1-5-2015

Evolution and ecology of two iconic Australian clades: the Meliphagidae (birds) and the Hakeinae (plants)

Eliot Trimarchi Miller
University of Missouri-St. Louis

Evolution and ecology of two iconic Australian clades:
The Meliphagidae (birds) and the Hakeinae (plants)

Eliot T. Miller
B.A., Biology, Vassar College – May 2005

A Dissertation Submitted to the Graduate School at the University of Missouri – St. Louis in partial fulfillment of the requirements for the degree

Doctor of Philosophy

in

Biology, with an emphasis on Ecology, Evolution and Systematics

October, 2014

Advisory Committee

Robert E. Ricklefs (Advisor)

John M. Bates, Ph.D.

Iván Jiménez, Ph.D.

Bette A. Loiselle, Ph.D.

Mark Westoby, Ph.D.

DISSERTATION ABSTRACT

The first part of this dissertation explores the evolution of two iconic groups of species through Australian climate space: the Meliphagidae, or honeyeaters, which are primarily nectar-feeding birds, and the Hakeinae, a section of the plant family Proteaceae. Both groups are inferred to have had their origins in Gondwanan rainforests that were widespread across Australia 45 million years ago and then diversified into more arid environments as the continent's climate became more arid. Accordingly, dry environments are inhabited by closely related (phylogenetically clustered) sets of species, although, in contrast to the honeyeaters, Hakeinae communities are characterized by more localized diversification. The impressive and rapid Hakeinae diversification may have been driven by specialization onto a variety of highly weathered, nutrient-poor soil types on the ancient Australian landmass.

The second part of this dissertation reviews a variety of methods to assess the phylogenetic structure of communities, such as local assemblages of honeyeaters and Hakeinae. Many published methods were found to be redundant, and some of the truly unique approaches do not measure what they purport to. Accordingly, only a small subset of phylogenetic community structure methods have merit.

In the third part of the dissertation, observations on foraging by 74 of 75 Australian honeyeater species are used to explore patterns of community assembly. Australian honeyeater communities reflect both stochastic and deterministic processes. Co-occurring species exhibit substantial overlap in foraging niche space, in contrast to predictions from assembly theory based on competition. At the same time, species tend to occupy characteristic portions of niche space and available niche space is smaller in the

arid regions of the continent. Within this smaller available niche space, arid-zone species tend to be more widely separated in niche space than species in more mesic environments.

ECOLOGY LETTERS

Ecology Letters, (2013) doi: 10.1111/ele.12156

LETTER

Niche conservatism constrains Australian honeyeater assemblages in stressful environments

E. T. Miller,[1,2]* A. E. Zanne[3,4] and R. E. Ricklefs[1]

Abstract

The hypothesis of phylogenetic niche conservatism proposes that most extant members of a clade remain in ancestral environments because expansion into new ecological space imposes a selectional load on a population. A prediction that follows is that local assemblages contain increasingly phylogenetically clustered subsets of species with increasing difference from the ancestral environment of a clade. We test this in Australian Meliphagidae, a continental radiation of birds that originated in wet, subtropical environments, but subsequently spread to drier environments as Australia became more arid during the late Cenozoic. We find local assemblages are increasingly phylogenetically clustered along a gradient of decreasing precipitation. The pattern is less clear along a temperature gradient. We develop a novel phyloclimatespace to visualise the expansion of some lineages into drier habitats. Although few species extend into arid regions, those that do occupy larger ranges and thus local species richness does not decline predictably with precipitation.

Keywords

Arid zone, Australia, biodiversity gradients, community assembly, Meliphagidae, phyloclimatespace, phylogenetic clustering, phylogenetic niche conservatism, phylogenetic structure, range size.

Ecology Letters (2013)

INTRODUCTION

Phylogenetic conservation of the niche, here defined broadly as the climate envelope within which a species occurs, has been invoked as a possible explanation for latitudinal gradients in species richness (Darlington 1959; Latham & Ricklefs 1993; Wiens & Donoghue 2004; Hawkins *et al.* 2005; Jablonski *et al.* 2006). This hypothesis predicts that evolutionary adaptation to novel climates is rare, and descendant species remain within climate space similar to that of their ancestors. Accordingly, as climate differs increasingly from the ancestral state of a particular clade, those species able to persist should belong to decreasing subsets of evolutionary lineages that have acquired adaptations to these different conditions. Thus, one expects to find increasing phylogenetic clustering in community structure along a gradient from ancestral to derived climate space.

Although phylogenetic community structure is often seen to shift along climate gradients, empirical evidence demonstrating the importance of phylogenetic niche conservatism in generating latitudinal diversity gradients has been mixed (Algar *et al.* 2009; Hortal *et al.* 2011; Parra *et al.* 2011). Indeed, phylogenetic niche conservatism, and the resulting predicted phylogenetic clustering away from the environment of initial radiation, need have no clear bearing on regional and local species richness patterns. Lineages that exhibit large shifts in climatic niche space might diversify more rapidly (Olalla-Tárraga *et al.* 2011) or have larger range sizes in novel habitats.

Across many regions of the world, the predominant environmental gradient reflects variation in temperature (Hawkins *et al.* 2005). In Australia, however, where the interior of the continent has become exceedingly arid compared to coastal areas over the past 20 Mya (Appendix S1), precipitation is the primary environmental driver. The north-south temperature gradient in Australia is less pronounced than present in northern hemisphere continents, owing to infrequency of freezing at higher latitudes in Australia, and in keeping with the trend of lower temperature seasonality in the southern hemisphere (Greenwood & Wing 1995; additional citations Appendix S1). Hawkins *et al.* (2005) demonstrated strong influences of water availability on bird richness patterns in Australia. Moreover, the continent has drifted equatorward coincident with a general cooling of the globe, leading to complex temperature changes over time (Appendix S1). Thus, the overall influence of temperature on the evolution of its biota is arguably less clear than that of the strong, directional trend in precipitation during this time. We focus on precipitation here, but also report temperature results.

The Australian Meliphagidae, or honeyeaters, comprise an abundant and widespread group of 75 bird species. At least one species can be found almost anywhere on the continent, and they are varied ecologically, from largely nectarivorous to almost entirely insectivorous (Higgins *et al.* 2001). The Meliphagidae diverged from other basal oscine passerines in the Eocene, approximately 45 Mya (Jønsson *et al.* 2011), when Australia was breaking away from Antarctica and what remained of Gondwana (Appendix S1). The family thus arose in a generally warm, wet world, on a continent that was much wetter than it is today; Meliphagidae likely originated in the wet forests that were widespread in Australia at that time (Appendix S1). The northward movement of the continent led to extensive aridification, which intensified in the mid- to late-Miocene, 5–15 Mya (Appendix S1). The new arid climate space would have provided

[1]*Department of Biology, University of Missouri, St. Louis, MO, 63121, USA*
[2]*Department of Biological Sciences, Macquarie University, Sydney, NSW, 2109, Australia*
[3]*Department of Biological Sciences, George Washington University, Washington, DC, 20052, USA*
[4]*Center for Conservation and Sustainable Development, Missouri Botanical Garden, St. Louis, MO, 63166, USA*
**Correspondence: E-mail: eliotmiller@umsl.edu*

substantial ecological opportunity for lineages that could adapt to the novel, physiologically stressful, open-vegetation environments. Because Meliphagidae are speciose, form a dominant part of Australian avian assemblages, span a range of climatic and ecological niches, radiated largely *in situ*, and face few dispersal limits within the continent, the family is an ideal taxon for analysis of evolution in climate space. Importantly, a recent molecular phylogeny is available (Nyári & Joseph 2011).

In this paper, we address the role of phylogenetic niche conservatism in the evolutionary radiation of Australian Meliphagidae. We develop a phyloclimatespace approach for visualising evolution through climate space, and use it to inform interpretation of patterns of phylogenetic community structure. We predict that evolution into new climate space is infrequent, and that local assemblages are composed of increasingly related species along a gradient of decreasing precipitation as compared to the ancestral climate of Meliphagidae. Because temperature has fluctuated throughout the evolution of this group, and in absolute terms the modern temperature gradient in Australia spans neither a notable portion of the global range in temperatures to which birds are subjected nor the range of temperatures to which the clade is thought to have been subjected over time, we do not expect to see clear results with respect to temperature. Nevertheless, *a priori*, we also predict that Meliphagidae assemblages should be increasingly phylogenetically clustered along a gradient away from the ancestral temperature regime. Despite these predicted relationships, and the linkage in the literature between these ideas and diversity gradients, we would not necessarily expect to see a strong relationship between climate and species richness, as species' range sizes and the diversification rates of particular lineages, among other factors, are also relevant. To address this potential disconnect, we explore species' range sizes, occupancy of suitable climate space, and species richness in local assemblages as functions of climate.

METHODS

Geographical data assembly

We obtained all sight and specimen records of Meliphagidae in Australia from the Global Biodiversity Information Facility (http://www.gbif.org/, n = 37 462), eBird (Sullivan *et al.* 2009, n = 28 056), and the Atlas of Living Australia (http://www.ala.org.au/, n = 2 296 074). We filtered the three databases in R (R Development Core Team 2011) to eliminate duplicate or non-georeferenced records, which left n = 2 273 404.

We generated a list of unique taxon names in this database (n = 385), determined their modern taxonomic interpretation (Toon *et al.* 2010; Nyári & Joseph 2011), and cleaned all names accordingly. Some of the taxa do not occur in Australia, and were therefore either incorrectly identified or poorly georeferenced. We discarded these, which left n = 2 269 088 across 75 species (minimum n = 130, *Meliphaga fordiana*; maximum n = 230 992, *Anthochaera carunculata*). We cleaned this initial database by visually inspecting all records on a species-by-species basis to eliminate poorly georeferenced points (n = 3075). The resulting point distributions were similar to, but more detailed than, available range maps. The final data set consisted of 2 269 088 unique records, because some of these records are associated with counts of multiple individuals, it contained 3 259 066 individuals total.

Climate data assembly

We described the climate niche of each species and grid cell with WorldClim layers (http://www.worldclim.org/bioclim). We divided Australia, including Tasmania, into equal-area grid cells ('local assemblages') of 100 × 100 km and summarised the mean of each layer for each grid cell. To determine the effect of spatial scale on our analyses (Cavender-Bares *et al.* 2006), we did the same for cells of 50 × 50 and 200 × 200 km. After exploring interrelationships among the 19 WorldClim variables, we chose to use mean annual temperature (MAT) and mean annual precipitation (MAP) to describe climate; these variables are uncorrelated in Australia (r^2 = 0.001). We used MAT instead of maximum, minimum or diurnal range in temperature for two reasons: (1) these were strongly correlated with MAP (r^2 greater than or equal to 0.21) and (2) many honeyeater species are nomadic, and temperature extremes may not be as biologically relevant if birds migrate or undertake local movements to avoid the harshest conditions (Higgins *et al.* 2001). We used the $\log_{10}$ of MAP because the distribution of precipitation is strongly right-skewed in Australia, and much interesting species turnover occurs among arid and semi-arid grid cells; the distribution of $\log_{10}$ MAP is close to normal (Shapiro–Wilk test, unlogged MAP W = 0.83, $\log_{10}$ MAP W = 0.96; the value of a normal distribution equals 1).

We defined the centre of each species' climatic niche as the mean MAT and MAP of unique grid cells in which the species occurred.

Community data matrix assembly and manipulation

For each grid cell, we used a split-apply-combine strategy (Wickham 2011) to generate two forms of spatially referenced data matrices (Webb *et al.* 2008), where species' abundances were calculated either as (1) the total number of records per species per grid or (2) the total number of individuals per species per grid. Since results were qualitatively similar for both matrices, and not all records were associated with count data, we report results only on the more conservative number of records.

Not all grid cells were evenly sampled. To account for this, we used rarefaction in the R package *vegan* (Oksanen *et al.* 2012) to restrict our analyses to grid cells for which at least 90% of the species were estimated to have been sampled (Chao 1987), and from which at least as many records existed as there were species in the most species-rich grid cell. Thus, in addition to cuts based on rarefaction, we excluded grid cells with fewer than 32, 33, and 36 unique records at the 50 × 50 km, 100 × 100 km and 200 × 200 km scales respectively. In total, these cuts removed 15, 22 and 43% of the original 50, 100 and 200 km grid cells, respectively, more or less evenly distributed throughout the continent (Appendix S5). Although it made no qualitative difference to results, to ensure all Meliphagidae were represented in the final matrix, we included a grid cell estimated to have had 84% of its species recorded, as otherwise *Lichenostomus hindwoodi* would have been excluded.

Range size was quantified as the number of grid cells in which a species occurred. We calculated each species' proportion of suitable climate space occupied as the number of grid cells occupied divided by the number of grid cells available within the range of climate space bounded by the 5 and 95% quantiles of its distribution in climate space. This was done separately for MAT and MAP. We regressed species richness, range size and the proportion of grid

cells occupied against MAP and MAT, accounting for potential spatial autocorrelation in species richness (Appendix S2).

Defining assemblages over a given scale is necessary in macroecological studies; we justify the scale we chose for this study in the following. First, Australia is relatively homogeneous topographically. Second, because we focus on phylogenetic niche conservatism, and the role it may have in mediating species occurrence patterns, whether the species in a grid cell interact is not critical. Third, in a separate study, ETM travelled extensively and studied the behaviour of all Australian Meliphagidae species. Both these observations and those of others (Higgins *et al.* 2001 and references therein) support the high vagility of these species. During this work, ETM occasionally recorded all birds seen during a single morning of travel by foot. From these lists, we conclude it is likely to observe a considerable portion of a grid cell's constituent Meliphagidae species at a single time and place (n = 27 mornings, mean proportion of species = 0.40 ± SD 0.16, range = 0.16–1). Finally, results were qualitatively similar across the 16-fold range in scale discussed above.

Assembly of the phylogeny

We used a modified version of a recently published phylogeny (Nyári & Joseph 2011). This tree, created from nuclear (Fib5) and mitochondrial (ND2) genes, was associated with branch lengths, but lacked nine of the 75 Australian species. We added these species manually, in one case (*Manorina*) incorporating molecular information available in GenBank (www.ncbi.nlm.nih.gov/genbank) to infer intrageneric relationships, and in another case (*Melithreptus*) incorporating more recent phylogenetic information (Toon *et al.* 2010). We assumed *Conopophila whitei* to be sister to *C. rufogularis/albogularis*, and *Xanthotis macleayanus* to be sister to *X. flaviventer*. We specified branch lengths from these new taxa to their nearest node by choosing biogeographically similar comparisons and assigning the new taxa the average branch lengths of their relevant comparisons. For instance, *X. flaviventer*, missing from the original phylogeny, was added to the terminal branch of its sister at a depth equal to the mean distance separating *C. rufogularis/albogularis*, *Meliphaga fordiana/albilineata*, *Ramsayornis fasciatus/modestus* and *Phylidonyris nigra/novaehollandiae*. Branch lengths used in phylogenetic analyses (except the ancestral state reconstruction with priors, see below) represent uncorrected genetic distances, though in figures we have scaled the phylogeny using a penalised likelihood approach (Sanderson 2002) to facilitate visualization.

Phylogenetic signal in climate niche

To test our hypothesis of phylogenetic niche conservatism in species' environmental niches, we assumed a drift (Brownian motion) model of evolution (Cooper *et al.* 2010) and calculated Pagel's λ (Pagel 1999) using the R package *phytools* (Revell 2012). This metric has recently been shown to perform well among those describing phylogenetic signal (Münkemüller *et al.* 2012). In practice, λ ranges from zero to one, where λ = 1 denotes that the trait in question is consistent with an underlying Brownian model of evolution. A P-value for λ is calculated with a likelihood ratio test, where the observed λ is compared to a trait distribution having no phylogenetic signal (Revell 2012). We ran this analysis with both the non-ultrametric and ultrametric (Sanderson 2002) form of the tree. Because results were qualitatively similar, we report only those for the non-ultrametric phylogeny (see also Litsios & Salamin 2012). Results of analyses using Blomberg's K (Blomberg *et al.* 2003) in the R package *picante* (Kembel *et al.* 2010) yielded similar results, and we do not report those here.

Ancestral state reconstruction

We reconstructed ancestral climate states using two approaches. First, we used restricted maximum likelihood (REML) ancestral state reconstruction (Schluter *et al.* 1997), as implemented in the R package *ape* (Paradis *et al.* 2004) to infer the most likely MAT and $\log_{10}$(MAP) climate values for the ancestor of modern Meliphagidae, assuming a Brownian model of evolution. This function returned similar results using least squares (Felsenstein 1985), maximum likelihood and REML.

Second, because the first approach does not consider the geologically and palynologically corroborated decrease in precipitation over the course of Meliphagidae evolution (Appendix S1), we used a Bayesian approach (Slater *et al.* 2012), where we fit models of evolution to species' current climate niches after placing priors on the root state. Our priors (mean MAP 1250 ± 275 SD mm yr^{-1}, mean MAT 19 ± 1.5 SD °C) are based on published literature (Appendix S1) and expert opinion (pers. comm. D. R. Greenwood, S. McLoughlin). We reconstructed ancestral precipitation based on the common logarithms of species' MAP values. The two alternatives we considered were Brownian and directional trend models of evolution. The latter is a Brownian model that incorporates an additional parameter, M, describing the expected value of the trait, in this case climatic niche, through time (Slater *et al.* 2012). The R function used, fitContinuousMCMC, will be incorporated in future versions of *geiger* (Harmon *et al.* 2008). We ran 10^7 generations of each model, sampling every 100 generations, and discarded the first 10^4 generations as burn-in. Number of generations needed was determined by repeated runs and comparisons of effective sample size with Tracer (http://beast.bio.ed.ac.uk/Tracer). We compared the fit of these different models with Akaike's information criterion for MCMC samples, using fitContinuousMCMC functions.

Phyloclimatespace

We visualised Meliphagidae exploration of climate space using an approach similar to a phylomorphospace (Sidlauskas 2008). In our case, our axes described the MAT and MAP of the extant taxa or the internal nodes as inferred by REML ancestral state reconstruction. Tips and internal nodes were plotted on this climate space, and the resulting points connected according to the underlying phylogeny. The branches were coloured by assigning all extant taxa a colour state of red. We divided the remaining nodes into four quantiles corresponding to distance from the root in the ultrametric tree, and assigned nodes colours as a function of their respective quantile (where blue was closest to the root). We used the R package *plotrix* (Lemon 2006) to colour branches by blending colours between two nodes according to a walk through RGB colour space.

We further explored a visual trend in the resulting figure by plotting the precipitation midpoint of each evolutionary vector (i.e. a branch from either an internal node to another such node or to an extant taxon) as a function of its angle through climate space.

Phylogenetic community structure

We used *picante* to calculate the mean phylogenetic pairwise distance (MPD) among the members of each grid cell (Webb 2000). This

index is not weighted by abundance. MPD increases with phylogenetic over-dispersion (or evenness, larger phylogenetic distances among the members of an assemblage) and decreases with clustering (shorter phylogenetic distances).

Abundance-weighted MPD is defined as the average phylogenetic distance between two randomly chosen individuals from the assemblage (Webb *et al.* 2008). It incorporates intraspecific phylogenetic distances of zero (assuming each taxon is represented by a single branch). However, our prediction that phylogenetic clustering increases away from ancestral environments concerns interspecific phylogenetic distances. By setting the diagonal element of the relative weight matrix used in the calculation of traditional abundance-weighted MPD equal to zero, we modified it to reflect only interspecific phylogenetic distances. We refer to this as interspecific abundance-weighted MPD, and its appropriate interpretation is the average phylogenetic distance among heterospecific individuals. Alternatively, it can be thought of as the MPD among species, where all distances are weighted by the number of individuals of each co-occurring species. Interspecific abundance-weighted MPD is particularly useful here in that it downweights the influence of vagrants on MPD scores.

We regressed both forms of MPD for each grid cell against the corresponding MAT and MAP value to test the prediction that phylogenetic clustering increases with distance from the ancestral climate. Because spatial autocorrelation is a potentially confounding issue of such analyses, we used spatial eigenvector mapping and variation partitioning to separate the components of spatial and environmental influences on the response variables (Appendix S2).

Though null models have been developed to explore the statistical significance of any given assemblage's phylogenetic structure (Kembel 2009), these standardise an observed score to a given set of assumptions. Our prediction was directly concerned with phylogenetic distances irrespective of species richness; we were interested in the relationship of raw MPD scores to climate. Accordingly, we developed null expectations of MPD under four scenarios (Appendix S3). We used the null expectations to calculate the 97.5 and 2.5% quantiles of the distribution of the metric at each value of species richness observed in the original data set. A given grid cell was considered 'overdispersed' or 'clustered' if the observed MPD score was greater or less than, respectively, the confidence intervals of the simulated scores at the corresponding richness (a two-tailed test).

RESULTS

Phylogenetic signal in environmental niche

Significant phylogenetic signal was observed in species' climate traits. For precipitation, $\lambda = 0.595$ ($P = 0.01$), and for temperature, $\lambda = 0.616$ ($P = 0.0005$). Thus, the observed phylogenetic trait distribution differed significantly from that expected given a star phylogeny (Revell 2012).

Ancestral state reconstruction

Our first method of reconstruction (REML) placed the ancestor of the Meliphagidae in an environment that received 748.6 mm yr^{-1} precipitation (Fig. 1, 95% CI = 447.5–1252.6, residual log-likelihood = 19.3), with a MAT of 21.1 °C (95% CI = 10.8–31.5 °C, residual log-likelihood = −518.4, subject to the known limitations of such reconstructions; Cunningham *et al.* 1998; Ané 2008; Slater *et al.* 2012; Appendix S4). This is moist by current Australian standards, and is at the upper range of precipitation that supports temperate woodland vegetation (Appendix S1).

Our second method, a Bayesian approach with a prior placed on the root (Slater *et al.* 2012), found, for MAP, highest support for a trend model of evolution with negative *M*, the parameter describing the expected value through time (on a $\log_{10}$ scale, mean = −0.21, 95% highest probability density = −0.48–0.05; due to the penalised likelihood smoothing approach, all tip to root distances equal 1). For MAT, a trend model of evolution was also best supported (mean $M = 2.20$, 95% HPD = −3.23–7.97). In neither case was the trend model strongly supported over a stationary Brownian model. For MAP, Akaike's difference score (dAIC) of the Brownian model was 2.45. For MAT, dAIC was 3.53. We therefore calculated the ancestral state at the root as the weighted average of these two models, based on the Akaike weights. We used kernel density estimates (Rosenblatt 1956), and calculated the HPD with the R package *hdrcde*. With this approach, the ancestral Meliphagidae were inferred to come from an environment characterised by mode MAP of 1205 mm yr^{-1} (95% HPD = 829–1779 mm yr^{-1}) and mode MAT of 19.3 °C (95% HPD = 16.2–22.0 °C). Inferred MAT is

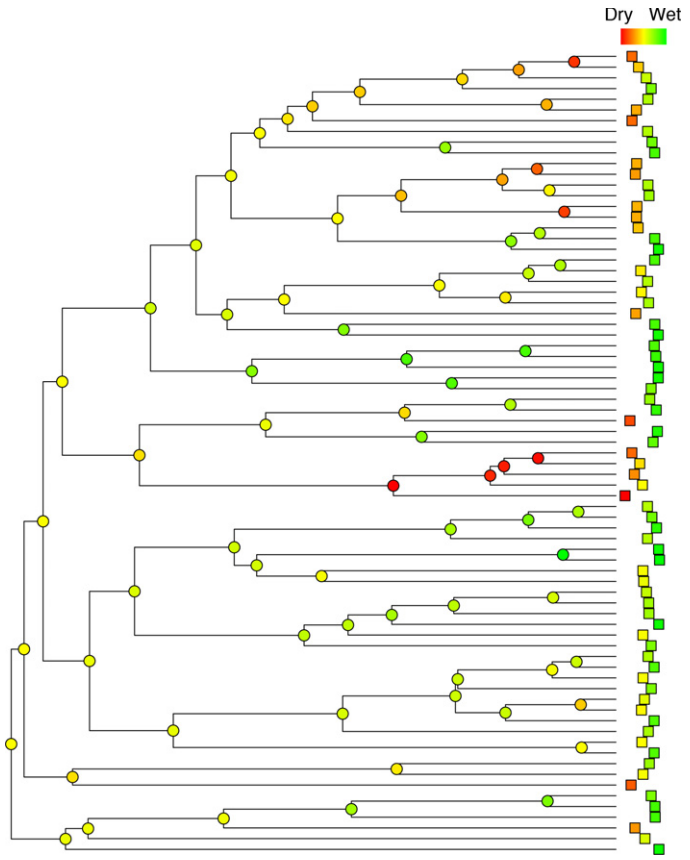

Figure 1 The Australian Meliphagidae phylogeny with mean annual precipitation depicted both across the tips and at the internal nodes (reconstructed with Brownian model of evolution and no trend). These values are represented both by the colour of the circles (internal nodes) and the squares (extant taxa) and, in the case of the extant taxa, by the distance of the squares from the tips of the phylogeny. Distances are proportional to the mean annual precipitation experienced by a given taxon. Colours range from red (taxa inhabiting driest areas) to orange to green (wettest areas). Observed $\lambda = 0.595$ ($P = 0.01$).

therefore approximately in the middle of current Australian temperature range, while the inferred MAP is much wetter than most of modern Australia (dashed lines Fig. 3).

Phyloclimatespace

Few lineages shifted out of the ancestral precipitation regime to invade the arid zone of Australia (Fig. 2a). In contrast, at moderate to high precipitation, evolution across broad ranges of temperature was frequent. Moving progressively from areas of high to low precipitation, we found that the orientation of evolutionary vectors in climate space narrowed significantly, with the lineages evolving towards drier climates remaining within narrow temperature ranges, and that lineages already in arid areas tended to evolve towards even drier climates (Fig. 2b).

Phylogenetic community structure

Local Meliphagidae assemblages were increasingly phylogenetically clustered along a gradient of decreasing precipitation from the inferred ancestral state of the Meliphagidae, whether measured in non-abundance-weighted (Fig. 3a, $r^2 = 0.496$, $P < 0.0001$, $n = 695$) or interspecific abundance-weighted MPD (Fig. 3c, $r^2 = 0.716$, $P < 0.0001$, $n = 695$). Honeyeaters that co-occur in drier areas are more closely related to each other than are species in wetter areas. Results were consistent across a 16-fold range in grid area; linear regressions of MPD against MAP were significant both at the 50 × 50 km (non-abundance-weighted $r^2 = 0.474$, $P < 0.0001$, $n = 1851$, interspecific abundance-weighted $r^2 = 0.648$, $P < 0.0001$, $n = 1851$) and the 200 × 200 km scales (non-abundance-weighted $r^2 = 0.558$, $P < 0.0001$, $n = 214$, interspecific abundance-weighted $r^2 = 0.753$, $P < 0.0001$, $n = 214$; see also Lanier *et al.* 2013). These results remained consistent after accounting for spatial autocorrelation; adjusted r^2 values after removal of spatial nuisance parameters for both forms of MPD at the 100 km scale were 0.496 and 0.716 respectively (Appendix S2).

The phylogenetic structure of Meliphagidae assemblages was poorly related to the temperature gradient in Australia. This was true irrespective of whether measured in non-abundance-weighted (Fig. 3b, $r^2 = 0.006$, $P = 0.039$, $n = 695$) or interspecific abundance-weighted MPD (Fig. 3d, $r^2 = 0.015$, $P = 0.001$, $n = 695$), and held across both changes in scale and after accounting for spatial autocorrelation (Appendix S2).

For non-abundance-weighted MPD, the assemblages of 40 of 695 total grid cells exhibited closer phylogenetic relationships than 97.5% of the richness null expectations at the corresponding species richness. Of these, 33 also exhibited significant phylogenetic clustering according to the frequency null expectations. The assemblages of seven grid cells were significantly overdispersed according to frequency null expectations, one of which was also considered overdispersed according to the richness null (Figs 3a,b and S3.2). For interspecific abundance-weighted MPD, 137 assemblages were con-

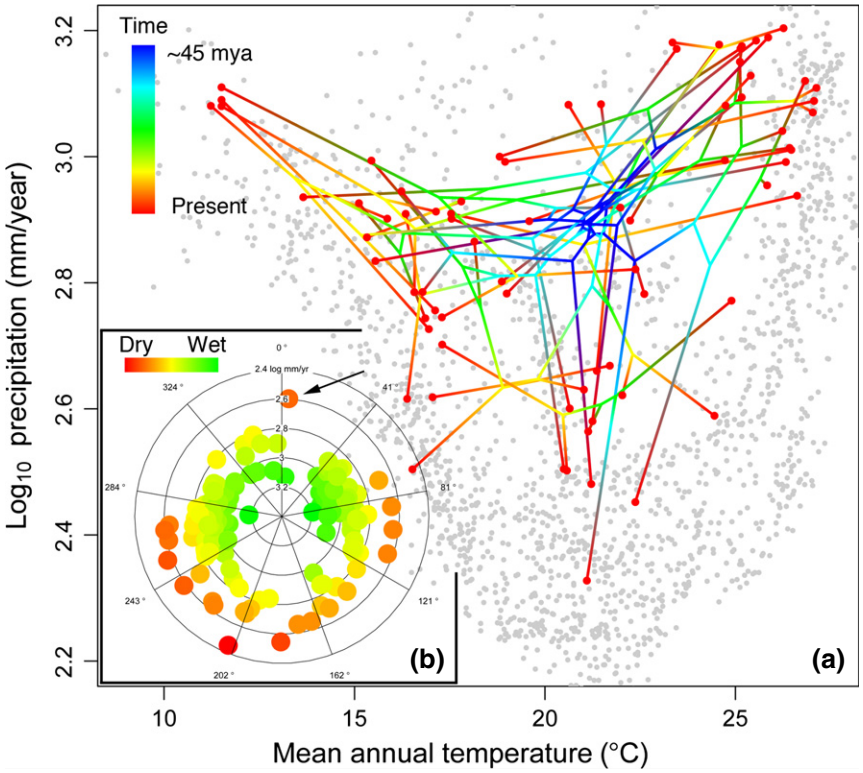

Figure 2 Meliphagidae evolution through climate space. (a) Extant taxa plotted as red points, positioned according to current climate niche. These are connected by the underlying phylogeny, with internal nodes placed with respect to inferred ancestral states (REML method). Colours in this panel represent distance of node from root (i.e. ± proportional to time). Grey points show modern range of Australian climate. The four species in the top left corner are Tasmanian endemics. (b) Precipitation midpoint of each vector as a function of angle through climate space. Like Fig. 1, colour in this panel represents precipitation, and the axis is inverted, such that lineages that evolved through wet climate space are plotted closest to origin. There is a tendency for lineages already in dry areas (outer ring of polar graph) not to evolve towards wetter climates (i.e. ± towards 0°). Outlier vector in this respect (small arrow) is discussed in Appendix S7.

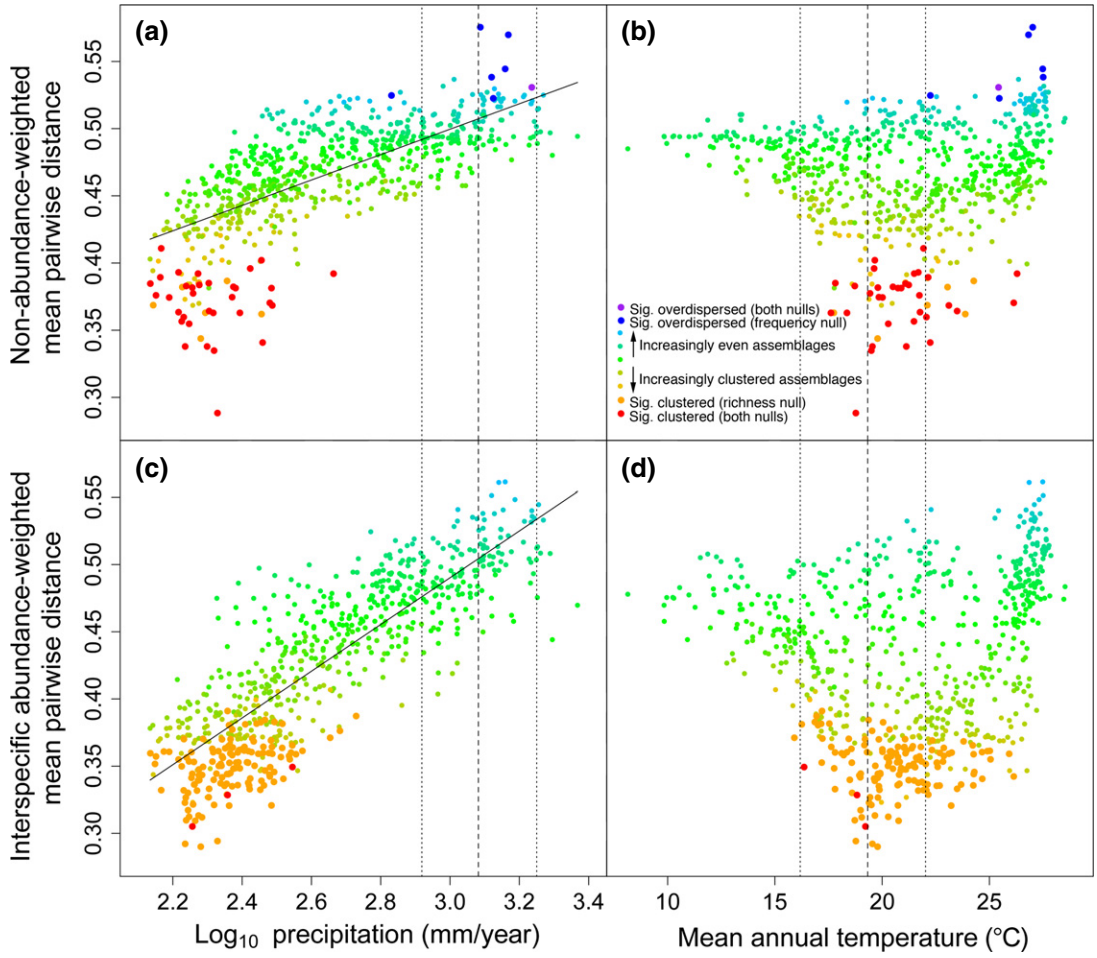

Figure 3 MPD as a function of climate. Points represent 100 × 100 km grids. Nonsignificant points coloured according to position between upper and lower confidence intervals (Appendix S3). Larger points deviate beyond one or more null model. Dashed lines represent inferred mode and 95% highest probability distribution for ancestral state at root (Bayesian approach with priors). Solid lines are ordinary least squares regressions. (a) Non-abundance-weighted MPD as function of $\log_{10}$ of MAP. Phylogenetic distances among assemblage members increase with precipitation ($r^2 = 0.496$, $P < 0.0001$, $n = 695$). (b) Non-abundance-weighted MPD as function of MAT. Phylogenetic distances are poorly related to temperature ($r^2 = 0.006$, $P = 0.039$, $n = 695$). (c) Interspecific abundance-weighted MPD as function of $\log_{10}$ of MAP ($r^2 = 0.716$, $P < 0.0001$, $n = 695$). (d) Interspecific abundance-weighted MPD as function of MAT ($r^2 = 0.015$, $P = 0.001$, $n = 695$).

sidered significantly clustered according to the richness null, but only 3 of these were significantly clustered using the frequency null (Figs 3c,d and S3.3).

Species richness

Species richness was positively correlated with MAP (Fig. 4a, Appendix S2, $r^2 = 0.245$, $P < 0.0001$, $n = 695$), as predicted by many hypotheses for the latitudinal diversity gradient and, since the ancestral state of the clade was inferred to have been an area of high precipitation, also in accordance with phylogenetic niche conservatism. It was, however, either weakly negatively correlated with MAT (Fig. 4b, $r^2 = 0.094$, $P < 0.0001$, $n = 695$) or, if spatial autocorrelation was accounted for, uncorrelated (Appendix S2). Regardless, neither climate variable explained much variation in species richness.

Range sizes

Range size was inversely related to MAP, such that species in arid areas occupy larger ranges than do species in wetter areas (Fig. 4c, $r^2 = 0.374$, $P < 0.0001$, $n = 75$). Range size was not related to MAT (Fig. 4d, $r^2 = 0.0004$, $P = 0.872$, $n = 75$). Moreover, species in arid areas occupy a larger proportion of available habitat space than do species in wetter areas (with respect to precipitation, $r^2 = 0.18$, $P = 0.0001$, $n = 75$, Fig. S6A; with respect to temperature $r^2 = 0.258$, $P < 0.0001$, $n = 75$, Fig. S6C). There was a weak but significant negative relationship between per cent of occupied temperature space and species' mean temperature niches ($r^2 = 0.056$, $P = 0.041$, $n = 75$, Fig. S6D).

DISCUSSION

Phylogenetic niche conservatism predicts descendant species remain in environmental space similar to that of their ancestors, with infrequent shifts into new climates (Latham & Ricklefs 1993; Wiens & Donoghue 2004). Accordingly, one expects increased phylogenetic clustering with increasing distance from the ancestral environment of a clade. For the Australian Meliphagidae, a diverse bird group distributed continent-wide, but believed to have originated in an area of high precipitation (Jønsson *et al.* 2011; Appendix S1; this

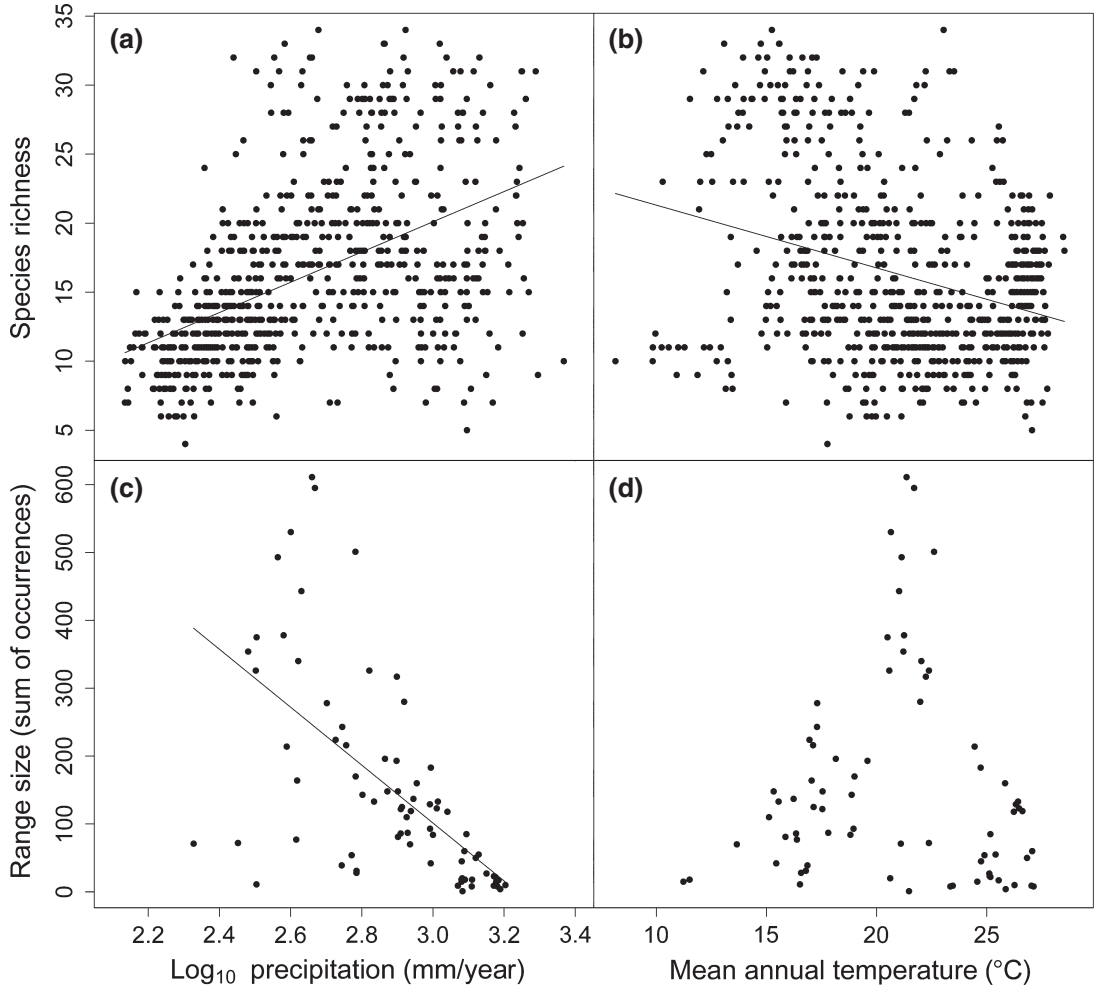

Figure 4 (a) Species richness per 100 × 100 grid cell as a function of MAP. More species are found in wetter areas, but little variation in species richness is explained by MAP (r^2 = 0.245, P < 0.0001, n = 695). (b) Species richness as function of MAT (r^2 = 0.094, P < 0.0001, n = 695). (c) Species range sizes (sum of grid cells in which a species occurs) as function of MAP (r^2 = 0.374, P < 0.0001, n = 75). Points in this and next panel represent individual species. The three outlying species with small range sizes in arid regions are *Ashbyia lovensis*, *Manorina melanotis* and *C. whitei*. The first two are habitat specialists with restricted ranges, while the third occurs widely throughout inland Australia but is rarely observed. (d) Species range sizes as function of MAT (r^2 = 0.0004, P = 0.87, n = 75).

study), we predicted increased phylogenetic clustering in increasingly arid climates. This was strongly supported; variation among assemblages in MAP explains much variation in phylogenetic community structure at a continental scale. We also predicted increased phylogenetic clustering away from the ancestral MAT of the clade. This was not supported, and may be related to fluctuating temperatures in Australia during Meliphagidae evolution, and the small extant temperature gradient in Australia (Appendix S1).

Our phyloclimatespace approach offers additional insight into the Australian Meliphagidae radiation. Shifts into novel climate space were rare; radiation into and within arid climates was particularly infrequent. In general, few lineages are characterised by long branches, which would suggest dramatic niche shifts. Evolution across broad swathes of Australian temperature regimes was evident among lineages inhabiting moist climates. Lineages that had moved into semi-arid habitats were the source of lineages that radiated into even more arid climates and, in keeping with the trend model of evolution being best supported, there appears to be a strong directionality to the evolution of these lineages. This is best seen in the winnowing of the distribution of evolutionary vectors in arid areas (Fig. 2b). Finally, few lineages evolved towards both hotter and drier habitats, and of these, none terminated in hot deserts. Because water availability decreases with increasing temperature, the adaptive load imposed on a population by a shift towards lower precipitation might be offset by parallel evolution to a lower temperature regime. In future studies, such questions might be better addressed by an analysis that considers species' entire climate envelopes or, ideally, their physiological tolerances (Vieites *et al.* 2009).

Despite strong support found here and by others (Algar *et al.* 2009; Hortal *et al.* 2011; Kooyman *et al.* 2011; Parra *et al.* 2011) for the phylogenetic niche conservatism hypothesis, i.e. increased phylogenetic clustering away from ancestral environments, species richness of Australian Meliphagidae declines only slightly with decreasing precipitation (Fig. 4a). This could have resulted from rapid diversification of the few lineages adapted to arid climates, although this does not seem to be the case (Fig. 2a). Rather, arid-adapted species tend to occupy larger geographical ranges (Fig. 4c) and a greater proportion of available climate space (Fig. S6) than mesic-restricted species.

Radiation into arid climes has been infrequent, but the increased phylogenetic clustering in these areas cannot be attributed to any

single clade. Instead, a few such clades within the Meliphagidae have entirely or partly radiated into dry areas. In total, 34 unique species occur in various combinations in significantly phylogenetically clustered assemblages. Of these, the Australian chats, long considered a separate family (Epthianuridae, Appendix S7), comprise one notable example. The *Ptilotula* clade (Nyári & Joseph 2011) of six species is another. The majority of these significantly clustered sites were located in the arid interior (Appendix S5).

Significantly overdispersed assemblages of species (Figs 3 and S3.2) might be interpreted as evidence for competitive exclusion, but we caution against this for three reasons: (1) we have not directly assessed competition among these species (Mayfield & Levine 2010), (2) seven (or one, depending on the null) significant sites is fewer than we would expect by chance (2.5%) to be significantly overdispersed and (3) the lack of significantly overdispersed sites when MPD is abundance-weighted suggests that vagrant and/or rare species might have influenced the non-abundance-weighted results.

Increased phylogenetic clustering away from an ancestral climate might be expected of a rapidly diversifying taxon with poor dispersal, irrespective of phylogenetic niche conservatism. However, the Australian Meliphagidae are highly mobile, and many species engage in migrations and/or nomadic movements (Higgins *et al.* 2001). Moreover, after correction for spatial autocorrelation, the results remained significant (Appendix S2). The strong pattern observed here seems unlikely to be the product of geographical inertia. Indeed, many Meliphagidae lineages likely underwent range shifts as the continent drifted northwards and the climate changed with it. Accordingly, phylogenetic clustering in arid-zone Meliphagidae represents the effect of an increasingly relevant habitat filter in drier areas. Numerous physiological adaptations for aridity have been documented in the Meliphagidae and other passerines (Williams & Main 1977; Maclean 1996; Tieleman 2005). In Australia, some arid areas are also among the warmest on the continent, which compounds physiological stresses (Maclean 1996; McKechnie & Wolf 2010). An alternative potential basis for this phylogenetic clustering, by no means mutually exclusive, is the lower productivity of arid regions (Boelman *et al.* 2003), combined with phylogenetically conserved differences in abilities to procure sufficient resources in such areas.

The Meliphagidae arose when Australia was much wetter than it is today, and was largely covered by Gondwanan forests (Appendix S1). As the continent drifted northwards, it experienced extensive aridification. A few clades have yielded lineages that invaded novel arid habitats, producing phylogenetic clustering in these areas. Such evolutionary shifts were presumably facilitated by ecophysiological adaptations to the new climates (Maclean 1996) and, perhaps, foraging adaptations associated with different vegetation structure and food resource characteristics of these new areas. Although phylogenetic niche conservatism may bear a complex relationship to patterns of local and regional species richness (Algar *et al.* 2009), it can clearly govern aspects of diversification, species' distributions and community assembly processes along strong gradients of environmental conditions.

ACKNOWLEDGEMENTS

ETM is grateful for support from the National Science Foundation (GRFP #1051698), the St. Louis Audubon Society, and a Trans-World Airlines Scholarship from the University of Missouri. We ran the null simulations on the University of Oslo Bioportal. We thank A. Nyári and L. Joseph for pre-publication access to the Meliphagidae phylogeny, M. Westoby, B. Loiselle and anonymous referees for insightful comments on previous drafts of the manuscript, J. Newell, T. Distler and J. Hidalgo for help with GIS, I. Jiménez for discussion and analysis of spatial autocorrelation and mapping of traits onto phylogenies, C. Trisos for discussion of null models, G. Slater for assistance with fitContinuousMCMC and discussion of different models of evolution, and D. Greenwood and S. McLoughlin for discussion of Australian paleoclimate.

AUTHORSHIP

ETM collected, prepared and analysed the data. AEZ and RER provided input on the design and implementation of the study from start to finish. ETM wrote the manuscript, and all authors contributed substantially to revisions.

REFERENCES

Algar, A.C., Kerr, J.T. & Currie, D.J. (2009). Evolutionary constraints on regional faunas: whom, but not how many. *Ecol. Lett.*, 12, 57–65.

Ané, C. (2008). Analysis of comparative data with hierarchical autocorrelation. *Ann. Appl. Stat.*, 2, 1078–1102.

Blomberg, S.P., Garland, Jr. T. & Ives, A.R. (2003). Testing for phylogenetic signal in comparative data: behavioral traits are more labile. *Evolution*, 71, 7–745.

Boelman, N.T., Stieglitz, M., Rueth, H.M., Sommerkorn, M., Griffin, K.L., Shaver, G.R., *et al.* (2003). Response of NDVI, biomass, and ecosystem gas exchange to long-term warming and fertilization in wet sedge tundra. *Oecologia*, 135, 414–421.

Cavender-Bares, J., Keen, A. & Miles, B. (2006). Phylogenetic structure of Floridian plant communities depends on taxonomic and spatial scale. *Ecology*, 87, S109–S122.

Chao, A. (1987). Estimating the population size for capture-recapture data with unequal catchability. *Biometrics*, 43, 783–791.

Cooper, N., Jetz, W. & Freckleton, R.P. (2010). Phylogenetic comparative approaches for studying niche conservatism. *J. Evol. Biol.*, 23, 2529–2539.

Cunningham, C.W., Omland, K.E. & Oakley, T.H. (1998). Reconstructing ancestral character states: a critical reappraisal. *Trends Ecol. Evolut.*, 13, 361–366.

Darlington, P.J. (1959). Area, climate, and evolution. *Evolution*, 13, 488–510.

Felsenstein, J. (1985). Phylogenies and the comparative method. *Am. Nat.*, 125, 1–15.

Greenwood, D.R. & Wing, S.L. (1995). Eocene continental climates and latitudinal temperature gradients. *Geology*, 23, 1044–1048.

Harmon, L.J., Weir, J.T., Brock, C.D., Glor, R.E. & Challenger, W. (2008). GEIGER: investigating evolutionary radiations. *Bioinformatics*, 24, 129–131.

Hawkins, B.A., Diniz-Filho, J.A.F. & Soeller, S.A. (2005). Water links the historical and contemporary components of the Australian bird diversity gradient. *J. Biogeogr.*, 32, 1035–1042.

Higgins, P.J., Peter, J.M. & Steele, W.K. (2001). *Handbook of Australian, New Zealand and Antarctic Birds. Vol. 5: Tyrant-flycatchers to Chats*. Oxford University Press, Melbourne, Australia.

Hortal, J., Diniz-Filho, J.A.F., Bini, L.M., Rodríguez, M.Á., Baselga, A., Nogués-Bravo, D., *et al.* (2011). Ice age climate, evolutionary constraints and diversity patterns of European dung beetles. *Ecol. Lett.*, 14, 741–748.

Jablonski, D., Roy, K. & Valentine, J.W. (2006). Out of the tropics: evolutionary dynamics of the latitudinal diversity gradient. *Science*, 314, 102–106.

Jønsson, K.A., Fabre, P.H., Ricklefs, R.E. & Fjeldså, J. (2011). Major global radiation of corvoid birds originated in the proto-Papuan archipelago. *PNAS*, 108, 2328–2333.

Kembel, S.W. (2009). Disentangling niche and neutral influences on community assembly: assessing the performance of community phylogenetic structure tests. *Ecol. Lett.*, 12, 949–960.

Kembel, S.W., Cowan, P.D., Helmus, M.R., Cornwell, W.K., Morlon, H., Ackerly, D.D., *et al.* (2010). Picante: R tools for integrating phylogenies and ecology. *Bioinformatics*, 26, 1463–1464.

Kooyman, R., Rossetto, M., Cornwell, W. & Westoby, M. (2011). Phylogenetic tests of community assembly across regional to continental scales in tropical and subtropical rain forests. *Global Ecol. Biogeogr.*, 20, 707–716.

Lanier, H.C., Edwards, D.L. & Knowles, L.L. (2013). Phylogenetic structure of vertebrate communities across the Australian arid zone. Published Early View online, *J. Biogeogr.*, 40, 1059–1070.

Latham, R.E. & Ricklefs, R.E. (1993). Global patterns of tree species richness in moist forests: energy-diversity theory does not account for variation in species richness. *Oikos*, 67, 325–333.

Lemon, J. (2006). Plotrix: a package in the red light district of R. *R-News*, 6, 8–12.

Litsios, G. & Salamin, N. (2012). Effects of phylogenetic signal on ancestral state reconstruction. *Syst. Biol.*, 61, 533–538.

Maclean, G.L. (1996). *The Ecophysiology of Desert Birds*. Springer, Berlin.

Mayfield, M.M. & Levine, J.M. (2010). Opposing effects of competitive exclusion on the phylogenetic structure of communities. *Ecol. Lett.*, 13, 1085–1093.

McKechnie, A.E. & Wolf, B.O. (2010). Climate change increases the likelihood of catastrophic avian mortality events during extreme heat waves. *Biol. Lett.*, 6, 253–256.

Münkemüller, T., Lavergne, S., Bzeznik, B., Dray, S., Jombart, T., Schiffers, K., *et al.* (2012). How to measure and test phylogenetic signal. *Methods Ecol. Evol.*, 3, 743–756.

Nyári, A.S. & Joseph, L. (2011). Systematic fragmentation of *Lichenostomus* improves the basis for understanding relationships within the honeyeaters (Meliphagidae) and historical development of Australo-Papuan bird communities. *Emu*, 111, 202–211.

Oksanen, J., Blanchet, F.G., Kindt, R., Legendre, P., Minchin, P.R. & O'Hara, R.B., *et al.* (2012). *vegan: Community Ecology Package*. R package version 2.0-7. Available at: http://CRAN.R-project.org/package=vegan

Olalla-Tárraga, M.Á., McInnes, L., Bini, L.M., Diniz-Filho, J.A.F., Fritz, S.A., Hawkins, B.A., *et al.* (2011). Climatic niche conservatism and the evolutionary dynamics in species range boundaries: global congruence across mammals and amphibians. *J. Biogeogr.*, 38, 2237–2247.

Pagel, M. (1999). Inferring the historical patterns of biological evolution. *Nature*, 401, 877–884.

Paradis, E., Claude, J. & Strimmer, K. (2004). APE: analyses of phylogenetics and evolution in R language. *Bioinformatics*, 20, 289.

Parra, J.L., Rahbek, C., McGuire, J.A. & Graham, C.H. (2011). Contrasting patterns of phylogenetic assemblage structure along the elevational gradient for major hummingbird clades. *J. Biogeogr.*, 38, 2350–2361.

R Development Core Team. (2011). *R: A Language and Environment for Statistical Computing*. R Foundation for Statistical Computing, Vienna, Austria, Available at: http://www.R-project.org. Last accessed 3 April 2013.

Revell, L.J. (2012). phytools: an R package for phylogenetic comparative biology (and other things). *Methods Ecol. Evol.*, 3, 217–223.

Rosenblatt, M. (1956). Remarks on some nonparametric estimates of a density function. *Ann. Math. Statist.*, 27, 832–837.

Sanderson, M.J. (2002). Estimating absolute rates of molecular evolution and divergence times: a penalized likelihood approach. *Mol. Biol. Evol.*, 19, 101–109.

Schluter, D., Price, T., Mooers, A.Ø. & Ludwig, D. (1997). Likelihood of ancestor states in adaptive radiation. *Evolution*, 51, 1699–1711.

Sidlauskas, B. (2008). Continuous and arrested morphological diversification in sister clades of characiform fishes: a phylomorphospace approach. *Evolution*, 62, 3135–3156.

Slater, G.J., Harmon, L.J. & Alfaro, M.E. (2012). Intergrating fossils with molecular phylogenies improves inference of trait evolution. *Evolution*, 66, 3931–3944.

Sullivan, B.L., Wood, C.L., Iliff, M.J., Bonney, R.E., Fink, D. & Kelling, S. (2009). eBird: a citizen-based bird observation network in the biological sciences. *Biol. Conserv.*, 142, 2282–2292.

Tieleman, B.I. (2005). Physiological, behavioral and life history adaptations of larks along an aridity gradient: a review. In: *Ecology and Conservation of Steppe-land Birds* (eds. Bota, G., Camprodon, J., Manosa, S. & Morales, M.). Lynx Editions, Barcelona, pp. 49–67.

Toon, A., Hughes, J.M. & Joseph, L. (2010). Multilocus analysis of honeyeaters (Aves: Meliphagidae) highlights spatio-temporal heterogeneity in the influence of biogeographic barriers in the Australian monsoonal zone. *Mol. Ecol.*, 19, 2980–2994.

Vieites, D.R., Nieto-Román, S. & Wake, D.B. (2009). Reconstruction of the climate envelopes of salamanders and their evolution through time. *PNAS*, 106, 19715–19722.

Webb, C.O. (2000). Exploring the phylogenetic structure of ecological communities: an example for rain forest trees. *Am. Nat.*, 156, 145–155.

Webb, C.O., Ackerly, D.D. & Kembel, S.W. (2008). Phylocom: software for the analysis of phylogenetic community structure and trait evolution. *Bioinformatics*, 24, 2098–2100.

Wickham, H. (2011). The split-apply-combine strategy for data analysis. *J. Stat. Software*, 40, 1–29.

Wiens, J.J. & Donoghue, M.J. (2004). Historical biogeography, ecology and species richness. *Trends Ecol. Evolut.*, 19, 639–644.

Williams, C.K. & Main, A.R. (1977). Ecology of Australian chats (Epthianura Gould): aridity, electrolytes and water economy. *Aust. J. Zool.*, 25, 673–691.

SUPPORTING INFORMATION

Additional Supporting Information may be downloaded via the online version of this article at Wiley Online Library (www.ecologyletters.com).

Editor, Arne Mooers
Manuscript received 18 February 2013
First decision made 1 April 2013
Second decision made 26 May 2013
Third decision made 4 June 2013
Fourth decision made 4 June 2013
Manuscript accepted 17 June 2013

Appendix S1:

Additional references for the paleoclimate of Australia

The climate history of the continent of Australia, from its Gondwanan origins to the present, has been fairly well studied. While gaps in our understanding remain to be filled, multiple approaches—particularly geological and palynological—have largely corroborated each other and helped to shape current knowledge of Australian paleoclimate. Due to space constraints in the main text, we offer a more complete bibliography here.

Australia began separating from Antarctica and what remained of Gondwana by the early Cenozoic (McLoughlin 2001; McGowran *et al.* 2004). The Meliphagidae diverged from other basal oscine passerines in the Eocene, approximately 45 Mya (Gardner *et al.* 2010; Jønsson *et al.* 2011). The family thus had its origin in a generally warm, wet world, on a continent that was much wetter than it is today (Huber & Goldner 2012); the Meliphagidae likely originated in the wet forests that were widespread in Australia at that time (Beadle 1981; Truswell 1993; Greenwood 1996; Greenwood *et al.* 2003). Since the Gondwanan breakup, Australia has continued equatorward movement, accompanied by extensive aridification that intensified in the mid- to late-Miocene, 5-15 Mya (Truswell 1993; Greenwood 1996; Hill *et al.* 1999; McLoughlin 2001; Greenwood *et al.* 2003; McGowran *et al.* 2004; Greenwood & Huber 2011; Herold *et al.* 2011; Huber & Goldner 2012). It also appears there has been an increase in the seasonality of this rainfall, resulting in drier dry seasons, as Australia has drifted towards the dynamic Intertropical Convergence Zone (Greenwood 1996; Huber & Goldner 2012). In summary, there has been a general, directional trend towards lower and less consistent annual precipitation across Australia since the origin of the Meliphagidae. Mean annual temperature, on the other hand, has fluctuated throughout Meliphagidae evolution, and though the world has generally

cooled during this time, Australia's simultaneous equatorward movement has generated a complex set of temperature shifts throughout its history (Truswell 1993; Greenwood *et al.* 2003; McGowran *et al.* 2004).

Additional references

1.

Beadle, N.C.W. (1981). *The vegetation of Australia*. Cambridge University Press, Cambridge, UK.

2.

Gardner, J.L., Trueman, J.W.H., Ebert, D., Joseph, L. & Magrath, R.D. (2010). Phylogeny and evolution of the Meliphagoidea, the largest radiation of Australasian songbirds. *Mol. Phylogenet. Evol*, 55, 1087–1102.

3.

Greenwood, D.R. (1996). Eocene monsoon forests in central Australia? *Aust. Syst. Bot.*, 9, 95–112.

4.

Greenwood, D.R. & Huber, M. (2011). Eocene precipitation: a global monsoon? Abstract T22C-07. Presented at the Fall Meeting, American Geophysical Union, 5-9 Dec, San Francisco, CA.

5.

Greenwood, D.R., Moss, P.T., Rowett, A.I., Vadala, A.J. & Keefe, R.L. (2003). Plant communities and climate change in southeastern Australia during the early Paleogene. In: *Causes and consequences of globally warm climates in the early Paleogene*, Special Paper (eds. Wing, S.L., Gingerich, P.D., Schmitz, B. & Thomas, E.). Geological Society of America, Boulder, Colorado, pp. 365–380.

6.

Herold, N., Huber, M., Greenwood, D.R., Müller, R.D. & Seton, M. (2011). Early to Middle Miocene monsoon climate in Australia. *Geology*, 39, 3–6.

7.

Hill, R.S., Truswell, E.M., McLoughlin, S. & Dettman, M.E. (1999). The evolution of the Australian flora: fossil evidence. In: *Flora of Australia*. CSIRO Publishing, Canberra, pp. 251–320.

8.

Huber, M. & Goldner, A. (2012). Eocene monsoons. *J. Asian Earth Sci.*, 44, 3–23.

9.

Jønsson, K.A., Fabre, P.H., Ricklefs, R.E. & Fjeldså, J. (2011). Major global radiation of corvoid birds originated in the proto-Papuan archipelago. *PNAS*, 108, 2328–2333.

10.

McGowran, B., Holdgate, G.R., Li, Q. & Gallagher, S.J. (2004). Cenozoic stratigraphic succession in southeastern Australia. *Aust. J. Earth Sci.*, 51, 459–496.

11.

McLoughlin, S. (2001). The breakup history of Gondwana and its impact on pre-Cenozoic floristic provincialism. *Aust. J. Bot.*, 49, 271–300.

12.

Truswell, E.M. (1993). Vegetation in the Australian Tertiary in response to climatic and phytogeographic forcing factors. *Aust. Syst. Bot.*, 6, 533–557.

Appendix S2:

Observed results cannot be explained solely as a product of spatial autocorrelation

Spatial autocorrelation is a potentially confounding issue in many ecological studies (Griffith & Peres-Neto 2006; Dormann *et al.* 2007; Bini *et al.* 2009; Beale *et al.* 2010; Peres-Neto & Legendre 2010). Since it is theoretically possible that any relationship we observed between mean pairwise phylogenetic distance (MPD) or richness and mean annual precipitation (MAP) or mean annual temperature (MAT) could be solely due to spatially contagious processes like dispersal and speciation, we employed spatial eigenvector mapping to partition out the contributions of environmental and spatial predictors on observed MPD and richness. Under some scenarios (dependent on the structure of the autocorrelation), this method has been shown to have type I error rates over 5% (Beale *et al.* 2010).

We used the procedure described in Dormann et al. (2007). However, because our goal was to test whether the environmental variables were significant in the face of spatial autocorrelation, we used a liberal approach in our selection of spatial eigenvectors. Specifically, we used all resulting 295 eigenvectors with positive eigenvalues as predictors in multiple regression models. Our results, therefore, represent a conservative estimate of the amount of variation in MPD (or richness) explained by the environmental variables after partitioning out the component of variation due solely to spatial autocorrelation (the spatial nuisance parameter; Peres-Neto & Legendre 2010).

As in the main text, we tested for the influence of MAT and MAP on MPD and richness separately. For each of these, we derived three regression models: (1) a model that incorporated the environmental variable in question and all spatial variables, including latitude and longitude; (2) a model that only incorporated the spatial variables; (3) a model that only incorporated the

environmental variable. We then partitioned the variation (Legendre & Legendre 1998) explained by these models into shared and unique components.

For non-abundance-weighted MPD, MAP remained significant after inclusion in model 1 with all variables ($P = 0.0002$). The adjusted (for multiple explanatory variables) R^2 for the entire model was 0.725. The proportion of variation that could be explained solely by the environment (fraction [a] in Legendre & Legendre 1998) was 0.006, while that which could be explained both by this and by spatially structured environmental data (fraction [ab], see also Peres-Neto & Legendre 2010) was 0.496. Thus, the adjusted R^2 of the spatial nuisance component of our results (fraction [b]) was 0.223. For interspecific abundance-weighted MPD, MAP also remained significant in model 1 ($P < 0.0001$), and the entire model adjusted $R^2 = 0.91$. Proportions of variation were adjusted R^2 [a] = 0.014, adjusted R^2 [ab] = 0.716, and adjusted R^2 [b] = 0.18.

For non-abundance-weighted MPD, MAT did not remain significant in model 1 ($P = 0.358$), and the entire model adjusted $R^2 = 0.716$. Proportions of variation were adjusted R^2 [a] = 0, adjusted R^2 [ab] = 0.005, and adjusted R^2 [b] = 0.711. For interspecific abundance-weighted MPD, MAT remained significant ($P = 0.0005$), and the entire model adjusted $R^2 = 0.899$. Proportions of variation were adjusted R^2 [a] = 0.003, adjusted R^2 [ab] = 0.014, and adjusted R^2 [b] = 0.882.

For richness, MAP remained significant in model 1 ($P = 0.02$), and the entire model adjusted $R^2 = 0.846$. Proportions of variation were adjusted R^2 [a] = 0.002, adjusted R^2 [ab] = 0.244, and adjusted R^2 [b] = 0.6. However, MAT was no longer significant after accounting for spatial autocorrelation ($P = 0.059$). The entire model adjusted $R^2 = 0.845$. Proportions of variation were adjusted R^2 [a] = 0.001, adjusted R^2 [ab] = 0.093, and adjusted R^2 [b] = 0.751.

Additional references

1.

Beale, C.M., Lennon, J.J., Yearsley, J.M., Brewer, M.J. & Elston, D.A. (2010). Regression analysis of spatial data. *Ecol. Lett.*, 13, 246–264.

2.

Bini, L.M., Diniz-Filho, J.A.F., Rangel, T.F.L.V.B., Akre, T.S.B., Albaladejo, R.G., Albuquerque, F.S., *et al.* (2009). Coefficient shifts in geographical ecology: An empirical evaluation of spatial and non-spatial regression. *Ecography*, 32, 193–204.

3.

Dormann, C.F., McPherson, J.M., Araújo, M.B., Bivand, R., Bolliger, J., Carl, G., *et al.* (2007). Methods to account for spatial autocorrelation in the analysis of species distributional data: a review. *Ecography*, 30, 609–628.

4.

Griffith, D.A. & Peres-Neto, P.R. (2006). Spatial modeling in ecology: the flexibility of eigenfunction spatial analyses. *Ecology*, 87, 2603–2613.

5.

Legendre, P. & Legendre, L. (1998). *Numerical ecology*. Elsevier Science, Amsterdam.

6.

Peres-Neto, P.R. & Legendre, P. (2010). Estimating and controlling for spatial structure in the study of ecological communities. *Global Ecol. Biogeogr.*, 19, 174–184.

Appendix S3:

A novel approach to significance testing of observed phylogenetic community structure

Typically, mean phylogenetic pairwise distance (MPD) scores are standardized by comparison to a null model, yielding the metric often referred to as net relatedness index (NRI, Webb 2000). In this manner the significance of the observed points is also assessed. However, as our prediction was concerned with raw MPD scores, a standardized score was, in our study, an unnecessary abstraction of our response variable. Moreover, had we had a time-calibrated phylogeny, observed MPD scores would have been directly interpretable as the average evolutionary time separating two species in an assemblage.

Despite this, we were still interested in the significance of our observed phylogenetic structure. Therefore, for both the unweighted and interspecific abundance-weighted MPD, we randomized the community data matrix using the richness and frequency shuffles in the R package *picante* (= four null models total; Kembel et al. 2010). However, rather than using these to standardize our MPD scores, we retained all randomizations and their associated species richness per scenario, and used them to calculate 95% confidence intervals at each unique species richness value that occurred in the observed dataset.

With unweighted MPD, a richness null calculated in this manner is equivalent to a traditional richness null, but a frequency null is quite different (Fig. S3.1). This is because the matrix randomization for the latter maintains species' occurrence frequencies by shuffling species among sites; the resulting random assemblages have a strong tendency towards the median number of species per assemblage in the observed dataset, and random assemblages of low and high species richness are infrequently sampled. Thus, observed sites are compared to randomized sites with a narrow distribution of species richness centered on the median of the

dataset, irrespective of the species richness of the observed site. Since the width of the confidence intervals are negatively correlated with species richness, such frequency nulls have high type I error risks (Hardy 2008), presumably particularly so at low species richness. Our approach avoids these shortcomings, though it is computationally intensive and, unless well-sampled species richness are discarded after sufficient sampling, observed scores will be compared to null expectations generated from unequal sampling. Code to calculate null expectations in this manner is available (http://www.umsl.edu/~emmq7).

With interspecific abundance-weighted MPD, our richness null compares observed assemblages to random assemblages of the corresponding species richness, where all species can occur with equal probability and rank abundance curves are sampled in proportion to their occurrence in the observed data. For instance, if half of the assemblages of a given species richness in the observed data contain a few very common species and many rare species, and the other half contains mostly moderately common species, this structure is maintained in the randomized data. Our frequency null compares observed assemblages to random assemblages of the same species richness, where species occur with a probability proportional to their occurrence in the original dataset, and with an abundance drawn from each species' specific observed abundance distribution (e.g., if a species is widespread but everywhere rare, this same structure is maintained in the randomized data).

We ran 10^5 iterations of each of the four null models. As expected, the frequency nulls infrequently sampled low and high species richness. We subsequently randomized the matrices as detailed, but this time only retained the first 100 random samples of each species richness. By combining these raw values with those from the corresponding 10^5 iterations, we ensured that all observed scores were compared to at least 100 random assemblages of equivalent species

richness. We compared these final confidence intervals to those generated from fewer iterations, and found that the positions of the confidence intervals—particularly at moderate to high species richness—remained quite stable after only a few hundred randomizations. Since, after secondary sampling for infrequently sampled species richness values, only random assemblages of high species richness (31-34 species) received fewer than 1,000 samples, and none of our significant grid cells contained this many species, we are confident that the significance of very few of our sites would change with additional iterations of the null models.

Additional references

1.

Hardy, O.J. (2008). Testing the spatial phylogenetic structure of local communities: statistical performances of different null models and test statistics on a locally neutral community. *J. Ecol.*, 96, 914–926.

2.

Kembel, S.W., Cowan, P.D., Helmus, M.R., Cornwell, W.K., Morlon, H., Ackerly, D.D., *et al.* (2010). Picante: R tools for integrating phylogenies and ecology. *Bioinformatics*, 26, 1463–1464.

3.

Webb, C.O. (2000). Exploring the phylogenetic structure of ecological communities: an example for rain forest trees. *Am. Nat.*, 156, 145–155.

70

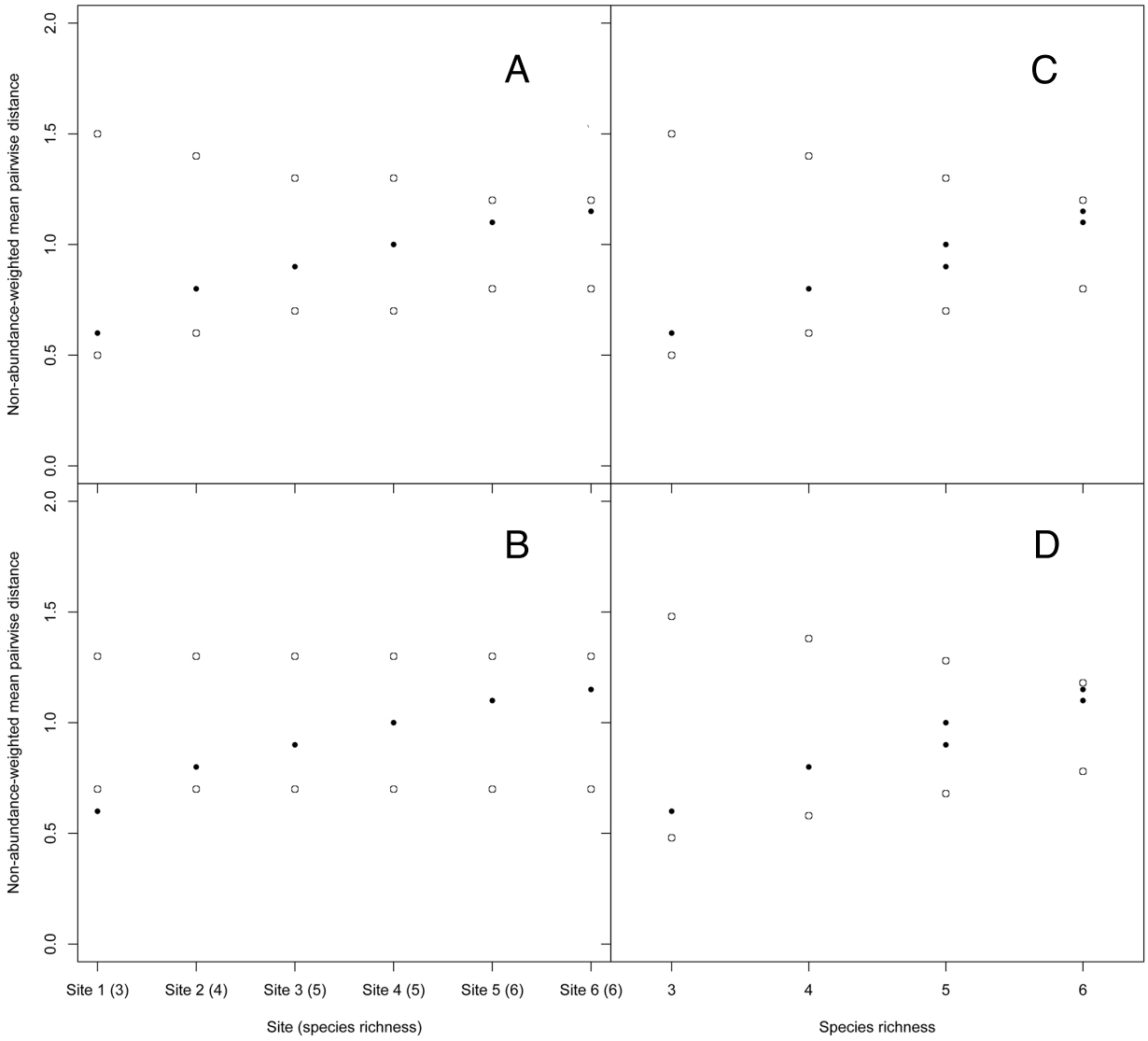

71

72

73 Figure S3.1. A schematic diagram, using simulated values, of the difference between a typical
74 null model approach and the approach we take in this study. (A) Matrix randomizations to
75 maintain species richness shuffle species within columns. All species can occur with equal
76 probability. Observed sites are compared to random values of corresponding species richness.
77 (B) Matrix randomizations to maintain species' occurrence frequencies shuffle species across

columns. Observed sites, irrespective of species richness, are compared to random values with an underlying distribution of species richness values centered on the median species richness in the observed dataset. (C) Results of a typical richness null and our approach are equivalent when the richness shuffle is used as, in either case, observed sites are compared to random values of corresponding species richness where all species can occur with equal probability. (D) Results of a typical frequency null and our approach differ when a frequency shuffle is used. Our approach compares observed sites to random sites of corresponding species richness.

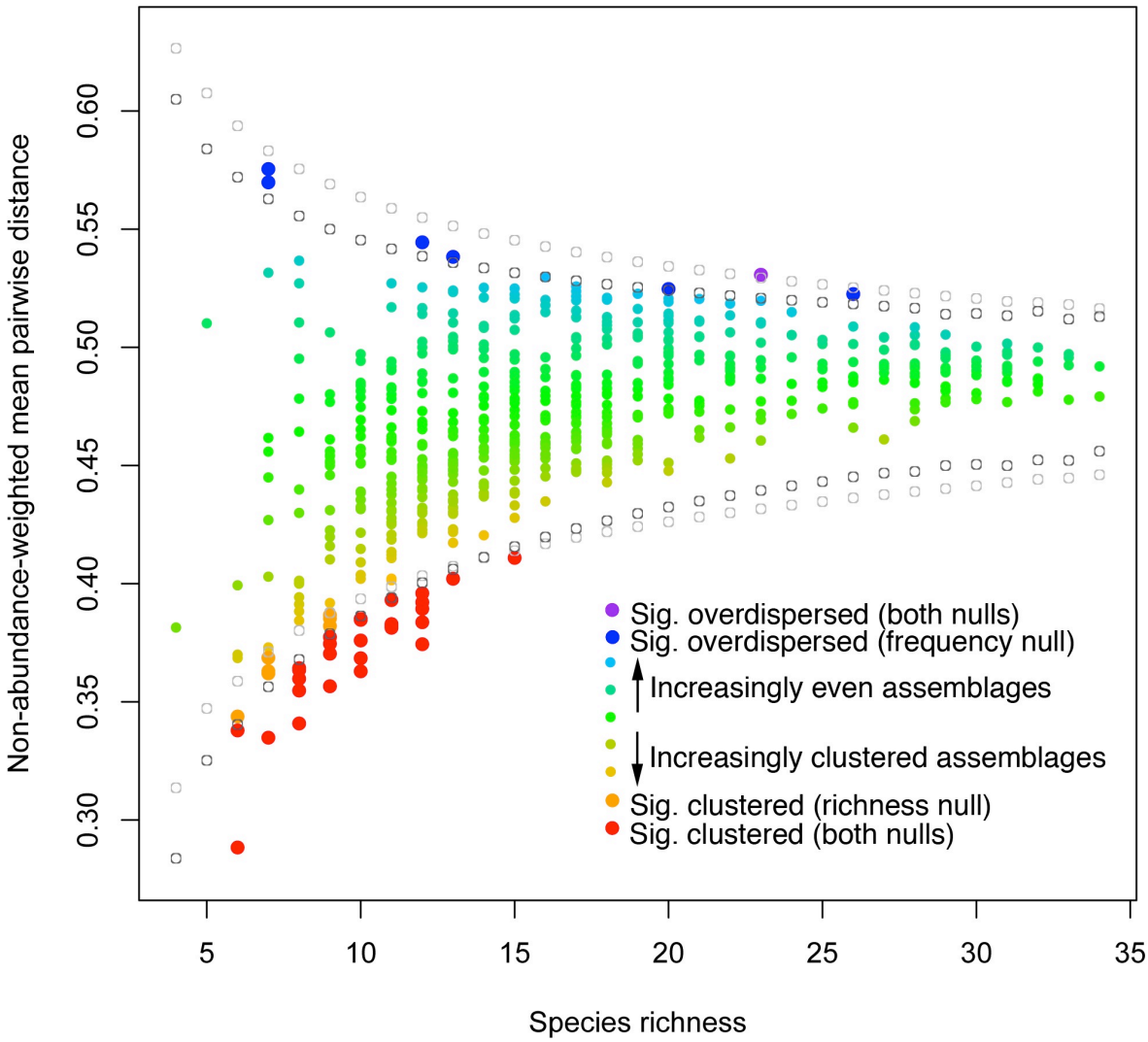

Figure S3.2. Observed and expected non-abundance-weighted mean pairwise phylogenetic distance among the members of n = 695 100 × 100 km grid cells. The non-significant sites are color-coded from light orange through light blue according to their position between the upper and lower confidence intervals. Null expectations for the richness null are plotted as light gray hollow circles, and those for the frequency null are dark hollow circles. Significant sites are also

93 color-coded: orange are clustered according to a richness null, red are clustered according to both
94 the richness and frequency nulls, blue are overdispersed according to a frequency null, and
95 purple are overdispersed according to both frequency and richness nulls.
96

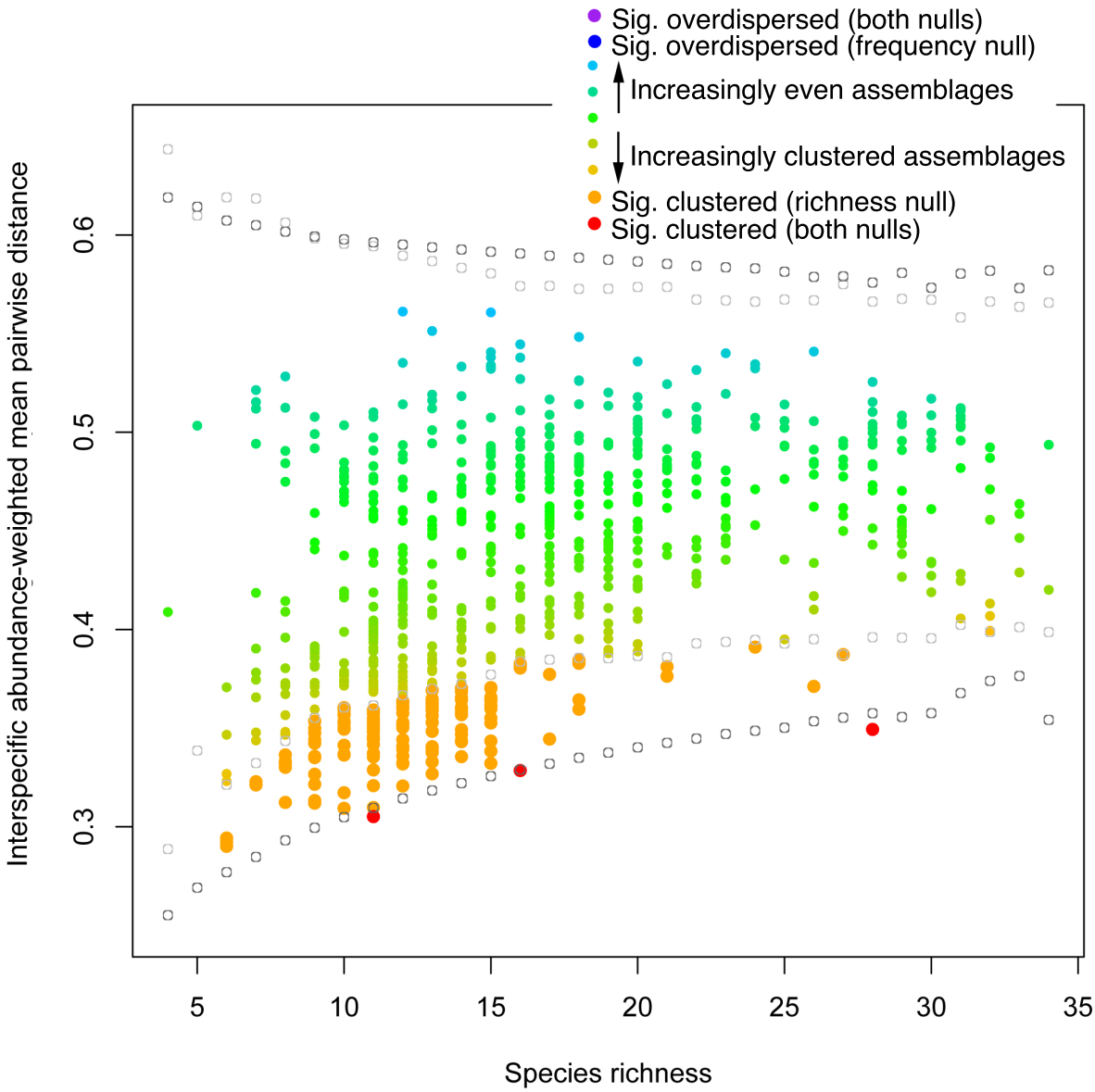

Figure S3.3. Observed and expected interspecific abundance-weighted mean pairwise phylogenetic distance among the members of n = 695 100 × 100 km grid cells. The non-significant sites are color-coded from light orange through light blue according to their position between the upper and lower confidence intervals. Null expectations for the richness null are plotted as light gray hollow circles, and those for the frequency null are dark hollow circles.

Significant sites are also color-coded: orange are clustered according to a richness null, and red are clustered according to both the richness and frequency nulls.

Figure S4. The Australian Meliphagidae phylogeny with mean annual temperature (MAT) depicted both across the tips and at the internal nodes (reconstructed assuming a Brownian model of evolution with no trend). These values are represented both by the color of the circles (internal nodes) and the squares (extant taxa) and, in the case of the extant taxa, by the distance of the squares from the tips of the phylogeny. Distances are proportional to the mean annual temperature experienced by a given taxon. The colors range from cyan (taxa inhabiting coldest areas) to orange to red (hottest areas). Observed Pagel's $\lambda = 0.616$ ($P = 0.0005$). Our restricted maximum likelihood reconstruction placed the ancestral Meliphagidae in an environment characterized by 21.1°C MAT (95% CI = 10.8-31.5°C, residual log-likelihood = -518.4).

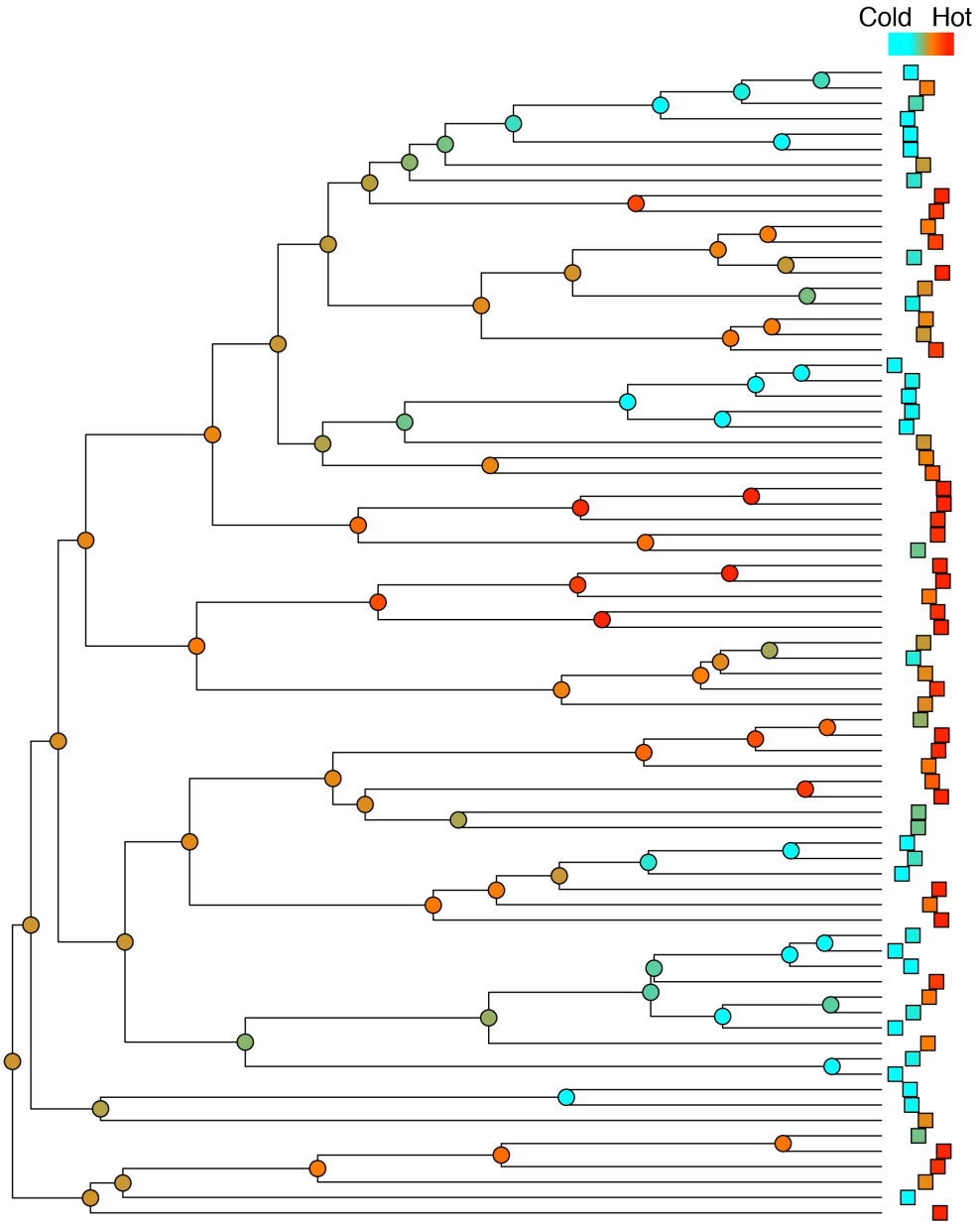
Cold
Hot

Figure S5.1. Non-abundance-weighted mean pairwise phylogenetic distance (MPD) mapped across Australia. Grid cells represent 100 × 100 km local assemblages, and are color-coded from red (more clustered) to blue (more even). When not abundance-weighted, co-occurring species are more closely related in the interior and west of the continent, while species in the east and particularly the north are less closely related. Figure S5.2 shows which of these grid cells deviate beyond null expectations.

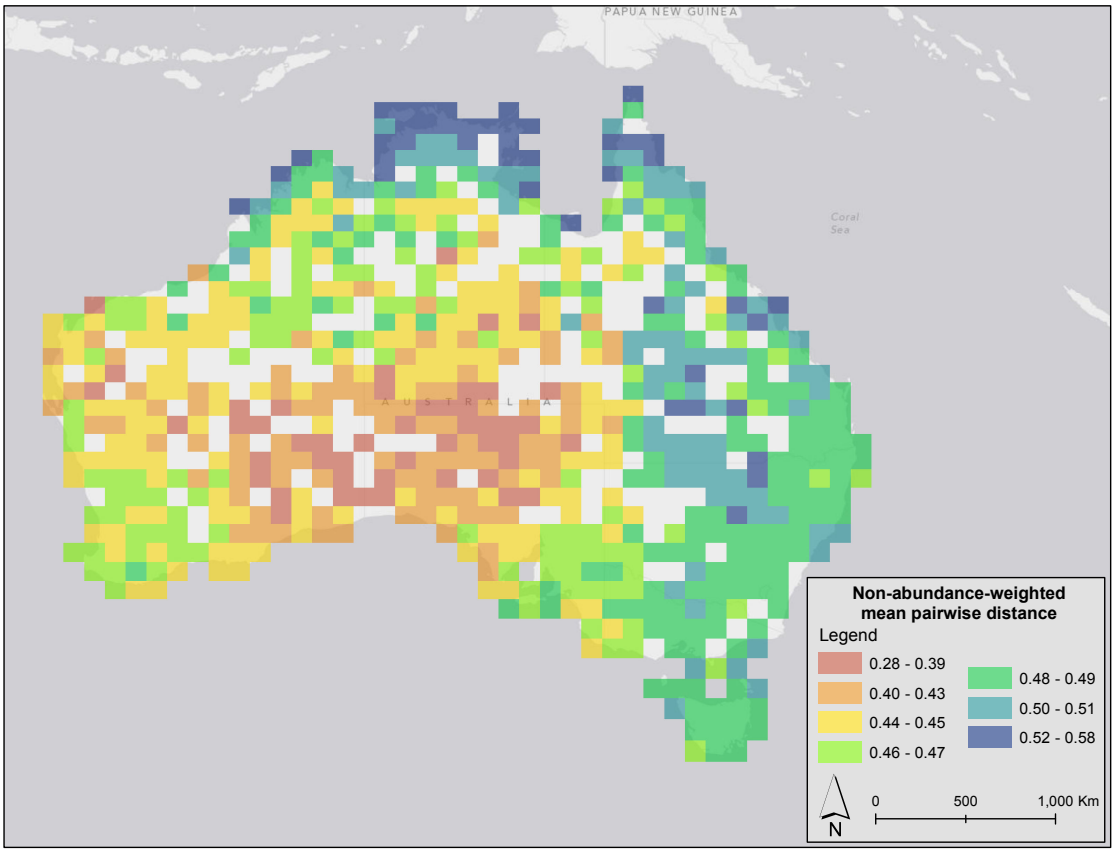

Figure S5.2. Significance, according to a frequency null, of observed non-abundance-weighted MPD mapped across Australia. Yellow grid cells did not deviate beyond expectations of a frequency null and, generally, a richness null (the 7 additional sites also considered clustered according to a richness null were all located in the interior of the continent). Red grid cells were significantly clustered, and blue significantly overdispersed. The single site also considered overdispersed according to a richness null was located on Cape York in the far northeast of the continent.

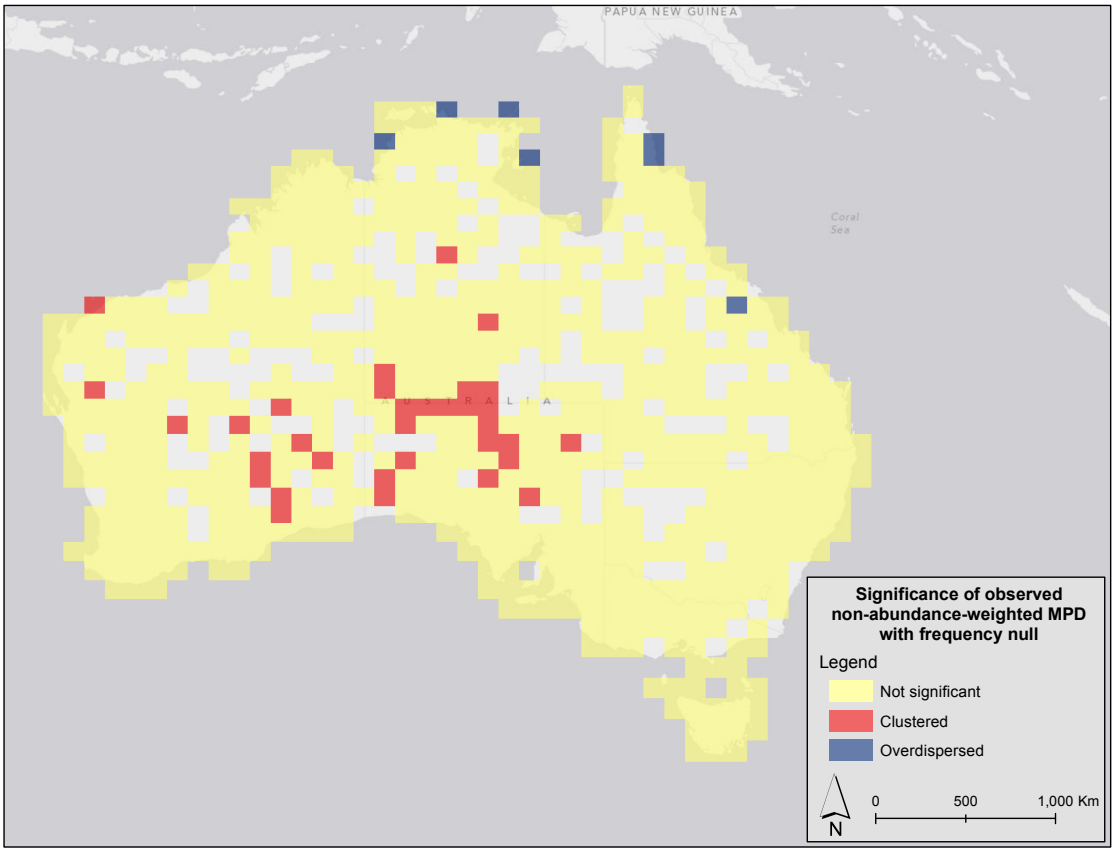

Figure S5.3. Interspecific abundance-weighted mean pairwise phylogenetic distance (MPD) mapped across Australia. Grid cells represent 100 × 100 km local assemblages, and are color-coded from red (more clustered) to blue (more even). When abundance-weighted, co-occurring species are more closely related in the interior and west of the continent, while assemblages along the north and northeast are composed of less closely related species. Figure S5.4 shows which of these grid cells deviate beyond null expectations.

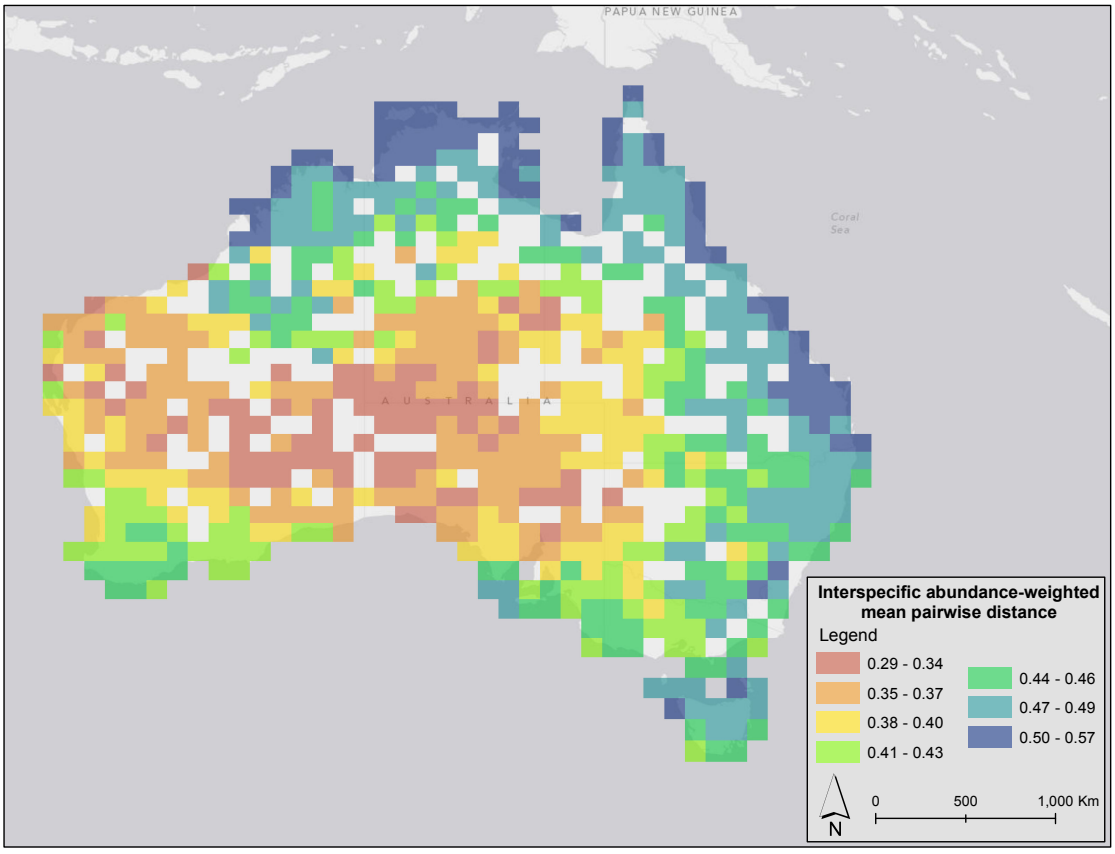

Figure S5.4. Significance, according to a richness null, of observed interspecific abundance-weighted MPD mapped across Australia. Yellow grid cells did not deviate beyond expectations of either a richness or a frequency null. Red grid cells were significantly clustered, and no sites were overdispersed. The three sites also considered clustered according to a frequency null were all located in the southern interior of the continent.

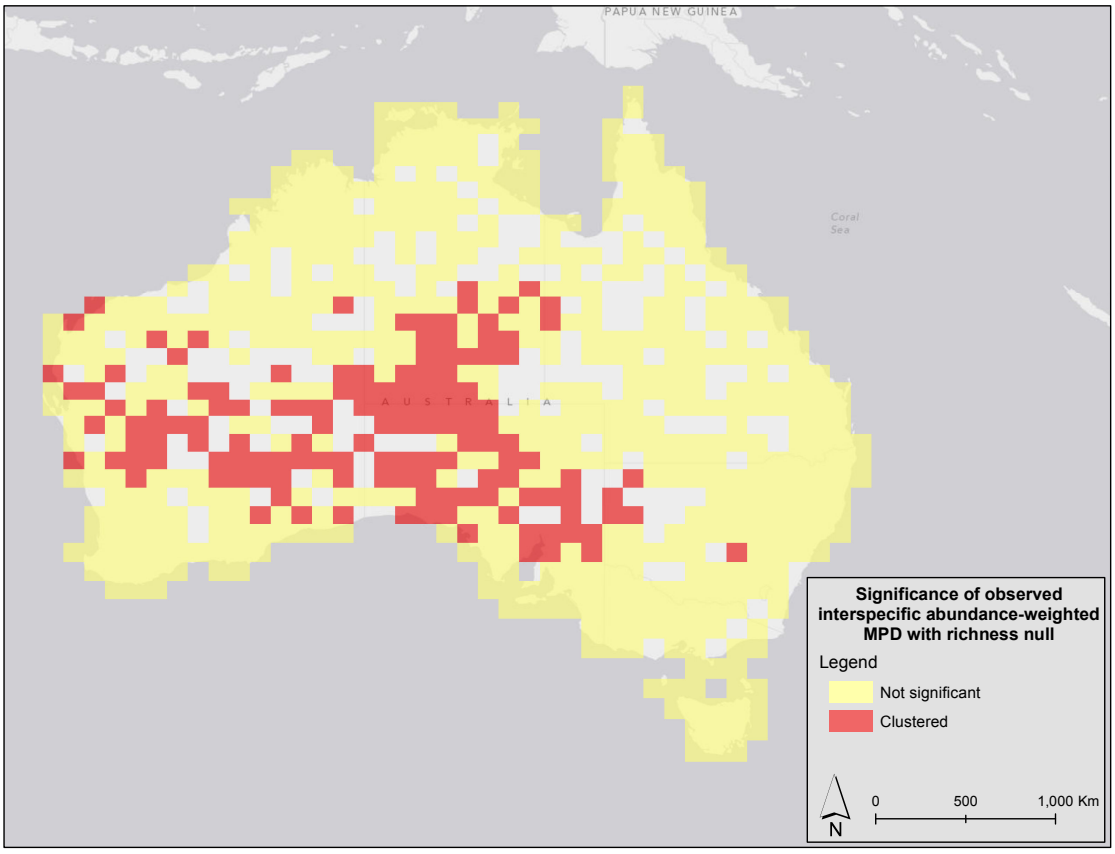

Figure S6. Percent of available climate space occupied by species as a function of their mean climate niches. This is calculated as the number of grid cells actually occupied divided by the total number of grid cells available within the range of climate space bounded by the 5 and 95% quantiles of a species' distribution in climate space. **(A)** The percent occupied of available precipitation space as a function of species' mean annual precipitation (MAP) niche ($r^2 = 0.18$, $P = 0.0001$, $n = 75$). The outlying point in the top right corner of this and panel C refers to *Lichenostomus hindwoodi*, a species represented by a single grid cell in the analysis. Because of this, its climate "range" is restricted to those cells with climates exactly matching the cell it occurs in. Like figure 4 in the main text, the three species in the bottom left of this and panel C are *Ashbyia lovensis*, *Manorina melanotis*, and *Conopophila whitei*. The first two are habitat specialists with restricted ranges, while the third occurs widely throughout inland Australia but is rarely observed. **(B)** Percent occupied of available precipitation space as a function of species' mean annual temperature (MAT) niche ($r^2 = 0.044$, $P = 0.07$, $n = 75$). **(C)** Percent occupied of available temperature space as a function of species' MAP niche ($r^2 = 0.258$, $P < 0.0001$, $n = 75$). **(D)** Percent occupied of available temperature space as a function of species' MAT niche ($r^2 = 0.056$, $P = 0.041$, $n = 75$).

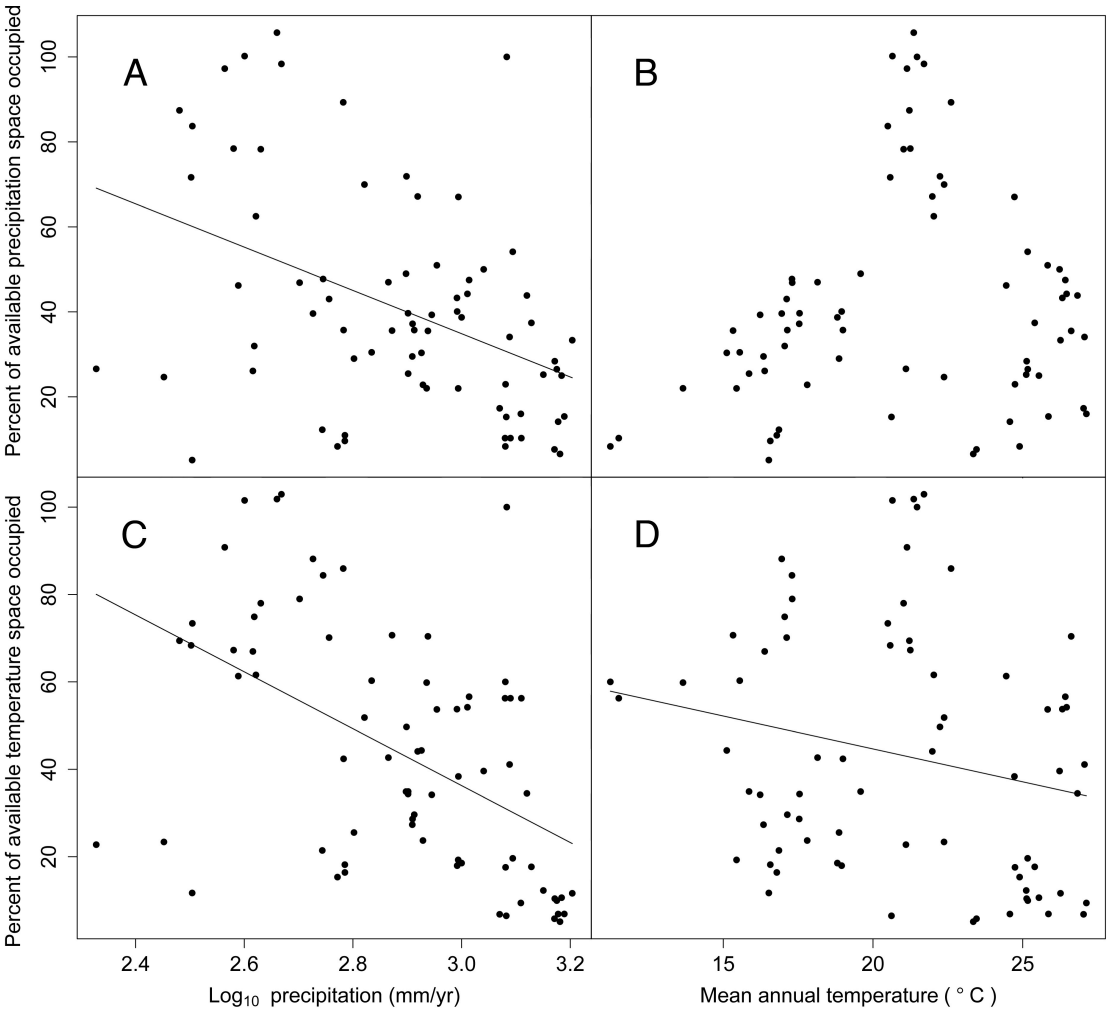
A
B
C
D
Percent of available precipitation space occupied
Percent of available temperature space occupied
20
40
60
80
100
2.4
2.6
2.8
3.0
3.2
15
20
25
Log10 precipitation (mm/yr)
Mean annual temperature (° C)

Figure S7. Meliphagidae evolution through climate space, and detail of Epthianurinae divergence. **(A)** Extant taxa are plotted as red points, positioned according to their current climate niche. These are connected by the underlying phylogeny, with internal nodes placed with respect to their inferred ancestral states (REML method). Colors in this panel represent the distance of the node from the root (i.e. color is approximately proportional to time in this panel). Gray points show the modern range of Australian climate. The four species in the top left corner are endemic to Tasmania. **(B)** Precipitation midpoint of each vector as a function of its angle through climate space. Like Figure 1, color in this panel represents precipitation, and the axis is inverted, such that lineages that evolved through wet climate space are plotted closest to the origin. There is a tendency for lineages already in dry areas (outer ring of polar graph) not to evolve towards wetter climates (i.e. ± towards 0°). The outlier vector in this respect (indicated with a small arrow) relates to an inferred divergence of small magnitude (13 mm/yr difference) between the ancestral Epthianurinae (*Ashbyia lovensis* + *Epthianura* spp.) and the four extant *Epthianura* spp., which suggests that *Epthianura*, an arid-adapted lineage, evolved a short distance back towards higher precipitation. Ancestral state reconstructions are subject to many limitations, but it is worth noting this result is probably driven by the extremely dry habitats preferred by *Ashbyia lovensis*, the sister to *Epthianura*; the reconstruction places the ancestral Epthianurinae in a drier habitat than three of the four *Epthianura* spp. **(C)** Detail of the Epthianurinae divergence, illustrating its small magnitude. Because the short branch leading to the ancestral *Epthianura* overlies the branch leading to the ancestral Epthianurinae, the internal node is difficult to discern. The bent arrow is a stylized representation of the direction of the evolutionary vector leading to *Epthianura*; the

internal node in question is immediately to the lower left of the bend in the arrow (between blue and cyan).

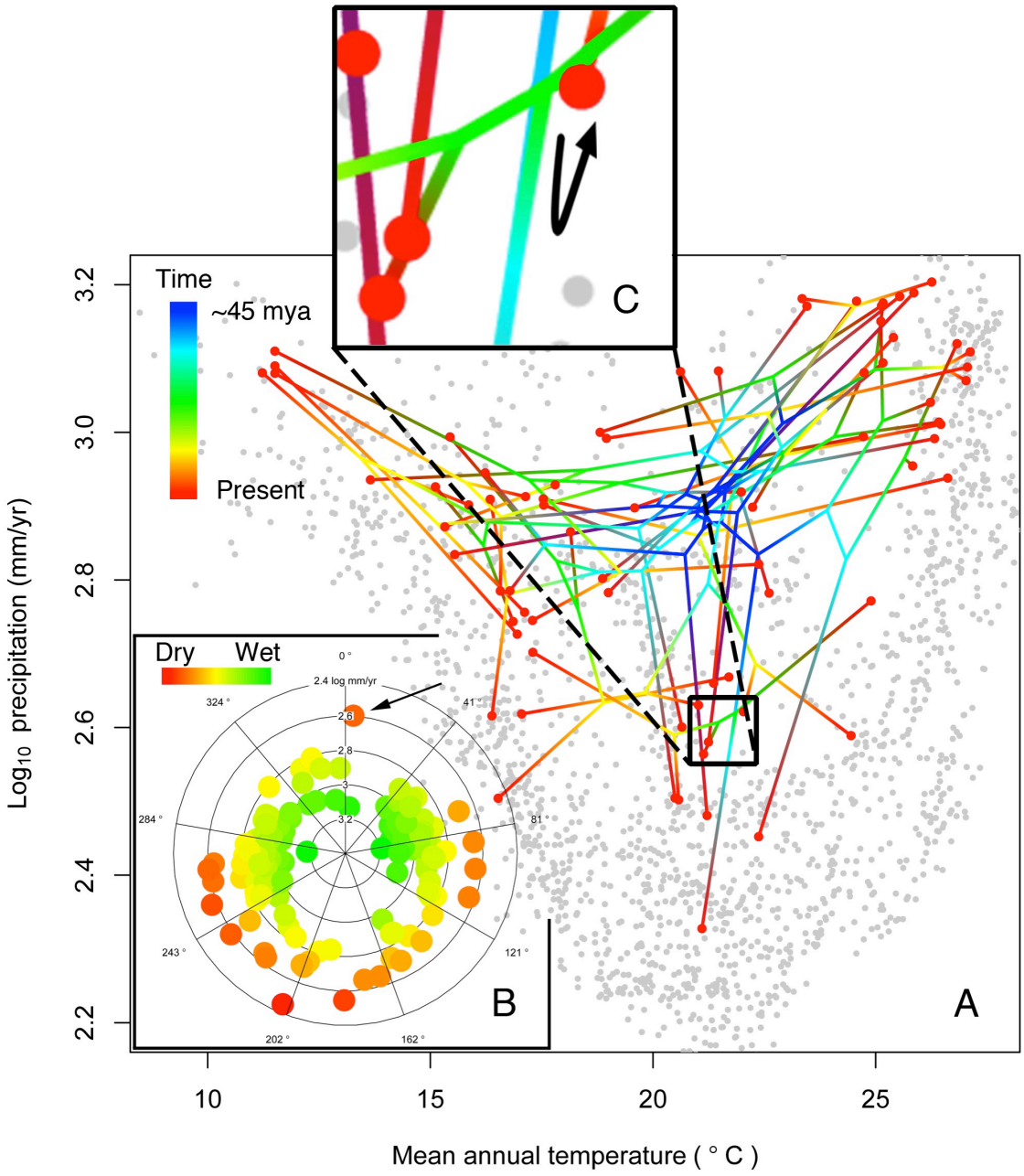

Title: Phylogenetic community structure metrics and null models: a review with new methods and software

Running title: Phylogenetic community structure methods

Word count: 8699 (including references, tables, figure legends and a text box)

Authors: Eliot T. Miller[1,2,*], Damien R. Farine[3,4,5], Christopher H. Trisos[3,6]

[1]Department of Biology, University of Missouri, St. Louis, MO 63121, USA; [2]Department of Biological Sciences, Macquarie University, NSW 2109, Australia; [3]Edward Grey Institute of Field Ornithology, Department of Zoology, University of Oxford, South Parks Road, Oxford OX1 3PS; [4]Smithsonian Tropical Research Institute, Ancon, Panama; [5]Department of Anthropology (Evolution Wing), University of California, Davis, CA 95616, USA; [6]South African Environmental Observation Network, SANBI, Cape Town, 7001, South Africa

* Correspondence author. Email: eliotmiller@umsl.edu; Phone: (314) 516-6200; Fax: (314) 516-6233; Address: R223, Research Bldg, 1 University Blvd., University of Missouri, St. Louis, St. Louis, MO, 63121

Summary

1. Competitive exclusion and habitat filtering are believed to have an important influence on the assembly of ecological communities, but ecologists and evolutionary biologists have not reached a consensus on how to quantify patterns that would reveal the action of these processes. No fewer than 22 phylogenetic community structure metrics and nine null models can be combined, providing 198 approaches to test for such patterns. Choosing statistically appropriate approaches is currently a daunting task.

2. First, we explored the statistical behavior of these metrics and null models, given random community assembly. This provides a baseline against which empirical results can be compared. Second, we developed spatially explicit, agent-based simulations where communities were created according to random, competitive exclusion or habitat filtering assembly rules, and then sampled from these communities to create realistic community data matrices. We quantified the performance of all 198 approaches against each of the three assembly processes.

3. Our first approach reduced to ca. 60 the number of truly unique approaches. Moreover, the second component of the analysis, our assessment of type I and II error rates, suggests that only 30 of these approaches are suitable for testing community assembly patterns.

4. While many reviewed methods performed poorly, we are able to recommend best practices for detection of significant phylogenetic community structure. We also introduce a new R package, *metricTester*, to facilitate robust analyses of method performance.

Key-words: Phylogenetic community structure, review, phylogenetic metric, null model, habitat filtering, competitive exclusion, phylogenetic clustering, phylogenetic overdispersion, community assembly, metricTester

Introduction

The idea that competition among species increases with relatedness goes back at least to Darwin (1859), who noted that more closely related species tend to be more ecologically similar and should therefore compete more intensely (reviewed in Cavender-Bares *et al.* 2009). Referred to as the competition-relatedness hypothesis (Cahill *et al.* 2008), this competitive exclusion is predicted to result in communities composed of less closely related species (phylogenetic overdispersion) than would be expected if communities were assembled entirely via stochastic processes (Elton 1946; Webb *et al.* 2002; but see Mayfield & Levine 2010), such as speciation and dispersal. In contrast to competitive exclusion, which limits similarity of co-occurring species, habitat filtering is the process whereby only those species possessing similar traits (i.e. those within a specific subset of trait space) are able to survive and reproduce within a given abiotic environment (Harper 1977; Keddy 1992). Thus, to the extent that such traits are evolutionarily conservative, habitat filtering results in local assemblages of species more closely related than expected by chance (phylogenetic clustering; Webb 2000; Cavender-Bares *et al.* 2009). Habitat filtering operates largely independently of individual interactions. In contrast, competitive exclusion occurs via either direct or indirect antagonistic interactions among individuals of different species. Thus, while the patterns thought to be indicative of habitat filtering and competitive exclusion represent opposite ends of a gradient, and the

two processes are often studied in concert, they are in fact rather dissimilar. Regardless, until recently, few methods existed to test for patterns of relatedness within communities, and those available took a taxonomic rather than a phylogenetic approach (Elton 1946; Vane-Wright *et al.* 1991).

Beginning in the early 1990s, a number of methods were developed to quantify phylogenetic patterns in community structure, by which one might infer the action of community assembly processes. However, misconceptions about the relationships of these metrics to each other and to species richness (reviewed in Box 1) have reduced their impact on our understanding of community assembly. Furthermore, while the metrics introduced by Webb and others (Webb 2000; Webb *et al.* 2002) have been most influential in community ecology, other metrics have also received widespread use, and their performance across different assembly processes has not been comprehensively assessed. Recent reviews (Kraft *et al.* 2007; Kembel 2009; Vamosi *et al.* 2009; Vellend *et al.* 2011) have addressed the performance of some of these metrics, but have evaluated only partially overlapping assortments of metrics, often using different methods. Consequently, results cannot be compared among studies, making the selection of appropriate metrics for empirical research difficult.

Assessing the significance of an observed phylogenetic community structure metric requires an expectation, generally produced by a null model. Since their introduction, these metrics have been linked to null models (Webb 2000), when, in fact, they are independent concepts. A null model requires a reference pool (e.g., a regional species pool, perhaps with abundance or frequency information), which is randomized with certain constraints, the details of which are defined by the null model used. These

randomized values are generally used to standardize observed metrics. Thus, the metric for a particular community and phylogeny is fixed, but the significance of that metric varies according to which null model is used (Connor & Simberloff 1979; Diamond & Gilpin 1982; Gotelli 2000). A good null model randomizes those structures in the observed data (e.g., individual co-occurrence patterns) relevant to the null hypothesis, and maintains structures in the dataset unrelated to the null hypothesis (e.g., species' abundance distributions) (Gotelli & Graves 1996). In practice, null model performance, specifically type I (false positive) and II (false negative) error rates, and redundancy among null models is rarely tested (but see Gotelli 2000).

Here, we compare the performance of 22 phylogenetic community structure metrics (Table 1) and 9 null models (Table 2). We develop spatially explicit, agent-based simulations of community assembly based on habitat filtering, competitive exclusion or the random placement of individuals, and then compare the ability (type I and II error rates) of each metric + null model combination to identify the correct assembly process. We quantify inter-correlations and document cases of equivalency among metrics. We also assess the response of both the metrics and the null models to variation in species richness. We conclude by discussing the implications of our findings for future tests of community assembly processes.

Methods

Null model background

We adopt the following terminology. The community is the spatial extent (i.e. study area) of interest. A research question pertinent at this scale might be, "what assembly

processes govern species composition in a rainforest community?" The quadrat is the sampling unit. For instance, 15, 1-ha forest plots in the Ecuadorian Amazon would be considered 15 quadrats of this rainforest community. We refer to the quadrat by species data matrix as the community data matrix (CDM).

We test the performance of nine null models (Table 2) designed to randomize patterns in species co-occurrence data. Perhaps the simplest of these is the richness null model, which randomizes species occurrences (or abundances) within quadrats, thereby maintaining species richness (and for abundance data: total abundance and the rank-abundance curve) of each quadrat. In contrast, a frequency null model randomizes occurrences within species in the CDM, which maintains species' occurrence frequencies (or abundances) but not quadrat species richness. For clarity, we refer to this null as the "frequency by quadrat" null, because in our implementation of it, metric values from randomized quadrat assemblages are grouped by the quadrat they are associated with, and then confidence intervals on metric values are calculated for each observed quadrat in the CDM. The species richness of the randomized assemblages resulting from the frequency by quadrat null approximates a normal distribution around the mean species richness in the observed CDM. Thus, this null model may exhibit high type I error rates, particularly at low species richness, as the large variance anticipated of repeated small samples from a larger pool (Efron 1979) is not incorporated in the expectation, and observed low species richness quadrats tend to be compared to randomized quadrats of the mean species richness. To account for this, Miller *et al.* (2013, Appendix 3 of that paper) developed the "frequency by richness" null model, wherein randomized quadrats are grouped by their species richness values. Confidence intervals on observed metric values are then derived

for each species richness value, thereby maintaining both species richness and species' occurrence frequency data structures in the null model. The "independent swap" null model also maintains these same two data structures (Gotelli 2000; Gotelli & Entsminger 2001), but we directly test that null here to confirm that it and the "frequency concatenated by richness" model perform similarly. We also examine the "trial swap" (Miklós & Podani 2004) and 1s (Hardy 2008) null models, which are functionally equivalent to the independent swap and richness null models, respectively (see Appendix S3 in Supporting Information), and are therefore excluded from analyses of statistical performance.

Prior to the development of abundance-weighted metrics, few null models intentionally maintained aspects of abundance distributions. For instance, a species might occur infrequently, but have high abundance when it is present. Hardy (2008) introduced the "2x" and "3x" null models to maintain both species richness and occurrence frequency, as well as either the species or quadrat-level structure of abundance data. The 2x maintains the total abundance and rank-abundance curve of each quadrat, but neither species' abundances nor the set of species-specific abundance distributions. In contrast, the 3x maintains species' abundances and the set of species-specific abundance distributions, but not the abundance distributions of each quadrat. No null model that we know of maintains species richness, species occurrence frequency, species-specific and quadrat-specific abundance distributions. We developed (Appendix S3) and tested a model that approximates this behavior, which we call the "regional null". It is meant to simulate a fixed propagule pressure on a local community, where local dynamics have no influence on the regional pool. Instead of using observed species abundance and

occurrence frequencies from the community (i.e. study area) of interest, information from a larger, regional pool is used to generate a null expectation; species' colonization probabilities are proportional to regional abundances.

metricTester

We wrote an R software package to run our analyses. This package is available from Github, along with associated documentation, and can be directly installed using the *devtools* package (*metricTester*, user name "eliotmiller"). *metricTester* interfaces with functions from the R packages *picante* (Kembel *et al.* 2010), *ape* (Paradis *et al.* 2004), *vegan* (Oksanen *et al.* 2013), *geiger* (Harmon *et al.* 2008), and *spacodiR* (Eastman *et al.* 2011), among others. It also interfaces with *ecoPD* (Cadotte *et al.* 2010). To simplify conflicts with *picante* we renamed some of the functions in *ecoPD* and rebuilt the package, hosted under the name *ecoPDcorr* in the same Github account.

General behavior of the metrics

To understand the behavior of the 19 focal metrics (Table 1) across variation in species richness we generated a phylogenetic tree that terminated at 50 species using a pure-birth model (birth=0.1), then assembled a CDM that included one "quadrat" at every species richness value between 10 and 40 species. We use the term quadrat loosely here, but in keeping with terminology throughout the paper (see *Null model background*). Specifically, we refer to a CDM row with no spatial association. These quadrats were created by randomly sampling from the tips of the phylogeny, and assigning selected

species abundances from a log-normal distribution (mean = 3, SD = 1). For each simulated CDM, we calculated the focal metrics for each quadrat, and retained those values. Using the same tree, we repeated this process 50,000 times, retaining the results from each. We then calculated the mean and 95% confidence intervals at every sampled species richness value, and plotted these across their respective species richness values.

We performed a Pearson correlation on the retained results to examine intercorrelations among metrics. Because of the large number of simulations, some metrics that appear exactly correlated do in fact differ subtly (Appendix S2). We used these correlations to generate a dendrogram and better visualize relationships among metrics.

General behavior of the null models

We explored the behavior of 9 null models (Table 2) across variation in species richness. We used MPD for this, since null model expectations (confidence intervals) of phylogenetic structure converged relatively quickly (exhibited less stochasticity) for this metric, and MPD is not inherently correlated with species richness (Fig. 1A). Using an abundance-weighted metric did not affect results (not shown). We also explored how expectations changed with increasing numbers of randomizations (Appendix S3). We did this by plotting the expected confidence intervals across the corresponding species richness while increasing the randomization of a given, initial CDM and phylogeny. In sum, this set of analyses identified null models that do or do not converge efficiently on a stable range of expected metric values, and identified functional equivalence among the null models. The trial swap and 1s null models were found to be functionally equivalent

to other null models (Appendix S3), and we therefore did not directly test their performance. This left seven focal models (Table 2).

Agent-based spatial simulations of community assembly to assess the performance of metric + null combinations

The first two sets of analyses illustrated the underlying behavior of each of the focal metrics and null models. In this third analysis, we assessed the ability of each metric + null model combination to detect a given assembly process. To generate test cases against which to assess each approach, we created CDMs with three types of spatially explicit community assembly simulations, intended to model the extremes of habitat filtering, competitive exclusion and random assembly. Because of the computing time required to run these tests (>>10,000 hr), we did not systematically examine sensitivity of results to simulation parameters, but results remained qualitatively the same after preliminary exploration of variation in parameters (Appendix S4), and *metricTester* is programmed in a manner to facilitate future study.

All spatial simulations produced 300 x 300 m communities according to one of three assembly rules: random assembly, habitat filtering, or competitive exclusion. We began by generating a phylogeny of 100 species using a pure-birth model (birth = 0.1) and log-normal rank abundance curve, and randomly assigned species abundances from this distribution. We expanded assigned abundances to create a vector of individuals with species identities. In the random assembly spatial simulation, these individuals were then randomly placed within the community.

In habitat filtering simulations, we independently evolved two traits according to a Brownian motion evolutionary process (sigma = 0.1). These traits are meant to mimic two independently evolving environmental preferences, e.g., soil moisture and pH. In our case, we treated these as spatial preferences (i.e. x and y-axis preferences), and scaled the simulated traits to match community bounds. We then placed individuals near their spatial preference, with a controllable degree of variation (exact parameters in Appendix S4). This simulation has the effect of placing related individuals near each other in space. We selected parameters that compromised between producing realistic-looking communities, and producing strong, readily detectable phylogenetic patterns. A consequence of this was that individuals were clumped near their preferred locations, which infrequently resulted in quadrats with < 2 species (example community in Appendix S4).

In competitive exclusion simulations, we first placed individuals using the random assembly process. Following this, each generation, we calculated the mean relatedness of every individual in the simulation to all individuals within 15 m, which we term the "interaction distance". We then identified the 20% of individuals with the highest mean relatedness. For each of these individuals, we identified the individual within their interaction distance to which they were most closely related. We randomly selected one of the two individuals to remove from the community. At the end of each generation, the same number of individuals as was removed was drawn from the original vector of individuals, and situated randomly in the community. This was repeated for 100 generations each competitive exclusion simulation. Preliminary analyses indicated that results were similar across different interaction distances and percentages of individuals

considered (Appendix S4). These simulations produced realistic-looking communities, with evenly spaced individuals, approximately the same number of individuals as would occur in a tropical rain forest of similar size (800 stems/ha, Murphy *et al.* 2013), and communities with phylogenetically overdispersed geographic neighborhoods (Appendix S4). The rank abundance curve of the final community was notably different than that of the initial community (Appendix S4).

In all spatial simulations, after a given community was assembled, we randomly placed 15, non-overlapping quadrats of 30 x 30 m within its confines. We recorded the individuals in each quadrat to create a CDM, and calculated observed metrics. To assess significance of these observed metrics, each CDM was randomized 1,000 times according to the null model being tested. We chose this number due to multiplicative increases in computing time required by additional randomizations. Results were qualitatively similar with additional randomizations (Appendix S4). For reasons explained below, rather than using these values to calculate standardized metric scores, as is often done (e.g., standardized MPD equals NRI, Box 1), we retained all randomized values and used these to construct 95% confidence intervals at each observed species richness (or for a given quadrat for the frequency by quadrat null). A quadrat was recorded as having significant phylogenetic structure if it was either above (overdispersed) or below (clustered) these confidence intervals.

Thus, for each of the 7 focal null models, 100 communities were assembled for competitive exclusion and another 100 for habitat filtering (1400 communities in total). A new phylogeny and log-normal rank abundance curve was used for generating each community. All 19 metrics were calculated and retained for each community after each of

1,000 randomizations of the initial CDM. Due to poor performance and the functional equivalence of some null models in the habitat filtering and competitive exclusion simulations, we only tested the results of the random assembly spatial simulations against the richness, independent swap, and regional null models (300 communities total). Some habitat filtering simulations resulted in < 2 species being sampled in a given quadrat, and such runs were discarded.

Type I and II error rates were assessed for each metric + null model approach as the proportion of the 100 communities for a given assembly process and null model for which these errors were recorded. For the habitat filtering and competitive exclusion simulations, we defined a type I error for a given community as occurring when at least one quadrat deviated beyond the 95% confidence interval in the opposite direction from that expected given the simulated assembly process. A type II error occurred when less than half of the quadrats deviated beyond confidence intervals in the expected direction. A successful run was when at least half of the quadrats deviated beyond the confidence intervals in the direction expected given the simulated assembly process. Thus, for each community, for a given metric + null test either a success or a type II error was recorded. In addition, a type I error could also be recorded for each community. For the random assembly spatial simulation only type I error rates were recorded. Here, a type I error was defined as at least one quadrat deviating beyond either of the 95% confidence intervals.

We have two reasons for tallying error rates like this. First, if 14 of 15 quadrats are within null model expectations but, for instance, one falls below the 95% confidence intervals, then a researcher might conclude a community showed evidence of habitat filtering, since >5% of plots showed that signal. Second, we believe it is not well

appreciated that null model expectations vary in metric-specific manners across species richness, and presenting results in this way emphasizes this point.

Results

General behavior of the metrics

We directly evaluated behavior of 19 focal community phylogenetic metrics (Table 1) across variation in community species richness. MPD, interspecific AW MPD, PSV and PAE were not correlated with species richness (Fig. 1A). Intraspecific AW MPD, complete AW MPD, PSE, IAC, H_{AED}, H_{ED}, SimpsonsPhy, PD, PD_c, and QE were positively correlated with species richness. MNTD, AW MNTD, PSC, and E_{ED} were negatively correlated with species richness. The intercorrelations (Fig. 1B, Appendix S5) among metrics and post-hoc plotting of absolute metric values against each other revealed that: (1) MPD is equivalent to PSV; (2) complete AW MPD is equivalent to SimpsonsPhy and QE, and approximately equal to intraspecific AW MPD (Appendix S2) and to PSE; and (3) PSC is equivalent to MNTD. Moreover, MPD, interspecific AW MPD, and intraspecific AW MPD are equivalent to $\Delta+$, Δ^*, and Δ, respectively, of Clarke & Warwick (1998) (Box 1, Appendix S2). Based on these intercorrelations (Fig. 1B), we classify the metrics into the following groups: Clade 1 are "total community relatedness" metrics; Clade 2 metrics focus on the relationship between "evolutionary distinctiveness and abundance" (Cadotte *et al.* 2010); Clade 3 are "nearest-relative" metrics; and Clade 4 metrics are closely correlated with species richness, and increase both with the addition of new species, and phylogenetically unique species.

General behavior of the null models

The confidence intervals from the richness null model matched statistical expectations (Fig. 2), with more variance observed at smaller subsamples of the regional species pool (i.e. a confidence funnel; Clarke & Warwick 1998). The 1s and richness null models were equivalent (Fig. S3.1). We found (Fig. S3.4) that the frequency by richness null was equivalent to the independent swap null. Moreover, the trial swap null seemed to converge slowly (i.e. after $>10^6$ randomizations) on the same expectations as these two nulls (Fig. S3.2). Because of this inefficiency, we did not assess the performance of the trial swap null model further. The confidence intervals of the frequency by quadrat null model did not form a confidence funnel. Instead, the value beyond which an observed metric needed to deviate to be considered significant was approximately the same for all quadrats, irrespective of underlying species richness of the quadrat (Fig. 2). We also found that the expectations from the 2x and 3x null models were equivalent, but varied inconsistently across species richness, and did not form a confidence funnel (Fig. 2, Fig. S3.5). Finally, expectations for the independent swap varied depending upon relationships between occurrence frequency and phylogenetic uniqueness. For instance, if phylogenetically unique species occurred more frequently in the input CDM, then confidence intervals were shifted upwards from those obtained without incorporating occurrence frequency (Fig. S3.6).

Performance of metric + null approaches

There was a great deal of variation in performance of different approaches. Across all metrics for both competitive exclusion and habitat filtering assembly simulations, the

frequency by quadrat null showed high rates of type I error, particularly for metrics that were correlated with species richness. The 2x and 3x nulls showed low type I error rates, but also a complete lack of power for all assessed metrics. The independent swap and frequency by richness null models performed reasonably well in habitat filtering simulations when used with some metrics (e.g., PD and MPD, Fig. 3), but poorly in competitive exclusion simulations with all metrics (Fig. 4). Finally, the richness and regional nulls performed well with most metrics in both the habitat filtering and competitive exclusion simulations.

These results suggested that additional exploration of the 2x, 3x and frequency by quadrat nulls was not worthwhile, and that these should not be considered accurate gauges of metric performance. Furthermore, because of the equivalence of the independent swap and frequency by richness nulls (Appendix S3), we only tested the performance of the metrics, given random community assembly, with the richness, independent swap, and regional null models (collectively, the "reasonable" models). Here, all metrics showed overall random phylogenetic community structure, but all also had type I error rates of 20-39% (Fig. S1.1).

Given a community assembled according to habitat filtering, PD and PD_c outperformed other metrics when using reasonable models as gauges of performance (Fig. 3). For Clade 1 metrics (Fig. 1B) with habitat filtering, the non-abundance-weighted metrics (PSV, MPD) showed higher type I error rates than other metrics from this clade. Given a community assembled according to competitive exclusion, PD and PD_c also performed well at detecting overdispersion (Fig. 4), though here they were outperformed by all Clade 1 metrics. If we take overall metric performance as the difference between

the sum of successful runs and the sum of type I errors across the reasonable models across both habitat filtering and competitive exclusion simulations, then PD and PD_c performed best overall, followed closely by the Clade 1 methods (Fig. 5). Clade 3 metrics never performed as well as Clade 1 metrics. Some metrics (PAE, H_{AED}) failed more often than they succeeded.

Discussion

The unification of phylogenetic community structure methods with age-old questions of community assembly has revolutionized the fields of ecology and evolution. Since Webb's seminal papers (Webb 2000; Webb *et al.* 2002), there has been an explosion of interest in these matters, including a wide variety of "improvements" upon existing measures (Box 1). Many of these, however, have never been adequately tested, and others are equivalent, as we show here (Fig. 1B). Our objective was to assess a wide range of available methods in order to identify those with demonstrable utility, and to identify those that measure unique aspects of phylogenetic community structure.

Which metrics are best? The results of our study suggest that the answer depends in part on which community assembly process are of interest, and which null models are used. However, some clear and general answers did emerge. Across all reasonable null models (richness, independent swap and regional) and community assembly simulations, PD (Faith 1992) consistently performed well (Fig. 5), showing low type I error rates and more power than most other metrics; it was particularly good at detecting the effects of habitat filtering (Fig. 3). Clade 1 ("total relatedness") metrics (Fig. 1) also performed well, particularly at detecting effects of competitive exclusion (Fig. 4). Like Kembel

(2009), and unlike Kraft *et al.* (2007), we found that Clade 3 ("nearest-relative") metrics were never as powerful as Clade 1 metrics. Abundance-weighted forms of Clade 1 metrics showed both lower type I error and less power than non-abundance-weighted forms, presumably because the latter can be strongly influenced by the presence or absence of a single individual. Finally, the metrics introduced by Cadotte *et al.* (2010) generally showed poor performance, particularly PAE and H_{AED} (PD_c is an exception, but see Box 1). As suggested by Cadotte *et al.* (2010), the metrics do indeed measure unique aspects of phylogenetic community structure (Fig. 1B). These aspects, however, do not seem to be related to traditionally recognized community assembly processes. Of the Cadotte metrics, IAC showed the greatest power to detect both non-random patterns, particularly when used with the regional null; this node-based metric does not incorporate branch length information. H_{ED} was closely correlated with PD (r = 0.94), but did not perform well.

Which null models are best? Again, our results suggest that the answer depends in part on the choice of metric and the community assembly process of interest. In general, we strongly recommend against the use of a frequency by quadrat null. The confidence intervals for this null model account for neither the increased variance in expectations at smaller subsamples of the regional species pool (Clarke & Warwick 1998), nor the correlation of many metrics with species richness (Fig. 1). This results in extremely high rates of type I error across all metrics, particularly those that are correlated with species richness (Fig. 3, 4). The 2x and 3x null models performed poorly. While they exhibited low type I error rates (Hardy 2008), they also never detected the expected phylogenetic signal in any of our simulations. We suspect that the extreme constraints imposed on the

matrix randomizations by these nulls resulted in a biased and inefficient exploration of reasonable phylogenetic space. Regardless of the reason, the instability across species richness shown by the confidence intervals for the 2x and 3x null models (Fig. 2) leads to the logically unappealing conclusion that the expectations for a given metric can change dramatically based on whether N or N+1 species are present in an observed community.

The regional null (Appendix S3) was designed to simulate propagule pressure/dispersal probability on a local community (study area) of interest, such that deviations from these dispersal pressures (e.g., the product of environmental filters) can be readily detected, and local community dynamics (e.g., competition) do not obfuscate expectations. For instance, given strong competitive exclusion, local communities may show widespread phylogenetic overdispersion, where certain species are generally excluded. When these observed occurrence frequencies are taken as regional occurrence frequencies and randomized accordingly (as in the independent swap), it becomes difficult to detect phylogenetic overdispersion, since the randomized CDMs will tend to contain distantly related species. The regional null avoids this issue by using expectations from a larger, fixed pool as the standard against which to compare observations from the study area, but it is difficult to quantify dispersal pressure on a community of interest, and this null model may not be practical for many researchers. Future studies should investigate what information might be used to construct these expectations (e.g., range sizes), and whether this null can be of widespread utility.

We emphasize that null model choice cannot be driven entirely by statistical properties. There may be sound biological reasons for why a given null should be employed (Gotelli & Graves 1996), even if its statistical performance is not on par with

others. For example, there could be instances where not every species in the pool could reasonably disperse to every site, and a constrained null model might need to be developed. However, such reasoning should not come at the expense of statistical common sense. For instance, if a phylogenetically unique species occurs only infrequently in observed communities, then a null such as the independent swap that maintains species' occurrence frequencies should be used; failure to do so would result in a loss of power to detect phylogenetic overdispersion. Conversely, if a CDM is not thought to be representative of a regional species pool (e.g., biased sampling across study areas), then the independent swap will only confuse interpretation of results.

What approach do we suggest? The richness null may offer the simplest results to interpret by making the clearest assumptions (any species can occur anywhere); more constrained null models raise questions of sampling artifacts and the efficiency of swap algorithms. We emphasize that little should be made of the deviation of any single community beyond null model expectations; the high type I error rates of most approaches casts doubt on the interpretation of single community tests. When multiple communities are available, these can be arranged along an environmental gradient to test hypotheses. Here, the slope of the overall relationship is of interest, rather than the significance of any given community (Miller *et al.* 2013). Hypothesis testing in this manner minimizes the necessity of a null model and, if the metrics in question are not correlated with species richness (e.g., PSV), also the need to standardize the metrics. Raw metric values, which often have intrinsic meaning, can then be used instead of standardized scores. For instance, the MPD of a community, given a time-calibrated phylogeny, is equal to the mean evolutionary time separating co-occurring taxa. Some

metrics, however, are correlated with species richness, and should be standardized if the researcher is interested in phylogenetic community structure (as opposed to, e.g., phylogenetic diversity itself). In short, researchers need to consider what they are measuring with their metric(s) of choice, whether they need to standardize those metrics, and why or why not they might procure significant results.

By making the assumption that the traits responsible for community assembly covary with phylogeny, this study maintains the sometimes questionable dogma that habitat filtering leads to phylogenetic clustering, and that competitive exclusion leads to phylogenetic overdispersion (Webb *et al.* 2002; Mayfield & Levine 2010). If trait data are available, we encourage researchers who use these methods to fit explicit models of evolution to traits pertinent to the assembly processes in question (Butler & King 2004), and to also investigate patterns of community structure in functional traits. In this study we did not test approaches that account for variation among quadrats in species co-occurrence probabilities (e.g., Cavender-Bares *et al.* 2004; Hardy & Senterre 2007), but *metricTester* could be adapted to investigate these metrics. There is also an expansive assortment of existing (and yet to be created), hypothetically useful null models whose behavior and performance remains to be tested (e.g., Ulrich & Gotelli 2010). Ultimately, advanced approaches (Ives & Helmus 2011) may prove more powerful and gain wider use than current phylogenetic community structure metrics, but the existing arsenal remains well suited to addressing a wide variety of questions.

Acknowledgements

We thank Vincenzo Ellis, Amy Zanne and the Ricklefs lab for input and feedback, and the Oslo Bioportal, the University of Missouri Lewis Cluster, and the Domino Data Lab for providing computing resources.

Data accessibility

metricTester is available from GitHub (https://github.com/eliotmiller/metricTester), and can be directly installed into an active R session using the *devtools* package. It requires the package *ecoPDcorr*, which can also be directly installed with *devtools* (https://github.com/eliotmiller/ecoPDcorr).

References

Allen, B., Kon, M. & Bar-Yam, Y. (2009). A new phylogenetic diversity measure generalizing the Shannon index and its application to phyllostomid bats. *The American Naturalist*, **174**, 236–243. Retrieved December 2, 2013,

Butler, M.A. & King, A.A. (2004). Phylogenetic comparative analysis: a modeling approach for adaptive evolution. *The American Naturalist*, **164**, 683–695.

Cadotte, M.W., Jonathan Davies, T., Regetz, J., Kembel, S.W., Cleland, E. & Oakley, T.H. (2010). Phylogenetic diversity metrics for ecological communities: integrating species richness, abundance and evolutionary history. *Ecology Letters*, **13**, 96–105. Retrieved December 2, 2013,

Cahill, J.F.J., Kembel, S.W., Lamb, E.G. & Keddy, P.A. (2008). Does phylogenetic relatedness influence the strength of competition among vascular plants?

Perspectives in Plant Ecology, Evolution and Systematics, **10**, 41–50. Retrieved May 1, 2014,

Cavender-Bares, J., Ackerly, D.D., Baum, D.A. & Bazzaz, F.A. (2004). Phylogenetic overdispersion in Floridian oak communities. *American Naturalist*, **163**, 823–843. Retrieved February 12, 2010,

Cavender-Bares, J., Kozak, K.H., Fine, P.V.A. & Kembel, S.W. (2009). The merging of community ecology and phylogenetic biology. *Ecology Letters*, **12**, 693–715. Retrieved February 12, 2010,

Clarke, K.R. & Warwick, R.M. (1998). A taxonomic distinctness index and its statistical properties. *Journal of Applied Ecology*, **35**, 523–531.

Clarke, K.R. & Warwick, R.M. (1999). The taxonomic distinctness measure of biodiversity: Weighting of step lengths between hierarchical levels. *Marine Ecology Progress Series*, **184**, 21–29.

Connor, E.F. & Simberloff, D. (1979). The assembly of species communities: chance or competition? *Ecology*, **60**, 1132–1140.

Darwin, C. (1859). *On the origin of species by means of natural selection, or the preservation of favoured races in the struggle for life*. John Murray, London.

Diamond, J.M. & Gilpin, M.E. (1982). Examination of the 'Null' Model of Connor and Simberloff for Species Co-Occurrences on Islands. *Oecologia*, **52**, 64–74.

Eastman, J.M., Paine, C.E.T. & Hardy, O.J. (2011). spacodiR: structuring of phylogenetic diversity in ecological communities. *Bioinformatics*, **27**, 2437–2438. Retrieved November 30, 2012,

Efron, B. (1979). Bootstrap methods: Another look at the jackknife. *The Annals of Statistics*, **7**, 1–26.

Elton, C. (1946). Competition and the structure of ecological communities. *Journal of Animal Ecology*, **15**, 54–68. Retrieved March 13, 2014,

Faith, D.P. (1992). Conservation evaluation and phylogenetic diversity. *Biological Conservation*, **61**, 1–10. Retrieved October 22, 2012,

Faith, D.P. (2007). The role of the phylogenetic diversity measure, PD, in bio-informatics: getting the definition right. *Evolutionary Bioinformatics Online*, **2**, 277–283. Retrieved February 10, 2014,

Giehl, E.L.H. & Jarenkow, J.A. (2012). Niche conservatism and the differences in species richness at the transition of tropical and subtropical climates in South America. *Ecography*, **35**, 933–943. Retrieved December 2, 2013,

Gotelli, N.J. (2000). Null model analysis of species co-occurrence patterns. *Ecology*, **81**, 2606–2621. Retrieved October 23, 2012,

Gotelli, N.J. & Entsminger, G.L. (2001). Swap and fill algorithms in null model analysis: rethinking the knight's tour. *Oecologia*, **129**, 281–291. Retrieved December 2, 2013,

Gotelli, N.J. & Graves, G.R. (1996). *Null models in ecology*. Smithsonian Institution Press, Washington.

Hardy, O.J. (2008). Testing the spatial phylogenetic structure of local communities: statistical performances of different null models and test statistics on a locally neutral community. *Journal of Ecology*, **96**, 914–926. Retrieved October 23, 2012,

Hardy, O.J. & Senterre, B. (2007). Characterizing the phylogenetic structure of communities by an additive partitioning of phylogenetic diversity. *Journal of Ecology*, **95**, 493–506.

Harmon, L.J., Weir, J.T., Brock, C.D., Glor, R.E. & Challenger, W. (2008). GEIGER: investigating evolutionary radiations. *Bioinformatics*, **24**, 129–131. Retrieved May 1, 2013,

Harper, J.L. (1977). *Population biology of plants.* Academic Press, London.

Helmus, M.R., Bland, T.J., Williams, C.K. & Ives, A.R. (2007). Phylogenetic measures of biodiversity. *The American Naturalist*, **169**, E68–E83.

Ives, A.R. & Helmus, M.R. (2011). Generalized linear mixed models for phylogenetic analyses of community structure. *Ecological Monographs*, **81**, 511–525. Retrieved February 2, 2014,

Keddy, P.A. (1992). Assembly and response rules: two goals for predictive community ecology. *Journal of Vegetation Science*, **3**, 157–164.

Kembel, S.W. (2009). Disentangling niche and neutral influences on community assembly: assessing the performance of community phylogenetic structure tests. *Ecology Letters*, **12**, 949–960.

Kembel, S.W., Cowan, P.D., Helmus, M.R., Cornwell, W.K., Morlon, H., Ackerly, D.D., Blomberg, S.P. & Webb, C.O. (2010). Picante: R tools for integrating phylogenies and ecology. *Bioinformatics*, **26**, 1463–1464.

Kraft, N.J.B., Cornwell, W.K., Webb, C.O. & Ackerly, D.D. (2007). Trait evolution, community assembly, and the phylogenetic structure of ecological communities. *The American Naturalist*, **170**, 271–283. Retrieved October 23, 2012,

Mayfield, M.M. & Levine, J.M. (2010). Opposing effects of competitive exclusion on the phylogenetic structure of communities. *Ecology Letters*, **13**, 1085–1093. Retrieved October 23, 2012,

Miklós, I. & Podani, J. (2004). Randomization of presence-absence matrices: comments and new algorithms. *Ecology*, **85**, 86–92. Retrieved December 2, 2013,

Miller, E.T., Zanne, A.E. & Ricklefs, R.E. (2013). Niche conservatism constrains Australian honeyeater assemblages in stressful environments. *Ecology Letters*, **16**, 1186–1194.

Murphy, H.T., Bradford, M.G., Dalongeville, A., Ford, A.J. & Metcalfe, D.J. (2013). No evidence for long-term increases in biomass and stem density in the tropical rain forests of Australia. *Journal of Ecology*, **101**, 1589–1597. Retrieved January 29, 2014,

Nipperess, D.A. & Matsen, F.A. (2013). The mean and variance of phylogenetic diversity under rarefaction. *Methods in Ecology and Evolution*. Retrieved December 2, 2013, from http://onlinelibrary.wiley.com/doi/10.1111/2041-210X.12042/full

Oksanen, J., Blanchet, F.G., Kindt, R., Legendre, P., Minchin, P.R., O'Hara, R.B., Simpson, G.L., Solymos, P., Stevens, M.H.H. & Wagner, H. (2013). *vegan: Community Ecology Package*. Retrieved from http://CRAN.R-project.org/package=vegan

Paradis, E., Claude, J. & Strimmer, K. (2004). APE: analyses of phylogenetics and evolution in R language. *Bioinformatics*, **20**, 289–290.

Rao, C.R. (1982). Diversity and dissimilarity coefficients: a unified approach. *Theoretical Population Biology*, **21**, 24–43. Retrieved December 2, 2013,

Simpson, E.H. (1949). Measurement of diversity. *Nature*, **163**, 688. Retrieved April 1, 2014,

Tsirogiannis, C. & Sandel, B. (2013). Computing the skewness of the phylogenetic mean pairwise distance in linear time. *Algorithms in Bioinformatics*, **8126**, 170–184. Retrieved December 2, 2013,

Ulrich, W. & Fattorini, S. (2013). Longitudinal gradients in the phylogenetic community structure of European Tenebrionidae (Coleoptera) do not coincide with the major routes of postglacial colonization. *Ecography*. Retrieved December 2, 2013, from http://onlinelibrary.wiley.com/doi/10.1111/j.1600-0587.2013.00188.x/full

Ulrich, W. & Gotelli, N.J. (2010). Null model analysis of species associations using abundance data. *Ecology*, **91**, 3384–3397. Retrieved May 1, 2014,

Vamosi, S.M., Heard, S.B., Vamosi, J.C. & Webb, C.O. (2009). Emerging patterns in the comparative analysis of phylogenetic community structure. *Molecular Ecology*, **18**, 572–592.

Vane-Wright, R.I., Humphries, C.J. & Williams, P.H. (1991). What to protect?—Systematics and the agony of choice. *Biological Conservation*, **55**, 235–254. Retrieved October 22, 2012,

Vellend, M., Cornwell, W.K., Magnuson-Ford, K. & Mooers, A.O. (2011). Measuring phylogenetic biodiversity. *Biological diversity: frontiers in measurement and assessment* pp. 193–206. Oxford University Press, Oxford.

Villalobos, F., Rangel, T.F. & Diniz-Filho, J.A.F. (2013). Phylogenetic fields of species: cross-species patterns of phylogenetic structure and geographical coexistence. *Proceedings of the Royal Society B: Biological Sciences*, **280**. Retrieved December 2, 2013, from http://rspb.royalsocietypublishing.org/content/280/1756/20122570.short

Warwick, R.M. & Clarke, K.R. (1995). New "biodiversity' measures reveal a decrease in taxonomic distinctness with increasing stress. *Marine Ecology Progress Series*, **129**, 301–305.

Warwick, R.M. & Clarke, K.R. (1998). Taxonomic distinctness and environmental assessment. *Journal of Applied Ecology*, **35**, 532–543.

Webb, C.O. (2000). Exploring the phylogenetic structure of ecological communities: an example for rain forest trees. *The American Naturalist*, **156**, 145–155.

Webb, C.O., Ackerly, D.D. & Kembel, S.W. (2008). Phylocom: software for the analysis of phylogenetic community structure and trait evolution. *Bioinformatics*, **24**, 2098–2100.

Webb, C.O., Ackerly, D.D., McPeek, M.A. & Donoghue, M.J. (2002). Phylogenies and community ecology. *Annual Review of Ecology and Systematics*, **33**, 475–505. Retrieved June 30, 2010,

Table 1. The 22 phylogenetic community structure metrics reviewed in this paper. We paraphrase (or sometimes directly quote) the original description of the metric. While some metrics we discuss are in fact equivalent, these original descriptions often emphasized their uniqueness. IAC is a node-based metric, and the only reviewed metric that increases in value with an increase in the relatedness of the species in the focal community set.

Metric	Abbreviation	Description	Citation
Quadratic entropy	QE	Within community diversity based on species dissimilarity.	(Rao 1982)
Phylogenetic diversity	PD	Sum of total branch lengths for a set of species, and length to root if set does not span it.	(Faith 1992)
Non-abundance-weighted mean pairwise phylogenetic distance	MPD	Mean of all pairwise branch lengths for a set of species.	(Webb 2000; Webb *et al.* 2002)
Non-abundance-weighted mean nearest taxon distance	MNTD	Mean of the branch lengths separating each species from its closest relative in the set of species.	(Webb 2000; Webb *et al.* 2002)
Taxonomic diversity*	Δ	Average phylogenetic distance between any two individuals from a set.	(Clarke & Warwick 1998)
Taxonomic distinctness*	Δ^*	Average phylogenetic distance between any two heterospecific individuals.	(Clarke & Warwick 1998)
Presence-absence case of taxonomic diversity*	$\Delta+$	Average phylogenetic distance between any two species from a set.	(Clarke & Warwick 1998)
Phylogenetic species variability	PSV	Measures how phylogenetic relatedness decreases the variance of a hypothetical Brownian motion trait shared by all species in the community.	(Helmus *et al.* 2007)

Table 1 *continued*

Metric	Abbreviation	Description	Citation
Phylogenetic species clustering	PSC	Modified form of PSV incorporating maximum off-diagonal element matrix of community phylogenetic correlation structure.	(Helmus *et al.* 2007)
Phylogenetic species evenness	PSE	Modified form of PSV incorporating species abundance.	(Helmus *et al.* 2007)
Phylogenetic form of Simpson's index	SimpsonsPhy	Extension of Simpson diversity index that incorporates phylogenetic information.	(Simpson 1949; Hardy & Senterre 2007)
Abundance-weighted MNTD	AW MNTD	Abundance-weighted form of MNTD.	(Webb *et al.* 2008)
Phylogenetic diversity without regard to a larger regional pool	PD_c	Sum of total branch lengths for a set of species, not including length to root.	(Faith 2007; Cadotte *et al.* 2010)
Phylogenetic abundance evenness	PAE	"Phylogenetic evenness of abundance distribution scaled by branch length."	(Cadotte *et al.* 2010)
Imbalance of abundance	IAC	IAC. "Relative per-node imbalance in individual distribution."	(Cadotte *et al.* 2010)
Community evolutionary distinctiveness	H_{ED}	"Entropic measure of diversity of evolutionary distinctiveness among species."	(Cadotte *et al.* 2010)
Equitability evolutionary distinctiveness	E_{ED}	"Equitability of H_{ED}."	(Cadotte *et al.* 2010)
Community abundance-weighted evolutionary distinctiveness	H_{AED}	"Entropic measure of diversity of evolutionary distinctiveness among individuals."	(Cadotte *et al.* 2010)

Table 1 *continued*

Metric	Abbreviation	Description	Citation
Equitability abundance-weighted evolutionary distinctiveness	E_{AED}	"Equitability of H_{AED}."	(Cadotte *et al.* 2010)
Complete abundance-weighted MPD	complete AW MPD	An abundance-weighted form of MPD. Average phylogenetic distance between two individuals from a set, possibly between the same individual.	(Webb *et al.* 2008, Appendix S2 of this paper)
Intraspecific abundance-weighted MPD	intra AW MPD	An abundance-weighted form of MPD. Average phylogenetic distance between any two individuals from a set.	(Appendix S2 of this paper)
Interspecific abundance-weighted MPD	inter AW MPD	An abundance-weighted form of MPD. Average phylogenetic distance between two heterospecific individuals.	(Miller *et al.* 2013, Appendix S2 of this paper)

* Denotes three metrics not directly assessed here due to equivalency with other metrics (see Appendix S2), leaving 19 focal metrics in this paper.

Table 2. The nine null models reviewed in this paper. A community data matrix (CDM) where quadrats (i.e. sites or samples) are rows and species are columns is used as the input. The citation lists either the simulation name from Gotelli (2000), or gives a more recent citation where necessary.

		Constraints (data features left unchanged after randomization)				
Null model	Description	Quadrat species richness	Quadrat rank-abundance curve (and quadrat total abundance)	Species occurrence frequency	Species-specific abundance distribution (and species total abundance)	Citation
Richness	Randomizes species' occurrences (or abundances) among species, independently within each quadrat.	X	X			SIM3
1s*	Randomizes species' occurrences (or abundances) among the tips of a phylogeny. With respect to the CDM, this shuffles entire columns among species.	X	X		†	Hardy (2008)
Frequency by quadrat	Often simply called a "frequency" null. Shuffles species' occurrences (or abundances) independently within each species.			X	X	SIM2
Frequency by richness	The same randomization as above null, but then groups randomized quadrats by their species richness. Observed values compared only to values from randomized quadrats of corresponding species richness.	X‡		X	X	Miller et al. 2013; Appendix S3
Independent swap	Transposes randomly chosen submatrices of the form (0,1)(1,) or (1,0)(0,1) in the CDM. When CDM contains abundance data, treats non-zero elements as 1.	X		X	§	SIM9

		Constraints (data features left unchanged after randomization)				
Null model	Description	Quadrat species richness	Quadrat rank-abundance curve (and quadrat total abundance)	Species occurrence frequency	Species-specific abundance distribution (and species total abundance)	Citation
Trial swap*	Same as independent swap, but guarantees equidistribution of results (evenly distributed randomized results).	X		X	§	Miklós & Podani (2004)
2x	Modified form of independent swap for abundance data. Transposes randomly chosen submatrices, switching elements of the submatrices within quadrats.	X	X	X		Hardy (2008)
3x	As for 2x, but switches elements within species.	X		X	X	Hardy (2008)
Regional	Described in detail in Appendix S3 of this paper.	X‡	Strictly maintains total abundance, approximately maintains rank-abundance curve	Approx.	Approx.	Appendix S3

* These were not included in tests of metric + null model performance due to equivalency with the richness and independent swap (Appendix S3), leaving seven focal models in this paper.

† Because columns are moved as a unit, each randomized CDM contains the same set of species-specific abundance distributions as the original CDM, though these abundance distributions are disassociated from their original species (i.e. the set of columns is the same, but each column is now associated with a different species).

‡ The randomized matrices do not always contain quadrats with species richness values the same as those of the original CDM, but by concatenating results later by randomized quadrat species richness, observed quadrats are compared to random quadrats of the same species richness.

§ Intended for use with presence/absence data, thus the fact that the *picante* (and *metricTester*) implementations also maintain column sums (and not just the sum of non-zero elements), and therefore also maintain species-specific abundance distributions is an unintentional consequence of the way these null models are coded.

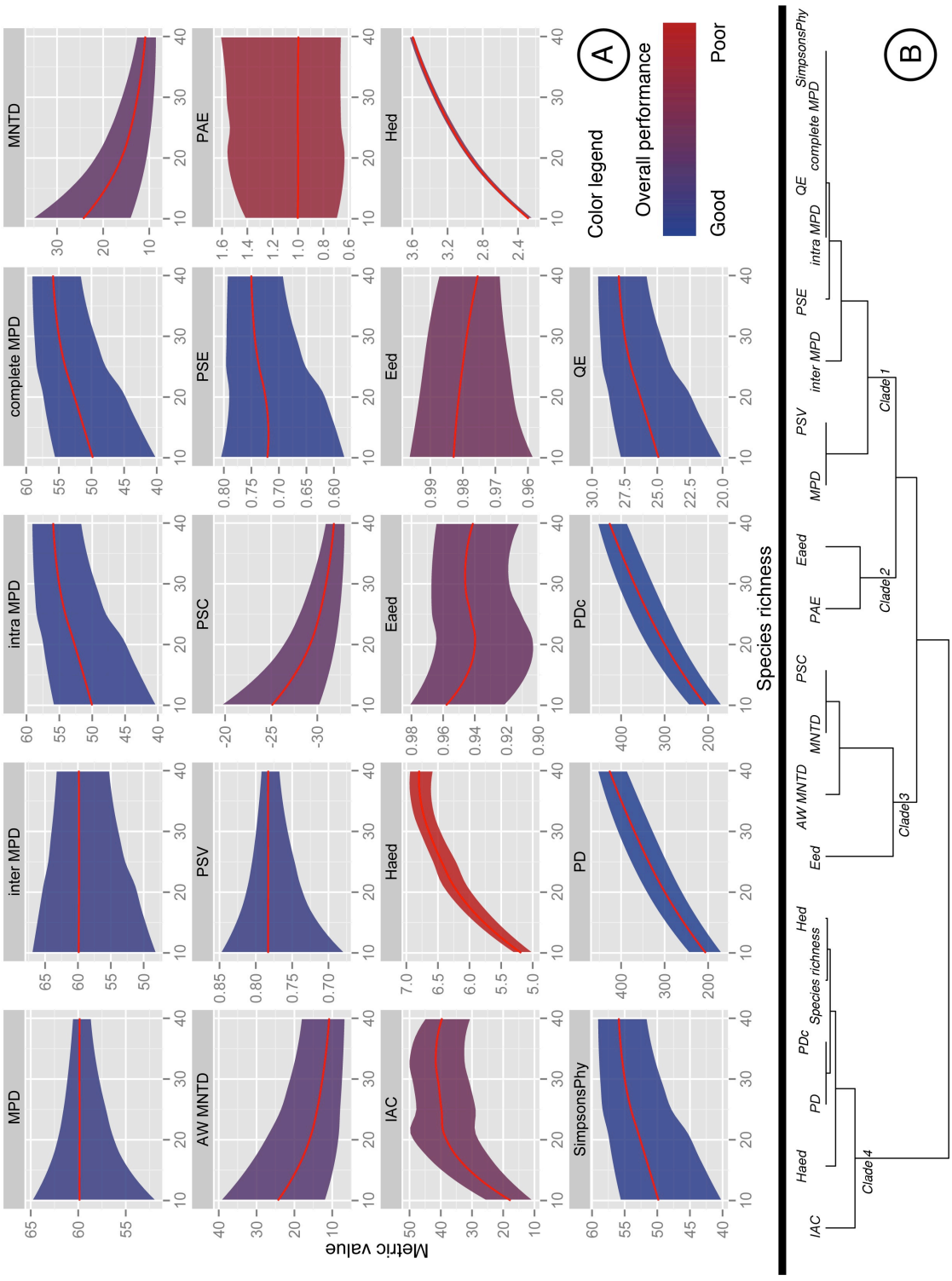
MPD
inter MPD
intra MPD
complete MPD
MNTD
AW MNTD
PSV
PSC
PSE
PAE
IAC
Haed
Eaed
Eed
Hed
SimpsonsPhy
PD
PDc
QE
Species richness
Metric value
Color legend
Overall performance
Good
Poor
A
B
Clade 1
Clade 2
Clade 3
Clade 4

Figure 1.

Figure 1. (A) Behavior of 19 focal phylogenetic community structure metrics (Table 1) across variation in species richness. Panels are color-coded from blue (good) to red (poor) according to sum of all successes (runs that successfully detected the simulated assembly process--either habitat filtering or competitive exclusion) minus sum of all type I errors encountered during the same runs for the richness, independent swap, and regional null models. **(B)** Dendrogram of intercorrelations among the phylogenetic community structure metrics (and species richness itself). Closely correlated metrics are annotated along branches. Clade 1 metrics focus on "total community relatedness"; Clade 2 metrics on the relationship between "evolutionary distinctiveness and abundance"; Clade 3 on "nearest-relative" measures of community relatedness; and Clade 4 metrics are particularly closely correlated with species richness.

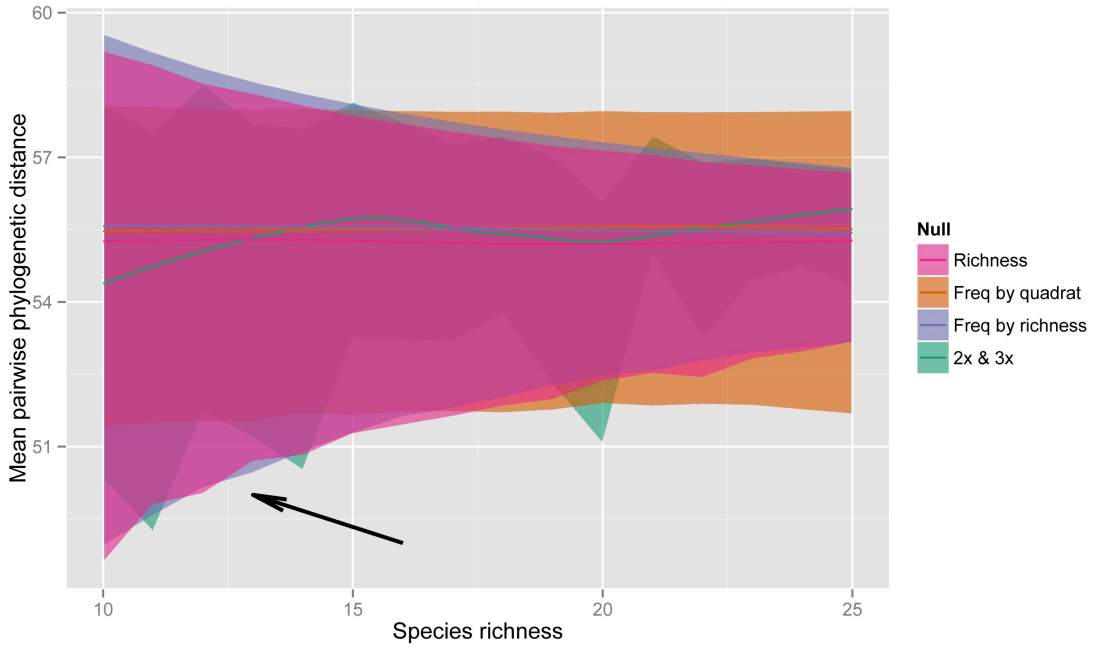

Figure 2. Confidence intervals (95%) for the richness, both forms of the frequency, 2x and 3x null models (Table 2) across variation in species richness. Expectations shown here are the result of 10^5 randomizations. Because the 2x and 3x nulls follow identical distributions (Fig. S3.5), only a single layer is included in this figure. The arrow indicates a region of particular concern for type I error when using the frequency by quadrat null. Other null model behavior (including the independent swap, trial swap, and regional models) is summarized in Appendix S3.

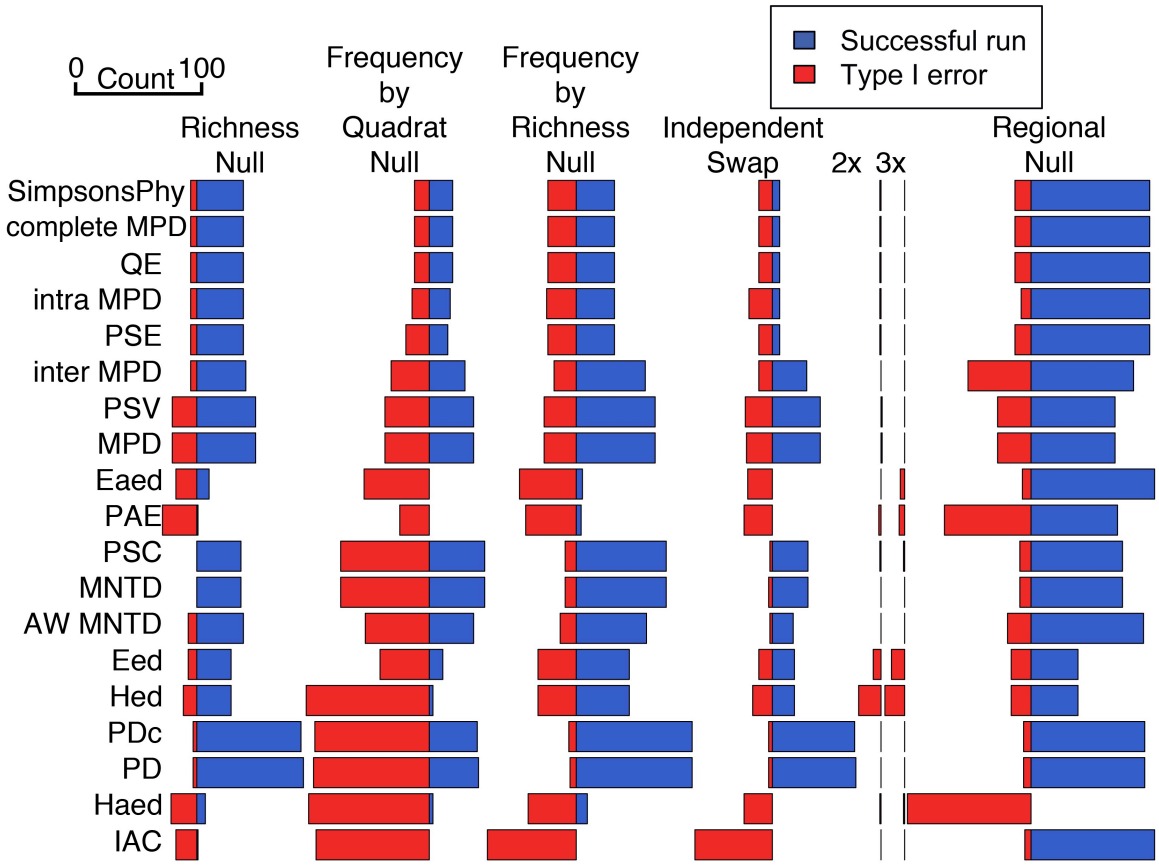

Figure 3. Performance of metric + null model approaches at detecting phylogenetic clustering given habitat filtering. A successful run was defined as over half of the quadrats in an arena showing significant phylogenetic clustering. Though occasional sampled quadrats contained < 2 species, and the entire iteration was discarded, results were scaled as if 100 iterations had been run, to facilitate visual comparison. Thus, results (i.e. each column of bars) are on the same scale. Actual sample sizes are given in Table S1.1 (smallest n = 84).

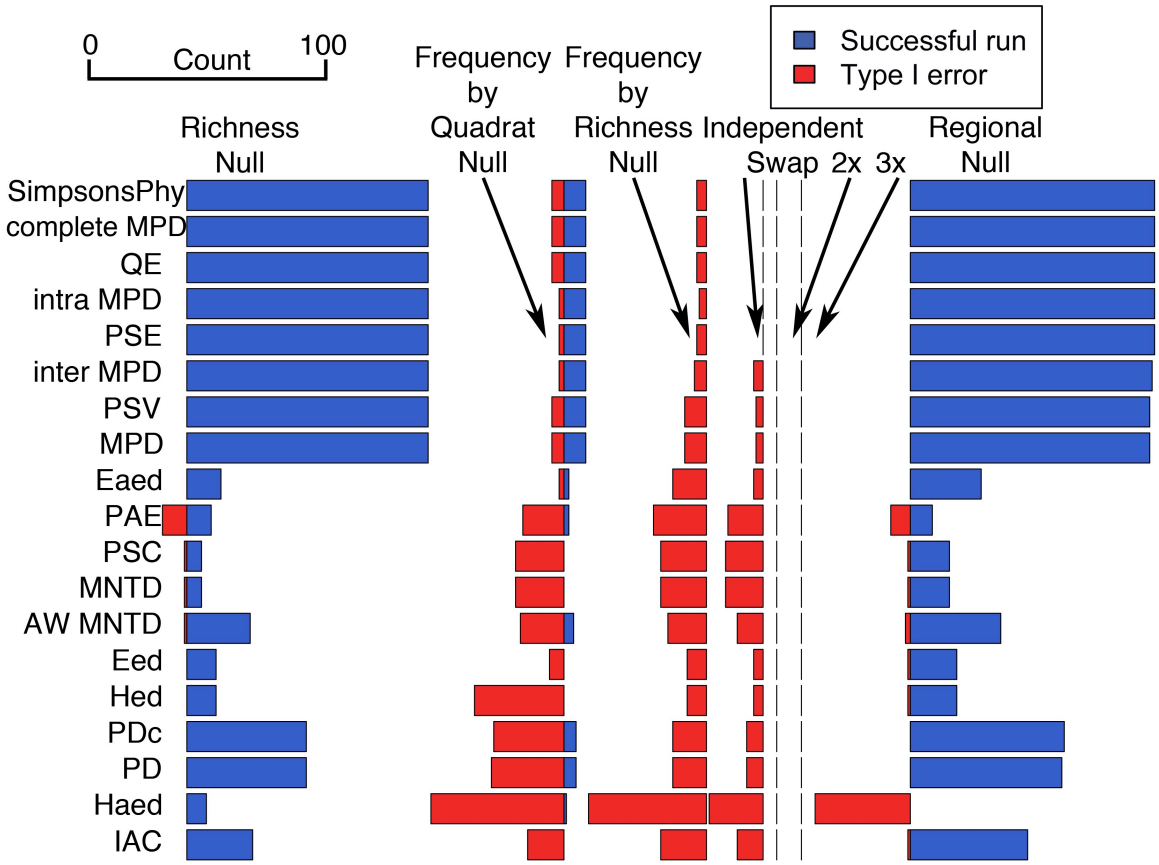

Figure 4. Performance of the different metric + null model approaches at detecting phylogenetic overdispersion given competitive exclusion. A successful run was defined as over half of the quadrats in an arena showing significant phylogenetic overdispersion. Results are on the same scale. Thus, for instance, the independent swap exhibited a high type II error rate.

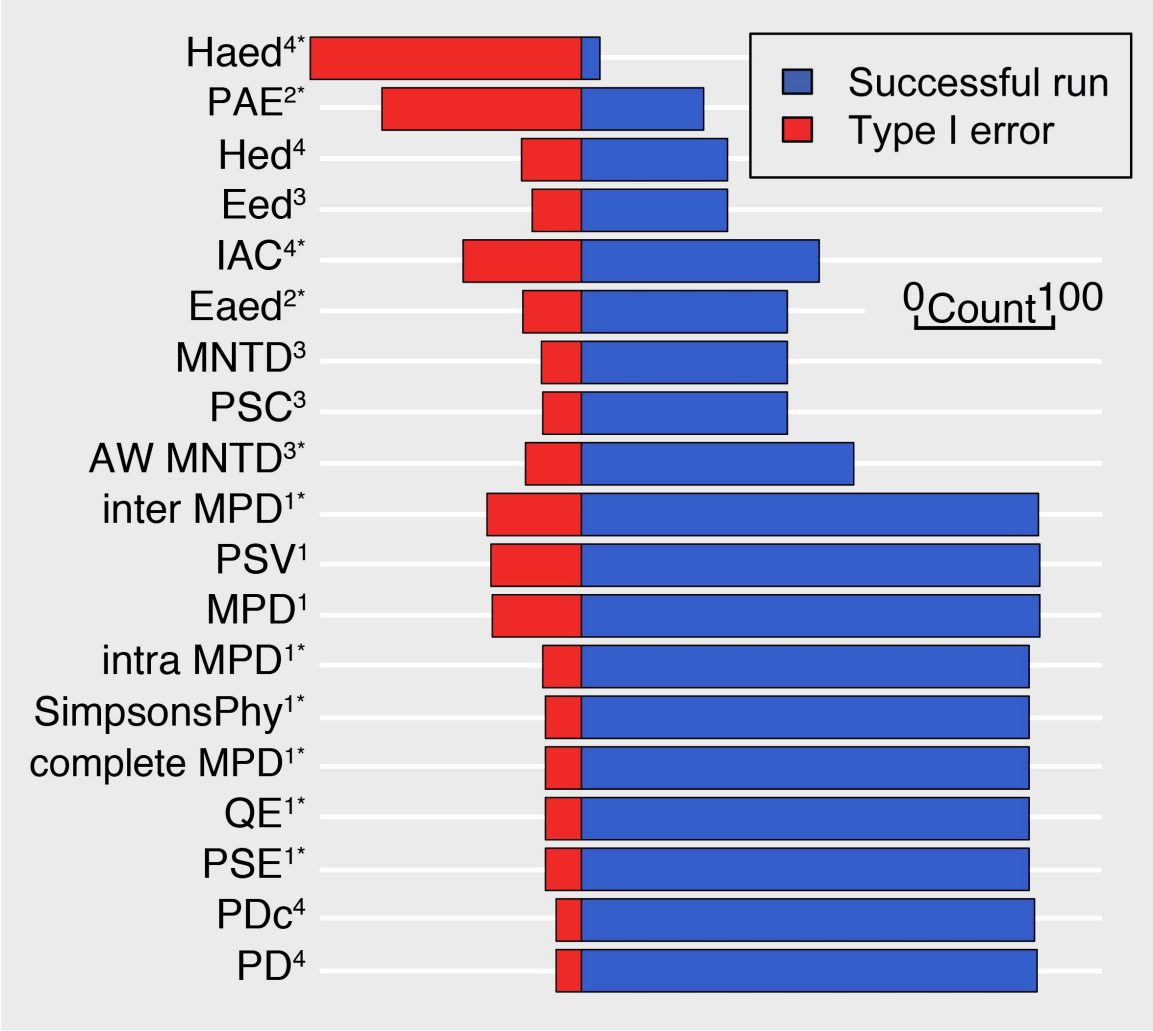

Figure 5. Overall performance of the different metrics using the richness, independent swap and regional null models. Blue bars are the sum of runs that successfully detected the simulated assembly process (either habitat filtering or competitive exclusion). Red bars are the sum of the type I errors encountered during the same runs. The results of 581 runs are shown (Table S1.1). Thus, the length (count) of the bar divided by 581 provides an estimate of overall power and type I error rates. Asterisks denote abundance-weighted metrics, and numbers refer to the Clade (Fig. 1B) they belong to.

Box 1: Abbreviated history of phylogenetic community structure metrics.

Faith (1992) introduced PD, a metric that quantifies the unique evolutionary history represented by co-occurring taxa. It was intended (and is often used) as a conservation tool. While PD built upon previous work by Vane-Wright *et al.* (1991) and others, it was the first to explicitly incorporate phylogeny. Since PD is the sum of all branch lengths connecting the species in a community (Table 1), the assumption that it increases with additional species, and is therefore correlated with species richness, was implicit (exact solution provided by Nipperess & Matsen 2013).

Subsequently, Clarke and Warwick introduced metrics (Δ, Δ+, Δ*) focused on the average branch length among a group of taxa or individuals, again linking their methodology to conservation decisions (Warwick & Clarke 1995, 1998; Clarke & Warwick 1998, 1999). Their pioneering papers explored some statistical properties of the metrics, including the fact that mean expected Δ+ is not correlated with species richness, but the width of its confidence intervals decreases with species richness (creating a "confidence funnel"). Yet, the conservation-specific scope of their papers limited their impact on community ecology. In fact, we were unaware of these metrics until after we had run our initial analyses.

Webb (2000) introduced two new metrics--MPD and MNTD--and the standardized forms of these, NRI (net relatedness index) and NTI (nearest taxon index). Initially, MPD was slightly different than Clarke and Warwick's metrics, only incorporating nodal distances, but by Webb *et al*. (2002) the definition had expanded to incorporate branch length, and was therefore equivalent to Δ+ (Appendix S2). Yet, by linking community assembly processes with these phylogenetic patterns, it was MPD and MNTD that

revolutionized the field of community ecology. Moreover, despite the equivalency of MPD and Δ+, Webb stated that both MPD and MNTD are correlated with species richness when only MNTD is (Fig. 1A), and devised standardization procedures to "correct" for this. This misperception occasionally persists to the present (e.g., Ulrich & Fattorini 2013), despite empirical solutions to the contrary (Tsirogiannis & Sandel 2013).

Helmus *et al.* (2007) introduced PSE, the "first" metric to incorporate abundance information. While this is not entirely true (Rao 1982; Warwick & Clarke 1995; Hardy & Senterre 2007), their focus on community assembly linked their approach with venerable evolutionary questions. Helmus *et al.* (2007) also introduced two other metrics intended to be similar but superior to NRI and NTI--PSV and PSC. The noted advantage to these is the lack of need for a reference species pool, and therefore the ability of these metrics to transcend the particulars of the phylogeny and community data matrix at hand, and allow raw metric values to be directly compared. However, these should therefore have been compared with MPD and MNTD, respectively. Had this been done, it would have been noted that PSV and PSC are directly proportional to MPD and MNTD, respectively, a still all but unknown fact (though see Vellend *et al.* 2011). Instead, PSV and PSC were compared with NRI and NTI. As a further complication, the PSC function in *picante* (Kembel *et al.* 2010) returns the inverse of PSC (M. Helmus, pers. comm.). This has confounded subsequent papers (e.g. Giehl & Jarenkow 2012; Villalobos *et al.* 2013). Some authors have incorrectly claimed that PSC is not inherently correlated with species richness.

Cadotte *et al.* (2010) introduced metrics focused on phylogenetic abundance distributions. We review seven of those here: PD_c (this was actually discussed earlier,

Faith (2007)), PAE, IAC, ED, H_{ED}, E_{ED}, H_{AED}, and E_{AED} (see Table 1). Cadotte *et al.* (2010) showed their metrics ranked communities differently than each other and than metrics like PSV and MNTD, but offered no discussion of the metrics' statistical properties, nor has any subsequent paper. The metrics are available in *ecoPD* (http://r-forge.r-project.org/projects/ecopd/).

We discuss six additional metrics in this paper: QE (Rao 1982), SimpsonsPhy (Hardy & Senterre 2007), abundance-weighted (AW) MNTD, and three variants of AW MPD (Table 1, Appendix S2). Both complete AW MPD and AW MNTD were introduced in *Phylocom* (Webb *et al.* 2008) and *picante* without accompanying publication, and their statistical properties and relationship to other metrics remains essentially unknown. Interspecific AW MPD was introduced in (Miller *et al.* 2013), and intraspecific AW MPD is "first" described in the current paper (Appendix 2), though as we subsequently discovered, it is equivalent to Δ (Clarke & Warwick 1998). Similarly, after exploring the behavior of QE and SimspsonsPhy and finding them equivalent, we realized this was already known (Hardy & Senterre 2007; Allen *et al.* 2009).

Appendix S1. Metric + null results for random community assembly, and sample sizes of all assembly simulations.

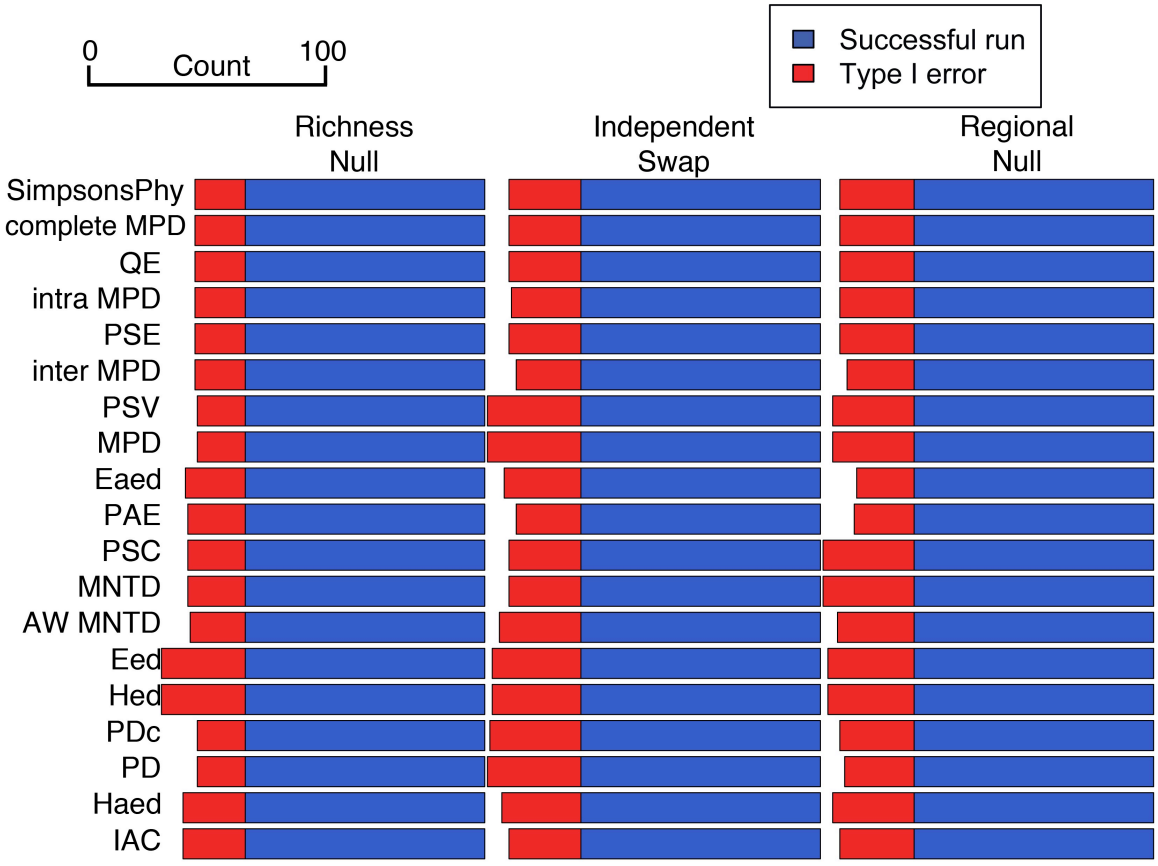

Figure S1.1. Performance of the different metric + null approaches given random community assembly. All metrics always detected an overall signal of random assembly for all three nulls, but occasional quadrats deviated beyond 95% expectations (20-39% of tests had at least one such quadrat, depending on the metric + null combination). The non-abundance-weighted metrics exhibited slightly higher type I error rates, presumably because of the large effect of the presence or absence of a single individual on the resulting metric value. All results in the figure are presented on the same scale.

Table S1.1. Sample sizes (iterations) for the different community assembly, null model analyses. Metric performance with random assembly was assessed with only the first three null models. Results are scaled (Fig. 3, 4, S1.1) to facilitate visual comparison.

	Habitat filtering	Competitive exclusion	Random
Richness	87	101	102
Frequency by quadrat	95	110	100
Frequency by richness	94	100	120
2x	84	100	
3x	95	100	
Independent swap	90	100	
Regional	103	100	

Appendix S2. Three forms of abundance-weighted MPD, and equivalency of some forms to Clarke and Warwick's metrics.

Three forms of abundance-weighted MPD

Abundance-weighted mean pairwise phylogenetic distance (MPD) and mean nearest taxon distance (MNTD) were introduced in *Phylocom* (Webb *et al.* 2008) without accompanying scientific papers. These methods have entered into common usage in the literature, but they have not been discussed at any length. A variation on abundance-weighted MPD was recently introduced that only accounts for interspecific phylogenetic distances (Miller *et al.* 2013). This is different than the implementation in *Phylocom* and *picante* (Kembel 2009).

There are at least three different possible forms of abundance-weighted MPD (Fig. S2.1). Consider a local assemblage of three species drawn from a regional species pool. Qualitatively, species A, B, and C are clustered in the phylogeny. But, how should the abundances of these three species affect the metric? In the simple case of an assemblage of two individuals of species A, and one each of species B and C, all of the potential interactions among individuals can be visualized schematically (Fig. S2.1).

If we include only interactions among heterospecific individuals to derive a matrix of abundance weights for the MPD calculation (Fig. S2.1, "interspecific"), we obtain the MPD among heterospecific individuals within the community. This is the same as the MPD among species, weighted by the number of individuals of each interacting species. It is also the same as Δ^* of Clarke & Warwick (1998) (see below). The resulting MPD calculated with this metric is slightly less than the unweighted version. This slight

decrease is due to down-weighting in the calculation of the contribution of the phylogenetic distance between individuals of the rarer species, B and C, compared to that of unweighted MPD (Fig. S2.1).

The interspecific metric will be useful when it is the phylogenetic distances among individuals of different species that are of interest. For example, when testing for habitat filtering or interspecific competition, given an increase in the number of individuals of species A, a researcher might prefer not to have the metric show a dramatic increase in the degree of clustering (as happens with alternative versions of the metric, see below and Fig. S2.2d). This is because it is the phylogenetic distances among individuals of different species that are hypothesized to be clustered and/or overdispersed. As another example, a researcher studying phylogenetic niche conservatism might be interested in how phylogenetic community structure changes along an environmental gradient. Given abundance data, he or she could study these changes along the gradient, down-weighting the importance of rarely recorded species (e.g., vagrants) and up-weighting the importance of abundant species.

Alternatively, one might wish to account for both inter- and intraspecific interactions to obtain the mean pairwise phylogenetic distance between any two individuals within the community (Fig. S2.1, "intraspecific"). Here, the two intraspecific interactions for species A, which correspond to phylogenetic distances of zero, are given weight when calculating MPD, considerably decreasing the resulting metric from the unweighted version. This intraspecific abundance-weighted MPD is equal to Δ of Clarke & Warwick (1998) (see below). It will likely be preferred when examining patterns in community phylogenetic structure predicted to arise from processes generating negative

density-dependence mediated by phylogenetic relatedness. For example, in the case of pathogen mediated species co-occurrence, the inclusion of both intra- and interspecific phylogenetic distances is important as both con- and heterospecific individuals represent potential hosts, and the expectation may be not only of even spacing among species, but even abundance distributions of individuals among species.

Lastly, abundance-weighted MPD, as currently implemented in *Phylocom* and *picante*, is calculated by accounting for all possible interactions, including those of an individual with "itself" (Fig. S2.1, "complete") (Webb *et al.* 2008; Kembel *et al.* 2010). The biological interpretation of this metric seems more complicated than those of the interspecific or intraspecific methods. The complete method might be likened, biologically, to including an individual's impact both on others and on itself; for example, an individual's use of environmental resources reducing availability for all individuals, including itself. The diagonal element in the abundance weight matrix of the complete method is equal to n^2, where n is the number of individuals of a species, while that in the intraspecific method is $n^2 - n$. Thus, the MPD values calculated with either version will converge rapidly as n increases (Fig. S2.3). Only at low total local assemblage abundance is the difference in MPD values between these metrics notable. Nevertheless, it seems that intraspecific MPD is a more accurate implementation of abundance-weighted MPD as defined by Webb *et al*. (2008) to be the average phylogenetic distance between any *two individuals* drawn from a sample.

Each of these methods corresponds to a different biological interpretation, and they performed similarly overall (Fig. 3-5). A few points should still be understood about the intraspecific and complete methods. Both intraspecific and complete abundance-

weighted MPD will correlate with assemblage species richness, since at lower richness, proportionally more intraspecific phylogenetic distances (i.e. distances of zero) are included in the mean (Fig. 1). Also, assemblages of uniform species abundances will have different MPD scores depending on whether they are abundance-weighted or not (Fig. S2.2). Finally, abundance-weighted MPD will always be less than the unweighted form (except in the unique case where all species in the assemblage are represented by a single individual, Fig. S2.2).

It is instructive to consider how these three different MPD metrics change as species abundances vary. If all species' abundances are increased, keeping relative abundances the same, the resulting metric is unchanged for the interspecific and complete methods, but decreases for the intraspecific method (it converges on the complete method with increasing total assemblage abundance, Fig. S2.3). If individuals of both species A and C are increased in tandem towards infinity, holding B constant, then the interspecific method converges on the phylogenetic distance between species A and C (4 in this example), while the latter two methods converge on the mean of the phylogenetic distance between species A and C and their intraspecific phylogenetic distance (2 in this example; the mean of 4 and zero). Similarly, with the interspecific method, adding individuals of species A only to the assemblage will increase the contribution of the phylogenetic distances between species A and other species, while with either of the other two methods, it will increase the contribution of both interspecific distances involving species A, and distances within species A (Fig. S2.2).

Some forms of MPD are equivalent to Clarke and Warwick's earlier metrics

While writing this manuscript, we became aware of three additional phylogenetic community structure metrics that were not incorporated in the main simulations (Clarke & Warwick 1998). This oversight was due in large part to the fact that these metrics have been more frequently used by conservation biologists than by community ecologists (Box 1). As we show here, they are equivalent to other metrics that we did assess, and consequently are expected to perform equivalently. Specifically, non-abundance-weighted MPD is equal to $\Delta+$, interspecific MPD is equal to $\Delta*$, and intraspecific MPD is equal to Δ (Fig. S2.4).

To demonstrate the equivalency of the metrics, we use our package *metricTester*, *geiger* (Harmon *et al.* 2008), *picante* (Kembel *et al.* 2010), and *vegan* (Oksanen *et al.* 2013), among others. Our package can be installed directly from GitHub using the *devtools* package (username = "eliotmiller"; note that the dependency *ecoPDcorr* must also be installed using the same username).

```
library(metricTester)
library(geiger)

#simulate tree with birth-death process
tree <- sim.bdtree(b=0.1, d=0, stop="taxa", n=50)

#generate log-normal abundance curve
sim.abundances <- round(rlnorm(5000, meanlog=2, sdlog=1))

#use this log-normal abundance curve to create a community
```

```
#data matrix (cdm) with 16 quadrats of species richness
#between 10 and 25.
cdm <- simulateComm(tree, min.rich=10, max.rich=25,
     abundances=sim.abundances)

#generate a phylogenetic distance matrix
dists <- cophenetic(tree)

#calculate the various forms of MPD using metricTester
naw.mpd <- modified.mpd(cdm, dists,
     abundance.weighted=FALSE)
inter.mpd <- modified.mpd(cdm, dists,
     abundance.weighted="interspecific")
intra.mpd <- modified.mpd(cdm, dists,
     abundance.weighted="intraspecific")

#calculate the various forms of Clarke and Warwick's
#metrics
temp.CW <- taxondive(cdm, dists)
delta <- temp.CW$D
delta.star <- temp.CW$Dstar
delta.plus <- temp.CW$Dplus

#Non-abundance-weighted MPD is equal to delta +. Also, call
```

```
#the raw values if you want to see those directly
plot(delta.plus~naw.mpd)

#Interspecific abundance-weighted MPD is equal to delta *
plot(delta.star~inter.mpd)

#Intraspecific abundance-weighted MPD is equal to delta
plot(delta~intra.mpd)
```

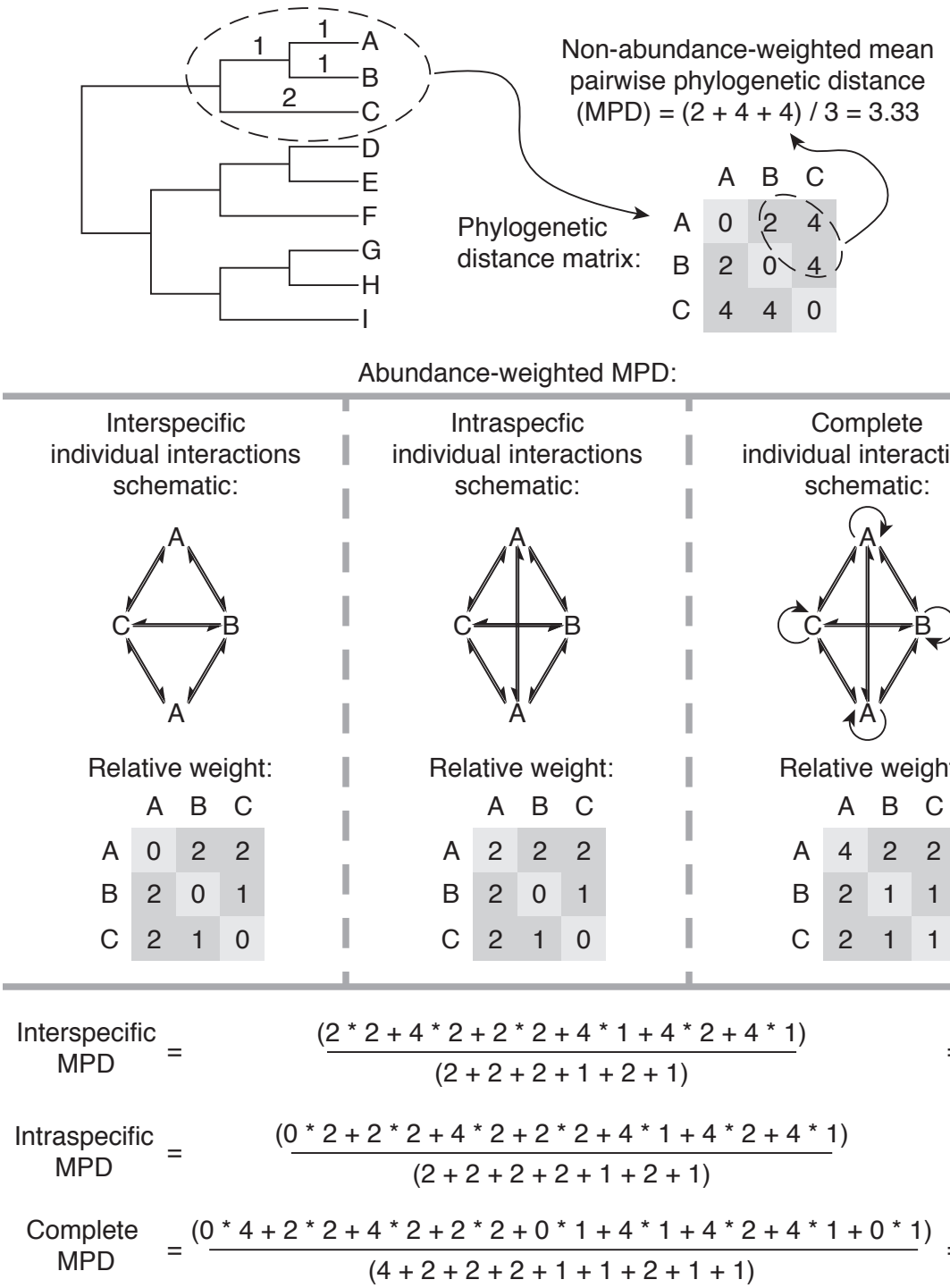

Figure S2.1. Schematic illustrating how non-abundance-weighted and three different forms of abundance-weighted MPD are calculated. Interspecific MPD accounts only for

phylogenetic distances among heterospecifics, intraspecific also accounts for distances among conspecifics, and complete also includes interactions of an individual with itself.

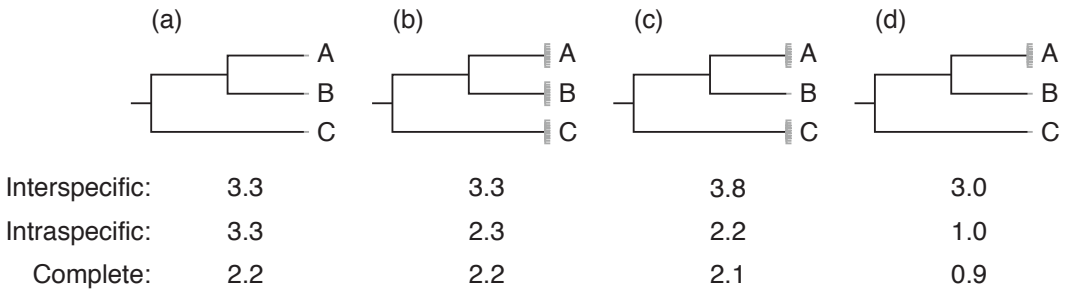

	(a)	(b)	(c)	(d)
Interspecific:	3.3	3.3	3.8	3.0
Intraspecific:	3.3	2.3	2.2	1.0
Complete:	2.2	2.2	2.1	0.9

Figure S2.2. Examples showing how varying species' abundances affects the different abundance-weighted MPD metrics. Branch lengths are the same as in Fig. S2.1. In all examples shown, unweighted MPD would be equal to 3.3. (a) Intraspecific MPD is equivalent to unweighted MPD in the special circumstance where one individual of each species is present, whereas the interspecific method is always equivalent to unweighted MPD when all species are equally abundant. (b) When all species' abundances are increased, keeping relative abundances constant, intraspecifc MPD decreases as more intraspecific distances are incorporated. (c) When individuals are added to species A and C, interspecific MPD increases, emphasizing the distance between these upweighted species. Intraspecific and complete MPD decrease, emphasizing the intraspecific phylogenetic distances within species A and C. (d) Intraspecific and complete MPD decrease dramatically when only individuals of species A are added, whereas interspecific MPD decreases only somewhat (as a result of a down-weighting of the phylogenetic distance between species B and C).

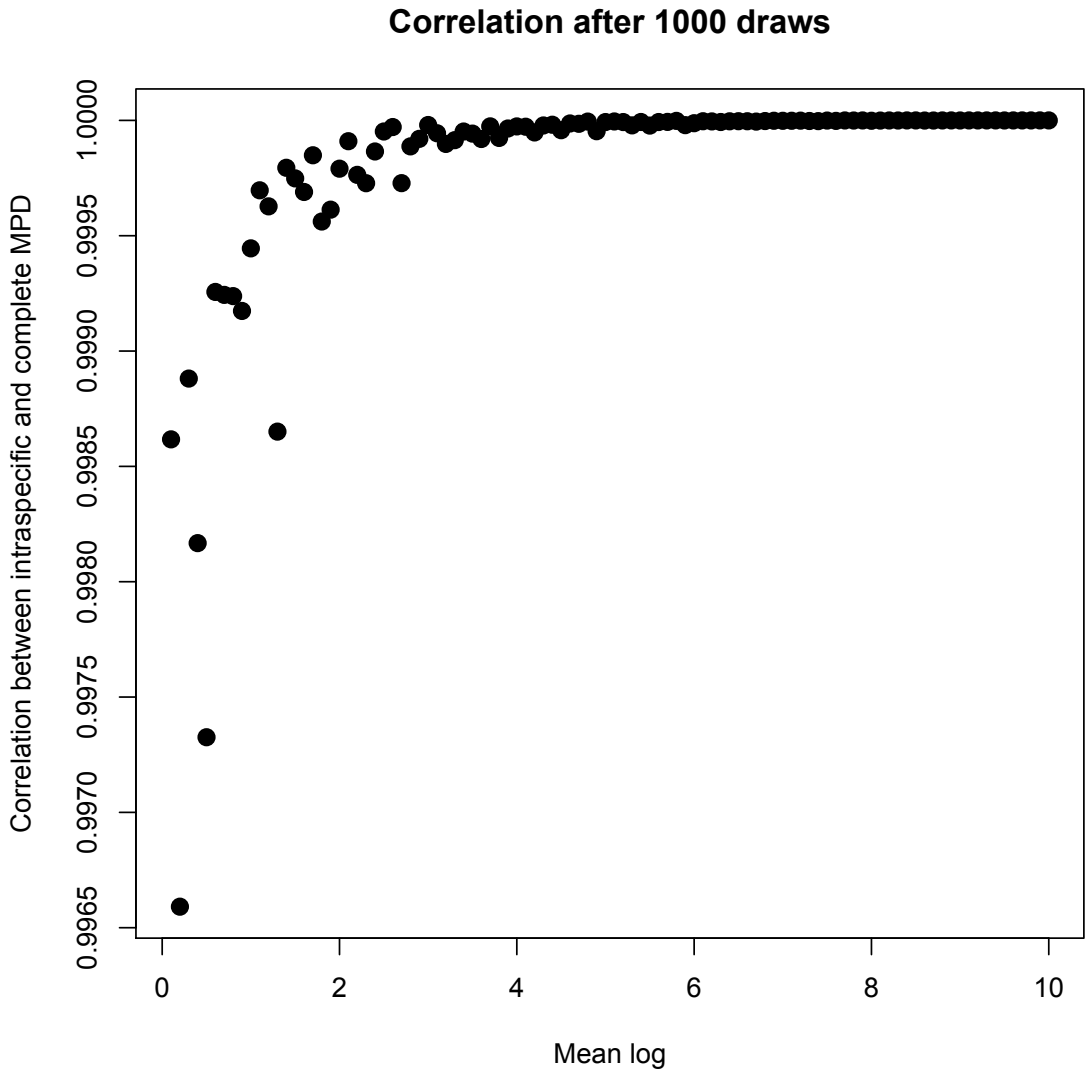

Figure S2.3. Intraspecific abundance-weighted MPD converges on complete abundance-weighted MPD with increasing total community size. To determine this, a series of 1,000 community data matrices were generated with the same phylogeny, number of species and number of quadrats, but the cells in the matrix were randomly filled by drawing from log-normal distributions with increasingly larger means.

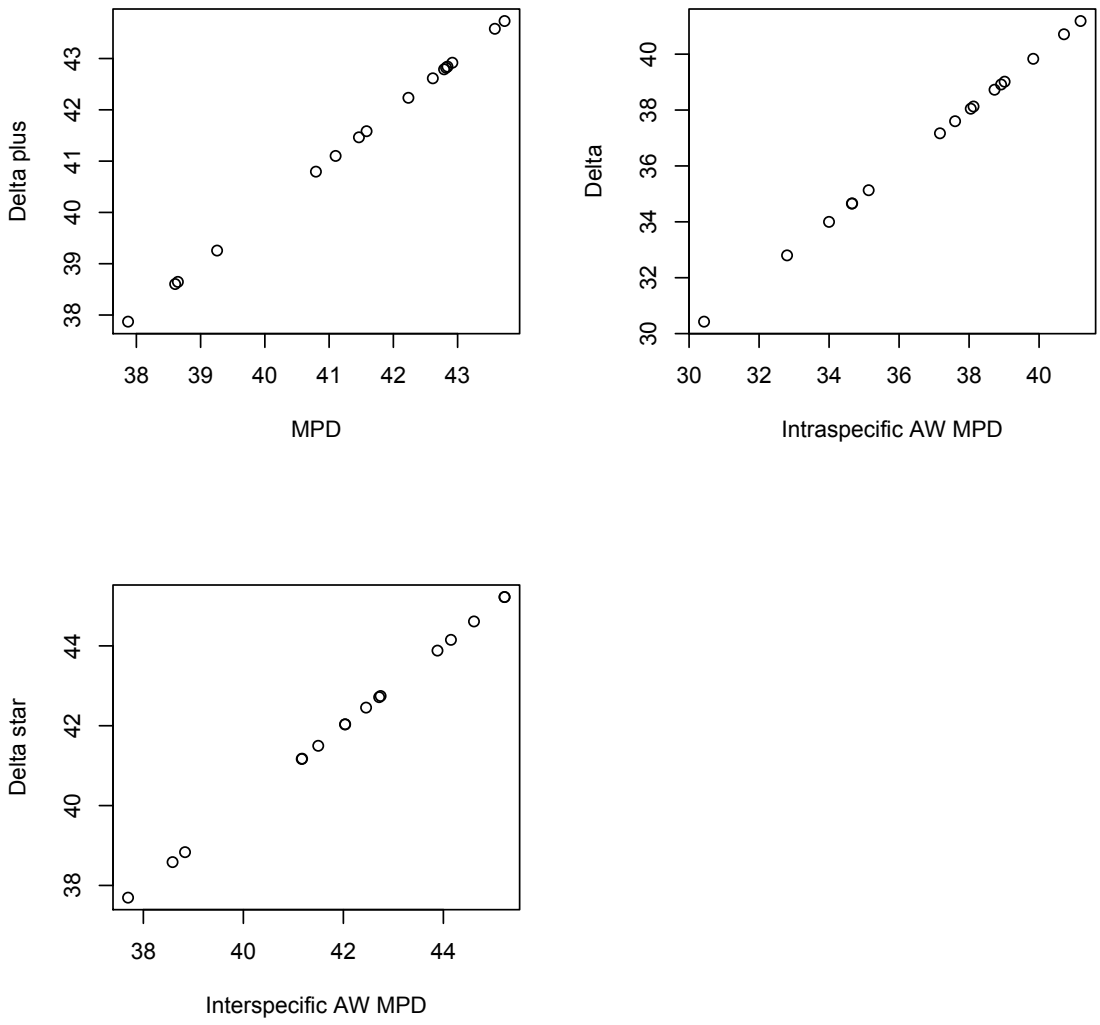

Figure S2.4. Scatterplots demonstrating the equivalency of Δ+ to MPD, Δ to intraspecific AW MPD, and Δ* to interspecific AW MPD. These plots were produced with the example code from *metricTester* shown above.

References

Clarke, K.R. & Warwick, R.M. (1998). A taxonomic distinctness index and its statistical properties. *Journal of Applied Ecology*, **35**, 523–531.

Harmon, L.J., Weir, J.T., Brock, C.D., Glor, R.E. & Challenger, W. (2008). GEIGER: investigating evolutionary radiations. *Bioinformatics*, **24**, 129–131.

Kembel, S.W. (2009). Disentangling niche and neutral influences on community assembly: assessing the performance of community phylogenetic structure tests. *Ecology Letters*, **12**, 949–960.

Kembel, S.W., Cowan, P.D., Helmus, M.R., Cornwell, W.K., Morlon, H., Ackerly, D.D., Blomberg, S.P. & Webb, C.O. (2010). Picante: R tools for integrating phylogenies and ecology. *Bioinformatics*, **26**, 1463–1464.

Miller, E.T., Zanne, A.E. & Ricklefs, R.E. (2013). Niche conservatism constrains Australian honeyeater assemblages in stressful environments. *Ecology Letters*, **16**, 1186–1194.

Oksanen, J., Blanchet, F.G., Kindt, R., Legendre, P., Minchin, P.R., O'Hara, R.B., Simpson, G.L., Solymos, P., Stevens, M.H.H. & Wagner, H. (2013). *vegan: Community Ecology Package*.

Webb, C.O., Ackerly, D.D. & Kembel, S.W. (2008). Phylocom: software for the analysis of phylogenetic community structure and trait evolution. *Bioinformatics*, **24**, 2098–2100.

Appendix S3. Null models: behavior across variation in species richness, documenting equivalency, and a new method.

Behavior of existing null models across species richness

As described in the main text, we were interested in quantifying the behavior of the null models (Table 2) across varying species richness. Basic principles of bootstrapping (Efron 1979) suggest that there should be more variance when small subsamples of a larger pool are taken. If two random taxa are drawn from a phylogeny, they could be close sister species, or they could span the root. The calculated phylogenetic community structure metrics from these two extremes could vary greatly. Alternatively, if all the species from a phylogeny are present in a community, we know what the calculated metric will be—no bootstrapping is necessary. This should lead to a confidence funnel (e.g., Clarke & Warwick 1998), with more variable expectations at lower species richness. But what sorts of expectations do the different nulls we tested generate? How do they differ from each other? What factors influence their distributions?

The richness null (=SIM3, Gotelli (2000)) we tested swaps abundances within quadrats. In other words, given a quadrat by species community data matrix (CDM), this null shuffles the contents of each row (a quadrat). Accordingly, species are sampled with equal frequency. We would expect that for metrics like mean pairwise phylogenetic distance (MPD) that are uncorrelated with species richness (Fig. 1), the mean expected value would not change with species richness. Simulations show this is the case (Fig. 2). This is a useful null to use as a benchmark against which to understand other more constrained nulls. Briefly, we note that a slight variations on this, the 1s null model

(Hardy 2008), converges on the same expectations as the richness null (Fig. S3.1). The 2s null (Hardy 2008) is Hardy's implementation of the richness null, and we examined it here simply to confirm that different R packages do indeed give similar solutions. There could be situations where these models do not converge, but we are unaware of what they are and we do not discuss either the 1s or 2s nulls further.

The frequency null we tested (=SIM2, Gotelli (2000)) swaps abundances within species. We refer to this as the frequency by quadrat null. Given a quadrat by species CDM, this null shuffles the contents of each column (a species). This means that species are not sampled with equal frequency. Importantly, it also means that the randomized quadrats tend to contain the mean number of species as were observed in the input CDM. For example, given a CDM with four quadrats, one of species richness 2, two of species richness 5, and one of species richness 8, randomized quadrats will tend to contain 5 species. Based on the principles of bootstrapping mentioned above, it should be clear why this would be problematic; the larger expected variance at low species richness will not be incorporated in the null model, and high type I error rates are expected (black arrow in Fig. 1 points to the region of concern).

To account for this, Miller *et al.* (2013) developed a method where the per quadrat raw metric values and associated species richness from a frequency null were retained. These values were concatenated by species richness, and observed values were compared to those expected at their corresponding species richness. We refer to this as the frequency by richness null.

Like the frequency by richness null, the derivation of a CDM where the randomized quadrats contain the same number of species as the input CDM, and

individual species occur with the same frequency as the input CDM are the goals of the independent swap (Gotelli & Entsminger 2001) and trial swap null models (Miklós & Podani 2004). The trial swap null model has been considered a more efficient implementation of the independent swap (Miklós & Podani 2004). In our simulations this was not the case. With increasing randomizations of a given CDM, the independent swap, trial swap and frequency by richness nulls all show increasingly stable expectations, but the trial swap seems to stabilize at a slower rate (Fig. S3.2). Regardless of the reason for this result, all three nulls seem to converge on the same solution (Figs. S3.3 and S3.4).

The 2x and 3x nulls (Hardy 2008) were developed to maintain not only aspects of species richness and occurrence frequency, but also either the quadrat-specific rank abundance curve or the species-specific abundance distribution, respectively. While these are aspects of a dataset that a researcher most certainly might wish to maintain, in practice, the extreme constraints imposed on the matrix randomizations seems to result in inefficient exploration of phylogenetic space. Both nulls also gave identical solutions (Fig. S3.5). We were unable to determine why these nulls behaved as they did, but the fact that their expectations wobble across species richness seems to be an undesirable property. Biologically, it is hard to construct a reason why one should expect dramatically different phylogenetic community structures with the presence or absence of a single species.

What determines how expectations for the independent swap (or frequency by richness or trial swap) vary from those given the richness null? It may not be intuitive to all readers that species within a phylogeny vary in their mean phylogenetic distance to other species in the phylogeny. In an ultrametric tree, all species are equidistant from the

root. How can one differ from another in its mean relatedness to other species? Consider the case of a single species that is sister to the rest of the phylogeny. This species is separated by larger average evolutionary distances than are the other species. The relationship between species' occurrence frequencies and their mean relatedness determines how the expectations for the independent swap shift from those of the richness null.

To illustrate this point, we generated a CDM as described in the main text. For every species in the CDM, we next calculated both its mean relatedness to the rest of the species and its occurrence frequency in the CDM. In the first simulation (Fig. S3.6, "sim1"), we then replaced species identities in the CDM such that species that were more closely related to the rest became the most frequent occurring species in the CDM. In other words, the most closely related species in the phylogeny also became the most common in the new CDM. We performed the opposite procedure in the second simulation ("sim2"). When distant relatives are also the least frequently observed species, the expectations are shifted downwards from those given a richness null. When distant relatives are the most frequently observed species, the expectations are shifted upwards (Fig. S3.6). Moreover, mean expected MPD, which is uncorrelated with species richness, begins to show some correlation with species richness when using a null model like this. This is because the probability of including rare species in the randomized matrices increases with larger samples. Thus, the expected MPD is positively correlated with species richness in the first simulation, and negatively correlated in the second.

Development of the regional null model.

No null model of community assembly that we know of maintains species richness, species occurrence frequency, and species abundance. The null models that come closest to achieving these objectives are the 2x and 3x nulls of (Hardy 2008), and these perform poorly. We develop a new null model aimed at achieving these goals. We do so both because of its theoretical value and, in particular, because our competitive exclusion simulations led us to recognize the importance of local interactions on species occurrence frequencies (Appendix S4). Specifically, our competitive exclusion simulations produce a local effect where some species that are regionally common become locally less so. Such species are closely related to species that are more common in the local community. When these local occurrence frequencies are used to inform a null model like the independent swap, short phylogenetic distances (like those between sister species) tend not to occur in the randomized matrices, which results in the expected phylogenetic community structure being shifted upwards from that given a null that maintains only species richness (Fig. S3.7). Accordingly, it becomes difficult to detect phylogenetic overdispersion.

In empirical situations, researchers are likely interested in testing for the effects of community assembly processes in a focused area (e.g., a forest plot, a grid cell on a map, a soil sample, etc.). The thought, likely, is that the focal area was historically or is currently subject to community assembly processes (e.g., competitive exclusion) that operate at a different scale than regional dispersal pressures on the focal area. The regional null is intended to simulate these regional dispersal probabilities (i.e. propagule pressure, with no intended implication of invasive biology). Based on our results in the main text, it performs well and, as we explain below, it largely accomplishes the

objectives of maintaining species richness, occurrence frequency, and abundance distributions. It requires, however, that a regional abundance vector (in the form of "sp1, sp1, sp1, sp2, sp2, …") be provided. Developing a vector like this is easy in our simulations, but may be more difficult in empirical situations. If a dataset consisted of evenly sampled sites, so as not to introduce biases in species occurrence frequencies, and the assumption was made that species abundances reflected their dispersal probability, then a vector of all individuals across the entire dataset could be used (use the function "abundanceVector" in our package to do so). Most real-world situations would be more complicated than this, and the practicality of the regional null remains to be demonstrated.

The regional null takes as input a regional abundance vector, as described above. For each quadrat in the randomized CDM, it then samples with equal probability from this vector the same number of individuals as were in that quadrat in the observed CDM. The metric of interest is calculated on the quadrats from this randomized CDM, and these values are retained, along with the associated species richness from each quadrat. This process is repeated many times. At the end of this process, the mean and 95% confidence intervals of all randomized values at each observed species richness value are then calculated. Thus, species richness is strictly maintained, as observed quadrats are only ever compared with the 95% CI from randomized sites of corresponding species richness.

Species occurrence frequencies are also approximately maintained with the regional null. For instance, after 1,000 randomized CDMs were generated with the regional null, we calculated the mean occurrence frequency across all randomized CDMs for each of the 50 species in community. These values were closely correlated with the

observed occurrence frequencies for the same 50 species ($r^2 = 0.83$, $p < 0.001$, Fig. S3.8). The abundance at which a species occurs in any given quadrat is also approximately maintained with the regional null. For instance, within a given quadrat from these same randomizations, a randomly selected species was mostly found as a single individual, occasionally as two individuals, and very infrequently at higher abundances (Fig. S3.9A). This is similar to the abundance distribution of the same species in the original CDM (Fig. S3.9B).

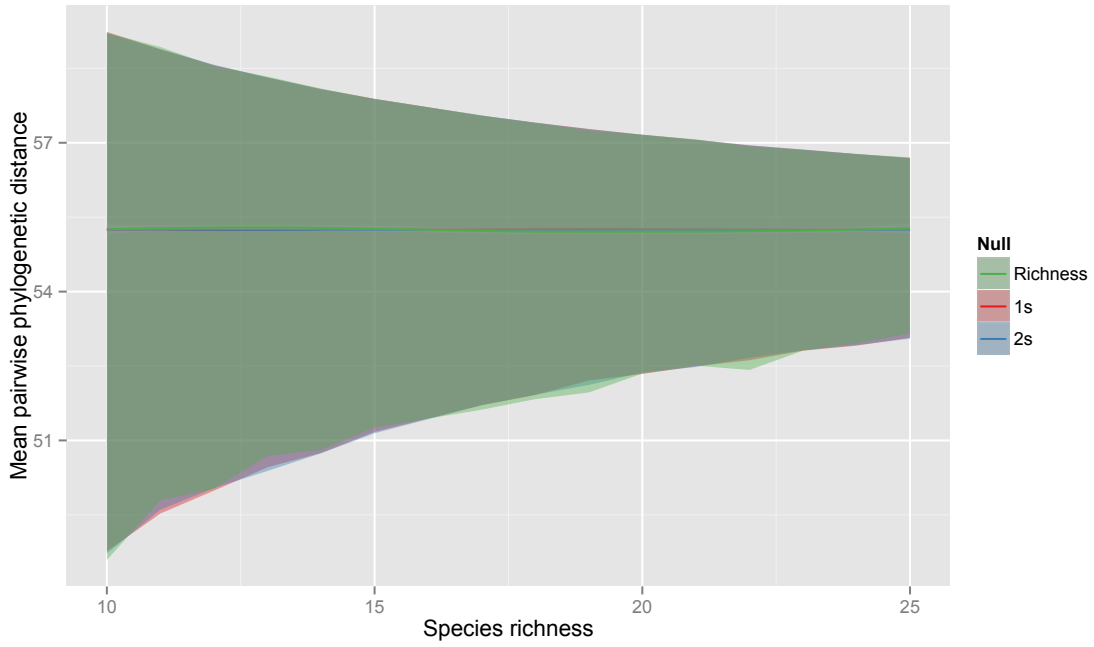

Figure S3.1. Confidence intervals (95%) for null models (shaded by color) across variation in species richness. The same initial CDM, phylogeny and number of randomizations as Fig. 1 were used. The richness and 1s null models provide identical expectations. The 2s null model also converges on the same expectation; this model is

simply the *spacodiR* implementation of what amounts to a richness null, but we include it here to confirm that different R packages provide similar results.

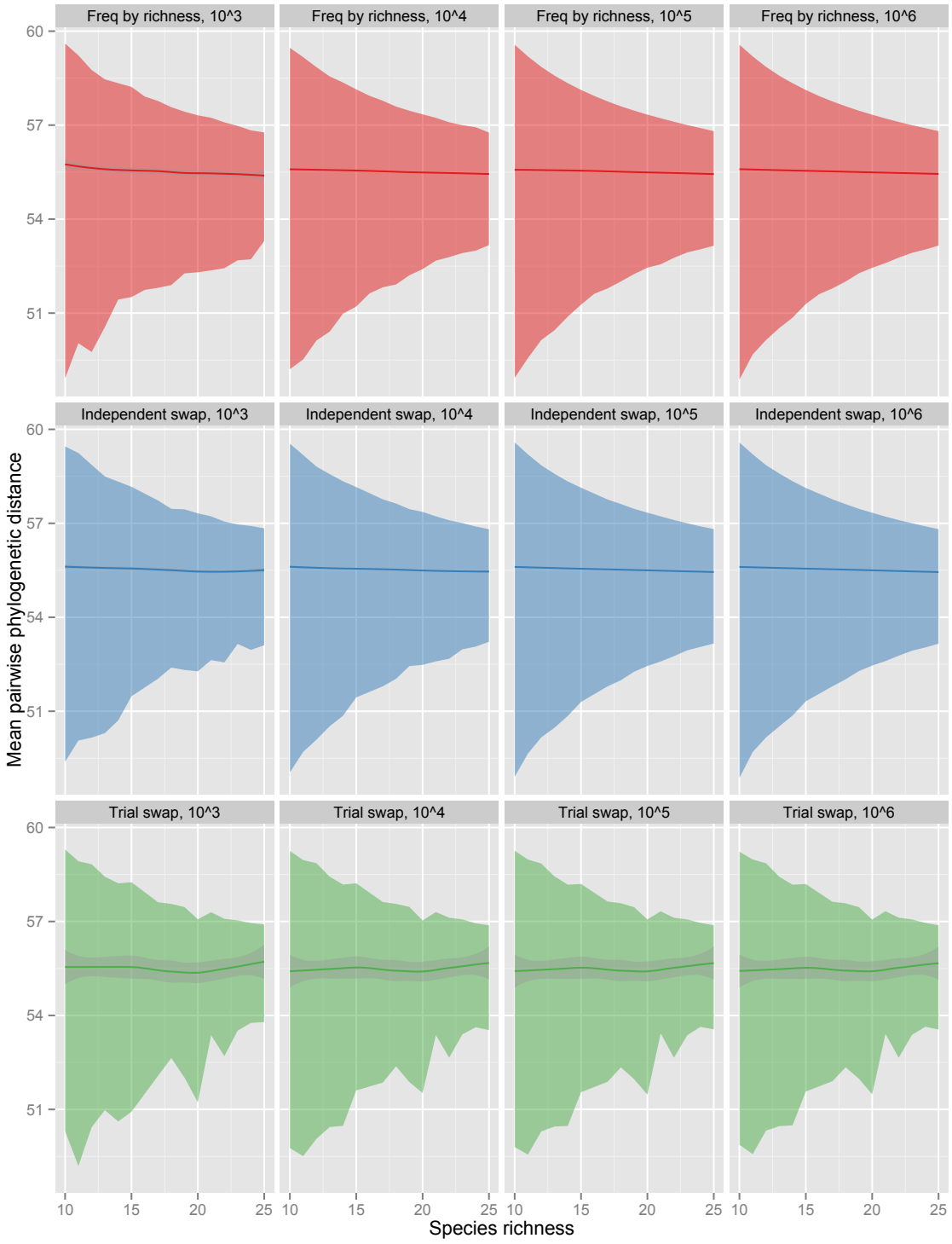

Figure S3.2. Confidence intervals (95%) for the frequency by richness, independent swap, and trial swap nulls across varying species richness and with increasing randomizations of an initial CDM. The darker lines in all panels represent mean trend lines. The shading around those lines represents confidence around that mean; the shading is only visible on the trial swap panels.

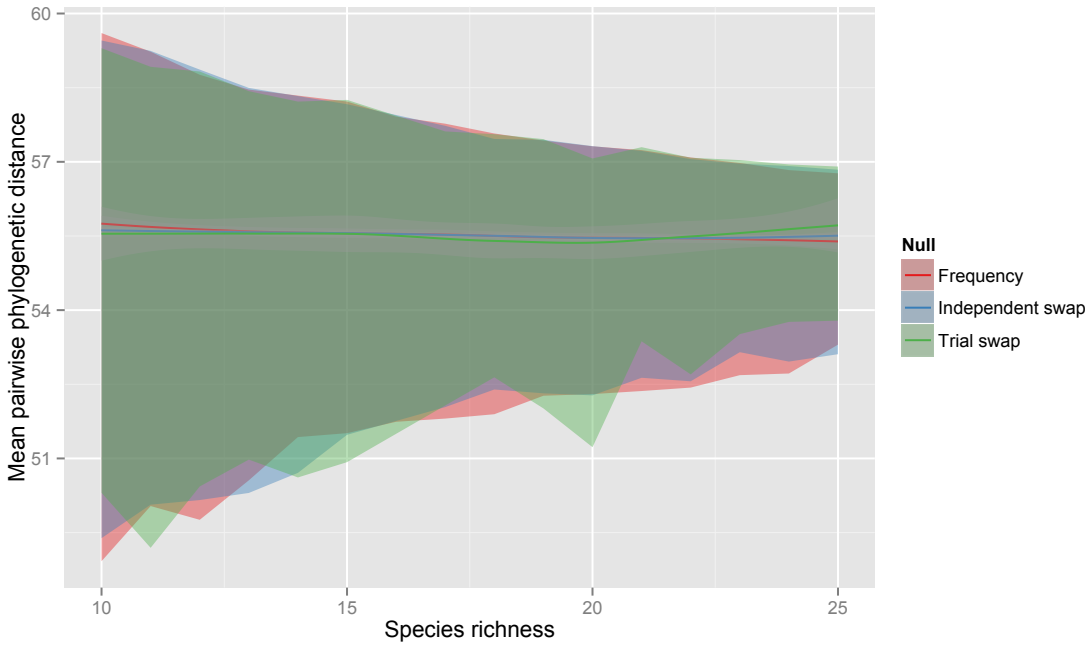

Figure S3.3. Confidence intervals (95%) for the frequency by richness, independent swap, and trial swap nulls across species richness (after 10^3 randomizations). These are the leftmost three panels from Fig. S3.2. Darker lines represent mean trends. Shading around those lines represents confidence around the mean; the shading is only visible for the trial swap mean.

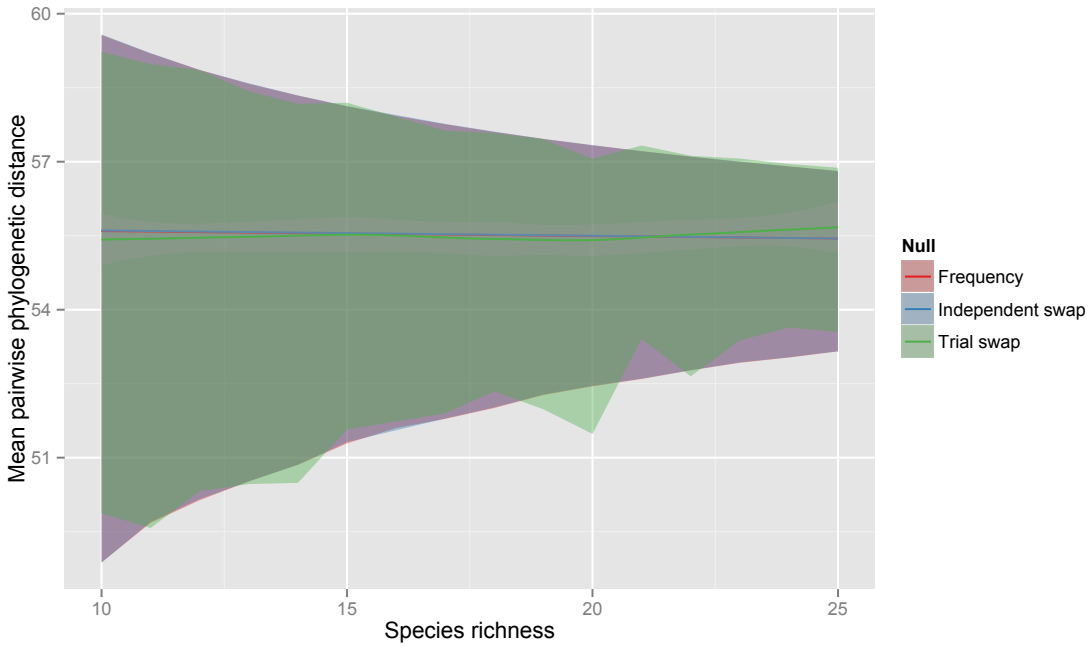

Figure S3.4. Confidence intervals (95%) for the frequency by richness, independent swap, and trial swap nulls across species richness (after 10^6 randomizations). These are the rightmost three panels from Fig. S3.2. Darker lines represent mean trends. Shading around those lines represents confidence around the mean; the shading is only visible for the trial swap mean.

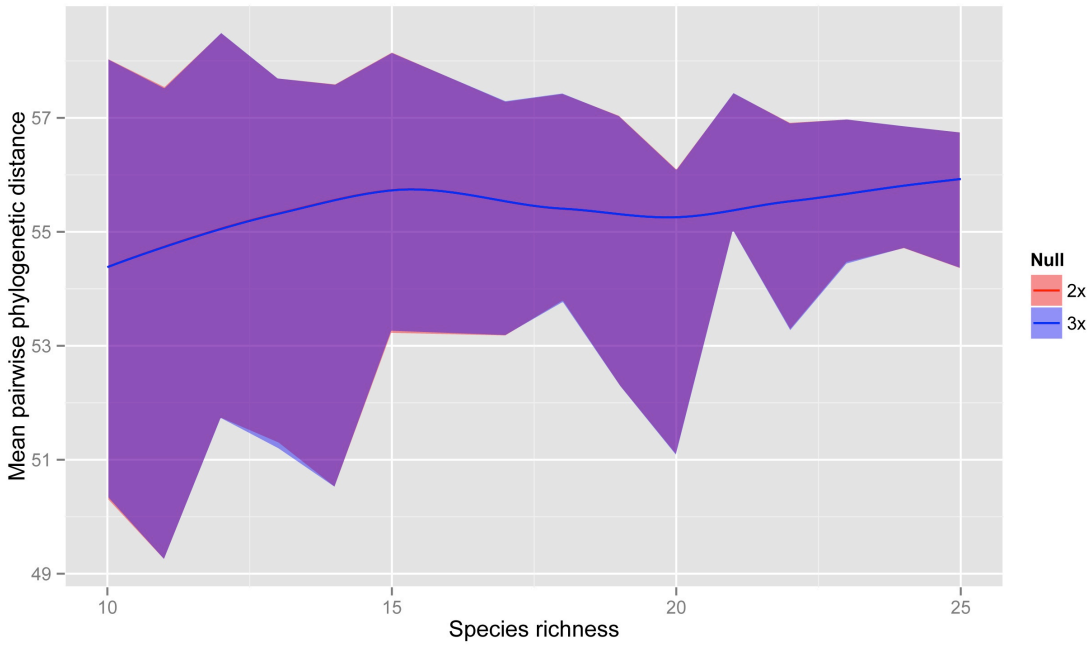

Figure S3.5. Confidence intervals (95%) for the 2x and 3x null models (Table 2) across variation in species richness. Expectations shown here are the result of 10^5 randomizations. The two null models follow identical distributions.

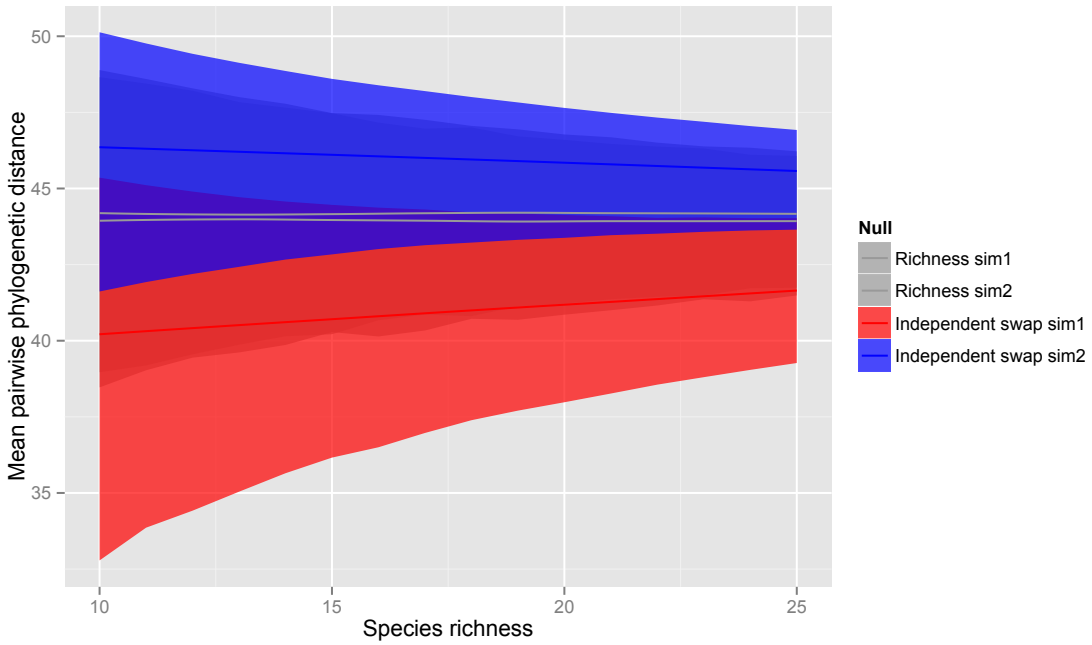

Figure S3.6. Results of two simulations varying the occurrence frequency of individual species in the CDM according to mean relatedness to the rest of the species in the phylogeny. In the first simulation, the most closely related species occurred most frequently. This pattern was reversed in the second simulation. Expectations do not shift notably when using the richness null.

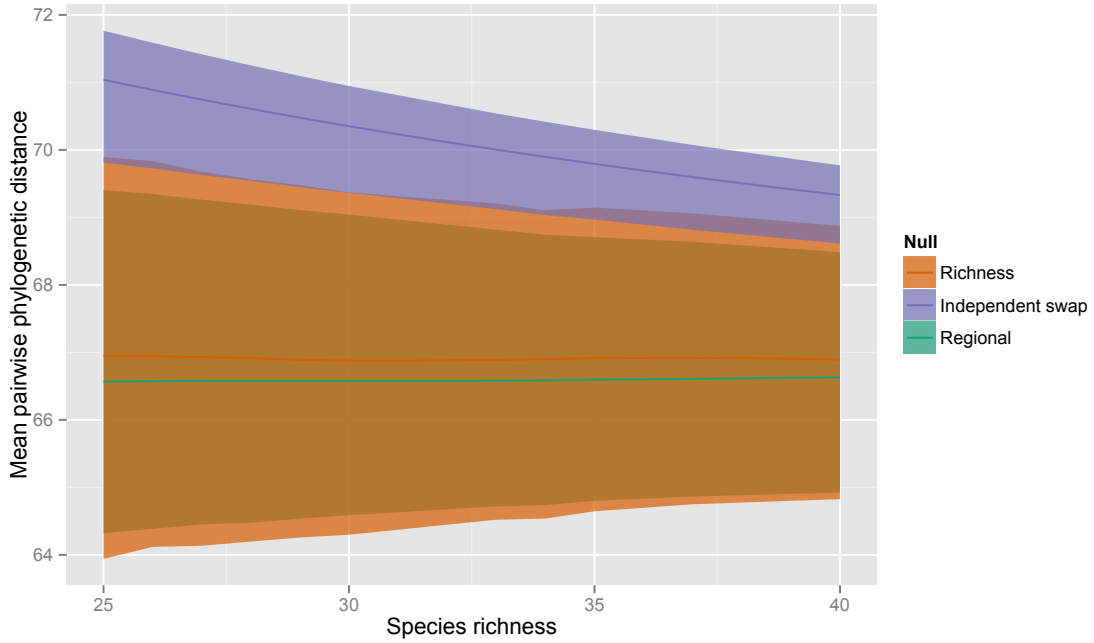

Figure S3.7. Confidence intervals (95%) for null models (shaded by color) across varying species richness. The arenas were constructed with the same parameters as described for the competitive exclusion simulations in the main text. The expectations shown here are the result 10^5 randomizations. After 100 generations of competition, the abundance of some species that are closely related to other species (i.e. “nested” in the phylogeny) decreases across the arena (Fig S4.11). Their occurrence frequency in random

quadrats, used to generate the CDM does as well. Thus, the expectations given an independent swap null, which accounts for occurrence frequency, are shifted notably upwards from those given a richness null. Moreover, some species are lost from the arena entirely, and the mean expectations for the richness null are therefore also shifted slightly up from those given the regional null.

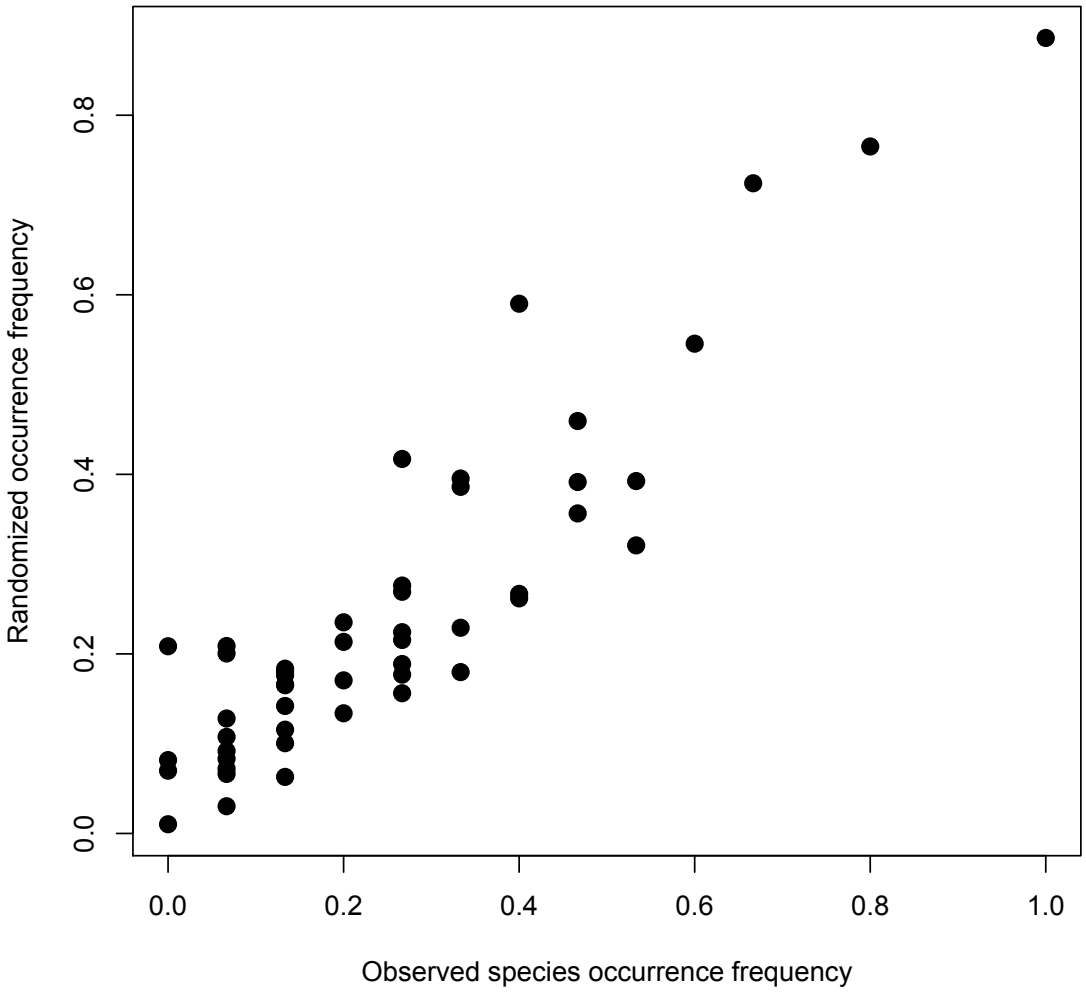

Figure S3.8. Mean occurrence frequency of 50 species, after 1000 randomizations with the regional null model, as compared with their initial occurrence frequency. Species tended to occur with a frequency proportional to their occurrence frequency in the observed matrix ($r^2 = 0.83$, $p < 0.001$).

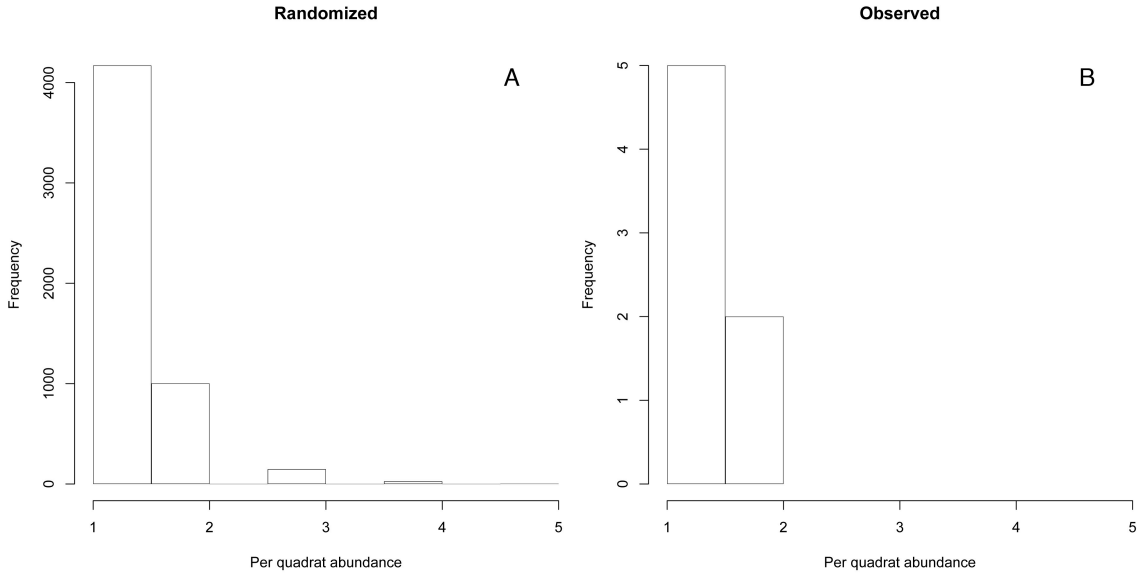

Figure S3.9. (**A**) Histogram of the abundance distribution of a randomly selected species across 1000 randomized community data matrices (after excluding all quadrats where it did not occur at all). (**B**) Histogram of the observed, original abundance distribution of the same randomly selected species as **A** (after excluding all quadrats where it did not occur at all).

References

Clarke, K.R. & Warwick, R.M. (1998). A taxonomic distinctness index and its statistical properties. *Journal of Applied Ecology*, **35**, 523–531.

Efron, B. (1979). Bootstrap methods: Another look at the jackknife. *The Annals of Statistics*, **7**, 1–26.

Gotelli, N.J. & Entsminger, G.L. (2001). Swap and fill algorithms in null model analysis: rethinking the knight's tour. *Oecologia*, **129**, 281–291.

Hardy, O.J. (2008). Testing the spatial phylogenetic structure of local communities: statistical performances of different null models and test statistics on a locally neutral community. *Journal of Ecology*, **96**, 914–926.

Miklós, I. & Podani, J. (2004). Randomization of presence-absence matrices: comments and new algorithms. *Ecology*, **85**, 86–92.

Miller, E.T., Zanne, A.E. & Ricklefs, R.E. (2013). Niche conservatism constrains Australian honeyeater assemblages in stressful environments. *Ecology Letters*, **16**, 1186–1194.

Appendix S4. Metric and null model approach results are robust to variation in spatial simulation parameters and number of randomizations of community data matrix.

In this study, we created community data matrices according to one of three community assembly processes: random assembly, habitat filtering and competitive exclusion. The random communities contained approximately the same number of individuals as stems recorded in forest plots of similar size (Murphy *et al.* 2013). Species within these communities were distributed according to a log-normal rank abundance curve (example community Fig. S4.1). The *metricTester*-specific parameters are listed below.

Simulate a phylogeny of 100 species with geiger:

```
tree <- sim.bdtree(b=0.1, d=0, stop="taxa", n=100)
```

Generate a random spatial community of 300 x 300 m, assigning species abundances from a log-normal distribution with mean log of 3.2:

```
arena <- randomArena(tree, x.min=0, x.max=300, y.min=0,
y.max=300, mean.log.individuals=3.2).
```

In the habitat filtering community assembly simulation, we set our parameters to compromise between producing realistic-looking communities, and producing strong and readily detectable phylogenetic patterns. A consequence of this was that individuals

tended to be distributed more densely in the center of the community, and more individuals were situated in the community than, e.g. stems in forest plots of similar size (Fig. S4.2). There is room for improvement in future simulations, but exploration of variation in these parameters yielded qualitatively identical results to those used in the main text (Fig. S4.3-5). The *metricTester*-specific parameters we used are listed below.

Generate a phylogeny of 100 species and allow two traits to evolve independently following a Brownian motion distribution:

```
temp <- phyloNtraits(100)
```

Scale those traits to match the size of the community:

```
scaled <- scaler(temp[[2]], min.arena=0, max.arena=300)
```

Place individuals down near their preferred spatial location. First determine how many individuals per species there are in the community by drawing from a log-normal distribution with mean of 5. Then create normal distributions of length = 100 and SD = 35 around the preferred X and Y location of each species. Draw as many individuals per species as were determined by the first process, and place them down at their selected X,Y location.

```
positions <- locationSampler(phyloNtraits.results=temp,
scaled.results=scaled, mean.log.individuals=5,
length.parameter=100, sd.parameter=35)
```

The competitive exclusion community assembly simulations began with a community created with the same parameters as the random community described above. Because the same numbers of individuals were removed as were added to the competitive communities, the communities likewise contained approximately the same number of individuals as the random communities (Fig S4.6). The *metricTester*-specific parameters we used are given below. The first two steps follow those of the random community above.

```
tree <- sim.bdtree(b=0.1, d=0, stop="taxa", n=100)
```

```
arena <- randomArena(tree, x.min=0, x.max=300, y.min=0,
y.max=300, mean.log.individuals=3.2)
```

Take the phylogeny and random community, set the interaction distance to be 15 m, the percent of individuals considered to be 20%, and run the competitive exclusion simulation for 100 generations.

```
comp <- competitionSimulator(tree=tree, initialArena=arena,
max.distance=15, percent.killed=0.2, iterations=100)
```

The competitive exclusion simulations were robust to parameter variation. Both variation in the interaction distance and in the percent of individuals "killed" per generation resulted in communities with regions of approximately equal genetic "overdispersion" (Fig. S4.7-8). These communities looked realistic and similar to the random communities, though the even spacing of close relatives was discernible (Fig. S4.9 and S4.10).

During the competitive exclusion simulations, some species that were initially common in the community became less so with each generation (Fig. S4.11). These species were those with many close relatives in the phylogeny. A null like the independent swap that incorporates species occurrence frequencies derives these from occurrence frequencies in the observed community data matrix (CDM). After the competitive exclusion simulations, therefore, longer than average branch lengths end up being frequently sampled in the randomized CDMs. Accordingly, the expected phylogenetic community structure is shifted upwards from that given a richness null, and it becomes difficult to detect phylogenetic overdispersion (Fig. S3.7). This occurs despite the fact that, throughout the competitive exclusion simulations, removed individuals were settled from the initial regional abundance pool. Our development of the regional null model (Appendix S3) was motivated in large part by this complication.

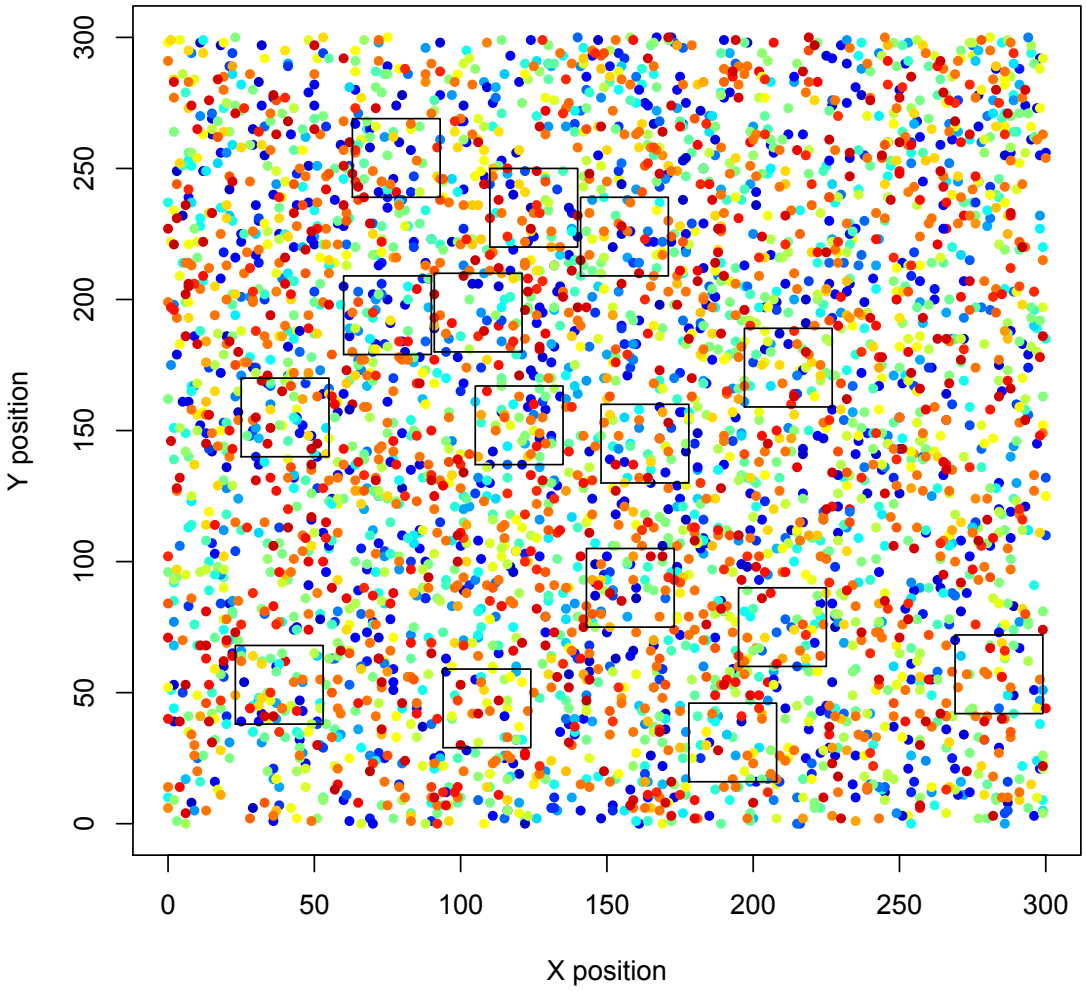

Figure S4.1. Example of a 300 x 300 m random assembly community, created using the same parameters as those in the study. The 15, 30 x 30 m quadrats are also plotted. Each species is assigned a unique color, though with 100 species they cannot be readily distinguished from one another.

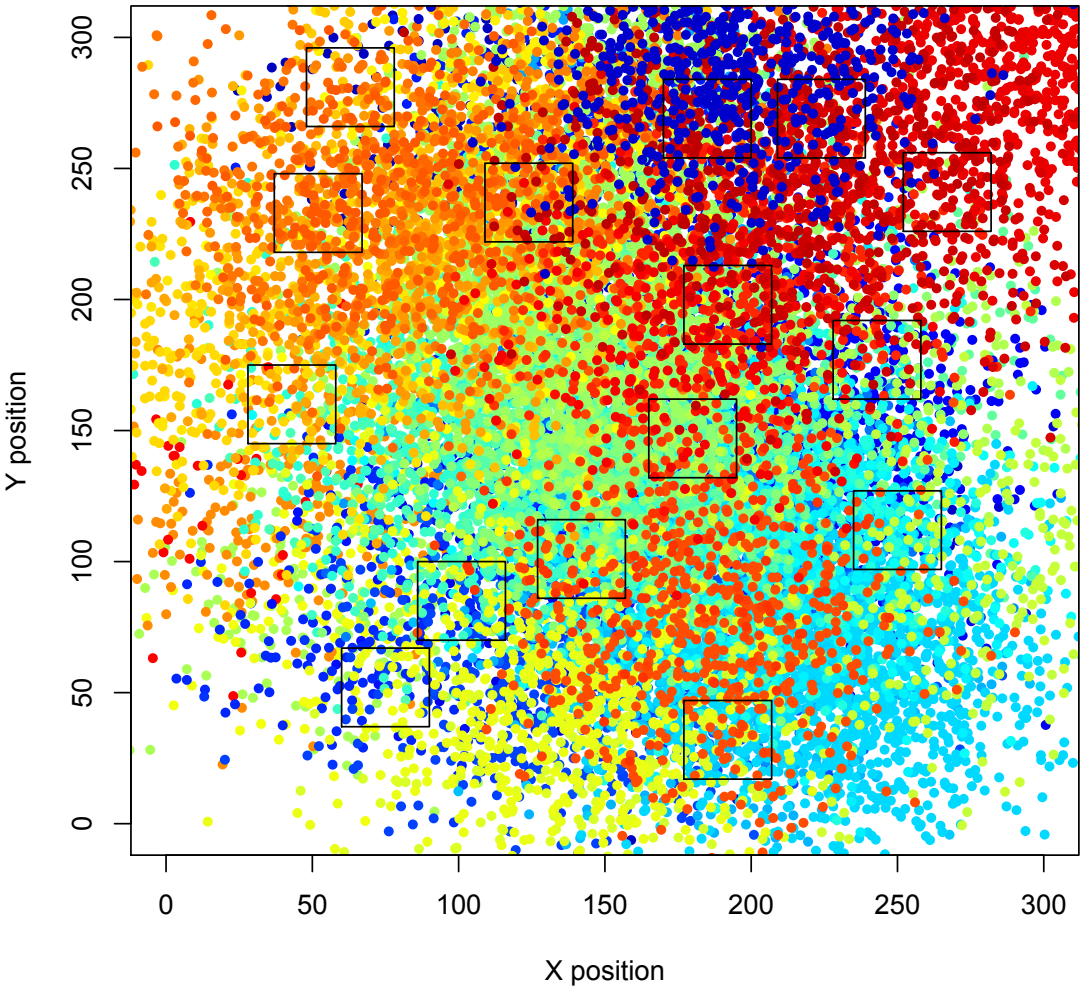

Figure S4.2. Example of a 300 x 300 m community, created using the same habitat filtering assembly parameters as those in the study. The 15, 30 x 30 m quadrats are also plotted. Each species is assigned a unique color.

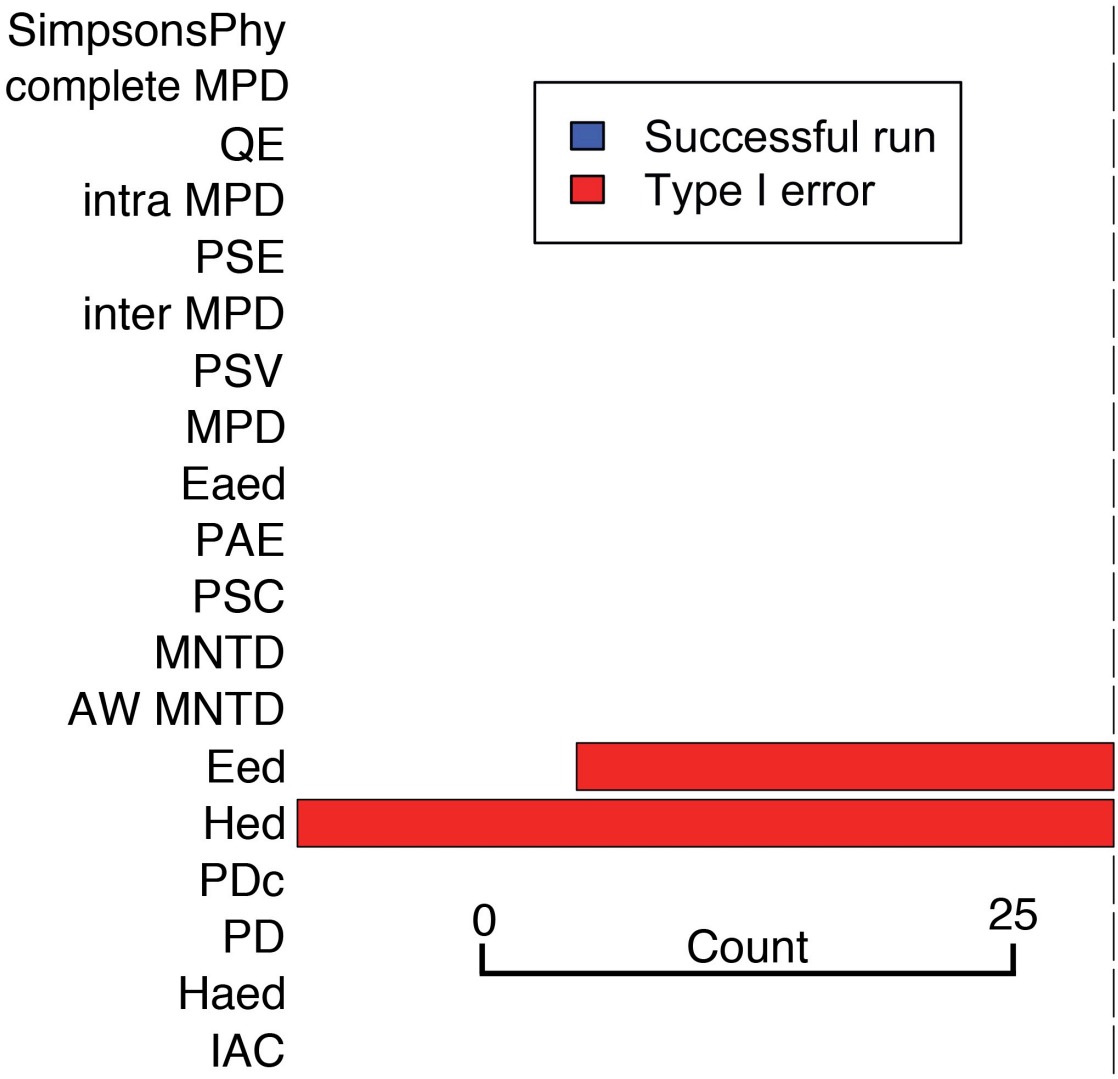

Figure S4.3. The results of a limited number of iterations testing the performance of the 19 phylogenetic community structure metrics with the 2x null (Hardy 2008) and a habitat filtering assembly process. To determine whether the lack of power in the initial metric + null performance results (Appendix S1.1) might have been a result of insufficient randomizations, each CDM was randomized 10,000 times in these tests. Due to the prohibitive computing time involved with this large number of randomizations, only 10

iterations were run and results were scaled up to 100, such that red bars represent type I error rates here (e.g., E_{ED} exhibited a 27% type I error rate).

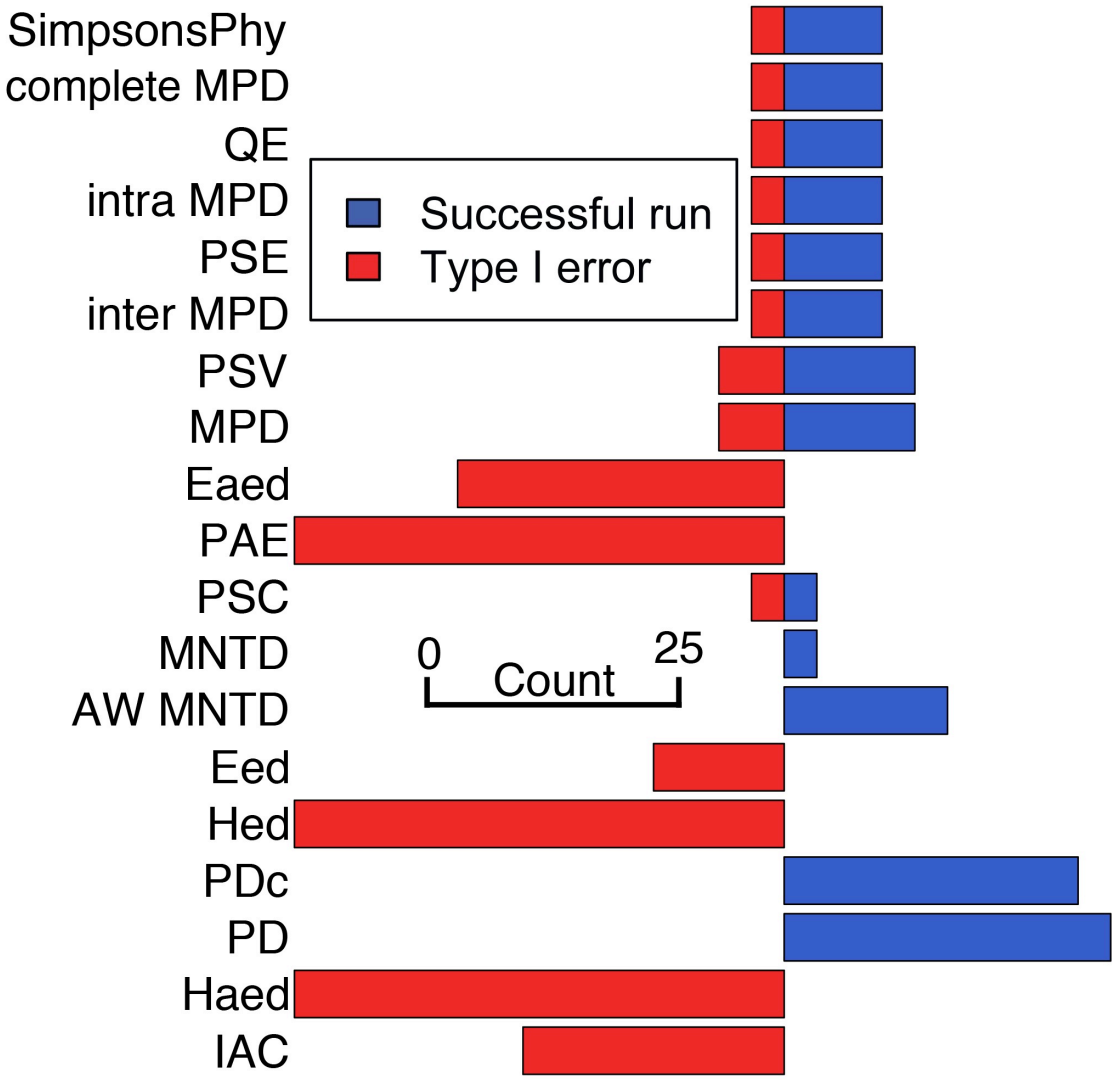

Figure S4.4. The results of 100 iterations testing the performance of the 19 phylogenetic community structure metrics with the richness null and a habitat filtering assembly process. To determine whether the initial metric + null performance results (Appendix S1.1) were sensitive to the number of individuals placed in the community, we set the

"mean.log.individuals" parameter to be equal to 3 in these tests. This generates communities with approximately the same number of individuals as the random and competitive exclusion simulations.

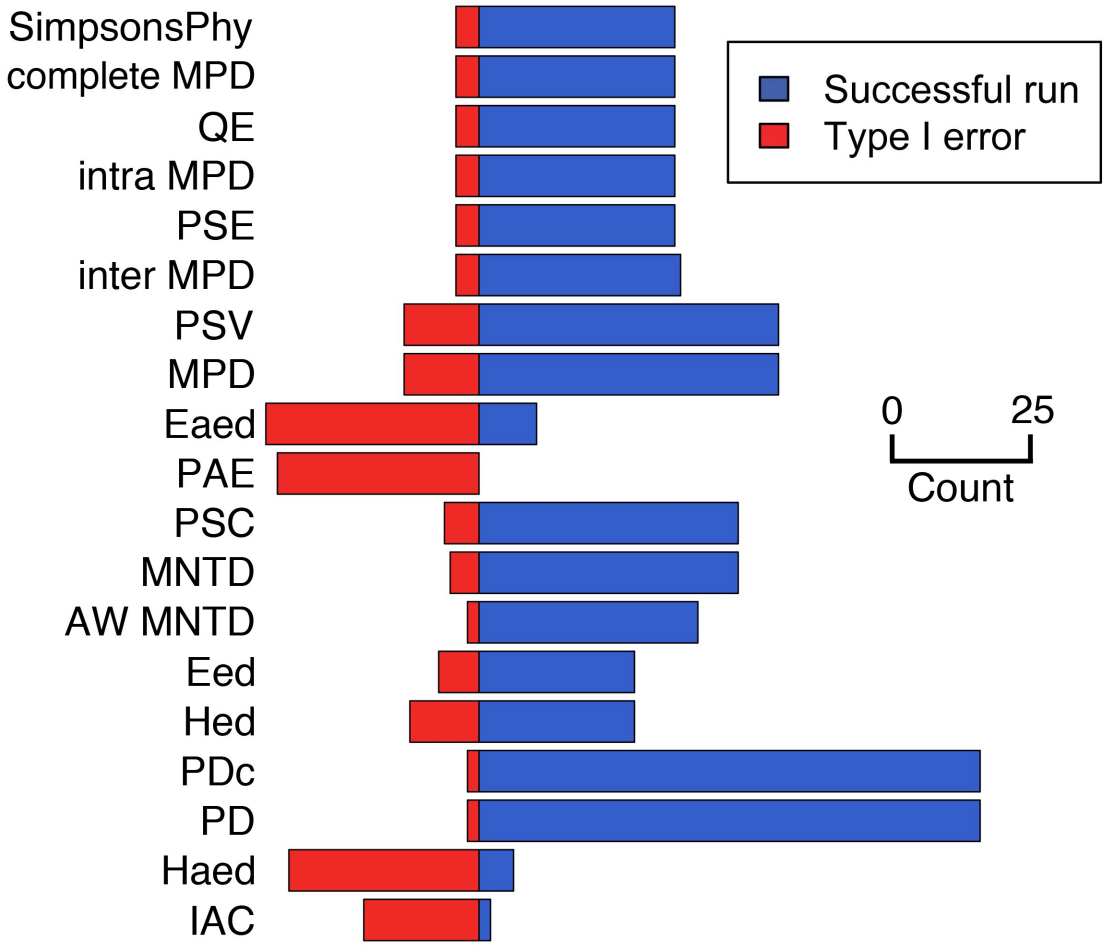

Figure S4.5. The results of 100 iterations testing the performance of the 19 phylogenetic community structure metrics with the richness null and a habitat filtering assembly process. To determine whether the initial metric + null performance results (Appendix S1.1) were sensitive to the number of randomizations of the CDM, each CDM was

randomized 10,000 times in these tests. Results were similar to those in the main text, though there is a slight increase in the power of the "tip-clustering" metrics PSC and MNTD.

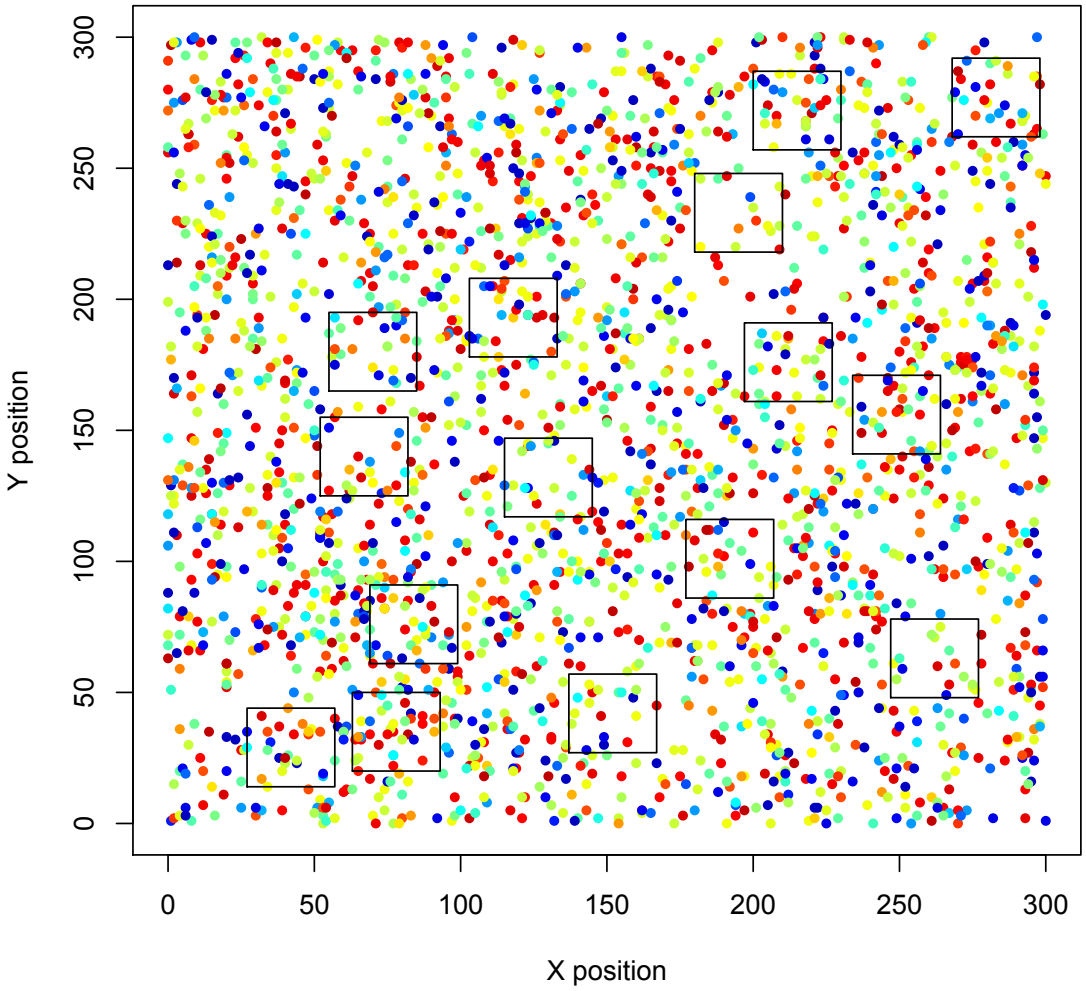

Figure S4.6. Example of a 300 x 300 m community, created using the same competitive exclusion assembly parameters as those in the study. The 15, 30 x 30 m quadrats are also plotted. Each species is assigned a unique color, though with 100 species they cannot be readily distinguished from one another.

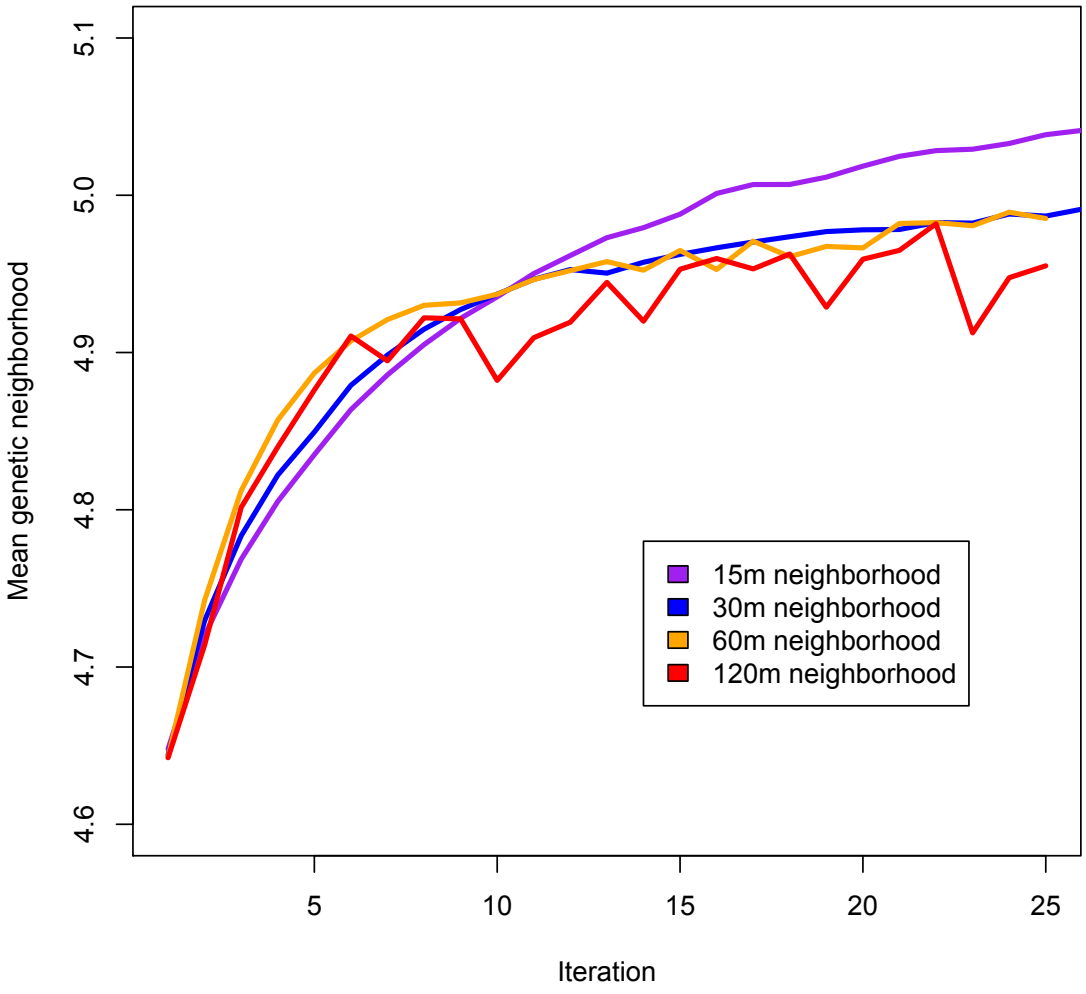

Figure S4.7. Change in the mean genetic neighborhood over 25 generations of the competitive exclusion assembly for four different interaction distances. The mean genetic neighborhood is defined as the mean of the mean of pairwise phylogenetic distances among an individual and all individuals within the interaction distance, for all individuals

in the community. Across a wide range of interaction distances, the general pattern of increasing phylogenetic overdispersion is evident.

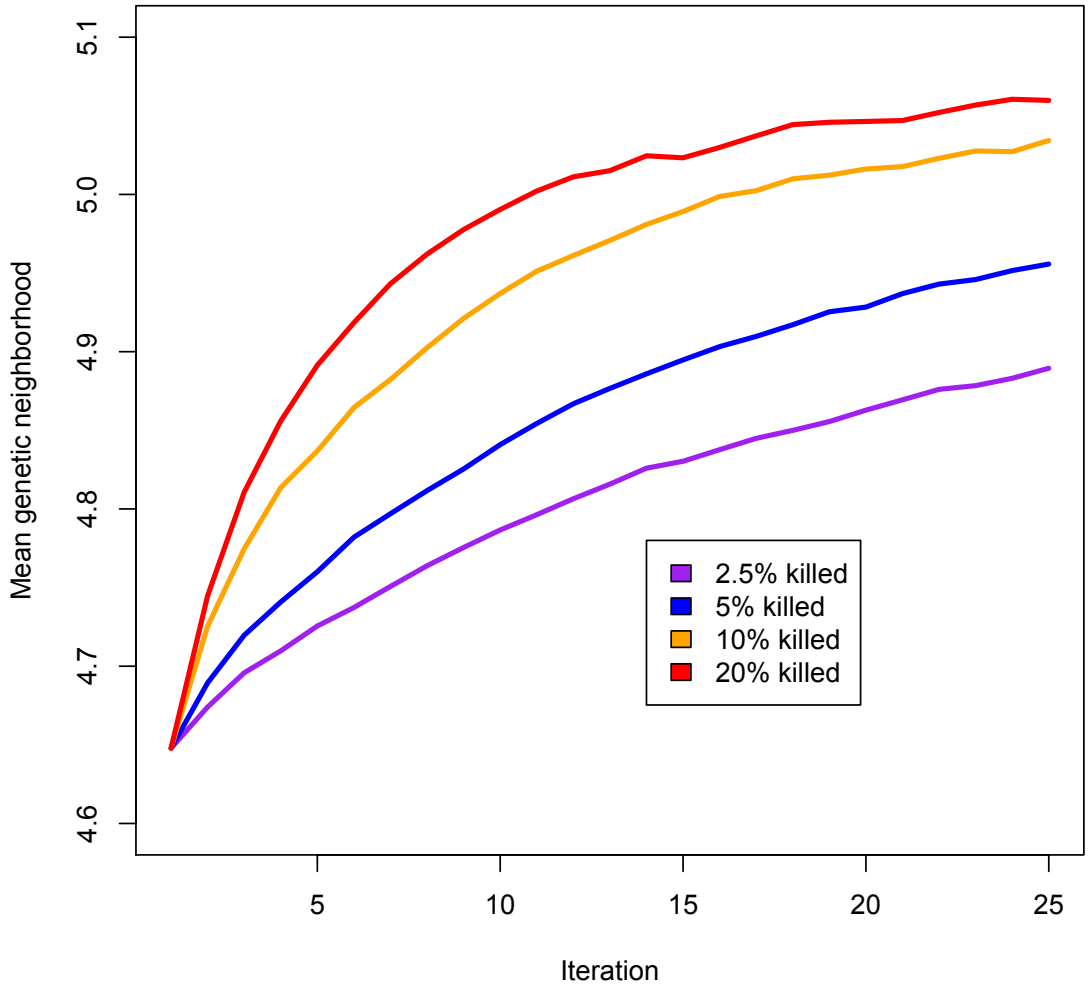

Figure S4.8. Change in the mean genetic neighborhood over 25 generations of the competitive exclusion assembly for four different percent killed parameters. The mean genetic neighborhood is defined as the mean of the mean of pairwise phylogenetic

distances among an individual and all individuals within the interaction distance, for all individuals in the community. Across a wide range of percent killed parameters, the general pattern of increasing phylogenetic overdispersion is evident. Based on these preliminary results, it appears that removing ("killing") a small percentage (e.g., 2.5%) of individuals each generation would ultimately generate a similar pattern to removing a large percentage (e.g., 20%).

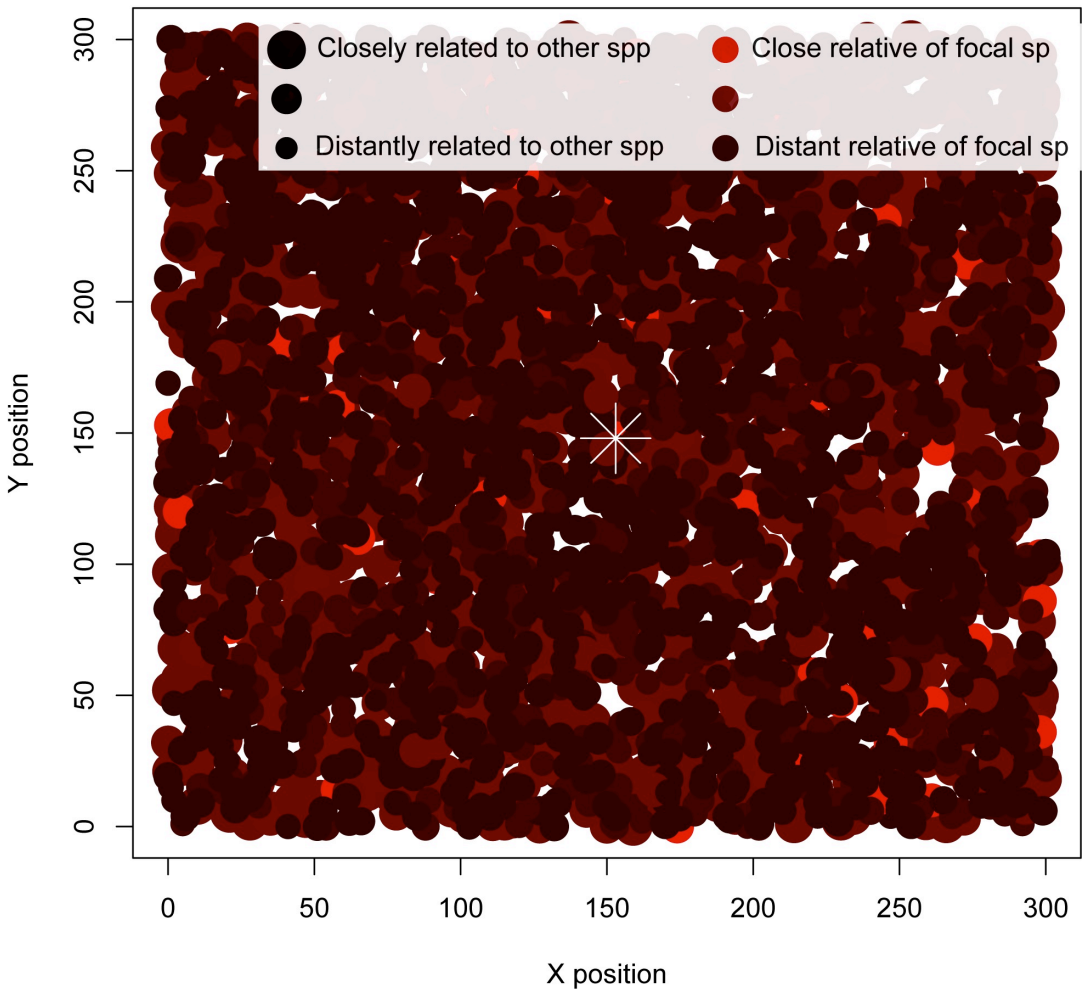

Figure S4.9. Example of a 300 x 300 m random assembly community, created using the same parameters as those in the study. Here, a random individual was selected near the center of the community (marked with a white asterisk). Individuals were then color-coded as a function of their relatedness to the focal individual, where bright red indicates a member of the same species. The size of individual dots was scaled according to their mean relatedness to all other species in the phylogeny, such that large dots indicate a member of a species with many close relatives. In this random community, bright red dots occasionally occur close together, and on average the plot is "redder" then Fig. S4.10. Also, the dots in the plot appear to be more uniform in size.

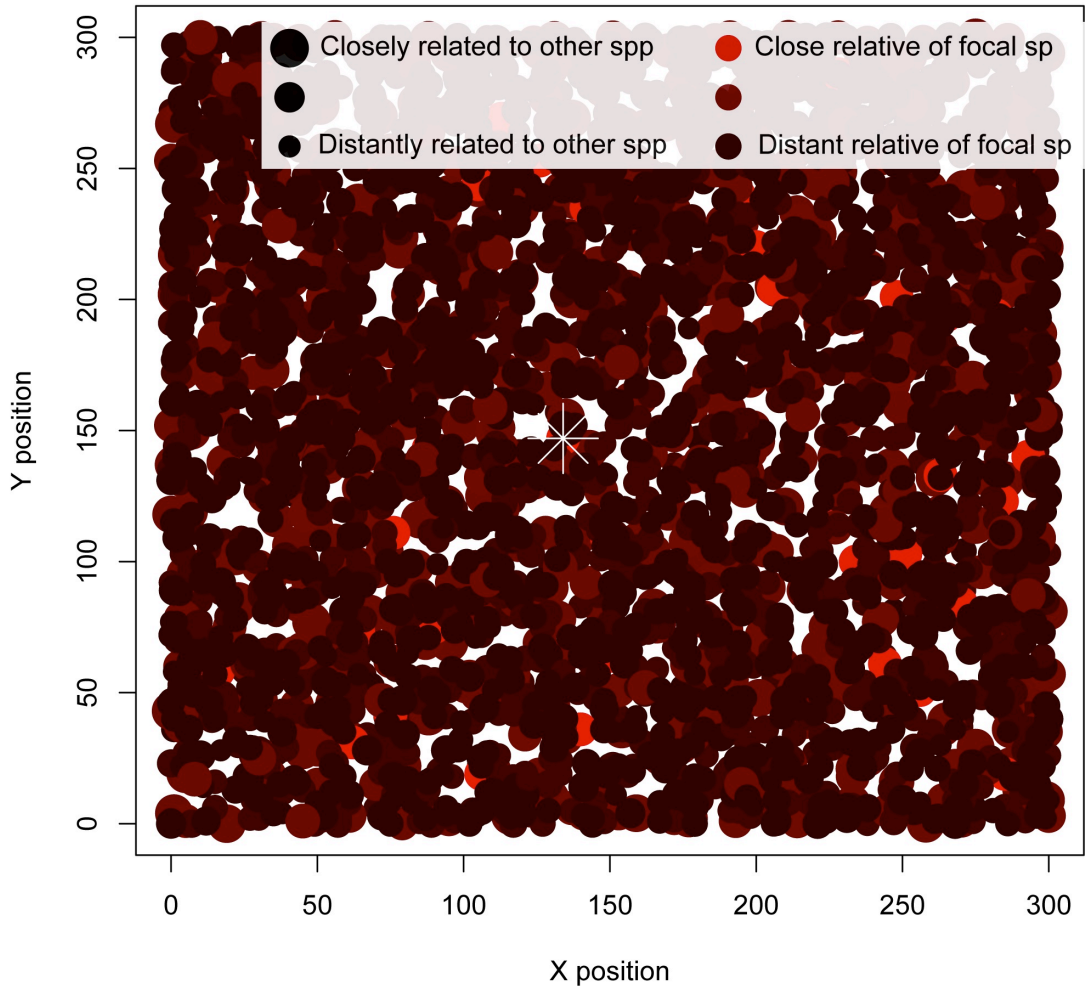

Figure S4.10. Example of a 300 x 300 m competitive exclusion community, created using the same parameters as those in the study. The community from Fig. S4.9 was used as a starting point. An individual of the same species as that figure was selected near the center of the community (marked with a white asterisk). Individuals were then color-coded as a function of their relatedness to the focal individual, where bright red indicates a member of the same species. The size of individual dots was scaled according to their mean relatedness to all other species in the phylogeny, such that large dots indicate a

member of a species with many close relatives. In this community, bright red dots appear regularly spaced, and on average the plot is “darker” then Fig. S4.9. Also, the dots in the plot appear to be more heterogeneous in size.

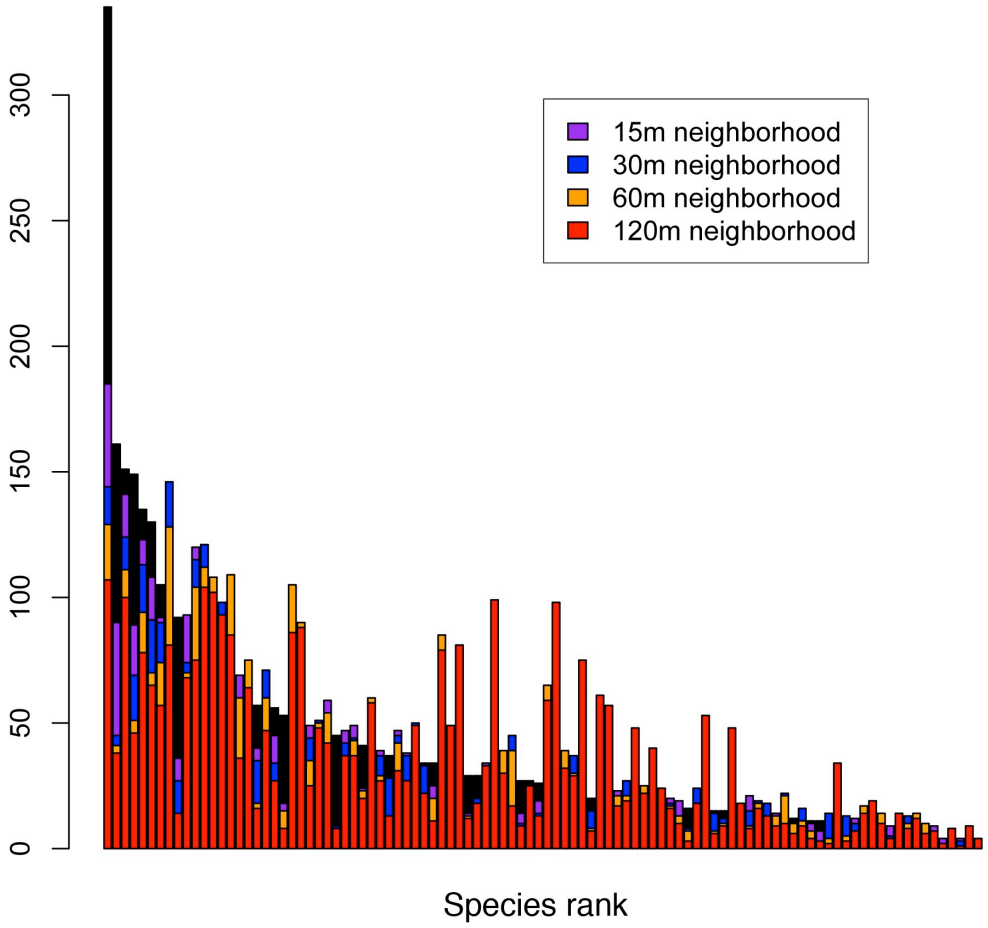

Figure S4.11. Changes in the rank abundance curve after 25 generations of the competitive exclusion assembly simulations. The initial rank abundance curve is shown in black. Increasing the interaction distance results in increasingly large deviations from

the initial rank abundance curve. Some species (e.g., 8 and 9) dramatically change abundance during these competition simulations. Four separate simulations with the same initial community and phylogeny are shown here. The similarities across the simulations are striking.

References

Hardy, O.J. (2008). Testing the spatial phylogenetic structure of local communities: statistical performances of different null models and test statistics on a locally neutral community. *Journal of Ecology*, **96**, 914–926.

Murphy, H.T., Bradford, M.G., Dalongeville, A., Ford, A.J. & Metcalfe, D.J. (2013). No evidence for long-term increases in biomass and stem density in the tropical rain forests of Australia. *Journal of Ecology*, **101**, 1589–1597.

Appendix S5. Intercorrelations among 19 phylogenetic community structure metrics.

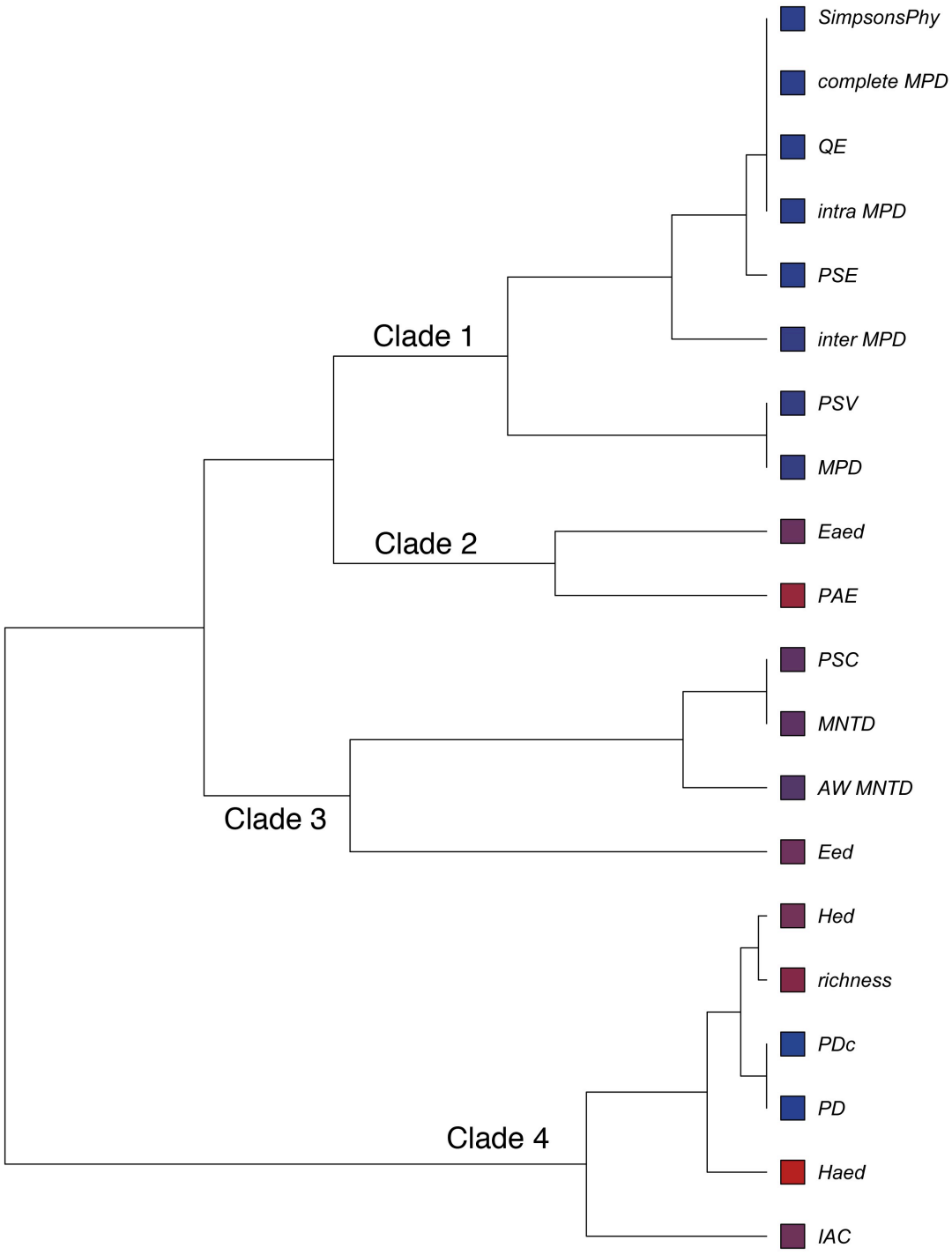

Figure S5.1. Dendrogram of intercorrelations among the phylogenetic community structure metrics (and species richness itself). This is the same topology as Fig. 2, repeated here for use with Table S5.1. Closely correlated metrics are annotated along branches. Clade 1 metrics focus on "total community relatedness"; Clade 2 metrics on the relationship between "evolutionary distinctiveness and abundance"; Clade 3 on "nearest-relative" measures of community relatedness; and Clade 4 metrics are particularly closely correlated with species richness. Tips are color-coded from blue (good) to red (poor) according to the sum of all successes (runs that successfully detected the simulated assembly process—either habitat filtering or competitive exclusion) minus the sum of all type I errors encountered during the same runs for the richness, independent swap, and regional null models.

Table S5.1. Pearson correlation coefficients among 19 phylogenetic community structure metrics. The raw values used to calculate these correlations were generated over 50,000 randomized community data matrices spanning a range of species richness values.

	Richness	MPD	Interspecific AW MPD	Intraspecific AW MPD	Complete AW MPD	MNTD	AW MNTD	PSV	PSC	PSE	PAE	IAC	Haed	Eaed	Eed	Hed	SimpsonsPhy	PD	PDc
Richness	1	0	0	0.52	0.53	-0.75	-0.61	0	-0.75	0.26	0	0.57	0.9	-0.09	-0.28	0.98	0.53	0.94	0.94
MPD	0	1	0.5	0.39	0.39	0.25	0.2	1	0.25	0.45	0	0.03	0	-0.02	0.19	0.01	0.39	0.18	0.18
Interspecific AW MPD	0	0.5	1	0.78	0.78	0.13	0.36	0.5	0.13	0.89	0.39	-0.18	0.09	0.45	0.1	0	0.78	0.08	0.08
Intraspecific AW MPD	0.52	0.39	0.78	1	1	-0.32	-0.06	0.39	-0.32	0.96	0.31	0.16	0.59	0.41	-0.07	0.53	1	0.57	0.57
Complete AW MPD	0.53	0.39	0.78	1	1	-0.33	-0.07	0.39	-0.33	0.95	0.31	0.17	0.6	0.4	-0.07	0.54	1	0.58	0.58
MNTD	-0.75	0.25	0.13	-0.32	-0.33	1	0.8	0.25	1	-0.09	0	-0.46	-0.78	-0.04	0.02	-0.8	-0.33	-0.58	-0.58
AW MNTD	-0.61	0.2	0.36	-0.06	-0.07	0.8	1	0.2	0.8	0.16	0.57	-0.52	-0.56	0.27	0.02	-0.64	-0.07	-0.47	-0.47
PSV	0	1	0.5	0.39	0.39	0.25	0.2	1	0.25	0.45	0	0.03	0	-0.02	0.19	0.01	0.39	0.18	0.18
PSC	-0.75	0.25	0.13	-0.32	-0.33	1	0.8	0.25	1	-0.09	0	-0.46	-0.78	-0.04	0.02	-0.8	-0.33	-0.58	-0.58
PSE	0.26	0.45	0.89	0.96	0.95	-0.09	0.16	0.45	-0.09	1	0.35	-0.04	0.34	0.51	0.01	0.26	0.95	0.33	0.33
PAE	0	0	0.39	0.31	0.31	0	0.57	0	0	0.35	1	-0.26	0.11	0.5	0	0	0.31	0	0
IAC	0.57	0.03	-0.18	0.16	0.17	-0.46	-0.52	0.03	-0.46	-0.04	-0.26	1	0.69	-0.4	-0.3	0.63	0.17	0.62	0.62
Haed	0.9	0	0.09	0.59	0.6	-0.78	-0.56	0	-0.78	0.34	0.11	0.69	1	0.08	-0.17	0.94	0.6	0.86	0.86
Eaed	-0.09	-0.02	0.45	0.41	0.4	-0.04	0.27	-0.02	-0.04	0.51	0.5	-0.4	0.08	1	0.32	-0.1	0.4	-0.18	-0.18
Eed	-0.28	0.19	0.1	-0.07	-0.07	0.02	0.02	0.19	0.02	0.01	0	-0.3	-0.17	0.32	1	-0.21	-0.07	-0.34	-0.34
Hed	0.98	0.01	0	0.53	0.54	-0.8	-0.64	0.01	-0.8	0.26	0	0.63	0.94	-0.1	-0.21	1	0.54	0.94	0.94
SimpsonsPhy	0.53	0.39	0.78	1	1	-0.33	-0.07	0.39	-0.33	0.95	0.31	0.17	0.6	0.4	-0.07	0.54	1	0.58	0.58
PD	0.94	0.18	0.08	0.57	0.58	-0.58	-0.47	0.18	-0.58	0.33	0	0.62	0.86	-0.18	-0.34	0.94	0.58	1	1
PDc	0.94	0.18	0.08	0.57	0.58	-0.58	-0.47	0.18	-0.58	0.33	0	0.62	0.86	-0.18	-0.34	0.94	0.58	1	1

Package 'metricTester'

May 1, 2014

Title Explore behavior of phylogenetic community structure metrics

Description Explore the behavior and performance of phylogenetic metrics and nulls

Version 0.1

Author Eliot Miller, Chris Trisos & Damien Farine

Maintainer Eliot Miller <eliot.isaac@gmail.com>

Depends R (>= 3.0.0), phylobase, ecoPDcorr, geiger, spacodiR

License GPL-3

LazyData true

R topics documented:

`abundanceVector` *Generate regional abundance vector*

Description

Given a community data matrix of sites by species, extract the column-wise sums (the total number of individuals of each species) and expand to create a regional abundance vector.

Usage

```
abundanceVector(cdm)
```

Arguments

`cdm`	Community data matrix in picante format

Details

Simple function to create a regional abundance vector given a "regional" community data matrix.

Value

A character vector in the form "s1, s1, s1, s2, s2, s3, etc".

References

Miller, Trisos and Farine.

Examples

```
library(plyr)
library(geiger)
library(picante)

#simulate tree with birth-death process
tree <- sim.bdtree(b=0.1, d=0, stop="taxa", n=50)

sim.abundances <- round(rlnorm(5000, meanlog=2, sdlog=1))

cdm <- simulateComm(tree, min.rich=10, max.rich=25, abundances=sim.abundances)

abund <- abundanceVector(cdm)
```

`allMetrics` *Calculate phylogenetic community structure metrics*

Description

Given a phylo object, and a picante-style community data matrix (sites are rows, species are columns), calculate all phylogenetic community structure metrics of interest.

Usage

```
allMetrics(tree, picante_cdm)
```

Arguments

`tree`	Phylo object
`picante_cdm`	A picante-style community data matrix with sites as rows, and species as columns

Details

Currently we are calculating 19 phylogenetic community structure metrics

Value

A data frame with the calculated 19 metrics and the associated species richness of all input "communities".

References

Miller, Trisos and Farine.

Examples

```
library(geiger)
library(picante)

#simulate tree with birth-death process
tree <- sim.bdtree(b=0.1, d=0, stop="taxa", n=50)

sim.abundances <- round(rlnorm(5000, meanlog=2, sdlog=1))

cdm <- simulateComm(tree, min.rich=10, max.rich=25, abundances=sim.abundances)

results <- allMetrics(tree, cdm)
```

`allMetricsNull` *Generate null expectations for community structure metrics*

Description

Given a phylo object, a picante-style community data matrix (sites are rows, species are columns), a desired null method (any of picante or also 2x, 3x, 1s, & 2s of spacodiR), a desired number of randomizations, and an output file name, will shuffle matrix according to null method, then calculate all phylogenetic community structure metrics as defined in the allMetrics() function, then save each iteration's worth of shufffled values to a csv file for later import. Also calculates the richness of the corresponding community.

Usage

```
allMetricsNull(tree, orig.matrix, null.method, regional.abundance,
  no.randomizations, temp.file)
```

Arguments

`tree`	Phylo object
`orig.matrix`	A picante-style community data matrix with sites as rows, and species as columns
`null.method`	A picante-style null, e.g. "richness" or "frequency", or "2x", "3x" "1s" or "2s", which will call spacodiR. It can also now accomodate calls to "regionalNull"
`regional.abundance`	Optional vector of species names repeated the number of times present in the regional abundance pool. For use with regionalNull.
`no.randomizations`	The desired number of no.randomizations the function will run, i.e. the number of times orig.matrix will be shuffled and the metrics calculated on it
`temp.file`	The desired name of the output csv file

Details

This runs much faster than trying to do this in memory in R. I will upload some of those type of functions in the near future anyhow. If you call null metrics 2x, 3x, 1s or 2s, it will call spacodiR for the resampling

Value

A csv file with each column equal to the value of a given metric for the shuffled community in question (a row in the input matrix).

References

Miller, Trisos and Farine.

Examples

```
library(geiger)
library(picante)
library(spacodiR)

#simulate tree with birth-death process
tree <- sim.bdtree(b=0.1, d=0, stop="taxa", n=50)

sim.abundances <- round(rlnorm(5000, meanlog=2, sdlog=1))

cdm <- simulateComm(tree, min.rich=10, max.rich=25, abundances=sim.abundances)

system.time(allMetricsNull(tree=tree, orig.matrix=cdm, null.method="richness",
no.randomizations=10, temp.file="output.csv"))
```

---

compareMins *Utility function to identify minimum values*

Description

Given a vector where the last element is the minimum, identifies which elements in that vector match the last element.

Usage

```
compareMins(x)
```

Arguments

x	A vector

Details

Simple utility function

Value

A logical vector of length input vector minus 1, corresponding to whether an element of the input vector equals the last element of the input vector.

References

Miller, Trisos and Farine.

Examples

```
#create a basic input vector
temp <- c(1,2,3,4,5,6,1)

#use the compareMins function
compareMins(temp)
```

`competitionLooper` *Test metrics across multiple competitive simulation arenas*

Description

Large, somewhat sloppy function tying many previous functions together into a single competitive exclusion simulator function that generates spatial arenas, samples quadrats, generates null expectations, tests for significance of observed metrics, and summarizes results as a matrix of type I and type II error rates.

Usage

```
competitionLooper(no.species, x.min, x.max, y.min, y.max, no.quadrats,
  quadrat_size, mean.log.individuals, max.distance, percent.killed,
  competition.randomizations, null.method, concatBYrichness = TRUE,
  no.randomizations, expectation, wrong, no.metrics, iterations, temp.file,
  output.file)
```

Arguments

`no.species`	Number of species in each arena
`x.min`	Minimum X coordinate of arena, e.g. 0
`x.max`	Maximum X coordinate of arena
`y.min`	Minimum Y coordinate of arena, e.g. 0
`y.max`	Maximum Y coordinate of arena
`no.quadrats`	Number of quadrats to sample
`quadrat_size`	Size of an individual quadrat
`mean.log.individuals`	Mean log of abundance vector from which species abundances will be drawn
`max.distance`	The geographic distance within which geographically neighboring indivduals should be considered to influence the individual in question.
`percent.killed`	The percent of individuals in the total arena that should be considered (as a proportion, e.g. 0.5 = half)
`competition.randomizations`	The number of generations per competitive exclusion arena simulation
`null.method`	A picante-style null, e.g. "richness" or "frequency"
`concatBYrichness`	Whether to concatenate null results by the richness of the randomized quadrat (the default), or by the quadrat ID (traditional method)
`no.randomizations`	Number of iterations the function should run, i.e. the number of times the orig.matrix will be shuffled and the metrics calculated on it
`expectation`	Expected value: 0=not significant, 1=clustered, 2=overdispersed
`wrong`	Value of a typeI error rate, e.g. 2 if expecting 1.
`no.metrics`	Need to specify how many metrics are being tested
`iterations`	Number of arenas to simulate and test
`temp.file`	File name of output file where null metric values are saved to. Re-written each iteration
`output.file`	File name of results file

Details

Could easily modify this function to save more information than it currently does, though obviously beware the additional space such an operation might require. A single null.csv file for 19 metrics by 1000 iterations is about ~50 megabytes. The results matrix is also written to csv in case the function crashes part-way through.

Value

Two csvs and a matrix of results summarizing the type I and type II errors across all metrics and spatial simulations. One csv is just a temporary file storing the null expectations, the other is a csv of the same thing as the output matrix.

References

Miller, Trisos and Farine.

Examples

```
library(ape)
library(geiger)
library(colorRamps)
library(plyr)
library(picante)

competitionLooper(no.species=50, x.min=0, x.max=300, y.min=0, y.max=300, no.quadrats=15,
quadrat_size=50, mean.log.individuals=3.2, max.distance=15, percent.killed=0.2,
competition.randomizations=25, null.method="richness", concatBYrichness=TRUE,
no.randomizations=2, expectation=2, wrong=1, no.metrics=19, iterations=2,
temp.file="deleteme.csv", output.file="confused.csv")
```

---

competitionSimulator *Simulate competitive exclusion over generations*

Description

Given a phylogenetic tree, a spatial arena of individuals with species identities, and arguments for the desired distance and percent removed, removes some of the most closely related individuals in the arena, settles individuals based on abundances from a regional species pool, and repeats across the desired number of generations.

Usage

```
competitionSimulator(tree, initialArena, max.distance, percent.killed,
  iterations)
```

Arguments

tree	Phylo object
initialArena	A spatial arena with three columns: individuals (the species ID), X (the x axis location of that individual), and Y (the y axis location). The initialArena actually needs a number of other elements in order for later functions to work properly, so any modifications to the code should take note of this.

max.distance	The geographic distance within which geographically neighboring indivduals should be considered to influence the individual in question.
percent.killed	The percent of individuals in the total arena that should be considered (as a proportion, e.g. 0.5 = half).
iterations	Number of generations to repeat simulation for.

Details

This function combines the killSome and settleSome functions into a loop that runs for the desired number of generations.

Value

A list of 5 elements: the average relatedness in the geographic neighbordhood of consideration (appended to any previous values that were fed into the function), the number of individuals killed, the original input regional abundance vector, the new spatial arena, and the dimensions of that arena. On the last iteration, it returns the arena BEFORE settling new individuals randomly.

References

Miller, Trisos and Farine.

Examples

```
library(geiger)

#simulate tree with birth-death process
tree <- sim.bdtree(b=0.1, d=0, stop="taxa", n=50)

#create a random arena
arena <- randomArena(tree, x.min=0, x.max=300, y.min=0, y.max=300, mean.log.individuals=3)

#run the competitionSimulator for 25 generations
temp <- competitionSimulator(tree, arena, 30, 0.2, 25)

#create a quick vector for plotting
generations <- 1:25

#plot the average relatedness in geographic neighborhoods over generations
plot(temp$related[2:length(temp$related)]~generations)
```

---

filteringLooper *Test metrics across multiple arenas*

Description

Large, somewhat sloppy function tying many previous functions together into a single habitat filtering simulator function that generates spatial arenas, samples quadrats, generates null expectations, tests for significance of observed metrics, and summarizes results as a matrix of type I and type II error rates.

Usage

```
filteringLooper(no.species, x.min, x.max, y.min, y.max, no.quadrats,
  quadrat_size, mean.log.individuals, length.parameter, sd.parameter,
  null.method, concatBYrichness = TRUE, no.randomizations, expectation, wrong,
  no.metrics, iterations, temp.file, output.file)
```

Arguments

no.species	Number of species in each arena
x.min	Minimum X coordinate of arena, e.g. 0
x.max	Maximum X coordinate of arena
y.min	Minimum Y coordinate of arena, e.g. 0
y.max	Maximum Y coordinate of arena
no.quadrats	Number of quadrats to sample
quadrat_size	Size of an individual quadrat
mean.log.individuals	Mean log of abundance vector from which species abundances will be drawn
length.parameter	Length of vector from which species' locations are drawn. Large values of this parameter dramatically decrease the speed of the function but result in nicer looking communities
sd.parameter	Standard deviation of vector from which species' locations are drawn
null.method	A picante-style null, e.g. "richness" or "frequency"
concatBYrichness	Whether to concatenate null results by the richness of the randomized quadrat (the default), or by the quadrat ID (traditional method)
no.randomizations	Number of iterations the function should run, i.e. the number of times the orig.matrix will be shuffled and the metrics calculated on it
expectation	Expected value: 0=not significant, 1=clustered, 2=overdispersed
wrong	Value of a typeI error rate, e.g. 2 if expecting 1.
no.metrics	Need to specify how many metrics are being tested
iterations	Number of arenas to simulate and test
temp.file	File name of output file where null metric values are saved to. Re-written each iteration
output.file	File name of results file

Details

Could easily modify this function to save more information than it currently does, though obviously beware the additional space such an operation might require. A single null.csv file for 19 metrics by 1000 iterations is about ~50 megabytes. The results matrix is also written to csv in case the function crashes part-way through.

Value

Two csvs and a matrix of results summarizing the type I and type II errors across all metrics and spatial simulations. One csv is just a temporary file storing the null expectations, the other is a csv of the same thing as the output matrix.

References

Miller, Trisos and Farine.

Examples

```
library(ape)
library(geiger)
library(colorRamps)
library(plyr)
library(picante)

filteringLooper(no.species=50, x.min=0, x.max=300, y.min=0, y.max=300, no.quadrats=15,
quadrat_size=50, mean.log.individuals=4, length.parameter=5000, sd.parameter=50,
null.method="richness", concatBYrichness=TRUE, no.randomizations=2, expectation=1,
wrong=2, no.metrics=19, iterations=3, temp.file="deleteme.csv",
output.file="confused.csv")
```

---

killSome *Remove most closely related individuals*

Description

Given a phylogenetic tree, a spatial arena of individuals with species identities, and arguments for the desired distance and percent removed, removes some of the most closely related individuals in the arena.

Usage

```
killSome(tree, arenaOutput, max.distance, percent.killed)
```

Arguments

tree	Phylo object
arenaOutput	A spatial arena with three columns: individuals (the species ID), X (the x axis location of that individual), and Y (the y axis location). The arenaOutput actually needs a number of other elements in order for later functions to work properly, so any modifications to the code should take note of this.
max.distance	The geographic distance within which geographically neighboring indivduals should be considered to influence the individual in question.
percent.killed	The percent of individuals in the total arena that should be considered (as a proportion, e.g. 0.5 = half).

Details

This function identifies individuals in the most genetically clustered geographic neighborhoods, continues on to identify the most closely related individual to a focal individual, and randomly chooses whether to remove that individual or the focal individual. It expects a list with a number of additional elements beyond the arena (currently, the mean genetic relatedness of geographic neighborhoods, a vector of regional abundance [where each element is a species name, repeated as many times as is present in pool], and the dimensions of the arena).

Value

A list of 5 elements: the average relatedness in the geographic neighbordhood of consideration (appended to any previous values that were fed into the function), the number of individuals killed, the original input regional abundance vector, the new spatial arena, and the dimensions of that arena.

References

Miller, Trisos and Farine.

Examples

```
library(geiger)

#simulate tree with birth-death process
tree <- sim.bdtree(b=0.1, d=0, stop="taxa", n=50)

arena <- randomArena(tree, x.min=0, x.max=300, y.min=0, y.max=300, mean.log.individuals=2)

new.arena <- killSome(tree, arenaOutput=arena, max.distance=50, percent.killed=0.2)

dim(arena$arena)
dim(arena$new.arena)
```

---

lengthNonZeros *Calculate the species richness of a community*

Description

Given a vector of abundances or presence/absences from a community data matrix, will calculate the species richness of that community.

Usage

```
lengthNonZeros(input.vector)
```

Arguments

input.vector	A vector from a community data matrix of abundances.

Details

An internal function to calculate richness of a cdm.

Value

A named vector of species richness.

References

Miller, Trisos and Farine.

Examples

```
library(geiger)
library(picante)

#simulate tree with birth-death process
tree <- sim.bdtree(b=0.1, d=0, stop="taxa", n=50)

sim.abundances <- round(rlnorm(5000, meanlog=2, sdlog=1))

cdm <- simulateComm(tree, min.rich=10, max.rich=25, abundances=sim.abundances)

#note that with this example, each community in the cdm will be labeled by its richness
apply(cdm, 1, lengthNonZeros)
```

---

locationSampler *Simulate spatially explicity community*

Description

Given the results of a call to phyloNtraits(), will generate a data frame with the spatial locations of individuals and their species' identity.

Usage

```
locationSampler(phyloNtraits.results, scaled.results, mean.log.individuals,
  length.parameter, sd.parameter)
```

Arguments

phyloNtraits.results	Results of a call to phyloNtraits()
scaled.results	Results of a call to scaler(). This is theoretically optional, but if not used, one probably has to provide just the data frame of the results from the phyloNtraits call
mean.log.individuals	Mean log of abundance vector from which species abundances will be drawn
length.parameter	Length of vector from which species' locations are drawn. Large values of this parameter dramatically decrease the speed of the function but result in nicer looking communities
sd.parameter	Standard deviation of vector from which species' locations are drawn

Details

Should be sped up by removing for loops and inserting new mini-functions then applying them with e.g. mapply(). Regardless, it works somewhat quickly. It takes results of calls to phyloNtraits() and, if desired, scaler(), and given the input parameters mean log of individuals in the resulting community, the length of the vector from which a species' X & Y coordinates will drawn, and the sd of that vector, it returns a dataframe of species and their X Y coordinates. The distribution of abundances among species follows a log-normal distribution. The distribution of individuals within species follows a normal distribution.

Value

A data frame with X & Y coordinates for all individuals and their species identity

References

Miller, Trisos and Farine.

Examples

```
library(geiger)

results <- phyloNtraits(50)

scaled <- scaler(results[[2]], min.arena=0, max.arena=300)

positions <- locationSampler(phyloNtraits.results=results, scaled.results=scaled,
mean.log.individuals=4, length.parameter=5000, sd.parameter=50)
```

---

modified.mpd *Calculate different versions of abundance-weighted MPD*

Description

Given a picante-style community data matrix (sites are rows, species are columns), a phylogenetic distance matrix, and a desired method of abundance-weighting, will calculate MPD.

Usage

```
modified.mpd(samp, dis, abundance.weighted = FALSE)
```

Arguments

samp	A picante-style community data matrix with sites as rows, and species as columns
dis	Phylogenetic distance matrix
abundance.weighted	One of either "FALSE", "interspecific", "intraspecific", or "complete"

Details

To be explained in forthcoming publication

Value

A vector of MPD values, calculated according to the abudance-weighted method specified

References

Miller, Trisos and Farine.

Examples

```
library(geiger)
library(picante)

#simulate tree with birth-death process
tree <- sim.bdtree(b=0.1, d=0, stop="taxa", n=50)

sim.abundances <- round(rlnorm(5000, meanlog=2, sdlog=1))

cdm <- simulateComm(tree, min.rich=10, max.rich=25, abundances=sim.abundances)

dists <- cophenetic(tree)

results <- modified.mpd(cdm, dists, abundance.weighted = "interspecific")
```

---

phyloNtraits *Generate phylogeny with trait data*

Description

Given a desired number of species, will generate a tree with that many species and associated trait data for two traits following a Brownian motion evolution model.

Usage

```
phyloNtraits(no.species)
```

Arguments

no.species	Desired number of species in resulting phylogeny

Details

Uses geiger's sim.bdtree function with b=0.1 and d=0. Evolves two traits up phylogeny with Brownian motion evolution process. Sigma from the Brownian motion process is set to 0.1 and cannot currently be manipulated without modifying and redefining the function itself.

Value

A list where the first object is a phylogeny with the desired number of species and the second object is a matrix of trait values for those species.

References

Miller, Trisos and Farine.

Examples

```
library(geiger)

results <- phyloNtraits(50)
```

psc.corr *Calculate corrected PSC*

Description

Given a phylo object and a picante-style community data matrix (sites are rows, species are columns), calculated corrected phylogenetic species clustering

Usage

```
psc.corr(samp, tree)
```

Arguments

tree	Phylo object
samp	A picante-style community data matrix with sites as rows, and species as columns

Details

Returns the inverse of psc as defined in picante

Value

A data frame of correctly calculated PSC values, with associated species richness and name of all communities in input cdm

References

Helmus et al 2007

Examples

```
library(geiger)
library(picante)

#simulate tree with birth-death process
tree <- sim.bdtree(b=0.1, d=0, stop="taxa", n=50)

sim.abundances <- round(rlnorm(5000, meanlog=2, sdlog=1))

cdm <- simulateComm(tree, min.rich=10, max.rich=25, abundances=sim.abundances)

results <- psc.corr(samp=cdm, tree=tree)
```

quadratContents *Identify individuals contained within a quadrat*

Description

Given a spatially explicit data frame of individual locations in a simulated arena, and the bounds of a series of quadrats, identifies the contents of each quadrat.

Usage

```
quadratContents(positions, quadrat_bounds)
```

Arguments

positions	Data frame of three columns: "individuals", "X", and "Y"
quadrat_bounds	Matrix of X Y coordinates of quadrats

Details

Takes a data frame like that returned from locationSampler(), and a matrix like that returned from quadratPlacer(), and returns the resulting community data matrix such as might be generated by someone surveying a forest plot. There is a check added so that if any quadrat has < 2 species the function returns FALSE. There is probably a better way to do this, but this works.

Value

A matrix with species as rows and quadrats as columns. Quadrats are unnamed

References

Miller, Trisos and Farine.

Examples

```
library(geiger)
library(colorRamps)

temp <- phyloNtraits(50)

scaled <- scaler(temp[[2]], min.arena=0, max.arena=300)

phydistmatrix <- cophenetic(temp[[1]])

#define a color for each species
cols <- blue2green2red(nrow(phydistmatrix))

positions <- locationSampler(phyloNtraits.results=temp, scaled.results=scaled,
mean.log.individuals=4, length.parameter=5000, sd.parameter=50)

#plot the arena. dont close the window
plot(positions$X, positions$Y, pch=20, cex=0.5, xlim=c(0,300), ylim=c(0,300),
col=cols[positions$individuals])
```

```
bounds <- quadratPlacer(no.quadrats=15, x.max=300, y.max=300, quadrat_size=50)

quadratPlotter(bounds)

#this community data matrix is not in picante format, use t()
temp.cdm <- quadratContents(positions, bounds)
```

---

quadratPlacer *Randomly place quadrats in arena*

Description

Given a desired number of quadrats, the arena size, and the quadrat size, will attempt to place quadrats down in a non-overlapping fashion

Usage

```
quadratPlacer(no.quadrats, x.max, y.max, quadrat_size)
```

Arguments

no.quadrats	Number of quadrats to place
x.max	Maximum x bounds of arena
y.max	Maximum y bounds of arena
quadrat_size	Size of desired quadrat

Details

Places quadrats down in non-overlapping fashion according to parameters supplied. Will run indefinitely if unacceptable parameters are supplied, but will not crash.

Value

A matrix with the X & Y coordinates of the four corners of each quadrat placed

References

Miller, Trisos and Farine.

Examples

```
bounds <- quadratPlacer(no.quadrats=15, x.max=300, y.max=300, quadrat_size=50)
```

quadratPlotter *Plot simulated quadrats in arena*

Description

Given a matrix of quadrat bounds, plots the quadrats in an already plotted, simulated arena

Usage

```
quadratPlotter(quadrat_bounds)
```

Arguments

quadrat_bounds	Matrix of quadrat bounds

Details

Plots quadrats as defined by the supplied matrix, e.g. a call to quadratPlacer An active plot with the simulated arena needs to already be open, see example.

Value

Plotted quadrats

References

Miller, Trisos and Farine.

Examples

```
library(geiger)
library(colorRamps)

temp <- phyloNtraits(50)

scaled <- scaler(temp[[2]], min.arena=0, max.arena=300)

phydistmatrix <- cophenetic(temp[[1]])

#define a color for each species
cols <- blue2green2red(nrow(phydistmatrix))

positions <- locationSampler(phyloNtraits.results=temp, scaled.results=scaled,
mean.log.individuals=4, length.parameter=5000, sd.parameter=50)

#plot the arena. dont close the window
plot(positions$X, positions$Y, pch=20, cex=0.5, xlim=c(0,300), ylim=c(0,300),
col=cols[positions$individuals])

bounds <- quadratPlacer(no.quadrats=15, x.max=300, y.max=300, quadrat_size=50)

quadratPlotter(bounds)
```

randomArena *Generate a random spatial arena*

Description

Given a phylogenetic tree, the desired dimensions of the arena, and the mean log of the regional abundance pool, randomly generates spatial arena.

Usage

```
randomArena(tree, x.min, x.max, y.min, y.max, mean.log.individuals)
```

Arguments

tree	Phylo object
x.min	The x minimum of the output arena, e.g. 0
x.max	The x maximum of the output arena
y.min	The y minimum of the output arena, e.g. 0
y.max	The y maximum of the output arena
mean.log.individuals	Mean of the log-normal distribution

Details

This function generates a log-normal regional abundance distribution and assigns those abundances to random species. It then draws from this regional abundance distribution to settle individuals at random in the landscape.

Value

A list of 4 elements: the mean of the genetic distance matrix of the input phylogeny, the regional abundance vector (where each element is a species name, repeated as many times as is present in pool), the spatial arena, and the dimensions of that arena.

References

Miller, Trisos and Farine.

Examples

```
library(geiger)
library(colorRamps)

#simulate tree with birth-death process
tree <- sim.bdtree(b=0.1, d=0, stop="taxa", n=50)

#generate the random arena
arena <- randomArena(tree, x.min=0, x.max=300, y.min=0, y.max=300, mean.log.individuals=2)

#calculate genetic distances
gen.dists <- cophenetic(tree)
```

```
#define species colors for plotting
cols <- blue2green2red(nrow(gen.dists))

#plot the arena
plot(arena$arena$X, arena$arena$Y, pch=20, cex=0.5, xlim=c(0,300), ylim=c(0,300),
col=cols[arena$arena$individuals])
```

`randomLooper` *Test metrics across multiple random arenas*

Description

Large, somewhat sloppy function tying many previous functions together into a single simulator function that generates random spatial arenas, samples quadrats, generates null expectations, tests for significance of observed metrics, and summarizes results as a matrix of type I and type II error rates.

Usage

```
randomLooper(no.species, x.min, x.max, y.min, y.max, no.quadrats, quadrat_size,
  mean.log.individuals, null.method, concatBYrichness = TRUE,
  no.randomizations, expectation, wrong, no.metrics, iterations, temp.file,
  output.file)
```

Arguments

`no.species`	Number of species in each arena
`x.min`	Minimum X coordinate of arena, e.g. 0
`x.max`	Maximum X coordinate of arena
`y.min`	Minimum Y coordinate of arena, e.g. 0
`y.max`	Maximum Y coordinate of arena
`no.quadrats`	Number of quadrats to sample
`quadrat_size`	Size of an individual quadrat
`mean.log.individuals`	Mean log of abundance vector from which species abundances will be drawn
`null.method`	A picante-style null, e.g. "richness" or "frequency"
`concatBYrichness`	Whether to concatenate null results by the richness of the randomized quadrat (the default), or by the quadrat ID (traditional method)
`no.randomizations`	Number of iterations the function should run, i.e. the number of times the orig.matrix will be shuffled and the metrics calculated on it
`expectation`	Expected value: 0=not significant, 1=clustered, 2=overdispersed
`wrong`	Value of a typeI error rate, e.g. 2 if expecting 1.
`no.metrics`	Need to specify how many metrics are being tested
`iterations`	Number of arenas to simulate and test
`temp.file`	File name of output file where null metric values are saved to. Re-written each iteration
`output.file`	File name of results file

Details

Could easily modify this function to save more information than it currently does, though obviously beware the additional space such an operation might require. A single null.csv file for 19 metrics by 1000 iterations is about ~50 megabytes. The results matrix is also written to csv in case the function crashes part-way through.

Value

Two csvs and a matrix of results summarizing the type I and type II errors across all metrics and spatial simulations. One csv is just a temporary file storing the null expectations, the other is a csv of the same thing as the output matrix.

References

Miller, Trisos and Farine.

Examples

```
library(ape)
library(geiger)
library(colorRamps)
library(plyr)
library(picante)

randomLooper(no.species=50, x.min=0, x.max=300, y.min=0, y.max=300, no.quadrats=15,
quadrat_size=50, mean.log.individuals=3.2, null.method="richness",
concatBYrichness=TRUE, no.randomizations=2, expectation=0, wrong=1|2, no.metrics=19,
iterations=2, temp.file="deleteme.csv", output.file="random.csv")
```

---

readIn *Batch read multiple csv files to list*

Description

Read in all the files from a given directory and save each to a different element of a list.

Usage

```
readIn(path, row.names = TRUE)
```

Arguments

path	The path of the directory containing the files to be read
row.names	Do the files to be read in have row names? Default is yes. If not, set this argument to FALSE.

Details

This function reads in all the files from a given directory and stores each as a separate element in a list. The names of the original files do not matter, but the function assumes all to be comma-delimited files with the row names stored in the first column and with each column having a name. Can modify this in the future if others find it useful.

Value

A list with each file stored as a separate element.

References

Miller, Trisos and Farine.

Examples

```
#path <- "/Users/eliotmiller/Desktop/delete"

#test <- readIn(path)

#output <- matrix(0, nrow=19, ncol=3)

#for(i in 1:length(test))
#{
# output <- output + test[[i]]
#}

#output <- t(output)

#ordr <- c("IAC","Haed","PD","PD_Cadotte","Hed","Eed","AW_MNTD","NAW_MNTD","PSC","PAE",
"Eaed","NAW_MPD","PSV","inter_MPD","PSE","intra_MPD","QE","complete_MPD","SimpsonsPhy")

#output <- output[,ordr]

#dimnames(output)[[2]] <- gsub("_", " ", dimnames(output)[[2]])

#quartz(height=6, width=12)

#par(mar=c(6.6,4.1,4.1,2.1))

#barplot(output, beside=TRUE, las=2, cex.names=1, col=c("red","gray","blue"),
xlab="Metric", ylab="Count")

#legend(x=65, y=85, c("Type I error","Type II error","Successful"), fill=c("red","gray","blue"))
```

`regionalNull` *Regional null model*

Description

Entirely vectorized null model that maintains species richness (approximately only during this phase of the calculation, but we do so strictly later on), species occurrence frequency, and species abundance distributions.

Usage

```
regionalNull(cdm, tree, regional.abundance)
```

Arguments

cdm	Picante-style community data matrix with communities/quadrats/plots/etc as rows and species as columns
tree	Ape-style phylogeny
regional.abundance	Vector of species names, where each species' name is repeated the number of times necessary to accomodate its abundance in the regional species pool

Details

Although not as fast as, e.g. randomizeMatrix, this functions does not contain any for loops and so still runs decently fast. It works by drawing the total number of individuals observed in the input plot from the regional abundance vector. Thus while a randomized quadrat will not necessarily have the same number of species as the observed quadrat, over many iterations it will likely be sampled. We can then concatenate the results by richness at the end which will only compare observed values to random quadrats of the same richness. As an example, an observed quadrat might have two individuals of speciesA and two of speciesB. If the regional abundance vector is c("spA","spA","spA","spA","spB","spB","spB","spC"), and we draw four individuals, it would be possible to draw 1, 2, or 3 species, but in general, two species would be seen in the randomized quadrats.

Value

A matrix with all species in the input tree in phylogenetic order, and the same number of randomized quadrats as used in the input community data matrix

References

Miller, Trisos and Farine.

Examples

```
library(ape)
library(geiger)
library(plyr)
library(picante)

tree <- sim.bdtree(stop="taxa", n=50)

arena <- randomArena(tree, 0, 300, 0, 300, 3.2)

bounds <- quadratPlacer(15, 300, 300, 30)

temp.cdm <- quadratContents(arena$arena, bounds)

cdm <- t(temp.cdm)

regionalNull(cdm, tree, arena$regional.abundance)
```

scaler *Scale output of phyloNtraits to arena size*

Description

Given a matrix of two traits, and the minimum and maximum extent of the desired arena, will return a data frame of species' traits scaled to the new arena size.

Usage

```
scaler(input.traits, min.arena, max.arena)
```

Arguments

input.traits	Second element of the results of a call to phyloNtraits()
min.arena	Minimum size of arena, e.g. 0
max.arena	Maximum size of arena

Details

Scales a matrix of species' traits to a desired mininimum-maximum range. Intended for use in a spatially explicit scenario with two traits, but could easily be co-opted.

Value

A scaled and named dataframe of species traits

References

Miller, Trisos and Farine.

Examples

```
library(geiger)

results <- phyloNtraits(50)

scaled <- scaler(results[[2]], min.arena=0, max.arena=300)
```

settleSome *Randomly settle individuals in a spatial arena*

Description

Given output from the killSome function, randomly settles individuals in the arena.

Usage

```
settleSome(killSomeOutput)
```

Arguments

killSomeOutput Output from the killSome function

Details

This function uses the number killed element of the killSome output to randomly draw from the regional abundance vector, then settles the individuals at random in the arena.

Value

A list of 4 elements: the average relatedness in the geographic neighbordhood of consideration (passed directly from the killSome output, not re-calculated here), the regional abundance vector, the new spatial arena, and the dimensions of that arena.

References

Miller, Trisos and Farine.

Examples

```
library(geiger)

#simulate tree with birth-death process
tree <- sim.bdtree(b=0.1, d=0, stop="taxa", n=50)

#create a random arena
arena <- randomArena(tree, x.min=0, x.max=300, y.min=0, y.max=300, mean.log.individuals=2)

#remove some of the most closely related individuals
new.arena <- killSome(tree, arenaOutput=arena, max.distance=50, percent.killed=0.2)

dim(arena$arena)
dim(arena$new.arena)

#now settle some indiviudals

newer.arena <- settleSome(new.arena)

dim(new.arena$arena)
dim(newer.arena$arena)
```

---

sigTest *Test significance of observed metrics*

Description

Given a table of results, where the expected confidence intervals are bound to the rows of observed scores, and the name of the metric of interest, returns a vector of 0, 1 and 2, where 0=not significant, 1=clustered, and 2=overdispersed.

Usage

```
sigTest(results.table, observed)
```

Arguments

results.table	Data frame of observed metrics with expected CIs bound in. See example
observed	Name of metric of interest

Details

The column names need to be fairly carefully labeled, so follow convention.

Value

A vector of 0s 1s and 2s, corresponding to not significant, clustered and overdispersed.

References

Miller, Trisos and Farine.

Examples

```
library(plyr)
library(geiger)
library(picante)

#simulate tree with birth-death process
tree <- sim.bdtree(b=0.1, d=0, stop="taxa", n=50)

sim.abundances <- round(rlnorm(5000, meanlog=2, sdlog=1))

cdm <- simulateComm(tree, min.rich=10, max.rich=25, abundances=sim.abundances)

system.time(allMetricsNull(tree=tree, orig.matrix=cdm, null.method="richness",
no.randomizations=10, temp.file="output.csv"))

possibilities <- read.csv("output.csv")

#call the summaries function from within a ddply statement
expectations <- ddply(possibilities, .(richness), summaries)

#calculate the observed metrics
observed <- allMetrics(tree, cdm)

#important merge command, confirm it works
results <- merge(observed, expectations, sort=FALSE)

oneMetric <- sigTest(results, "PSV")

#example of how to loop it over a table of results
metric.names <- names(observed)[3:21]

sig.results <- list()

for(i in 1:length(metric.names))
{
sig.results[[i]] <- sigTest(results, metric.names[i])
}

sig.results <- as.data.frame(sig.results)
```

```
names(sig.results) <- metric.names
```

`simulateComm` *Generate a simulated community data matrix*

Description

Given a phylo object, desired min and max species richnesses, and a vector of potential species abundances, will generate a community data matrix with these characteristics.

Usage

```
simulateComm(tree, min.rich, max.rich, abundances)
```

Arguments

`tree`	Phylo object
`min.rich`	Minimum richness of the resulting cdm
`max.rich`	Maximum richness of the resulting cdm
`abundances`	A vector of potential abundances, e.g. a log-normal distribution

Details

There is currently no implementation to control the frequency with which a given species is selected.

Value

A community data matrix (a data frame) with species as columns and sites as rows.

References

Miller, Trisos and Farine.

Examples

```
library(geiger)
library(picante)

#simulate tree with birth-death process
tree <- sim.bdtree(b=0.1, d=0, stop="taxa", n=50)

sim.abundances <- round(rlnorm(5000, meanlog=2, sdlog=1))

cdm <- simulateComm(tree, min.rich=10, max.rich=25, abundances=sim.abundances)
```

`singleMetric` *Calculate specific phylogenetic community structure metric*

Description

Given a phylo object, and a picante-style community data matrix (sites are rows, species are columns), calculate a phylogenetic community structure metric of interest.

Usage

```
singleMetric(tree, picante_cdm, metric)
```

Arguments

`tree`	Phylo object
`picante_cdm`	A picante-style community data matrix with sites as rows, and species as columns
`metric`	A phylogenetic community structure metric of interest. Options are: "mpd" (non-abundance weighted MPD), "interspecific" (interspecific abundance-weighted MPD), "intraspecific", "complete", "mntd" (non-abundance weighted MNTD), "aw.mntd", "psv", "psc", "pse", "pae", "iac", "haed", "eaed", "eed", "hed", "simpson", "pd", "pd.c" (Cadotte's re-defined PD), and "qe".

Details

Useful wrapper function to calculate a number of phylogenetic community structure metrics from different packages.

Value

A data frame with the calculated metric and the associated species richness of all input "communities".

References

Miller, Trisos and Farine.

Examples

```
library(geiger)
library(picante)

#simulate tree with birth-death process
tree <- sim.bdtree(b=0.1, d=0, stop="taxa", n=50)

sim.abundances <- round(rlnorm(5000, meanlog=2, sdlog=1))

cdm <- simulateComm(tree, min.rich=10, max.rich=25, abundances=sim.abundances)

results <- singleMetric(tree, cdm, "mpd")
```

`singleMetricNull` *Generate null expectations for a single community structure metric*

Description

Given a phylo object, a picante-style community data matrix (sites are rows, species are columns), a desired null method (any of picante or also 2x, 3x, 1s, & 2s of spacodiR), a desired number of randomizations, and an output file name, will shuffle matrix according to null method, then calculate the desired community structure metric as defined in the metric argument, then save each iteration's worth of shufffled values to a csv file for later import. Also calculates the richness of the corresponding community.

Usage

```
singleMetricNull(tree, orig.matrix, metric, null.method, regional.abundance,
  no.randomizations, temp.file)
```

Arguments

`tree`	Phylo object
`orig.matrix`	A picante-style community data matrix with sites as rows, and species as columns
`metric`	The community structure metric of choice. Options are as in singleMetric
`null.method`	A picante-style null, e.g. "richness" or "frequency", or "2x", "3x" "1s" or "2s", which will call spacodiR. It can also now accomodate calls to "regionalNull"
`regional.abundance`	Optional vector of species names repeated the number of times present in the regional abundance pool. For use with regionalNull.
`no.randomizations`	The desired number of no.randomizations the function will run, i.e. the number of times orig.matrix will be shuffled and the metric calculated on it
`temp.file`	The desired name of the output csv file

Details

This runs much faster than trying to do this in memory in R. I will upload some of those type of functions in the near future anyhow. If you call null metrics 2x, 3x, 1s or 2s, it will call spacodiR for the resampling. Note that if you have many quadrats (sites, communities, etc., i.e. rows in your community data matrix), some with repeated species richness, this may be more efficient than using a function like ses.pd() or ses.mpd() from picante (though it is almost entirely dependent on code from that package).

Value

A csv file with each column equal to the value of a given metric for the shuffled community in question (a row in the input matrix).

References

Miller, Trisos and Farine.

Examples

```
library(geiger)
library(picante)
library(spacodiR)

#simulate tree with birth-death process
tree <- sim.bdtree(b=0.1, d=0, stop="taxa", n=50)

sim.abundances <- round(rlnorm(5000, meanlog=2, sdlog=1))

cdm <- simulateComm(tree, min.rich=10, max.rich=25, abundances=sim.abundances)

system.time(singleMetricNull(tree=tree, orig.matrix=cdm, metric="mpd",
null.method="richness", no.randomizations=10, temp.file="output.csv"))
```

---

summaries *Return average and CIs of input vector*

Description

Given a vector of numbers, such as a column from a data frame of null expectations, returns the average and 95 percent CIs of that vector

Usage

```
summaries(null.output)
```

Arguments

null.output	Vector of numbers

Details

Took out the call to iterations, but if you want that back it's just the length of v. Note that it's very important when you run this to have your null output be a file that has one column called richness, and all others be various metrics you want confidence intervals returned for. Note also that this function must be used from within a ddply statement in order to work as desired, see example.

Value

temp

References

Miller, Trisos and Farine.

Examples

```
library(plyr)
library(geiger)
library(picante)

#simulate tree with birth-death process
tree <- sim.bdtree(b=0.1, d=0, stop="taxa", n=50)

sim.abundances <- round(rlnorm(5000, meanlog=2, sdlog=1))

cdm <- simulateComm(tree, min.rich=10, max.rich=25, abundances=sim.abundances)

system.time(allMetricsNull(tree=tree, orig.matrix=cdm, null.method="richness",
no.randomizations=10, temp.file="output.csv"))

possibilities <- read.csv("output.csv")

#call the summaries function from within a ddply statement
expectations <- ddply(possibilities, .(richness), summaries)
```

---

typeI *Test for type I errors*

Description

Sloppy function that needs work. Intended to test for type I and II errors of results of testing of various metrics against a single spatial simulations.

Usage

```
typeI(significance.results, expectation, wrong)
```

Arguments

`significance.results`	Data frame of significance results from call to sigTest()
`expectation`	Expected value: 0=not significant, 1=clustered, 2=overdispersed
`wrong`	Value of a typeI error rate, e.g. 2 if expecting 1.

Details

Note that IAC is thought to detect clustering if observed is greater than upper CIs, so we have to explicitly flip our expectations in the function. See example below for how to test for type I error rates if expecting random community structure. Note that it is possible to have a type I error irrespective of power of test, so a row can have more than one 1 in it.

Value

Matrix with rows corresponding to metrics, and columns for type I errors, "NoSignal" (i.e. < 50 community data matrix exhibiting expected pattern), and "Good" (i.e. > 50 pattern). Values in table are 0s and 1s, where 1 corresponds to a confirmation of the pattern in question.

References

Miller, Trisos and Farine.

Examples

```
library(plyr)
library(geiger)
library(picante)

#simulate tree with birth-death process
tree <- sim.bdtree(b=0.1, d=0, stop="taxa", n=50)

sim.abundances <- round(rlnorm(5000, meanlog=2, sdlog=1))

cdm <- simulateComm(tree, min.rich=10, max.rich=25, abundances=sim.abundances)

system.time(allMetricsNull(tree=tree, orig.matrix=cdm, null.method="richness",
no.randomizations=10, temp.file="output.csv"))

possibilities <- read.csv("output.csv")

#call the summaries function from within a ddply statement
expectations <- ddply(possibilities, .(richness), summaries)

#calculate the observed metrics
observed <- allMetrics(tree, cdm)

#important merge command, confirm it works
results <- merge(observed, expectations, sort=FALSE)

oneMetric <- sigTest(results, "PSV")

#example of how to loop it over a table of results
metric.names <- names(observed)[3:21]

sig.results <- list()

for(i in 1:length(metric.names))
{
sig.results[[i]] <- sigTest(results, metric.names[i])
}

sig.results <- as.data.frame(sig.results)

names(sig.results) <- metric.names

error.summ <- typeI(sig.results, expectation=1, wrong=2)

#if you are expecting 0s (random structure), then use: expectation=0, wrong=1|2
```

Index

In and out of the rainforest and the loss of another iconic Australian genus

Eliot T. Miller

Austin R. Mast

Peter H. Weston

Robert O. Makinson

Peter Olde

Amanda Cubes

Eric H. Jones

Amy E. Zanne

Robert E. Ricklefs

Mark Westoby

ABSTRACT

Aim: The genera *Hakea* and *Grevillea*, members of Hakeinae, account for much floral diversity in Australia. We reconstructed the phylogenetic history of Hakeinae, and tested the prediction that this impressive radiation was driven by shifts to novel arid climates and shorter growth forms. We also examined to what extent Hakeinae assemblages appear shaped by phylogenetic niche conservatism.

Location: Australia.

Methods: We sequenced 148 species of *Hakea* and *Grevillea* (and a wide breadth of outgroups) to create a phylogeny to test our predictions. We used this molecular tree and new methods described here to create complete phylogenies that included all 517

Australian species. We quantified range sizes, heights, diversification rates, climate niches, and phylogenetic community structure, and compared the interrelationships among these variables.

Results: We show that *Hakea* is nested within *Grevillea*. While the entire clade traces its origins to ca. 45 mya, many of these species appear to have originated in the last 5 mya. This rapid diversification was not driven by a shift out of rainforests, nor by a shift to smaller-stature plants, nor by species with intermediate ranges. Phylogenetic relationships among co-occurring Hakeinae species share some characteristics with the previously studied bird family Meliphagidae, in that Hakeinae assemblages are more closely related away from the inferred ancestral climate state.

Main conclusions: Hakeinae diversification appears to have a geographic signal, and may have been driven by ongoing nutrient depletion from Australian soils, with concomitant radiation into specialized edaphic zones; the highest rates of radiation are seen in the most recently geologically active region of southeast Australia, where the weatherization process is more recent than in southwest Australia. Total species richness is highest in southwest Australia. The clade may trace its origins to open, oligotrophic habitats in that part of the continent. Hakeinae phylogenetic community structure bears a strong signal of localized radiations, particularly in temperate Australia.

INTRODUCTION

Two related iconic Australian genera, *Hakea* and *Grevillea*, comprise a notable portion of floral diversity of the continent (517 species total). Fossil evidence points to recent rapid radiation in the group. This diversification has been concomitant with radical shifts in

Australian climate. What was the relationship between this dramatic diversification and aridification? Where, geographically and climatically, did the Hakeinae originate? What biogeographic patterns exist, and what do they tell us about drivers of extant Australian biodiversity? Finally, is there any evidence that diversification rates in the group are associated with shifts to arid habitats or smaller-stature plants?

Species of *Hakea* and *Grevillea*, along with six additional species in the genera *Opisthiolepis*, *Buckinghamia*, and *Finschia*, form the almost entirely Australian subtribe Hakeinae (Weston & Barker 2006; Sauquet *et al.* 2009). For brevity, hereafter Hakeinae refers to the clade excluding *Opisthiolepis* and *Buckinghamia*. Hakeinae species exhibit phenomenal diversity, often within a site; they vary from stunted, clambering heath plants to rainforest trees. Many species within the group are bird-pollinated (Ford *et al.* 1979), but they span a range of pollinator strategies (Mast *et al.* 2012). As members of the family Proteaceae, Hakeinae species contribute a considerable component of the worldwide leaf economics spectrum; without Proteaceae, worldwide plant trait diversity would be notably shifted towards traits characteristic of faster growth (Cornwell *et al.* 2014).

The Proteaceae are an ancient Gondwanan group, with a long-history in the fossil record (reviewed in Carpenter 2012), and a crown age of 126-85 mya (APG 2003). While most modern Australian genera (notable exceptions include *Hakea* and *Grevillea*) contain few species and are restricted to regions of high precipitation (Johnson & Briggs 1975), this was not always the case. The palynological record and macrofossils of leaf (Vadala & Greenwood 2001; Carpenter 2012) and reproductive structures (Dettmann & Clifford 2005) mutually support the former widespread Australian distribution of Proteaceae. For

instance, plants similar to *Athertonia* and *Megahertzia*, now monotypic genera of trees restricted to high elevation rainforest, ranged throughout inland New South Wales and southern Victoria 30-20 mya (Vadala & Greenwood 2001). The fossil record indicates that the family was diverse (more so than today) in form and likely formed an important component of the flora by ca. 60 mya (Dettmann & Jarzen 1998; Carpenter 2012). Despite this fairly robust historical record of Proteaceae, Hakeinae fossil evidence is, given its current extent, exceedingly sparse. Fossil fruits of a taxon that looks like extant members of the *Grevillea* Hilliana and Heliosperma groups were uncovered from sediments estimated to be 30-20 mya in Victoria (Dettmann & Clifford 2005), and pollen similar to some species of *Grevillea* occurs in sediments from ca. 72 mya, also from Victoria (Dettmann & Jarzen 1998). More recent fossils (< 4 mya) are known (Pole & Bowman 1996; Jordan *et al.* 1998); unless the fossil record is remarkably biased, a diverse Hakeinae appears to be a recent phenomenon.

Phylogenetically diverse assemblages of Proteaceae began disappearing in conjunction with dramatic climate changes on the continent. Australia completed its high-latitude separation from Antarctica and the remnants of Gondwana in the early Cenozoic and began moving rapidly northwards ca. 55 mya (McLoughlin 2001; McGowran *et al.* 2004; Vasconcelos *et al.* 2008). As the continent has drifted, it has experienced extensive aridification that intensified 15-5 mya and continues to the present (Truswell 1993; Greenwood 1996; Hill *et al.* 1999; Greenwood *et al.* 2003; Greenwood & Huber 2011; Herold *et al.* 2011; Huber & Goldner 2012). Unlike the clear signal of increasing aridity during this time, temperature in Australia has fluctuated as the continent has shifted towards the equator coincident with overall global cooling (Greenwood *et al.* 2003).

While the continent as a whole has experienced extensive aridification, the process has not been spatiotemporally even. For instance, much of eastern Australia still receives substantial precipitation, and cool-temperate rainforests dominated by *Nothofagus*, Araucariaceae, and Podocarpaceae, among others, existed in regions of southeastern continental Australia until at least the late Miocene 11-5 mya (Hill 2004). In contrast, evidence of xeromorphic characters appeared earlier in the southwest than the southeast, and fossil floras from the early Eocene to mid-Pliocene in southwest and central Australia have been interpreted as coming from a vegetation mosaic, e.g. a riparian forest zone with adjacent sclerophyllous shrublands (Christophel *et al.* 1992; Dodson & Macphail 2004; Carpenter *et al.* 2014). Do the Hakeinae trace their origins to these early heterogeneous habitats?

Many species of Proteaceae, and Hakeinae in particular, present extreme examples of low leaf nitrogen and specific leaf area (SLA, leaf area to dry mass), hallmarks of scleromorphy (Hill 1998). However, such species also tend to live in arid areas, and a number of traits characteristic of xeromorphic (dry-adapted) vegetation are also exhibited by scleromorphic (low nutrient-adapted) species, which has confounded the study of these traits' origins (Hill 1998; Fonseca *et al.* 2000). The evolution of scleromorphy in the Proteaceae specifically may have been driven by low nutrient levels, and/or high solar radiation (Jordan *et al.* 2005), and/or elevated atmospheric CO_2 (Jordan *et al.* 1998). Regardless of the reason, given the origins of these traits prior to the aridification of Australia (Dettmann & Jarzen 1998), and the later, seeming exaptation of some of these same traits to xeric conditions, it is thought that early scleromorphic traits may have subsequently facilitated the success of lineages like the Hakeinae in modern

Australia (Jordan *et al.* 2008; Crisp & Cook 2013). Was scleromorphy a key trait that drove modern Hakeinae diversity?

Australian soils are low in nutrients important to plant growth, particularly phosphorus, and have been this way for a long time (Orians & Milewski 2007; Vasconcelos *et al.* 2008). The continent receives little airborne nutrient input, and has been largely geologically stable throughout its independent history (Orians & Milewski 2007). Exceptions to this stability did occur. The most notable geological feature in modern Australia is the Great Dividing Range, a series of low ranges and isolated mountaintops along the eastern and southeastern margin of the continent. While much of the range was likely in place before the Cenozoic, ca. 66 mya (Young & McDougall 1993), uplift, warping and subsidence continue today.

There has also been considerable volcanism in these areas, beginning ca. 70 mya in the central eastern ranges. The center of volcanism has "shifted" as the continent drifted northwards, arriving in central Victoria ca. 6 mya (Vasconcelos *et al.* 2008). This volcanism, basin formation, erosion of ranges and shifting of river valleys in this southeast region have been associated with a complex topographical and edaphic history (Holdgate *et al.* 2008). Until at least the late Miocene, these ranges were largely covered by rainforests, but as the continent has continued to dry and cool, most have been replaced by sclerophyll forest (Hill 2004), a process likely expedited by nutrient depletion (Beadle 1966).

Another notable biogeographic barrier is the Nullarbor Plain, which separates southeast from southwest Australia. This large, semi-circular area of limestone initially formed by incursion from the Great Australian Bight (Frakes 1999). While it appears to

have been in place as a marine barrier by 30 mya (Frakes 1999), its uplift ca. 14 mya has been associated with vicariance events in a number of plant taxa (Crisp & Cook 2007). The degree to which the Nullarbor has shaped Australian floras has been a long-standing matter of discussion (Hopper & Gioia 2004), and appears to vary between taxa (Crisp *et al.* 2004). It has never been adequately addressed in the Hakeinae, but the existence of both endemic and shared taxonomic groups between the southwest and southeast has been noted (Barker *et al.* 1999; Makinson 2000). What role have these biogeographic barriers played in Hakeinae diversification?

Range size could serve as a proxy for the recalcitrant idiosyncrasies of range contraction and expansion that ultimately drive diversification. For instance, since large-ranged species should only infrequently be subject to complete population splitting, and small-ranged species may be at increased risk of extinction, species with intermediate range sizes may show the fastest rates of diversification (Rosenzweig 1995). Do Hakeinae with intermediate ranges diversify at a faster rate than others? In Appendix S1, we also ask to what degree Hakeinae obey Rapoport's rule (Stevens 1989).

There is strong evidence that phylogenetic niche conservatism can shape the geographical distribution of lineages within a large continental radiation. This can be detected in the phylogenetic community structure of co-occurring species. Such a process is predicted to leave a signature of increasing phylogenetic clustering away from the clade's climate of origin. Recent support for this was found in the Australian Meliphagidae (Miller *et al.* 2013), a speciose group of birds whose diversification was contemporaneous with that of the Hakeinae. Do the same principles apply to the Hakeinae?

The apparent rapid diversification and ecological success of the Hakeinae are a matter of great biological interest. Based on climatic and geological history and previous suggestions (e.g., Jordan *et al.* 2008), we hypothesize that the proto-Hakeinae (Johnson & Briggs 1975) were sclerophyllous, rainforest trees. These proto-Hakeinae would have grown as canopy or sub-canopy trees in oligotrophic soils on the margins of rainforests, or perhaps in light gaps within such forests. As Australia began drying out, the proto-Hakeinae diversified into a number of lineages that radiated throughout the continent. We hypothesize that the geographic heterogeneity of the aridification process, in combination with edaphic specialization, drove the apparent rapid diversification of the Hakeinae. In accordance with this hypothesis, we predict that speciation rates in the clade are negatively correlated with height, which we use as a rough proxy for scleromorphy. We also predict that diversification rates are negatively correlated with precipitation and, to a lesser extent, temperature. We emphasize that diversification is fundamentally a process of populations splitting and not interbreeding or going extinct if and when they come back into contact. Thus, in the Hakeinae, we predict that diversification rates show a unimodal response with geographic range size, with the highest rates exhibited by intermediate ranged species. Finally, we predict that Hakeinae assemblages are increasingly related along gradients of decreasing precipitation and, to a lesser extent, temperature.

METHODS

Geographical data assembly

We initially obtained 146,538 collections from the Atlas of Living Australia (ALA, http://www.ala.org.au/). These represented 737 unique, matched species names. This is fewer than the 3,090 unique names in the ALA system before internal cleaning, but it is more than modern estimates (e.g., 511, Weston & Barker 2006). First, we matched all unique names to their modern interpretation (excluding three and five extralimital *Finschia* and *Grevillea* species, respectively). After this, and exclusion of points identified by ALA as climatic outliers (using a reverse jackknife procedure, Chapman 2005), the dataset consisted of 126,936 collections across 517 species. Finally, we went through all collections, species-by-species in a geographic context, bringing all taxonomy and distribution up to treatment in the Flora of Australia (FOA) (Barker *et al.* 1999; Makinson 2000), or in some cases more recent treatments (e.g., Downing *et al.* 2004). This included manually adding in collections excluded as climatic outliers. We used digitally available information to decide whether to keep points outside the accepted range. If the collection was modern and had been identified by a recognized authority, we generally kept it. Other points were removed, either because they were demonstrably badly georeferenced, or because they were georeferenced to general locality. Our final dataset consisted of 125,696 collections across 517 species (Fig. S4.1).

Climate data assembly

We used the WorldClim (http://www.worldclim.org/bioclim) climate layers, with the addition of a moisture index (MI) layer (Willmott & Feddema 1992), derived using a potential evapotranspiration layer from Australia's Bureau of Meteorology. We focus on mean annual temperature (MAT) and mean annual precipitation (MAP), although we also

use BIO4 (temperature seasonality) and BIO15 (precipitation seasonality, Appendix S1). We summarized climate layers in grid cells of 100 x 100 km.

Plant height data assembly

We obtained height data from Makinson (2000) and Barker *et al.* (1999). We always used the tallest value when ranges were given or subspecies were listed separately. Some species have been described since the publication of the flora. For these we used the maximum height recorded on a specimen label (checked through ALA).

Community data matrix assembly and manipulation

For each grid cell described above, we summarized the number of specimens per species to create a "community" data matrix (CDM). We used rarefaction in the R (R Development Core Team 2011) package *vegan* (Oksanen *et al.* 2013) to restrict our analyses to cells that were estimated to have had at least 70% of their constituent species sampled (Chao 1987), and from which at least two species had been collected from the cell.

Molecular phylogeny assembly

Our methods are detailed in Appendix S2.

Complete phylogeny assembly

All species of Hakeinae have been placed by experts in named, hierarchically clustered taxonomic groups (Barker *et al.* 1999; Makinson 2000). Since we were interested in

exploring some questions best suited to complete phylogenies, we developed a method to add missing taxa into the molecular phylogeny. Existing methods (see Kuhn *et al.* 2011) differ primarily in how branch lengths are partitioned after adding taxa. An alternative is to consider the possible extremes of missing information; if results are consistent, they can be considered more strongly supported. With this in mind, one extreme to consider is that all missing taxa diverged from the stem-lineage of their taxonomic group. The opposite extreme is that all missing taxa diverged more recently than any of the sequenced species in their taxonomic group.

We wrote an R function (https://github.com/arborworkflows/aRbor/blob/master/R/randomlyAddTaxa.R) that, for each missing species A, finds a member of its taxonomic group, species B, that is in the tree. We used the function in three ways. With the "crown" option, species A was bound at a distance midway between the parent node to species B and the tips of the phylogeny (Fig. S4.2). With the "stem" option, if species B was sister to species C, both of which were in the same taxonomic group as species A, species A was bound at a distance midway between the parent and grandparent nodes of species B and C (Fig. S4.2). If there was no such species C, then species A was bound crownwards from B. This is necessary, as if species C belonged to another taxonomic group, binding A to its stem-lineage would render clade (A,B) paraphyletic. Finally, with the "random" option, species A was bound randomly either crownwards or stemwards according to the rules above.

We generated 1,000 trees with each of these methods. For some of our analyses we used the entire set of trees and averaged results (see below). For diversification rate

analyses we could not do this. Accordingly, we used TreeAnnotator (Appendix S2) to create maximum clade credibility (MCC) trees that maintained the target tree node heights.

Ancestral state reconstruction and phyloclimatespace

We reconstructed ancestral states using two methods for both the molecular tree and for the complete MCC tree obtained with the random method above (hereafter, we refer to this as the randomMCC tree, and the other two complete phylogenies as the stemMCC and crownMCC). First, for height and climatic niche, we calculated the maximum likelihood ancestral states using the R package *phytools* (Revell 2012). This method assumes a Brownian model of evolution, e.g., that climatic niches were not under selection during Hakeinae radiation. This assumption is likely incorrect. Thus, we also employed a Bayesian approach with *geiger* (Harmon *et al.* 2008) to derive ancestral climatic niches after placing priors on the root of the tree. These priors (MAP 1250 ± 275 SD mm/yr, MAT 19 ± 1.5 SD °C) are based on continent-wide estimates, as described in Miller *et al*. (2013). With this approach, we fit and compared three different models of climatic niche evolution, a Brownian and a directional trend model with priors on the root state, and a Brownian model without priors (Slater *et al.* 2012). Per model, we ran 10^7 and 10^8 generations for the randomMCC and molecular tree, and sampled every 10^3 and 10^4 generations, respectively. We discarded the first 10% of generations as burn-in. All runs achieved a root-state ESS of > 200. We compared the fit of these different models with the Akaike information criterion.

We explored Hakeinae radiation through climate using a phyloclimatespace approach (Miller *et al.* 2013), now available in *phytools*. We implemented this approach using both the molecular and randomMCC tree and both the results of the maximum likelihood ancestral state reconstructions and those of the best-fit Bayesian approaches.

Evolution across geographic space

We visualized Hakeinae radiation across the Australian continent with the program *phylowood* (Landis & Bedford 2014). To do so, we wrote an R package *R2phylowood* (https://github.com/eliotmiller/R2phylowood) that takes as input a Nexus file and species' centroids of distribution, and generates the necessary *phylowood* inputs. The geographic positions of ancestral nodes are calculated by maximum likelihood ancestral reconstruction from extant centroids. While this is certainly a simplistic approach, and given both historical climate change and geographic shifts in Australia little should be made of the specific locations of these ancestral nodes, particularly the latitudinal positions, we suggest it is informative with respect to longitudinal spread of the clade.

To directly examine the influence of the Nullarbor Plain on Hakeinae diversification, we explicitly defined southwest and southeast endemic taxa as species that occurred South of Karratha, Western Australia and either West of 129° E or East of Port Augusta, South Australia, respectively. We then pruned the molecular and randomMCC trees to species endemic to these areas, and calculated the per-node proportion of descendant species from each region. Nodes with only southeast or southwest taxa descending from them were considered to define endemic clades. We then

visualized the timing of diversification in these two regions by looking at endemic clade accumulation over time (i.e. node through time plots).

Range size analyses

We calculated range size as the number of 100 x 100 km grid cells a species occurs in.

Phylogenetic community structure

We used *picante* (Kembel *et al.* 2010) to calculate non-abundance-weighted mean pairwise phylogenetic distance (MPD) among constituent species in each grid cell. We did so using the molecular phylogeny and each of the three, entire sets (n = 1000) of complete trees (see *Complete phylogeny assembly*). We summarized the results from each of the complete trees by taking the mean of the per-grid MPD values.

Diversification rate analyses

We used the program BAMM (Rabosky 2014) to quantify rates of diversification in the Hakeinae, using the molecular tree and the three complete MCC trees. We ran these analyses for between 10^6 and 10^9 generations, sampling between every 10^3 and 5 x 10^4 generations. For all four runs, the ESS exceeded 200, the recommended minimum for BAMM. We discarded the first 10% of generations as burn-in. For the molecular tree, we accounted for missing taxa by setting the global sampling fraction to 0.279, and we did not set clade-specific sampling fractions, since sampling was not taxonomically biased (chi-squared test, p=0.99).

We used the R package *BAMMtools* (Rabosky *et al.* 2014) to explore variation in diversification rates. BAMMtools provides lineage-specific speciation and extinction rates. For the four models (one from each of tree), we extracted the per-species average speciation rates, and identified the single best shift configuration. This summarizes the set of shifts in diversification rate across the phylogeny with the highest maximum *a posteriori* probability.

Geographical scale statistical analyses

To explore geographic variation and potential drivers of macroecological patterns, we summarized per-grid species richness, diversification rates (the mean of the constituent species' per-species average speciation rates), median height, mean range size, and MPD. We derived linear models between these responses and potential climatic drivers: MAT, MAP, MI, and, for mean range size, also temperature and precipitation seasonality (Appendix S1).

To directly compare phylogenetic community structure patterns in the Hakeinae with those in the Meliphagidae, we used *picante* to calculate net-relatedness indices (NRI) using a null model that maintained per-grid species richness (10^4 randomizations of CDM). We then derived a per-grid index equal to the Hakeinae NRI score minus that of the Meliphagidae. Large values of this index correspond to grid cells where Hakeinae phylogenetic community structure is overdispersed relative to that of the Meliphagidae, while small values correspond to grid cells where the Hakeinae structure is clustered compared to the Meliphagidae.

Species level statistical analyses

We tested our prediction that increased diversification rates are associated with decreases in plant height and increases in temperature and precipitation with two approaches. First, we used ordinary least squares (OLS) regression to compare the per-species average speciation rates with the height and climate traits. Second, we fit phylogenetic generalized least squares (PGLS) regressions. To better interpret PGLS results, we simulated 1,000 sets of Brownian motion trait evolution on the four phylogenies, and compared the correlation coefficients of these simulated traits with those of the observed traits.

RESULTS

Molecular phylogeny

We found that all species of *Hakea*, *Finschia*, and sequenced non-Australian *Grevillea* were nested within an expanded *Grevillea* (Fig. 1). Like recent previous studies, *Buckinghamia* and then *Opisthiolepis* were sister to *Grevillea*. In contrast to previous suppositions, rainforest taxa (e.g. *G. baileyana*, *G. robusta*) were not resolved as the basal-most taxa. Instead, these species were nested in an early diverging lineage. The species that was sister to all others was the 1-3 m tall shrub *G. endlicheriana*, currently found in a rather small area inland from Perth, Western Australia. Some members of the Hilliana group (e.g., *G. glauca*, *G. myosodes*), which has also been postulated to be a basal lineage within the genus (Makinson 2000), were indeed resolved to have originated at an early stage of the *Grevillea* radiation (see also Dettmann & Clifford 2005)

Where, geographically and climatically, did the Hakeinae originate?

Using maximum likelihood the ancestral precipitation regime of the Hakeinae was inferred to have been 550 mm/yr (95% CI = 137-2239) and 607 mm/yr (95% CI = 313-1178) with the randomMCC and molecular tree, respectively. The ancestral MAT was inferred to have been 19.7 °C (95% CI = 10.2-29.2) and 19.6 °C (95% CI = 15.0-24.2). Of the Bayesian models for the molecular tree, the trend and Brownian motion model with priors on the root were the best-supported models for precipitation and temperature, respectively. The trend parameter was negative, indicating a progression towards lower precipitation regimes. For the randomMCC tree, the Brownian motion models with priors received the most support. With these models, the ancestral precipitation regime of the Hakeinae was inferred to have been 1284 mm/yr (95% CI = 1276-1292) and 1198 mm/yr (95% CI = 1133-1267) with the molecular and randomMCC trees, respectively. The ancestral MAT was inferred to have been 18.7 °C (95% CI = 18.7-18.8) and 19.9 °C (95% CI = 19.4-20.3). These are all still running. They proceed painfully slowly. These are initial results, and subject to change. The molecular tree is likely to have ESS way over 200, but it's not clear this will happen with the randomMCC tree.

The phyloclimatespace (Fig. 2, S4.3) shows major diversification of the Hakeinae within cooler regions of Australia, including arid climates. Many species within these regions directly abut the limits of available climate space, i.e. they are "pushed" against the left margin of gray points. In contrast, only some lineages have transitioned to warm and wet regions, where few species are found today. The results of the Bayesian analysis did not change these conclusions (Fig. S4.4-5).

The proto-Hakeinae are inferred to have lived in inland southwest Australia, near present-day Yeo Lake (-28.09°, 124.43°). Almost identical results were returned with all four trees.

What was the relationship between Hakeinae diversification and climate changes?

The best model of diversification for the molecular tree showed speciation rates increasing at a decreasing rate towards the present, with no significant shifts in any clades' diversification rate (Fig. S4.6). Where missing species were added had a large influence on inferred diversification rates through time. When added to their stem-lineage, diversification rates were inferred to have declined towards the present, with a single burst in diversification ca. 22 mya (Fig. S4.7-8). When added to their crown-lineage, rates were inferred to have increased rapidly until ca. 30 mya, and then declined until a recent burst in speciation (Fig. S4.9-10). When added randomly either stemwards or crownwards, the Hakeinae were inferred to have diversified at a similar rate to the results from the molecular tree, though there is a clear recent (ca. 3 mya) rise in rates (Fig. 3a, S4.11).

Despite these overall differences in diversification rates among the four trees, there were general similarities in which clades, if any, were identified as showing shifts in diversification rate. For brevity, we discuss only those from the randomMCC tree. The best model with this tree identified two clades that have diversified at an increased rate compared to the background rate of the Hakeinae. These two clades, composed largely of members of the *Grevillea* Linearifolia and Pteridifolia groups (Makinson 2000) (Fig. 3, S4.11, S4.21-25), account for much of the recent increase in speciation rates.

In an OLS framework, per-species, model-averaged speciation rates (randomMCC) were weakly negatively correlated with species' MAT ($R^2 = 0.1$, $p < 0.001$). Speciation rates were weakly positively correlated with MAP ($R^2 = 0.1$, $p < 0.001$). These results were qualitatively identical irrespective of the tree used. Neither MAT nor MAP was correlated with speciation rate in a PGLS framework. Indeed, the observed traits showed less correlation with speciation rate than did many simulated traits (Fig. S4.12). There is little to support the hypothesis that Hakeinae diversification has been driven entirely (or even partly) by climate change.

Are shifts to shorter plants associated with increased diversification rates?

Modern Hakeinae tend to be shrub-sized (median = 2 m, mean = 3 m, SD = 3.25). The proto-Hakeinae were inferred to be somewhat taller, however (4.9 m and 5.4 m with the randomMCC and molecular tree, respectively), and some modern species are as tall as 40 m. These tall species are concentrated in the mesic northeast of the continent (Fig. S4.13).

Like climate change, there is little evidence that shifts to shorter statures drove Hakeinae diversification. In an OLS framework, per-species, model-averaged speciation rates were very weakly negatively correlated with height ($R^2 = 0.02$, $p = 0.0005$). These were not at all correlated in a PGLS framework (Fig. S4.12).

What was the geographic pattern of Hakeinae diversification?

We present linear models between possible environmental drivers and grid-cell averaged species richness, height, and diversification rates in Appendix S3.

In contrast to the weakly supported climatic and height correlates (preceeding two sections), there appears to be a clear geographic pattern to diversification rates. Specifically, when the molecular, randomMCC or crownMCC trees are used (Fig. 4, S4.14-15), rapid rates of speciation are concentrated in and around the Great Dividing Range, particularly the recently geologically active South. When the stemMCC tree is used, rapid diversification was inferred to have occurred in the northwest of the continent (Fig. S4.16), but note the unusual tree shape produced when binding many missing species stemwards (Fig. S4.8). The rapid diversification rates seen in the southeast are a product of multiple, disparate Hakeinae lineages co-occurring there. Animated reconstruction of the geographic radiation shows early and continued diversification within the southwest, with subsequent invasion of eastern Australia by some lineages, and rapid radiation within the southeast in recent times (i.e. < 5mya, Appendix S5).

With respect to the Nullarbor Plain, endemic southwest clades trace their origins to 34-28 mya (Fig. S4.17-18). Endemic, extant southeast clades first arose 12-11 mya. They quickly accumulated species, suggesting a possible role for the Nullarbor at this time. That said, some lineages may have "crossed" the Nullarbor as recently as 8 mya, perhaps via regions North of the Plain.

What is the relationship between diversification and range sizes in the Hakeinae?

Speciation rate was weakly negatively correlated with range size ($R^2 = 0.05$, $p < 0.001$), and fitting the predicted quadratic relationship was not able to explain notably more of the variation in speciation rate.

Does phylogenetic niche conservatism shape Hakeinae geographical distribution?

MPD was weakly positively correlated with MAT (randomMCC, $R^2 = 0.08$, $p < 0.001$, Fig. S4.19) and negatively correlated with MAP ($R^2 = 0.02$, $p = 0.0008$, Fig. S4.20) and MI ($R^2 = 0.05$, $p < 0.001$). MPD showed a unimodal response to temperature; the most overdispersed grid cells occurred around the ancestral temperature regime of ca. 20 °C. These results were qualitatively identical irrespective of the tree used. Our purpose is to highlight the lack of explanatory power of these models. We therefore do not account for spatial autocorrelation, which would likely change the significance of these weak but nominally significant relationships.

Hakeinae phylogenetic community structure differed from that of the Meliphagidae. In particular, large parts of the interior were phylogenetically overdispersed relative to the Meliphagidae, while northern Australia and particularly the southwest and southeast were phylogenetically clustered relative to the Meliphagidae (Fig. 5).

DISCUSSION

The subtribe Hakeinae includes some of Australia's most well known plants, species of *Hakea* and *Grevillea*, and it comprises a notable portion of floral diversity on the continent. Based on fossil evidence, its successful spread through the landscape has been a recent phenomenon. Presumably, its diversification into 525 extant species, 517 of which are Australian, also occurred rapidly. What drove this diversification?

While the monophyly of *Grevillea* with respect to *Hakea* has been questioned, *Hakea* species are morphologically distinct and, prior to this study, *Hakea* itself was

thought to be monophyletic (Barker *et al.* 1999; Makinson 2000). The molecular tree (Fig. 1) confirms this, showing conclusively that monophyletic *Hakea* (and *Finschia*) is nested within *Grevillea*.

Based on our molecular results, we conclude that extant Hakeinae diversity arose quite recently. Indeed, a considerable portion of species appear to have arisen in the last 5 my (Fig. 3a). Given the dramatic aridification that occurred during this time (Truswell 1993), and the purported scleromorphic proto-Hakeinae (Hill 1998), we hypothesized that the Hakeinae radiated out from rainforest margins into newly opened, low-nutrient shrublands, and that their success was facilitated by the utility of their scleromorphic traits in xeric conditions. Yet, in reality there are at least three kinks in this linear story.

First, Hakeinae do not necessarily seem to trace their origins to rainforest. While the rainforest taxa like *G. baileyana* and *robusta* appear to have diverged fairly early in the radiation (Fig. 1), the proto-Hakeinae were inferred to be shrubs or short trees in open, mid-precipitation conditions. The immediate sisters to an expanded *Grevillea*, *Buckinghamia* and *Opisthiolepis*, are rainforest-restricted. Presumably the larger clade would trace its origins to the rainforest. This is similar to recent evidence suggesting that some clades of Australian marsupials secondarily re-invaded the rainforests from arid regions (Mitchell *et al.* 2014).

Second, we predicted that diversification rates would be correlated with decreases in height (our proxy of scleromorphy) and shifts to drier and colder climates. This was not well supported. While we recognize that height is an imperfect proxy, we suggest it is unlikely that a better measure would yield different results.

Third, speciation generally requires populations becoming isolated in some manner. Since geography is the most common means by which this might happen (Rieseberg & Willis 2007), and range size should serve as some measure of population interconnectedness, we also anticipated a unimodal relationship between range size and diversification rate (Rosenzweig 1995). In retrospect, this is a naïve approach to the problem. If a process like centrifugal speciation (Brown 1957) was relevant, the diversification rate of the parent species would not be expected to propagate down the phylogeny. Instead, we might expect to see parent species lying sister to a swarm of small-ranged daughter species. Interestingly, visual inspection of range size plotted across the Hakeinae phylogeny suggests this hypothesis warrants further investigation. Regardless, our initial prediction was not supported, and we conclude that our initial story of Hakeinae diversification was overly simplistic.

What did emerge in our analyses was a clear geographic signal of speciation. Speciation rates are highest in the southeast, particularly in the region of greatest recent volcanism and geological shifts (Fig. 4, Vasconcelos *et al.* 2008). At the same time, overall richness is highest in the southwest (Fig. S3.1). We attribute this pattern to the following modified scenario. Around 45 mya, the proto-Hakeinae lived along forest margins, or perhaps in oligotrophic or otherwise higher-light, lower-nutrient sites. Our simple ancestral state reconstruction suggested the Hakeinae arose near present-day Yeo Lake. This may be true, given that 45 mya the climate in this region could conceivably have been similar to the inferred ancestral climate regime of the Hakeinae. However, it seems equally likely that the geographic origin of the Hakeinae may have been elsewhere; basal members of the group (e.g., *Grevillea glauca*, *G. endlicheriana*) today

occur in widely separated areas. Regardless of the geographic origin, it appears clear that the Hakeinae began diversifying early on in the southwest, and that this process has continued to the present day (Fig. S4.17-18). As Australia first began drying out, southwestern vegetation likely consisted of heterogeneous mixtures of closed forest with shrublands on more xeric sites (Vadala & Greenwood 2001). Such a scenario would offer spatial configurations conducive to speciation, particularly as the aridification intensified and marooned the early Hakeinae in disjunct habitats. Moreover, much of the southwestern diversity seems to owe its origins to edaphic specialization (Hopper & Gioia 2004), and it is likely that speciation into new edaphic zones would have also played an important role in this process. Finally, geographic areas covered by southwestern flora may once have been notably larger in extent (Burbidge 1960), and accordingly the region could in effect be a modern-day refugium.

The development of proteoid roots (Purnell 1960) may have contributed to modern Hakeinae diversity. These near-surface roots excrete acids to solubilize and absorb otherwise inaccessible soil phosphate (Lambers *et al.* 2008). Not only are many Hakeinae species able to persist on extraordinarily poor soils, but they may actually deplete the soils beyond levels acceptable to most other plants (Pate *et al.* 2001). While the current diversity of low-nutrient edaphic zones would not always have been available, we speculate that as the weathering of soils proceeded in the southwest, new edaphic zones would have opened up and been colonized by Hakeinae. Gene flow between adjacent, differentially weathered zones derived from diverse parent material could have been inhibited by selection against hybrids, and by newly opened edaphic zones being initially colonized by members of extant Hakeinae lineages with pre-established post-

zygotic reproductive barriers between them. It is conceivable that this diversification could have involved a process where species radiated into suitable edaphic zones, drew down soil nutrients and, subject to strong selective pressure (phosphorus limitation), quickly diverged from their progenitors. Such a process would be difficult to test for, and it does not preclude scleromorphy, aridification, or range size as being important aspects of Hakeinae diversification, but these latter factors alone do not appear to have produced the diversity of forms and species we see today. An additional factor not addressed here, but which also may have been involved in this rapid diversification, was the onset of fire as a driving force structuring Australian vegetation (Orians & Milewski 2007).

The apparent recent and rapid diversification in southeastern Hakeinae offers some support for this admittedly speculative hypothesis. Specifically, the complex topographical history of the southeast would have provided both ecological opportunity and the splitting and isolation of habitats conducive to speciation (Holdgate *et al.* 2008). Much of the Great Dividing Ranges were until recently covered in wet forests. In the last 5 my, however, most of these forests have given way to dry sclerophyll forests and shrublands (Beadle 1966; Hill 2004). Members of the *Grevillea* Linearifolia group account for much of this recent diversification (Fig. 3, S4.21, S.4.23). These species have radiated into a number of habitats, particularly patches of heath and isolated rocky mountain slopes under *Eucalyptus* canopies on soil types that are rare in Australia.

The other group that showed a significant increase in diversification rate was a clade composed of members of the *Grevillea* Pteridifolia group (Fig. 3, S4.22, S4.24). This pan-Australian group is almost entirely bird-pollinated (Makinson 2000), which might be expected to increase gene flow and thereby decrease diversification rate (Toon

et al. 2014). Both the Pteridifolia and Linearifolia groups (the latter of which exhibits a range of pollinator syndromes), contain some of Australia's best-known bird-pollinated species (Fig. S4.25). While it is tempting to suppose that birds were involved in elevating speciation rates in these clades, some other bird-pollinated clades within the Hakeinae did not show increases in diversification rates. Sister to the Pteridifolia group are rainforest taxa like *G. baileyana* and *robusta*. It is possible that rather than an increase in speciation rate of the Pteridifolia group, there has been an increase in the extinction rate of these rainforest taxa. These questions await reanalysis with a complete molecular phylogeny and better understanding of pollinator syndromes across the clade.

The Nullarbor Plain and its influence on the diversification of the rich endemic southwest and southeast floras has long been a central theme in Australian botany (Hooker 1860; Burbidge 1960; Mast & Givnish 2002; Crisp *et al.* 2004; Jabaily *et al.* 2014). Our animated reconstruction of Hakeinae geographic diversification suggests that the first eastern lineages began to arrive ca. 17 mya (Appendix S5). These lineages appear to have given rise to endemic southeast clades that quickly began accumulating species 12-11 mya. This is consistent with the purported uplift of the Nullarbor Plain 14 mya and subsequent endemic diversification in the southeast and southwest (Crisp & Cook 2007). Despite the divide, some clades were able to cross the Nullarbor after the uplift, presumably via refugia like the MacDonnell Ranges. There may also have been limited recent dispersal of southeast lineages back to the southwest. While we caution that such conclusions based on the animated geographic reconstruction are subject to more careful analysis, they certainly support the notion that the Nullarbor Plain was a

significant but not impermeable barrier to Hakeinae dispersal, and that this barrier may account for much of the endemism seen in modern-day temperate Hakeinae.

By filtering out some lineages physiologically unable to persist in climates different than their ancestral climate regime, phylogenetic niche conservatism has been shown to shape which lineages occur where (Algar *et al.* 2009; Miller *et al.* 2013). This process should lead to a pattern of increasing phylogenetic clustering away from the climate of origin of the clade in question. We found weak support for the relationship in the Hakeinae, where the most phylogenetically clustered areas were found in colder and warmer regions than the inferred moderate temperature ancestral region, and precipitation explained little of the variation in lineage co-occurrence patterns. Compared with the Meliphagidae, the Hakeinae showed considerable phylogenetic clustering in the southwest and southeast of the continent. This emphasizes the limited dispersal potential of Hakeinae, and a number of localized, endemic radiations, especially in the southwest and southeast. Arid interior Hakeinae assemblages showed more phylogenetic overdispersion than Meliphagidae, reflecting the differing origins of these groups; the Hakeinae appear to have originated somewhere in the interior of the continent, in a fairly dry area, while the Meliphagidae likely originated in rainforests. Phylogenetic niche conservatism does not seem able to explain much of the variation in lineage co-occurrence patterns of this non-vagile group.

ACKNOWLEDGEMENTS

ETM is grateful for financial support from the National Science Foundation (GRFP #1051698), the St. Louis Audubon Society, a Trans-World Airlines Scholarship from the

University of Missouri, and Macquarie University Higher Degree Research Office. For discussion and/or help in the field that lead to many of the hypotheses in the paper, we recognize: Brian Venebles, Darren Crayn, Rob Kooyman, Dick and Wendy Cooper, Craig Costion, Fay Adams, Hillary Cherry, Glen Sanders, Dan Metcalfe, Garry and Nada Sankowsky, Alison Downing, Jill Newland, Rigel Jensen, Andrew Ford, Steven Murphy, Wade Tozer, Sean Gleason, Don Butler, Bryan Suson and Sarah Wagner. Some of our analyses were run on the University of Missouri Lewis Cluster and the Domino Data Lab.

LITERATURE CITED

1.

Algar, A.C., Kerr, J.T. & Currie, D.J. (2009). Evolutionary constraints on regional faunas: whom, but not how many. *Ecol. Lett.*, 12, 57–65.

2.

APG, I. (2003). The Angiosperm Phylogeny Group. 2003. An update of the Angiosperm Phylogeny Group classification for the orders and families of flowering plants: APG II. *Bot. J. Linn. Soc.*, 141, 399–436.

3.

Barker, R.M., Haegi, L. & Barker, W.R. (1999). Hakea. In: *Flora Aust. Vol. 17B Proteaceae 3*. CSIRO Publishing, Melbourne, Australia, pp. 31–170.

4.

Beadle, N.C.W. (1966). Soil phosphate and its role in molding segments of the Australian flora and vegetation, with special reference to xeromoprhy and sclerophylly. *Ecology*, 47, 992–1007.

5.

Brown, W.L., Jr. (1957). Centrifugal speciation. *Q. Rev. Biol.*, 32, 247–277.

6.

Burbidge, N.T. (1960). The phytogeography of the Australian region. *Aust. J. Bot.*, 8, 75–211.

7.

Carpenter, R.J. (2012). Proteaceae leaf fossils: phylogeny, diversity, ecology and austral distributions. *Bot. Rev.*, 78, 261–287.

8.

Carpenter, R.J., McLoughlin, S., Hill, R.S., McNamara, K.J. & Jordan, G.J. (2014). Early evidence of xeromorphy in angiosperms: Stomatal encryption in a new eocene species of Banksia (Proteaceae) from Western Australia. *Am. J. Bot.*, 101, 1486–1497.

9.

Chao, A. (1987). Estimating the population size for capture-recapture data with unequal catchability. *Biometrics*, 43, 783–791.

10.

Chapman, A.D. (2005). *Principles and Methods of Data Cleaning: Primary Species and Species-occurrence Data*. Global Biodiversity Information Facility.

11.

Christophel, D.C., Scriven, L.J. & Greenwood, D.R. (1992). An Eocene megafossil flora from Nelly Creek, South Australia. *Trans. R. Soc. S. Aust.*, 116, 65–76.

12.

Cornwell, W.K., Westoby, M., Falster, D.S., FitzJohn, R.G., O'Meara, B.C., Pennell, M.W., *et al.* (2014). Functional distinctiveness of major plant lineages. *J. Ecol.*, 102, 345–356.

13.

Crisp, M., Cook, L. & Steane, D. (2004). Radiation of the Australian flora: what can comparisons of molecular phylogenies across multiple taxa tell us about the evolution of diversity in present–day communities? *Philos. Trans. R. Soc. Lond. B. Biol. Sci.*, 359, 1551–1571.

14.

Crisp, M.D. & Cook, L.G. (2007). A congruent molecular signature of vicariance across multiple plant lineages. *Mol. Phylogenet. Evol.*, 43, 1106–1117.

15.

Crisp, M.D. & Cook, L.G. (2013). How was the Australian flora assembled over the last 65 million years? A molecular phylogenetic perspective. *Annu. Rev. Ecol. Evol. Syst.*, 44, 303–324.

16.

Dettmann, M.E. & Clifford, H.T. (2005). Fossil fruit of the Grevilleeae (Proteaceae) in the Tertiary of eastern Australia. *Mem. Qld. Mus.*, 51, 359–374.

17.

Dettmann, M.E. & Jarzen, D.M. (1998). The early history of the Proteaceae in Australia: the pollen record. *Aust. Syst. Bot.*, 11, 401–438.

18.

Dodson, J.. & Macphail, M.. (2004). Palynological evidence for aridity events and vegetation change during the Middle Pliocene, a warm period in Southwestern Australia. *Hum. Dimens. Nat. Process. Environ. Change*, 41, 285–307.

19.

Downing, T.L., Duretto, M.F. & Ladiges, P.Y. (2004). Morphological analysis of the

Grevillea ilicifolia complex (Proteaceae) and recognition of taxa. *Aust. Syst. Bot.*, 17, 327–341.

20.

Fonseca, C.R., Overton, J.M., Collins, B. & Westoby, M. (2000). Shifts in trait-combinations along rainfall and phosphorus gradients. *J. Ecol.*, 88, 964–977.

21.

Ford, H.A., Paton, D.C. & Forde, N. (1979). Birds as pollinators of Australian plants. *N. Z. J. Bot.*, 17, 509–519.

22.

Frakes, L.A. (1999). Evolution of Australian environments. In: *Flora Aust.* CSIRO Publishing, Melbourne, Australia.

23.

Greenwood, D.R. (1996). Eocene monsoon forests in central Australia? *Aust. Syst. Bot.*, 9, 95–112.

24.

Greenwood, D.R. & Huber, M. (2011). Eocene precipitation: a global monsoon? Abstract T22C-07. Presented at the Fall Meeting, American Geophysical Union, 5-9 Dec, San Francisco, CA.

25.

Greenwood, D.R., Moss, P.T., Rowett, A.I., Vadala, A.J. & Keefe, R.L. (2003). Plant communities and climate change in southeastern Australia during the early Paleogene. In: *Causes Consequences Glob. Warm Clim. Early Paleogene*, Special Paper (eds. Wing, S.L., Gingerich, P.D., Schmitz, B. & Thomas, E.). Geological Society of America, Boulder, Colorado, pp. 365–380.

26.

Harmon, L.J., Weir, J.T., Brock, C.D., Glor, R.E. & Challenger, W. (2008). GEIGER: investigating evolutionary radiations. *Bioinformatics*, 24, 129–131.

27.

Herold, N., Huber, M., Greenwood, D.R., Müller, R.D. & Seton, M. (2011). Early to Middle Miocene monsoon climate in Australia. *Geology*, 39, 3–6.

28.

Hill, R.S. (1998). Fossil evidence for the onset of xeromorphy and scleromorphy in Australian Proteaceae. *Aust. Syst. Bot.*, 11, 391–400.

29.

Hill, R.S. (2004). Origins of the southeastern Australian vegetation. *Philos. Trans. R. Soc. Lond. B. Biol. Sci.*, 359, 1537–1549.

30.

Hill, R.S., Truswell, E.M., McLoughlin, S. & Dettman, M.E. (1999). The evolution of the Australian flora: fossil evidence. In: *Flora Aust.* CSIRO Publishing, Canberra, pp. 251–320.

31.

Holdgate, G.R., Wallace, M.W., Gallagher, S.J., Wagstaff, B.E. & Moore, D. (2008). No mountains to snow on: major post-Eocene uplift of the East Victoria Highlands; evidence from Cenozoic deposits. *Aust. J. Earth Sci.*, 55, 211–234.

32.

Hooker, J.D. (1860). *The botany of the Antarctic voyage of H.M. Discovery ships* Erebus *and* Terror *in the Years 1839-1843, under the command of Captain Sir James Clark Ross. Part III. Flora Tasmaniae.* Reeve Brothers, London.

33.

Hopper, S.D. & Gioia, P. (2004). The southwest Australian floristic region: evolution and conservation of a global hot spot of biodiversity. *Annu. Rev. Ecol. Evol. Syst.*, 623–650.

34.

Huber, M. & Goldner, A. (2012). Eocene monsoons. *J. Asian Earth Sci.*, 44, 3–23.

35.

Jabaily, R.S., Shepherd, K.A., Gardner, A.G., Gustafsson, M.H.G., Howarth, D.G. & Motley, T.J. (2014). Historical biogeography of the predominantly Australian plant family Goodeniaceae. *J. Biogeogr.*

36.

Johnson, L.A.S. & Briggs, B.G. (1975). On the Proteaceae—the evolution and classification of a southern family*. *Bot. J. Linn. Soc.*, 70, 83–182.

37.

Jordan, G.J., Carpenter, R.J. & Hill, R.S. (1998). The macrofossil record of Proteaceae in Tasmania: a review with new species. *Aust. Syst. Bot.*, 11, 465–501.

38.

Jordan, G.J., Dillon, R.A. & Weston, P.H. (2005). Solar radiation as a factor in the evolution of scleromorphic leaf anatomy in Proteaceae. *Am. J. Bot.*, 92, 789–796.

39.

Jordan, G.J., Weston, P.H., Carpenter, R.J., Dillon, R.A. & Brodribb, T.J. (2008). The evolutionary relations of sunken, covered, and encrypted stomata to dry habitats in Proteaceae. *Am. J. Bot.*, 95, 521–530.

40.

Kembel, S.W., Cowan, P.D., Helmus, M.R., Cornwell, W.K., Morlon, H., Ackerly, D.D., *et al.* (2010). Picante: R tools for integrating phylogenies and ecology. *Bioinformatics*, 26, 1463–1464.

41.

Kuhn, T.S., Mooers, A.Ø. & Thomas, G.H. (2011). A simple polytomy resolver for dated phylogenies. *Methods Ecol. Evol.*, 2, 427–436.

42.

Lambers, H., Raven, J.A., Shaver, G.R. & Smith, S.E. (2008). Plant nutrient-acquisition strategies change with soil age. *Trends Ecol. Evol.*, 23, 95–103.

43.

Landis, M.J. & Bedford, T. (2014). Phylowood: interactive web-based animations of biogeographic and phylogeographic histories. *Bioinformatics*, 30, 123–124.

44.

Makinson, R.O. (2000). Grevillea. In: *Flora Aust. Vol. 17A Proteaceae 2*. CSIRO Publishing, Melbourne, Australia, pp. 1–460.

45.

Mast, A.R. & Givnish, T.J. (2002). Historical biogeography and the origin of stomatal distributions in Banksia and Dryandra (Proteaceae) based on their cpDNA phylogeny. *Am. J. Bot.*, 89, 1311–1323.

46.

Mast, A.R., Milton, E.F., Jones, E.H., Barker, R.M., Barker, W.R. & Weston, P.H. (2012). Time-calibrated phylogeny of the woody Australian genus Hakea (Proteaceae) supports multiple origins of insect-pollination among bird-pollinated ancestors. *Am. J. Bot.*, 99, 472–487.

47.

McGowran, B., Holdgate, G.R., Li, Q. & Gallagher, S.J. (2004). Cenozoic stratigraphic succession in southeastern Australia. *Aust. J. Earth Sci.*, 51, 459–496.

48.

McLoughlin, S. (2001). The breakup history of Gondwana and its impact on pre-Cenozoic floristic provincialism. *Aust. J. Bot.*, 49, 271–300.

49.

Miller, E.T., Zanne, A.E. & Ricklefs, R.E. (2013). Niche conservatism constrains Australian honeyeater assemblages in stressful environments. *Ecol. Lett.*, 16, 1186–1194.

50.

Mitchell, K.J., Pratt, R.C., Watson, L.N., Gibb, G.C., Llamas, B., Kasper, M., *et al.* (2014). Molecular phylogeny, biogeography, and habitat preference evolution of marsupials. *Mol. Biol. Evol.*, 31, 2322–2330.

51.

Oksanen, J., Blanchet, F.G., Kindt, R., Legendre, P., Minchin, P.R., O'Hara, R.B., *et al.* (2013). *vegan: Community Ecology Package*.

52.

Orians, G.H. & Milewski, A.V. (2007). Ecology of Australia: the effects of nutrient-poor soils and intense fires. *Biol. Rev.*, 82, 393–423.

53.

Pate, J.S., Verboom, W.H. & Galloway, P.D. (2001). TURNER REVIEW No. 4. Co-occurrence of Proteaceae, laterite and related oligotrophic soils: coincidental associations or causative inter-relationships? *Aust. J. Bot.*, 49, 529–560.

54.

Pole, M.S. & Bowman, D.M.J.S. (1996). Tertiary plant fossils from Australia's' Top End'. *Aust. Syst. Bot.*, 9, 113–126.

55.

Purnell, H.M. (1960). Studies of the family Proteaceae. I. Anatomy and morphology of the roots of some Victorian species. *Aust. J. Bot.*, 8, 38–50.

56.

Rabosky, D.L. (2014). Automatic Detection of Key Innovations, Rate Shifts, and Diversity-Dependence on Phylogenetic Trees. *PLoS ONE*, 9, e89543.

57.

Rabosky, D.L., Grundler, M., Anderson, C., Title, P., Shi, J.J., Brown, J.W., *et al.* (2014). BAMMtools: an R package for the analysis of evolutionary dynamics on phylogenetic trees. *Methods Ecol. Evol.*, 5, 701–707.

58.

R Development Core Team. (2011). *R: A language and environment for statistical computing*. R Foundation for Statistical Computing, Vienna, Austria, http://www.R-project.org.

59.

Revell, L.J. (2012). phytools: an R package for phylogenetic comparative biology (and other things). *Methods Ecol. Evol.*, 3, 217–223.

60.

Rieseberg, L.H. & Willis, J.H. (2007). Plant speciation. *Science*, 317, 910–914.

61.

Rosenzweig, M.L. (1995). *Species diversity in space and time*. Cambridge University Press, Cambridge, UK.

62.

Sauquet, H., Weston, P.H., Anderson, C.L., Barker, N.P., Cantrill, D.J., Mast, A.R., *et al.* (2009). Contrasted patterns of hyperdiversification in Mediterranean hotspots. *Proc. Natl. Acad. Sci.*, 106, 221–225.

63.

Slater, G.J., Harmon, L.J. & Alfaro, M.E. (2012). Intergrating fossils with molecular phylogenies improves inference of trait evolution. *Evolution*, 66, 3931–3944.

64.

Stevens, G.C. (1989). The latitudinal gradient in geographical range: how so many species coexist in the tropics. *Am. Nat.*, 240–256.

65.

Toon, A., Cook, L.G. & Crisp, M.D. (2014). Evolutionary consequences of shifts to bird-pollination in the Australian pea-flowered legumes (Mirbelieae and Bossiaeeae). *BMC Evol. Biol.*, 14, 43.

66.

Truswell, E.M. (1993). Vegetation in the Australian Tertiary in response to climatic and phytogeographic forcing factors. *Aust. Syst. Bot.*, 6, 533–557.

67.

Vadala, A.J. & Greenwood, D.R. (2001). Australian Paleogene vegetation and environments: evidence for palaeo-Gondwanic elements in the fossil records of Lauraceae and Proteaceae. In: *Faunal Flor. Migr. Evol. Southeast Asia–Australasia* (eds. Metcalfe, I., Smith, J.M.B. & Davidson, I.). Swets & Zeitlinger, Lisse, pp. 196–221.

68.

Vasconcelos, P.M., Knesel, K.M., Cohen, B.E. & Heim, J.A. (2008). Geochronology of the Australian Cenozoic: a history of tectonic and igneous activity, weathering, erosion, and sedimentation*. *Aust. J. Earth Sci.*, 55, 865–914.

69.

Weston, P.H. & Barker, N.P. (2006). A new suprageneric classification of the Proteaceae, with an annotated checklist of genera. *Telopea*, 11, 314–344.

70.

Willmott, C.J. & Feddema, J.J. (1992). A more rational climatic moisture index. *Prof. Geogr.*, 44, 84–88.

71.

Young, R. & McDougall, I. (1993). Long-term landscape evolution: Early Miocene and modern rivers in southern New South Wales, Australia. *J. Geol.*, 35–49.

FIGURE LEGENDS

Figure 1. Time-calibrated molecular phylogeny of the Australian *Hakea* and *Grevillea*. Branches are colored from blue to red as a function of the model-averaged lineage-specific speciation rate as calculated in BAMM.

Figure 2. Phyloclimatespace figure showing Hakeinae radiation across mean annual temperature and precipitation. Branches are colored from blue to red as a function of distance from the root. Light gray points represent grid-cell averaged climate values, used to show the breadth of climate space available to the Hakeinae in Australia. The phylogeny used in this figure is the randomMCC tree, and ancestral states are reconstructed with maximum likelihood.

Figure 3. Speciation rate through time of the entire Hakeinae and the two clades that were detected as exhibiting significantly elevated rates of speciation. The phylogeny used in this figure is the randomMCC tree.

Figure 4. Grid-cell averaged diversification rates across Australia, where red represents the fastest rates. The phylogeny used in this figure is the randomMCC tree.

Figure 5. Map of differences in phylogenetic community structure between the Meliphagidae, a bird family, and the Hakeinae. Red colors correspond to areas where the Hakeinae are more phylogenetically clustered than the Meliphagidae, while blues correspond to areas where the Hakeinae are phylogenetically overdispersed as compared with the Meliphagidae.

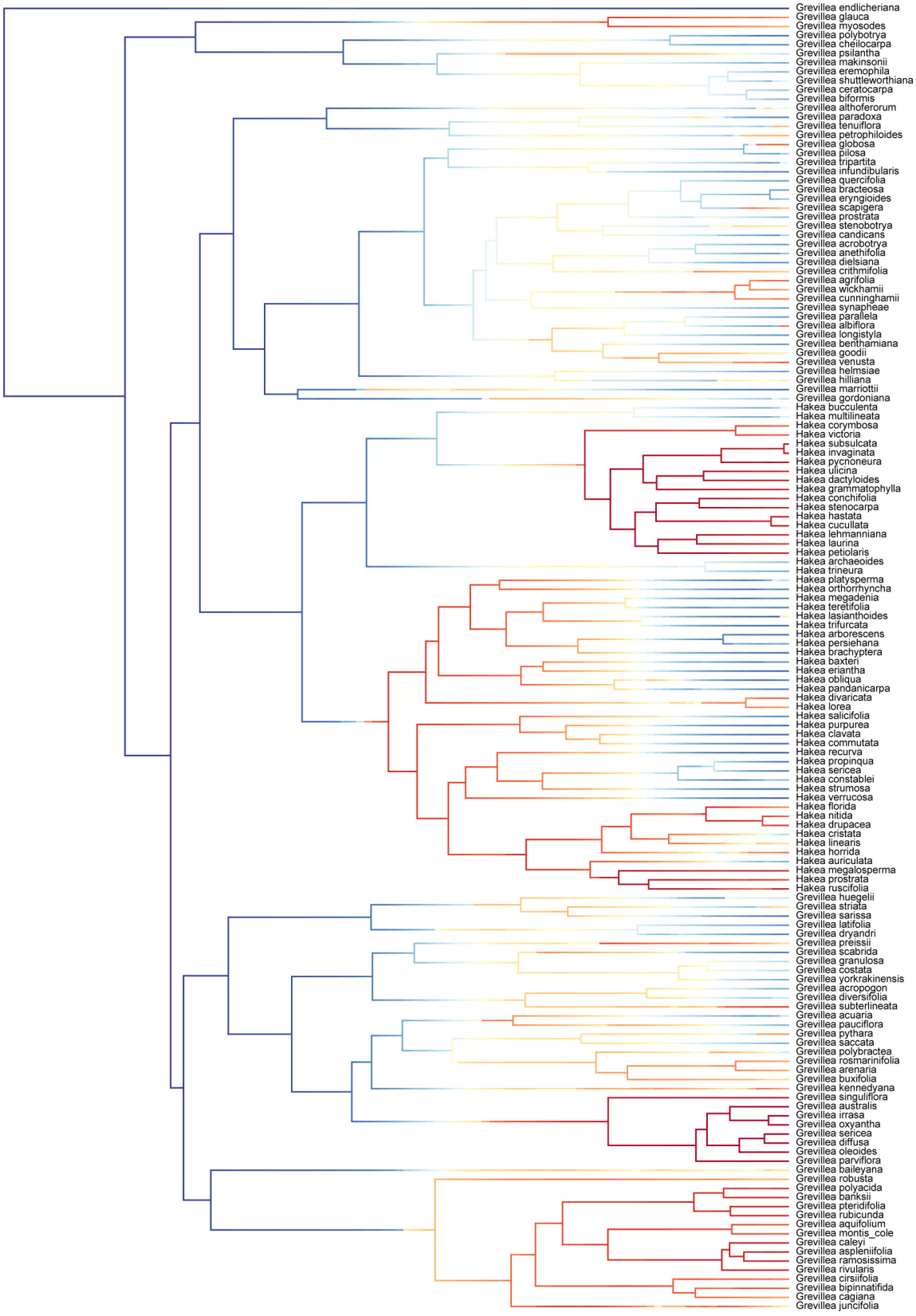
Grevillea endlicheriana
Grevillea glauca
Grevillea myosodes
Grevillea polybotrya
Grevillea cheilocarpa
Grevillea psilantha
Grevillea makinsonii
Grevillea eremophila
Grevillea shuttleworthiana
Grevillea ceratocarpa
Grevillea biformis
Grevillea althoferorum
Grevillea paradoxa
Grevillea tenuiflora
Grevillea petrophiloides
Grevillea globosa
Grevillea pilosa
Grevillea tripartita
Grevillea infundibularis
Grevillea quercifolia
Grevillea bracteosa
Grevillea eryngioides
Grevillea scapigera
Grevillea prostrata
Grevillea stenobotrya
Grevillea candicans
Grevillea acrobotrya
Grevillea anethifolia
Grevillea dielsiana
Grevillea crithmifolia
Grevillea agrifolia
Grevillea wickhamii
Grevillea cunninghamii
Grevillea synapheae
Grevillea parallela
Grevillea albiflora
Grevillea longistyla
Grevillea benthamiana
Grevillea goodii
Grevillea venusta
Grevillea helmsiae
Grevillea hilliana
Grevillea marriottii
Grevillea gordoniana
Hakea bucculenta
Hakea multilineata
Hakea corymbosa
Hakea victoria
Hakea subsulcata
Hakea invaginata
Hakea pycnoneura
Hakea ulicina
Hakea dactyloides
Hakea grammatophylla
Hakea conchifolia
Hakea stenocarpa
Hakea hastata
Hakea cucullata
Hakea lehmanniana
Hakea laurina
Hakea petiolaris
Hakea archaeoides
Hakea trineura
Hakea platysperma
Hakea orthorrhyncha
Hakea megadenia
Hakea teretifolia
Hakea lasianthoides
Hakea trifurcata
Hakea arborescens
Hakea persiehana
Hakea brachyptera
Hakea baxteri
Hakea eriantha
Hakea obliqua
Hakea pandanicarpa
Hakea divaricata
Hakea lorea
Hakea salicifolia
Hakea purpurea
Hakea clavata
Hakea commutata
Hakea recurva
Hakea propinqua
Hakea sericea
Hakea constablei
Hakea strumosa
Hakea verrucosa
Hakea florida
Hakea nitida
Hakea drupacea
Hakea cristata
Hakea linearis
Hakea horrida
Hakea auriculata
Hakea megalosperma
Hakea prostrata
Hakea ruscifolia
Grevillea huegelii
Grevillea striata
Grevillea sarissa
Grevillea latifolia
Grevillea dryandri
Grevillea preissii
Grevillea scabrida
Grevillea granulosa
Grevillea costata
Grevillea yorkrakinensis
Grevillea acropogon
Grevillea diversifolia
Grevillea subterlineata
Grevillea acuaria
Grevillea pauciflora
Grevillea pythara
Grevillea saccata
Grevillea polybractea
Grevillea rosmarinifolia
Grevillea arenaria
Grevillea buxifolia
Grevillea kennedyana
Grevillea synguliflora
Grevillea australis
Grevillea irrasa
Grevillea oxyantha
Grevillea sericea
Grevillea diffusa
Grevillea oleoides
Grevillea parviflora
Grevillea baileyana
Grevillea robusta
Grevillea polyacida
Grevillea banksii
Grevillea pteridifolia
Grevillea rubicunda
Grevillea aquifolium
Grevillea montis_cole
Grevillea caleyi
Grevillea asplenifolia
Grevillea ramosissima
Grevillea rivularis
Grevillea cirsiifolia
Grevillea bipinnatifida
Grevillea cagiana
Grevillea juncifolia

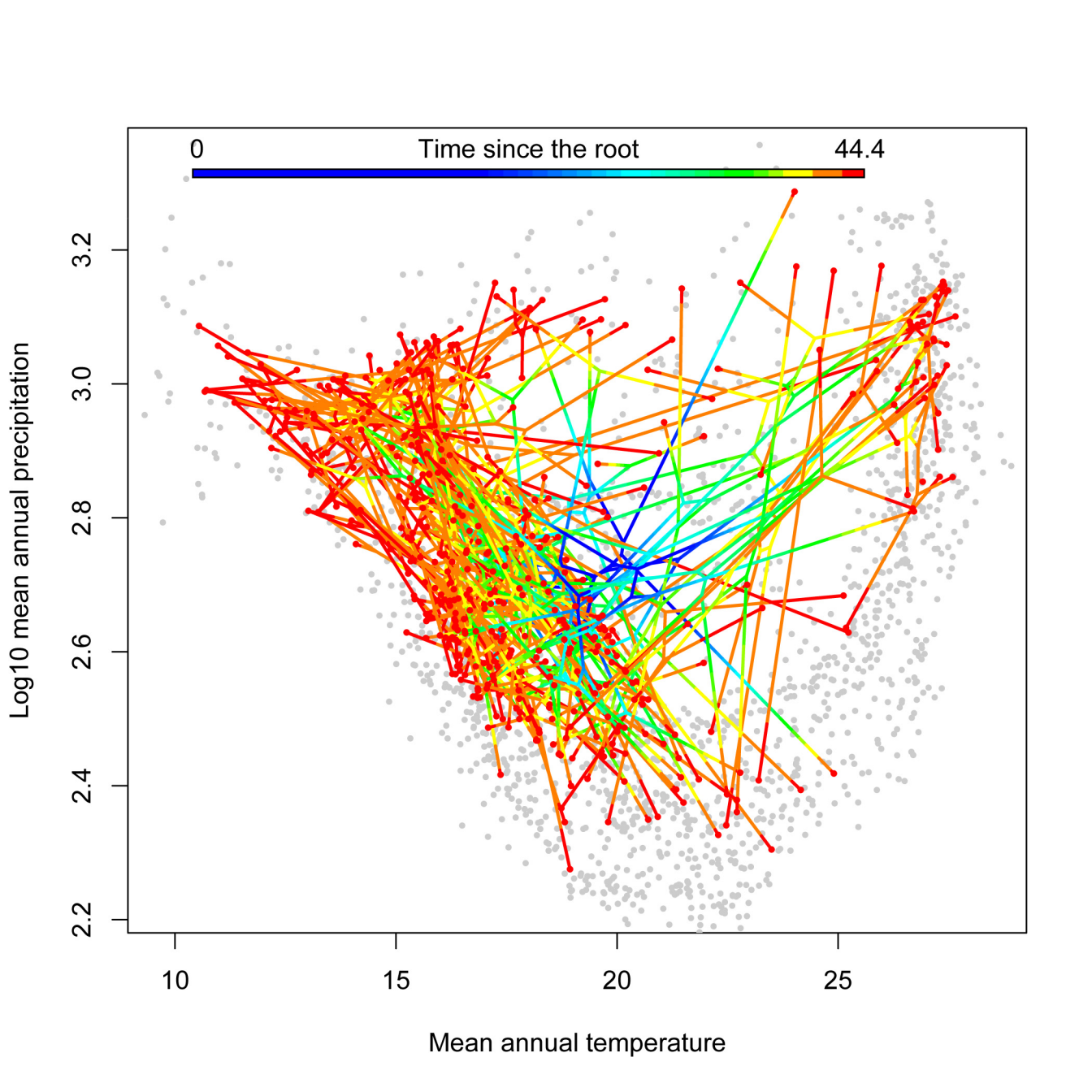
0
Time since the root
44.4
Log10 mean annual precipitation
3.2
3.0
2.8
2.6
2.4
2.2
10
15
20
25
Mean annual temperature

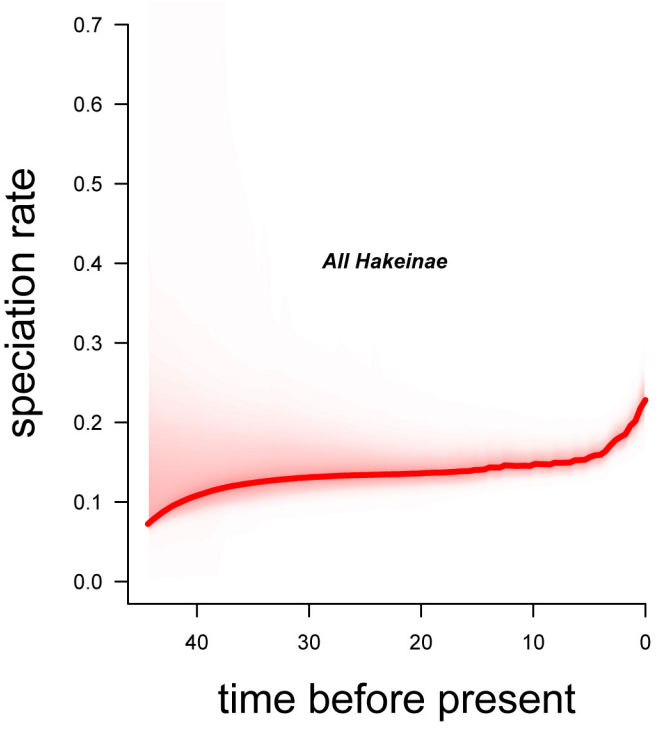
speciation rate
0.0
0.1
0.2
0.3
0.4
0.5
0.6
0.7
All Hakeinae
40
30
20
10
0
time before present

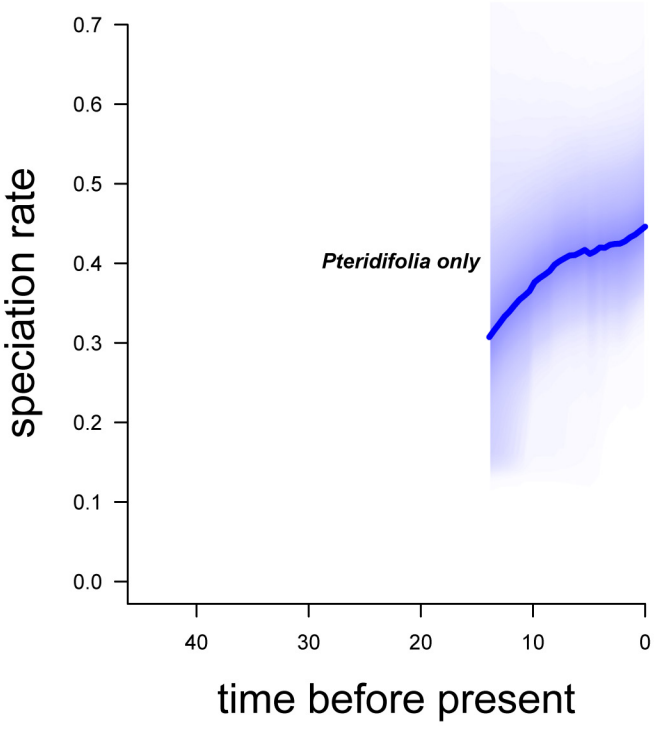
speciation rate
0.0
0.1
0.2
0.3
0.4
0.5
0.6
0.7
Pteridifolia only
40
30
20
10
0
time before present

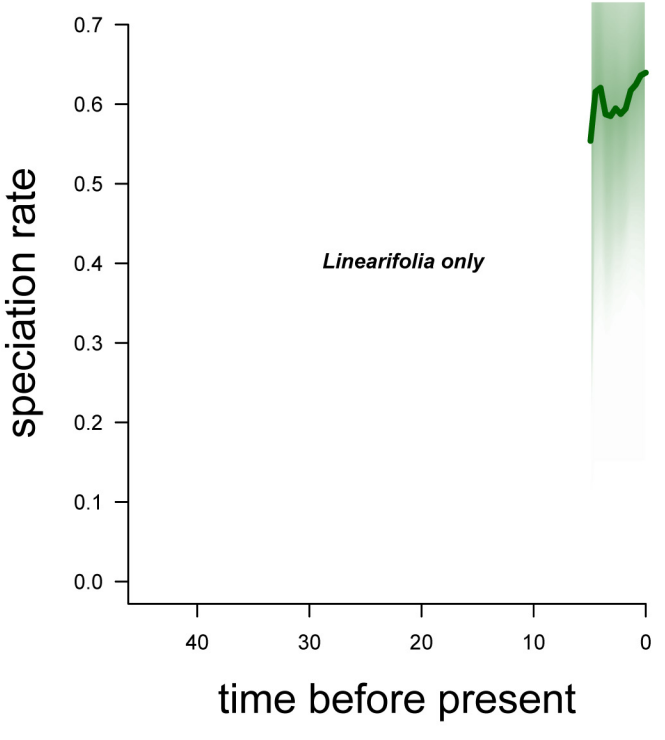
speciation rate
0.0
0.1
0.2
0.3
0.4
0.5
0.6
0.7
Linearifolia only
40
30
20
10
0
time before present

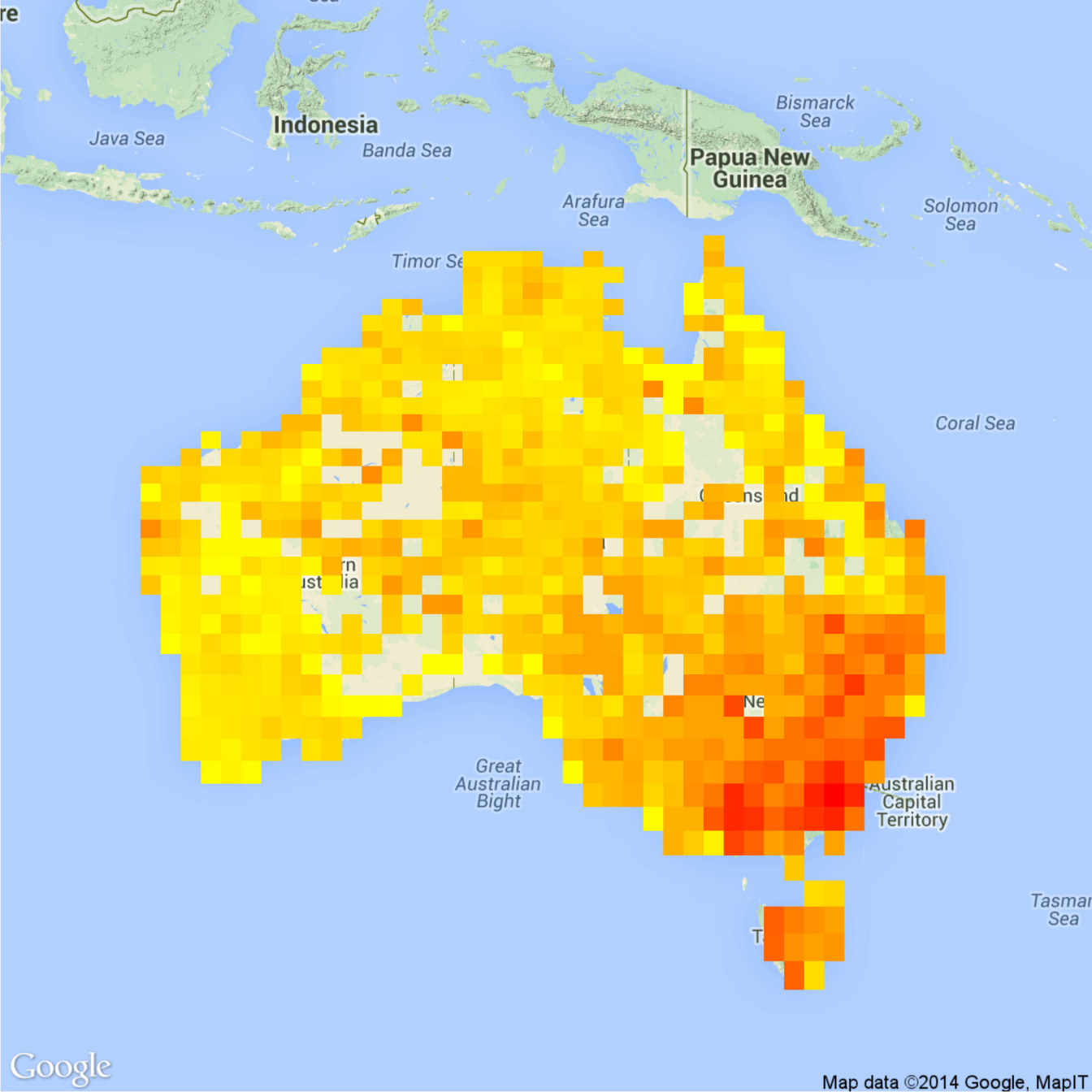
Indonesia
Java Sea
Banda Sea
Bismarck Sea
Papua New Guinea
Arafura Sea
Solomon Sea
Timor Se
Coral Sea
Great Australian Bight
Australian Capital Territory
Tasman Sea
Google
Map data ©2014 Google, MapIT

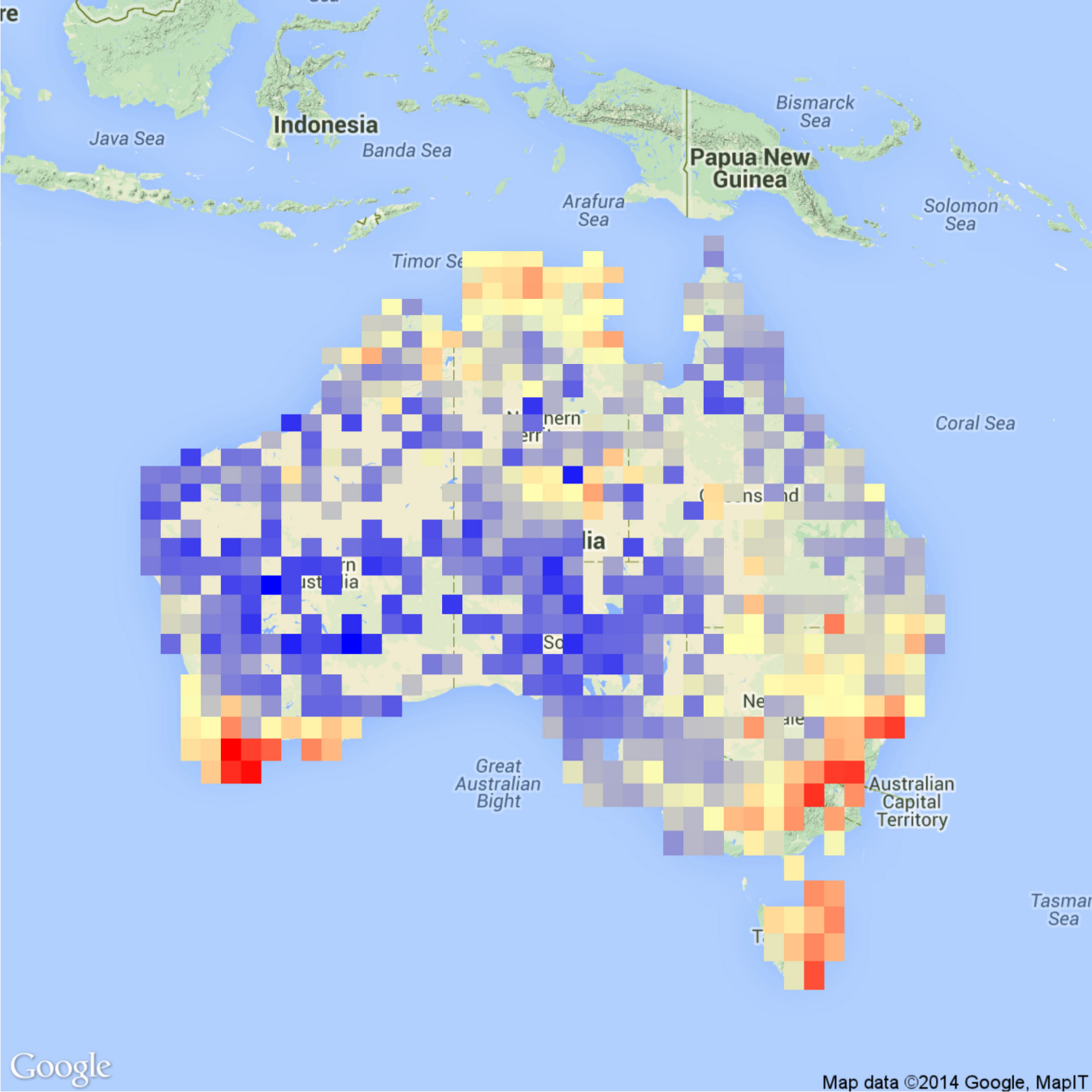
Indonesia
Java Sea
Banda Sea
Bismarck Sea
Papua New Guinea
Arafura Sea
Solomon Sea
Coral Sea
Great Australian Bight
Australian Capital Territory
Tasman Sea
Google
Map data ©2014 Google, MapIT

Appendix S1. Range size distributions among Hakeinae assemblages, and relation to Rapoport's rule

Rapoport's rule, as originally formulated, proposed that species range sizes are positively correlated with latitude (Stevens 1989). The focus on latitude has shifted over the years, and one modern interpretation of the rule states that climate stability may buffer small-ranged species from extinction, leading to a correlation between seasonality and range size. Recent support for the "rule" has been weak (Gaston *et al.* 1998), though some have found support for it (Morueta-Holme *et al.* 2013). In this appendix, we test the support for this interpretation of the rule, and also examine other aspects of range size distributions across the Australian continent.

As described in the main text, we calculated range size per species as the number of 100 x 100 km grid cells that species occurs in. Then, per-grid, we calculated the mean, standard deviation, kurtosis and skewness (the four moments) of the distribution of range sizes of the constituent species. To visually summarize these different aspects of range size distributions, we ordinated the four moments with a principal coordinates analysis, with the variables scaled and centered. We then took the position of each grid cell along the first three PC axes and used this to create an RGB color scale. Here, the red, green and blue components of the scale were functions of the position of the grid cell along axes 1, 2 and 3, respectively.

We found that average range sizes of species are clearly largest in the center and north of the continent (Fig. S1.1). Standard deviation in range size follows a similar pattern (Fig. S1.2). Differences between the southwest and southeast Hakeinae are

apparent in the kurtosis (Fig. S1.3) and skew (Fig. S1.4) of the constituent species. Southwestern sites have more small-ranged species than do southeastern sites, in addition to a number of large-ranged species that also occur in the southwest. This can be seen in the PCA map (Fig. S1.5), where southwestern sites are colored less red, due to kurtosis and skew being strongly negatively loaded on PC1 (Table S1).

We found that average range size was positively correlated with MAT ($R^2 = 0.27$, $p < 0.001$) and negatively correlated with MAP ($R^2 = 0.24$, $p < 0.011$) and MI ($R^2 = 0.38$, $p < 0.001$). More relevantly, it was also positively correlated with precipitation seasonality and particularly with temperature seasonality. These two seasonality variables are negatively correlated with each other; a multiple regression with a significant interaction term between temperature and precipitation seasonality explained much of the variation in range size ($R^2 = 0.46$, $p < 0.01$).

We therefore find some support for Rapoport's rule in the Australian Hakeinae, where a combination of temperature and precipitation seasonality was able to explain much of the variation in average range size. That said, highly seasonal climates characterize large areas of the Australian continent; species in seasonal regions have more space across which to spread. In general, we echo Gaston *et*. *al*'s sentiments that at best this pattern should be called the Rapoport effect. While it may well be a general macroecological phenomenon, future research would be better aimed towards understanding the mechanisms that might generate differential extinction patterns across different climate regimes, rather than addressing the generality of the rule per se.

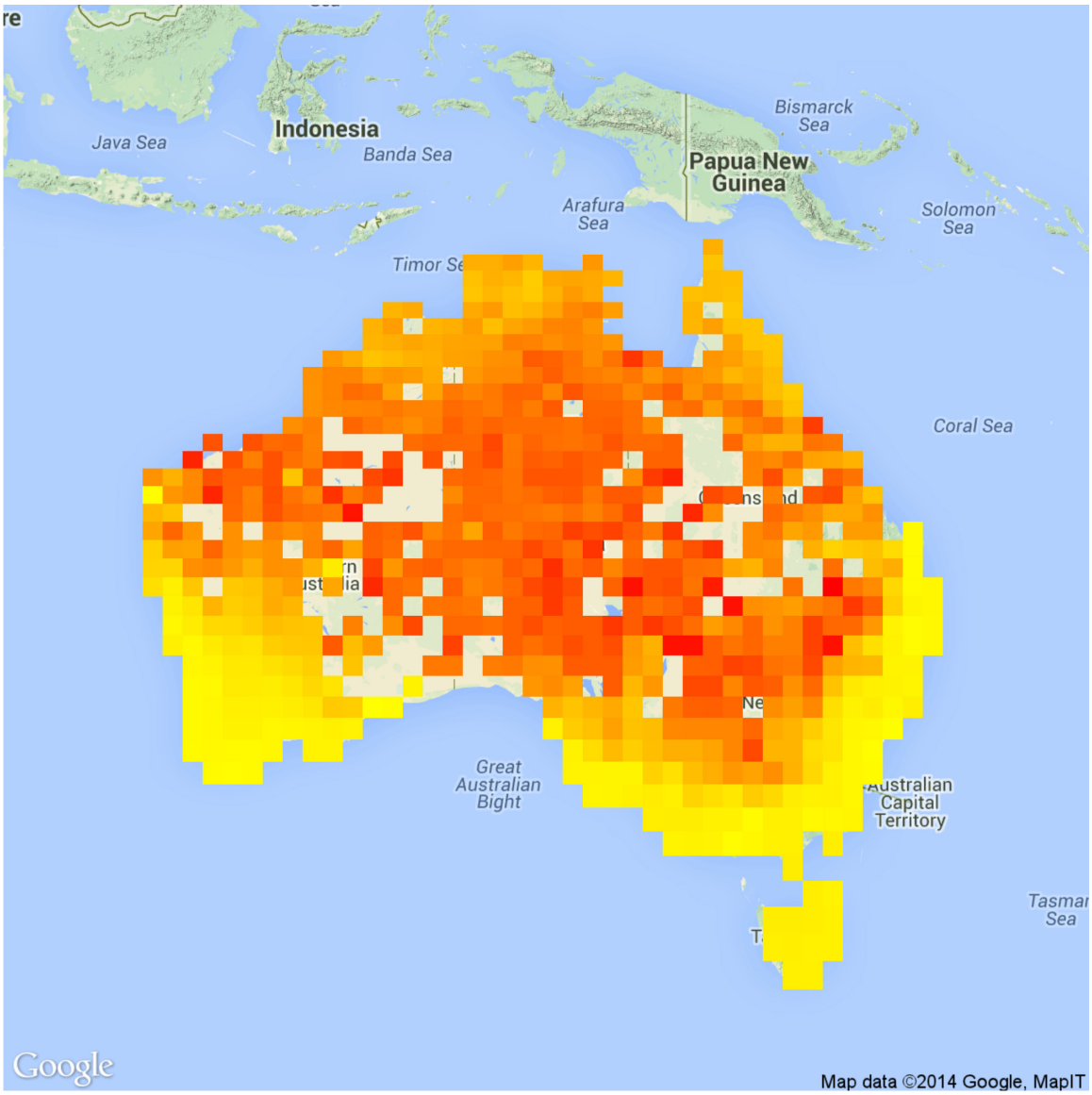

Figure S21. Map of average range size per grid cell across Australia.

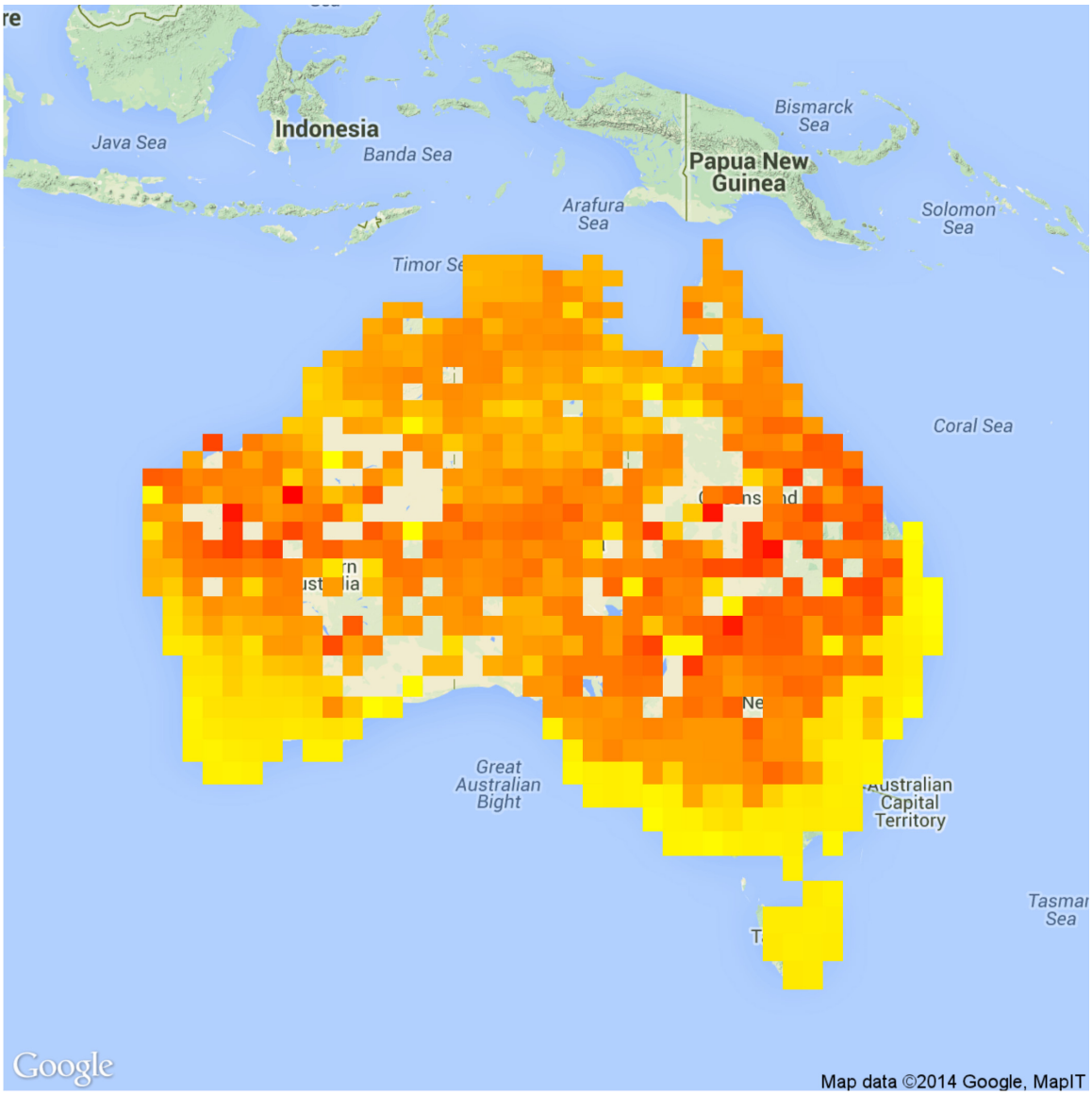

Figure S22. Map of standard deviation in range size per grid cell across Australia.

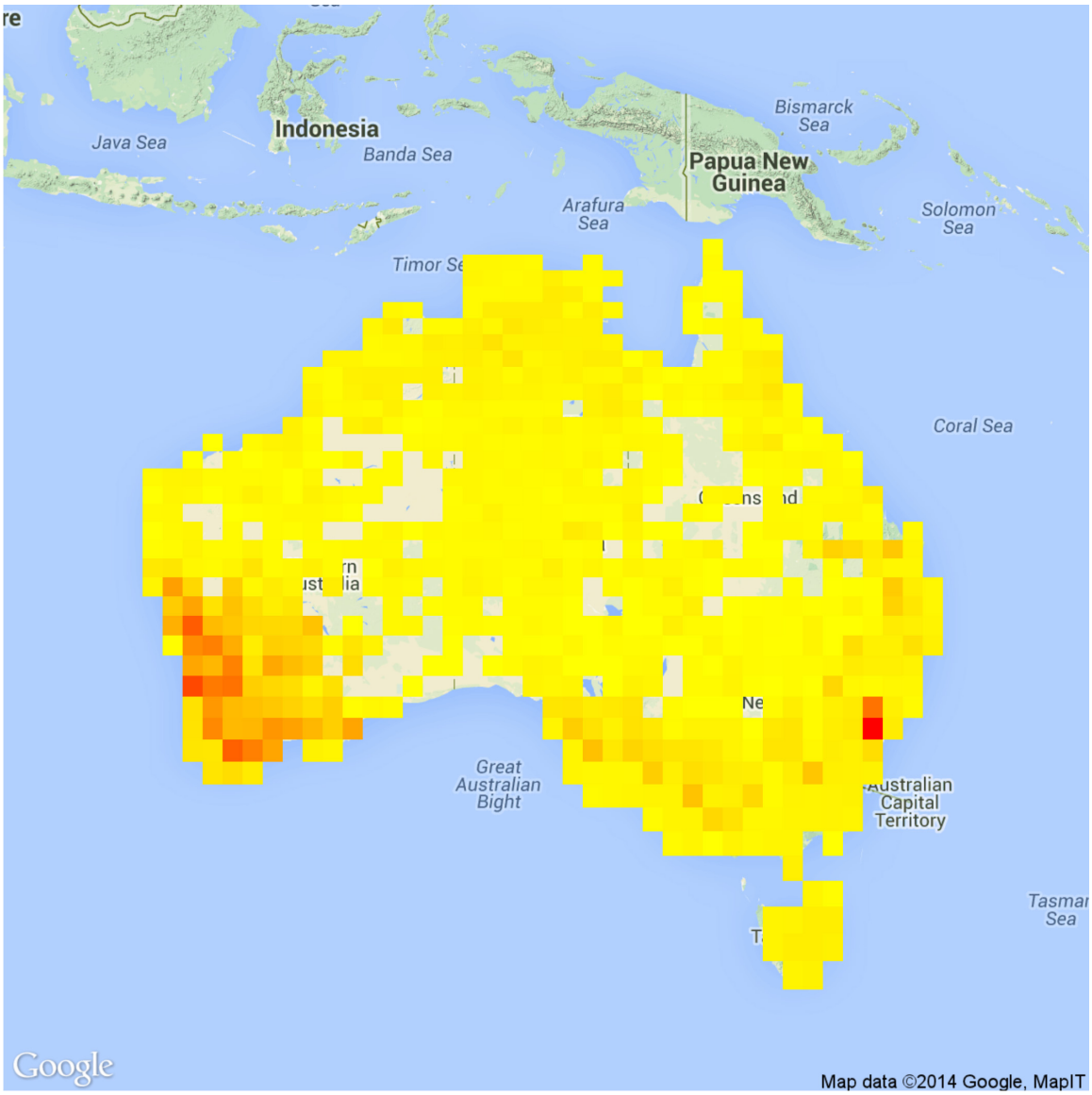

Figure S23. Map of the kurtosis in range size per grid cell across Australia.

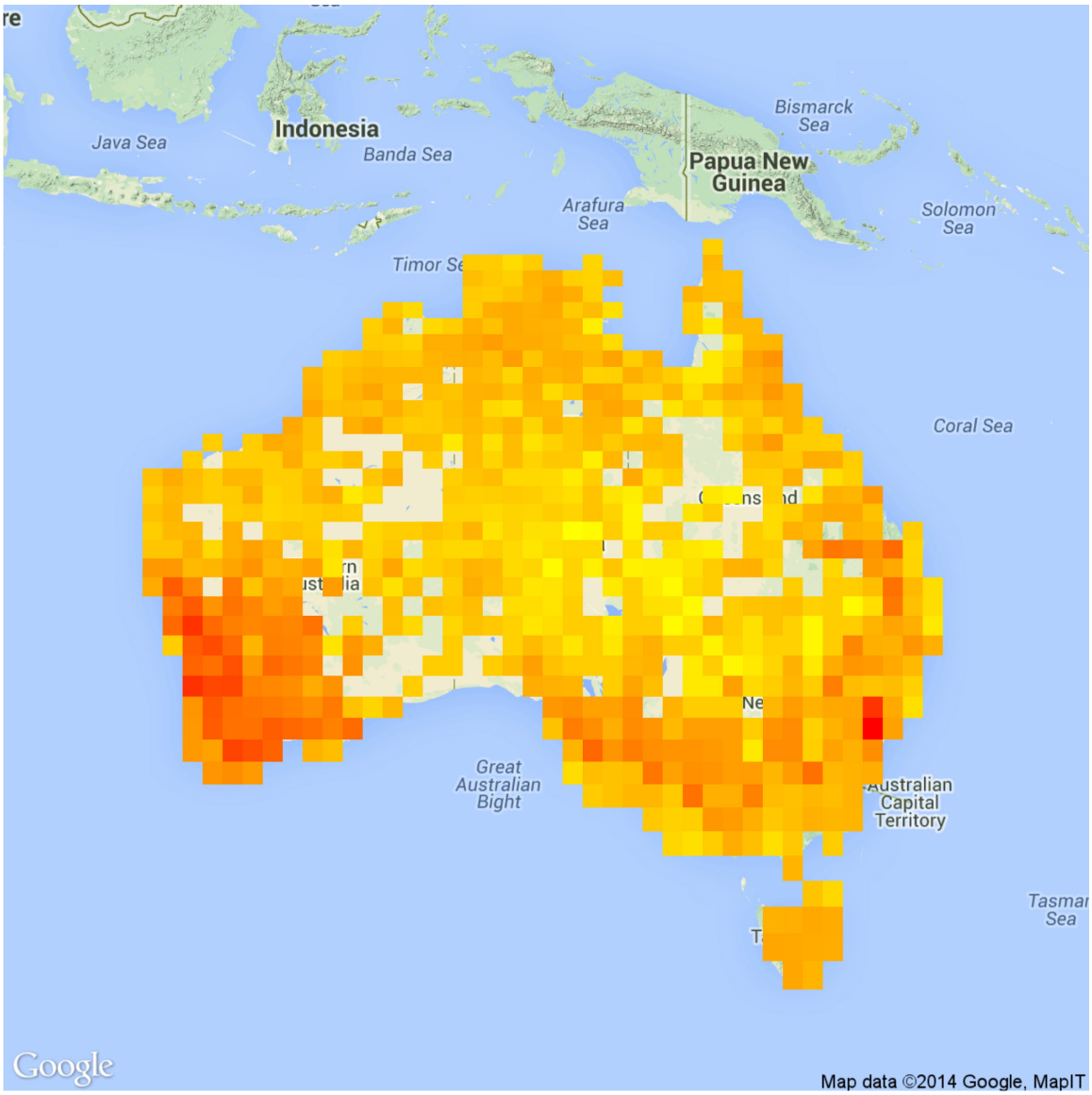

Figure S24. Map of the skewness in range size per grid cell across Australia.

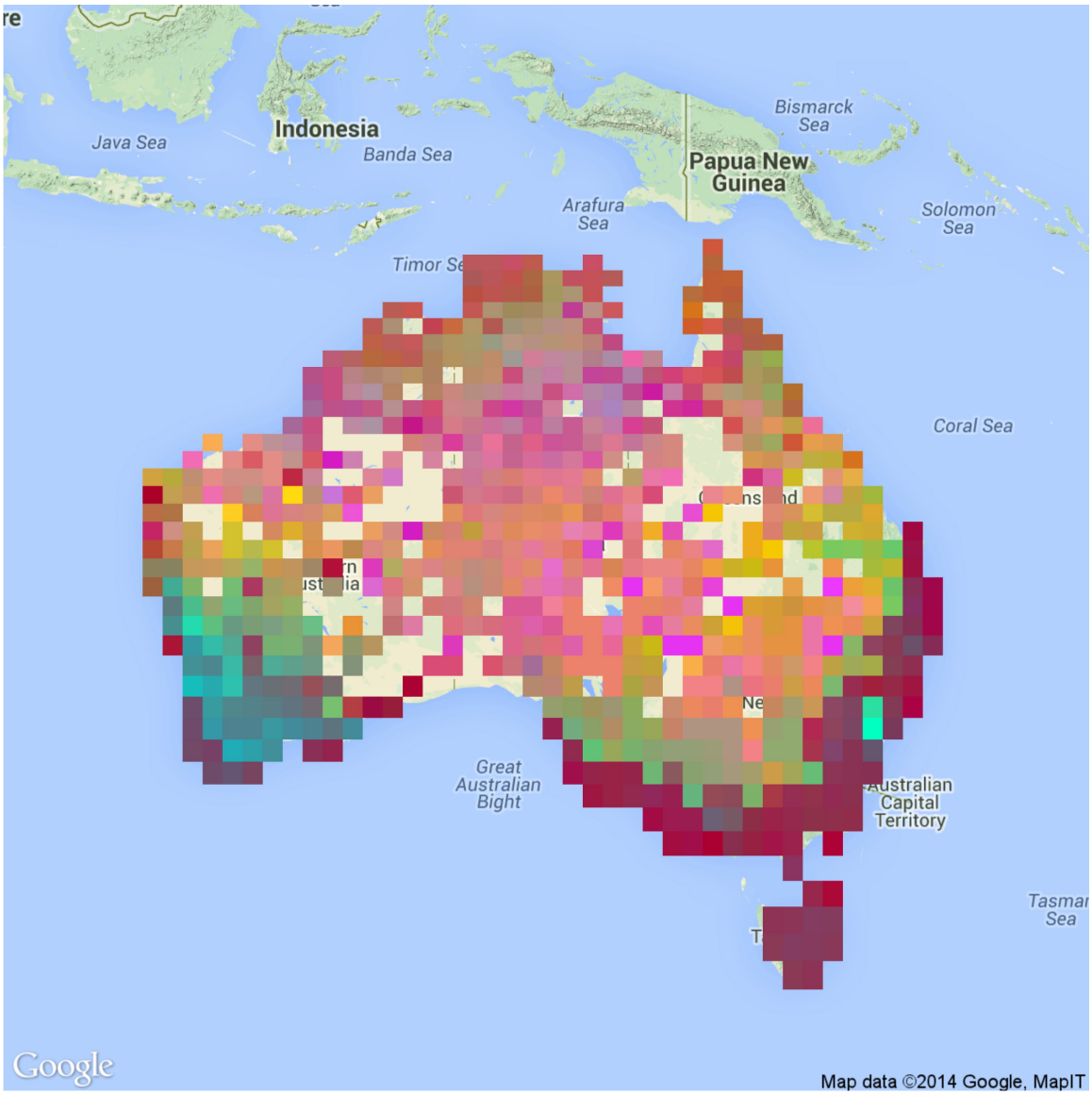

Figure S1.5. Map of the four moments (mean, standard deviation, kurtosis, skewness) of range size per grid. The moments were ordinated with a PCA, then grid cells were assigned colors as a function of their position along PC1 (red), PC2 (green) and PC3 (blue). The loadings for these axes are given in Table S1. As an example, the unique teal color of the southwest reflects the negative position of its grid cells along PC1 (small average range and standard deviation in range), and strongly positive positions along PC2 and PC3 (large kurtosis and skew in range size distribution per cell).

	PC1	PC2	PC3	PC4
Mean	0.52	0.25	0.80	0.14
Std. deviation	0.36	0.80	-0.46	-0.12
Kurtosis	-0.55	0.35	0.36	-0.67
Skewness	-0.55	0.41	0.11	0.72

Table 1. Loadings on a scaled and centered PCA of each of the four moments of range size distributions across grid cells among Australian Hakeinae.

REFERENCES

1.

Gaston, K.J., Blackburn, T.M. & Spicer, J.I. (1998). Rapoport's rule: time for an epitaph? *Trends Ecol. Evol.*, 13, 70–74.

2.

Morueta-Holme, N., Enquist, B.J., McGill, B.J., Boyle, B., Jørgensen, P.M., Ott, J.E., *et al.* (2013). Habitat area and climate stability determine geographical variation in plant species range sizes. *Ecol. Lett.*, 16, 1446–1454.

3.

Stevens, G.C. (1989). The latitudinal gradient in geographical range: how so many species coexist in the tropics. *Am. Nat.*, 240–256.

Appendix S2. Methods of molecular phylogenetic reconstruction

We created a molecular dataset of four chloroplast DNA (cpDNA) regions from up to 171 accessions, representing 93 species of *Grevillea*, 55 of *Hakea*, and 1 species from each of the other 10 genera in tribe Embothrieae (to which subtribe Hakeinae belongs), 1 species from each of the other 3 tribes in subfamily Grevilleoideae (to which Embothrieae belongs), 1 species from each of the other 4 subfamilies in Proteaceae, and 1 species from each of the other 2 families in the order Proteales (following Weston & Barker 2006). Our sampling of *Grevillea* was taxonomically even, with 1-12 representatives from 40 of the 41 informal groups recognized by Olde & Marriott (1994), and 1-12 representatives from each of the 33 informal groups recognized by Makinson (2000). Olde and Marriott's (1994) monotypic Group 24, composed of *Grevillea papuana* from Papua New Guinea, was not sampled.

We extracted genomic DNA using the DNEasy Plant Mini Kit (Qiagen, Valencia, California, USA). The four cpDNA regions that we sampled are the *matK*, *atpB*, and *ndhF* genes and the *rpl16* intron. We amplified and sequenced all DNA regions, except the *rpl16* intron, following Mast *et al.* (2008). We sequenced the *rpl16* intron following Mast *et al.* (2005). We aligned and edited using Sequencher (Gene Codes Corporation 2005). We compared chloroplast sequences to the complete chloroplast of *Nicotiana tabacum* (GenBank accession number NC 001879) to determine beginning and ending points of each cpDNA region and check that frameshifts were not implied by insertion of gaps in the alignment. We did not use *rpl16* intron sequence data for taxa outside subtribe

Hakeinae. For the purpose of modeling nucleotide substitutions in the data, we recognized each of the regions as separate data partitions.

We used the Akaike information criterion (AIC) in MrModelTest 1.1b (http://www.abc.se/ca. nylander/) to select an adequately parameter-rich model of nucleotide substitution for each of the DNA regions. These models were then used for their respective partitions in the Bayesian analyses in BEAST version 1.7.1 (Drummond *et al.* 2012). We prepared the XML file using BEAUTi version 1.7.1 (Drummond *et al.* 2012). We constrained the clade of Platanaceae and Proteaceae to be monophyletic, and chose an uncorrelated lognormal relaxed clock model (Drummond *et al.* 2006), the parameters of which we had BEAST estimate. We chose a Yule Process tree prior (Yule 1925; Gernhard 2008) and, as a starting tree, gave BEAST a 50% majority rule tree from a MrBayes (Ronquist & Huelsenbeck 2003) analysis of the data after randomly resolving polytomies with branches of length 0.001 in Mesquite (Maddison & Maddison 2009). We set the prior of the mean for the uncorrelated lognormal relaxed clock parameter as an exponential distribution with a mean of 1, the priors for the two calibration nodes as described below, and accepted the default prior for the remaining parameters. We unlinked the substitution models and linked the clock models and trees. The Markov Chain Monte Carlo (MCMC) algorithm for each analysis was run for 50×10^6 generations (sampled every 10^3 generations) twice with the data and once without the data to determine the marginal prior densities for each parameter. We considered the first quarter of the samples to represent the burn-in for the MCMC run. This number of generations was sufficient to produce very similar marginal posterior densities for each parameter, effective sample sizes (ESS) >200 (and typically >1000), and posterior

densities that differed from most prior densities, as determined in Tracer version 1.5 (http://beast.bio.ed.ac.uk/Tracer). We combined post-burn-in trees from multiple runs of BEAST in LogCombiner v. 1.7.1 (distributed with BEAST), then produced a maximum clade credibility tree showing node heights at the median sampled ages and 95% highest posterior density for the ages of branches with ≥95% p.p. in Tree Annotator v. 1.7.1 (also distributed with BEAST).

We used two priors on the age of nodes in the analysis. Each of the node age priors was described as a normal distribution. We gave the prior age for the MRCA (most recent common ancestor) of Proteaceae and Platanaceae a mean of 112.3 and a standard deviation of 6.48. This results in a bound of 99.6 (equivalent to 99.6 Ma) for the 2.5% quantile and a bound of 125.0 (equivalent to 125.0 Ma) for the 97.5% quantile. 125 Ma is the approximate time of appearance in the fossil record of the tricolpate pollen of the eudicots (Magallon *et al.* 1999), of which Proteales is an early diverging branch. It has been used elsewhere as a calibration for the MRCA of the eudicots (e.g., Bell *et al.* 2005), for the MRCA of Proteales and Sabiaceae (Sauquet *et al.* 2009), and for the MRCA of Proteaceae and Platanaceae (Mast *et al.* 2008, 2012). 99.6 Ma is the upper boundary of the Albian (Gradstein *et al.* 2004), the earliest period from which fossil inflorescences have been recovered that can be assigned to Platanaceae (e.g., Crane *et al.* 1993) using shared derived features (Crepet *et al.* 2004; Anderson *et al.* 2005). This is slightly older than the occurrence of the oldest fossil that can be assigned to Proteaceae based on its position in parsimony analyses (Sauquet *et al.* 2009): *Triorites africaensis* (Dettmann & Jarzen 1998) is from the Upper Cenomanian to Turonian (ca. 94 Ma ago) of Senegal and Gabon. We gave the prior age for the MRCA of *Embothrium* and its sister,

Telopea, a mean of 37.5 and a standard deviation of 1.07. This results in a bound of 35.4 (equivalent to 35.4 Ma) for the 2.5% quantile and a bound of 39.6 (equivalent to 39.6 Ma) for the 97.5% quantile. 35.4 Ma is the estimated age of occurrence of pollen of *Granodiporites nebulosus* (Macphail & Truswell 1989). *G. nebulosus* was resolved as sister to *Embothrium* by Sauquet *et al*. (2009). Barker *et al.* (2007) and Sauquet *et al.* (2009) both used this fossil calibration in their studies of the family. 39.6 Ma is the upper bound of the 95% credible interval determined for the MRCA of *Embothrium* and *Telopea* by Mast *et al*. (2012) using Multidivtime (http://statgen.ncsu.edu/thorne/multidivtime.html, Thorne & Kishino 2002). For analysis of the *rpl16* intron dataset, which did not include taxa outside subtribe Hakeinae, we assigned the MRCA of *Buckinghamia*, *Grevillea*, *Hakea*, and *Finschia* a prior with a mean of 35.05 and standard deviation of 4.955. This results in a bound of 25.34 (equivalent to 25.34 Ma) for the 2.5% quantile and a bound of 44.76 (equivalent to 44.75 Ma) for the 97.5% quantile. Sauquet *et al*. (2009) estimated the mean age of this node as 35.05 Ma with a bound of 25.34 for the 2.5% quantile and a bound of 45.64 for the 97.5% quantile. Barker *et al*. (2007) use a second calibration within tribe Embothrieae (the fossil pollen species *Propylipollis ambiguus*), but we do not use it here because Sauquet *et al*. (2009) demonstrated that it cannot be assigned such precision with confidence. Sauquet *et al*. (2009) also demonstrated that *Hakeidites martinii*, a pollen fossil previously assigned to *Hakea* by Khan (1976), cannot be assigned this precision with confidence.

REFERENCES

1.

Anderson, C.L., Bremer, K. are & Friis, E.M. (2005). Dating phylogenetically basal eudicots using rbcL sequences and multiple fossil reference points. *Am. J. Bot.*, 92, 1737–1748.

2.

Barker, N.P., Weston, P.H., Rutschmann, F. & Sauquet, H. (2007). Molecular dating of the "Gondwanan" plant family Proteaceae is only partially congruent with the timing of the break-up of Gondwana. *J. Biogeogr.*, 34, 2012–2027.

3.

Bell, C.D., Soltis, D.E. & Soltis, P.S. (2005). The age of the angiosperms: a molecular timescale without a clock. *Evolution*, 59, 1245–1258.

4.

Crane, P.R., Pedersen, K.R., Friis, E.M. & Drinnan, A.N. (1993). Early Cretaceous (early to middle Albian) platanoid inflorescences associated with Sapindopsis leaves from the Potomac Group of eastern North America. *Syst. Bot.*, 328–344.

5.

Crepet, W.L., Nixon, K.C. & Gandolfo, M.A. (2004). Fossil evidence and phylogeny: the

age of major angiosperm clades based on mesofossil and macrofossil evidence from Cretaceous deposits. *Am. J. Bot.*, 91, 1666–1682.

6.

Dettmann, M.E. & Jarzen, D.M. (1998). The early history of the Proteaceae in Australia: the pollen record. *Aust. Syst. Bot.*, 11, 401–438.

7.

Gradstein, F.M., Ogg, J.G., Smith, A.G., Bleeker, W. & Lourens, L.J. (2004). A new geologic time scale, with special reference to Precambrian and Neogene. *Episodes*, 27, 83–100.

8.

Khan, A.M. (1976). Palynology of Tertiary sediments from Papua New Guinea. I. New form genera and species from Upper Tertiary sediments. *Aust. J. Bot.*, 24, 753–781.

9.

Macphail, M.K. & Truswell, E.M. (1989). Palynostratigraphy of the central west Murray Basin. *J. Aust. Geol. Geophys.*, 11, 301–331.

10.

Magallon, S., Crane, P.R. & Herendeen, P.S. (1999). Phylogenetic pattern, diversity, and diversification of eudicots. *Ann. Mo. Bot. Gard.*, 297–372.

11.

Mast, A.R., Milton, E.F., Jones, E.H., Barker, R.M., Barker, W.R. & Weston, P.H. (2012). Time-calibrated phylogeny of the woody Australian genus Hakea (Proteaceae) supports multiple origins of insect-pollination among bird-pollinated ancestors. *Am. J. Bot.*, 99, 472–487.

12.

Mast, A.R., Willis, C.L., Jones, E.H., Downs, K.M. & Weston, P.H. (2008). A smaller *Macadamia* from a more vagile tribe: inference of phylogenetic relationships, divergence times, and diaspore evolution in *Macadamia* and relatives (tribe Macadamieae; Proteaceae). *Am. J. Bot.*, 95, 843–870.

13.

Sauquet, H., Weston, P.H., Anderson, C.L., Barker, N.P., Cantrill, D.J., Mast, A.R., *et al.* (2009). Contrasted patterns of hyperdiversification in Mediterranean hotspots. *Proc. Natl. Acad. Sci.*, 106, 221–225.

14.

Thorne, J.L. & Kishino, H. (2002). Divergence time and evolutionary rate estimation with multilocus data. *Syst. Biol.*, 51, 689–702.

Appendix S3. Results of linear models between macroecological patterns and potential environmental drivers

As described in the main text, we used rarefaction to determine which grid cells had been adequately sampled. After removing insufficiently sampled grid cells, 749 remained. This is the sample size for the following linear models. Since our purpose in presenting these results is to highlight the lack of explanatory power of these models, we do not account for spatial autocorrelation, which would surely change the significance of many of these weak but nominally significant relationships.

Species richness per grid cell was negatively correlated with MAT ($R^2 = 0.07$, $p < 0.001$), and positively correlated with $\log_{10}$ MAP ($R^2 = 0.015$, $p = 0.0009$) and MI ($R^2 = 0.017$, $p = 0.0004$). Regions of intermediate temperature and precipitation, particularly the southwest, showed the highest species richness (Fig. S3.1).

Median grid-cell height was positively correlated with temperature ($R^2 = 0.31$, $p < 0.001$; this is an exception to the weak correlations among most of these variables). It was positively ($R^2 = 0.006$, $p = 0.042$) and negatively ($R^2 = 0.01$, $p = 0.007$) correlated with MAP and MI, respectively.

Grid-cell averaged diversification rates were negatively correlated with MAT (with randomMCC tree, $R^2 = 0.26$, $p < 0.001$) and positively correlated with MAP ($R^2 = 0.01$, $p = 0.002$) and MI ($R^2 = 0.1$, $p < 01.001$). These results were qualitatively identical irrespective of the tree used, with the exception of results from the stemMCC tree (see *What was the geographic pattern of Hakeinae diversification?* main text). Here, a

positive correlation of MAT with diversification rate was observed ($R^2 = 0.02$, $p < 0.001$).

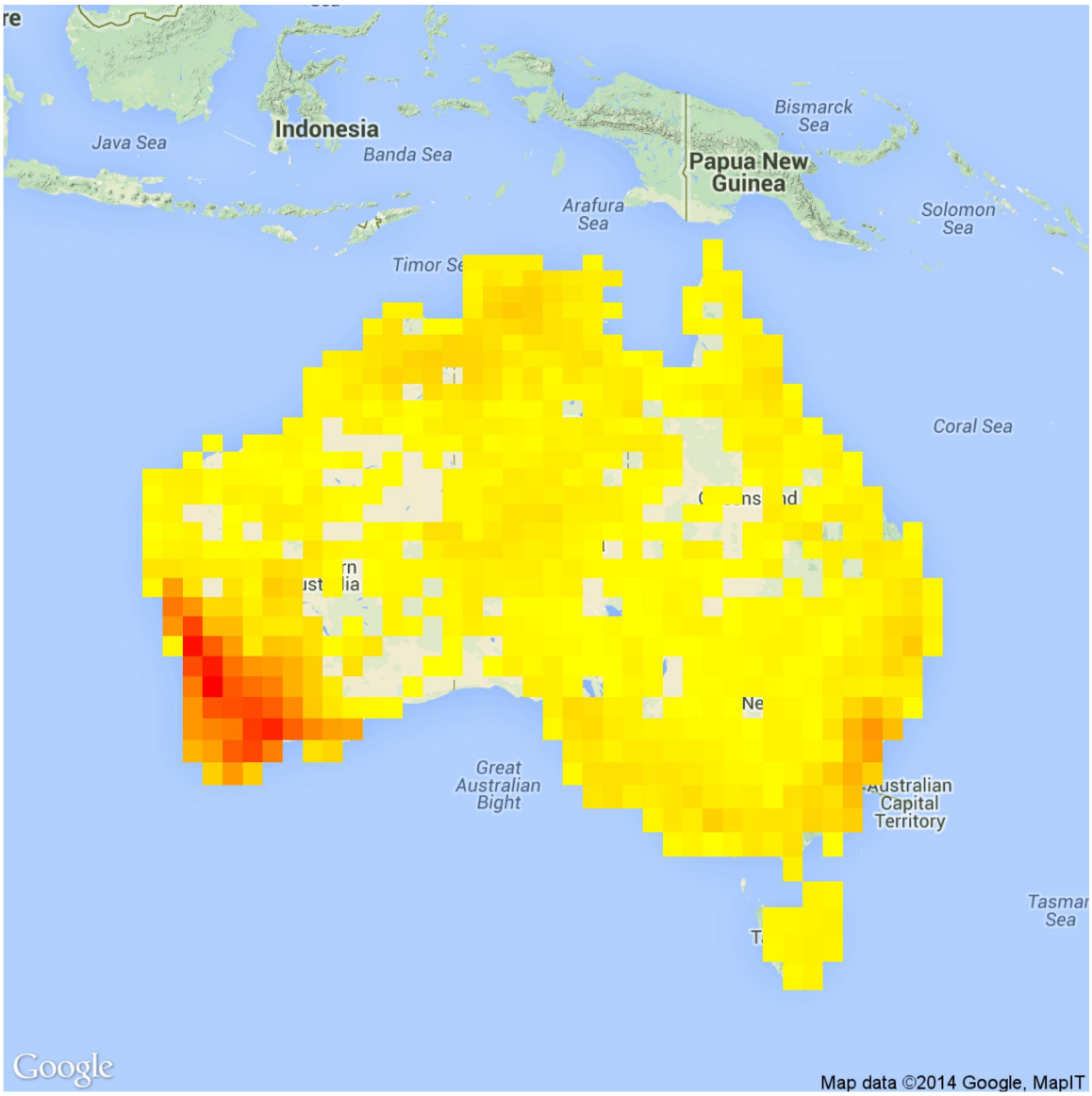

Figure S3.1. Map of Hakeinae species richness, where red corresponds to the most speciose cells.

Appendix S4. Supplementary figures

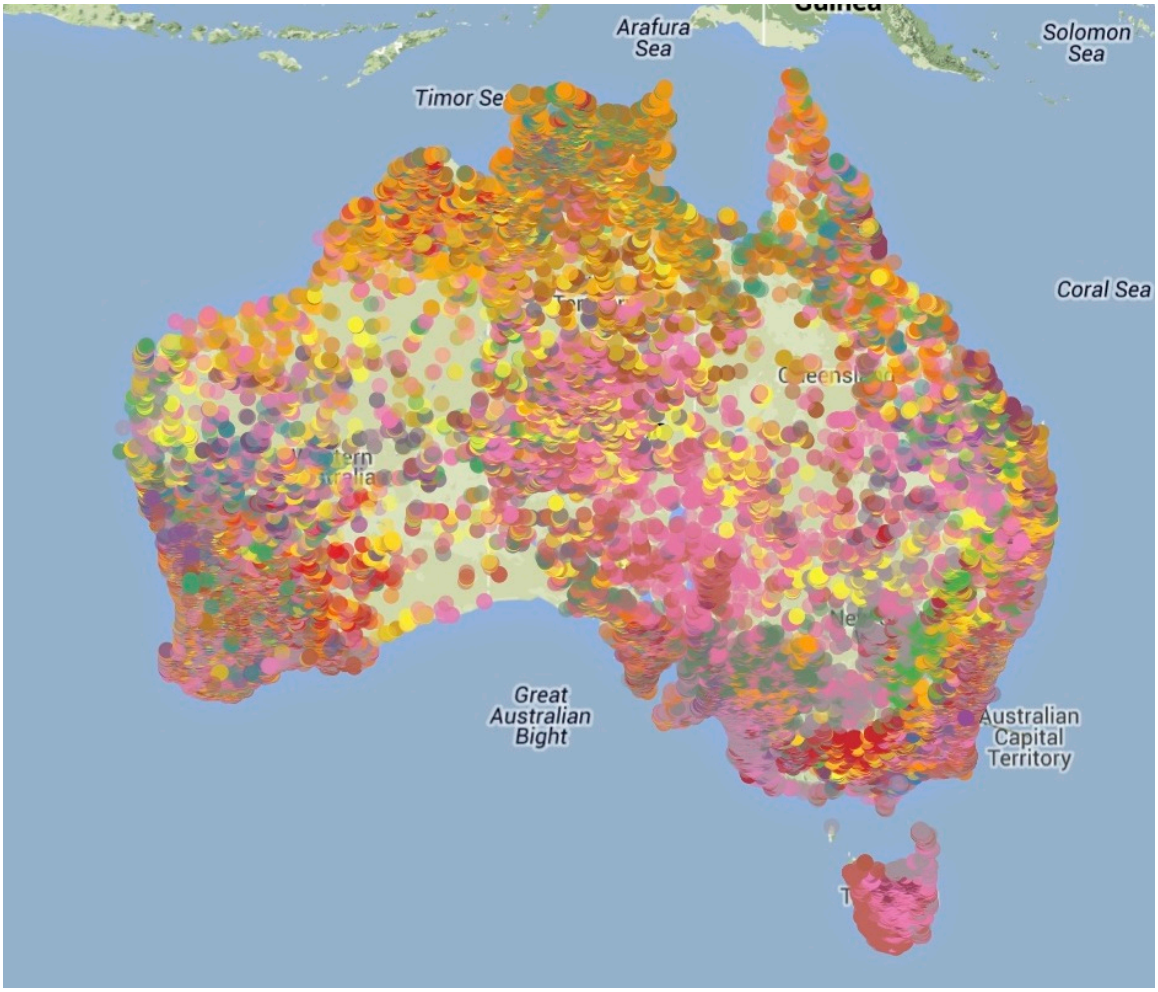

Figure S4.1. Map of the 125,696 Hakeinae collections used in this study. Each of the 517 unique species is illustrated with its own color.

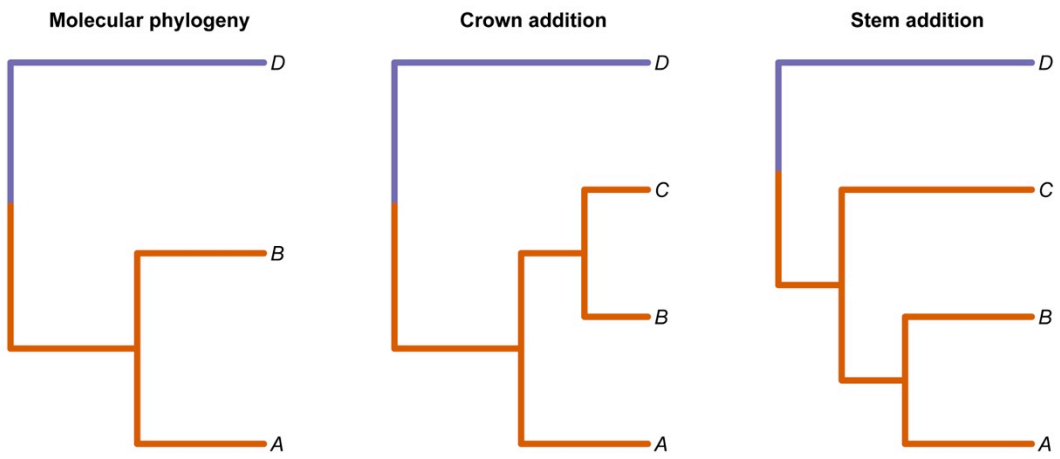

Figure S4.2. Schematic diagram illustrating the different ways that missing taxa can be added to a molecular tree. Assuming missing species C is part of the same taxonomic group as A and B, if crownwards addition is chosen, C will be bound either as illustrated here, or with similar branch lengths but sister to species A. If stemwards addition is chosen, C will be added sister to A and B. Note that if species B was not in the same taxonomic group as A and C, the algorithm would automatically add C crownwards and sister to A.

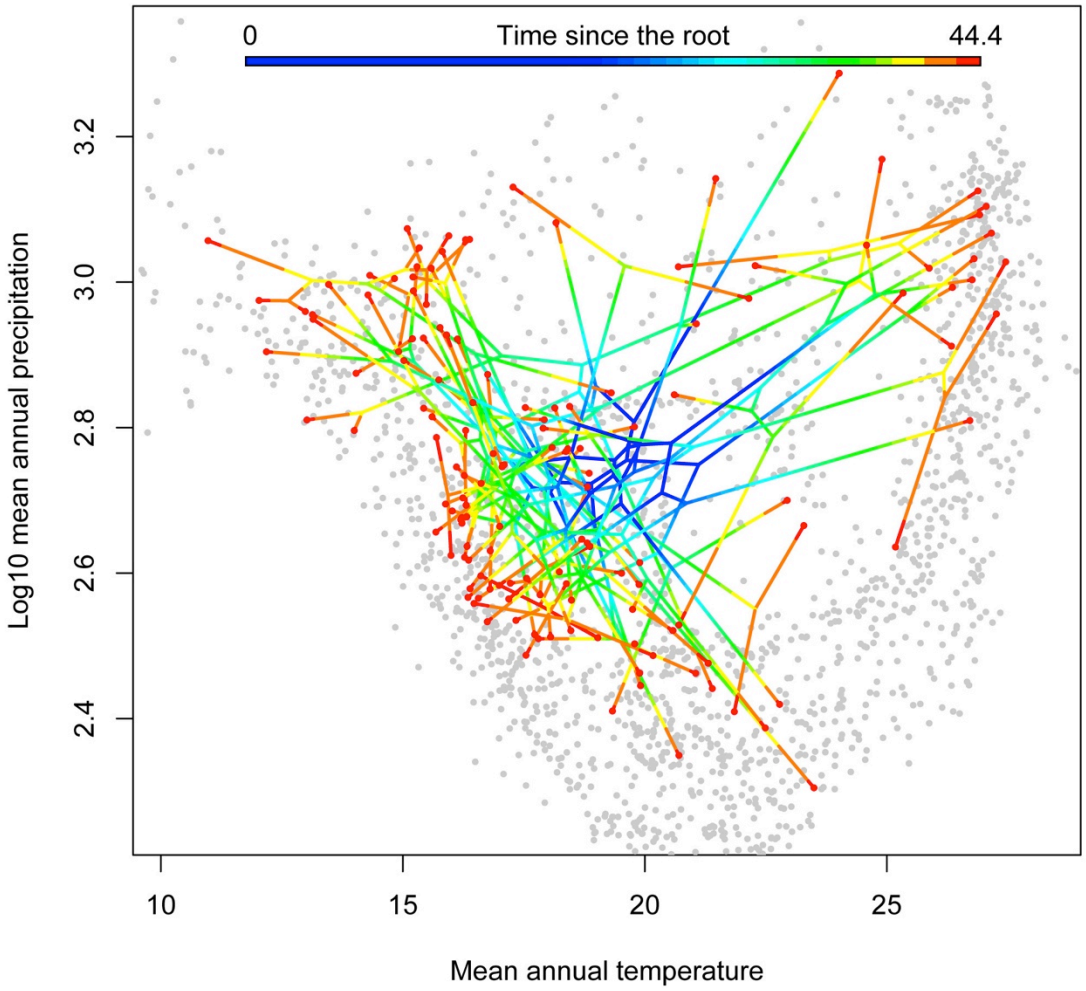

Figure S4.3. Phyloclimatespace figure showing Hakeinae radiation across mean annual temperature and precipitation. Branches are colored from blue to red as a function of distance from the root. Light gray points represent grid-cell averaged climate values, used to show the breadth of climate space available to the Hakeinae in Australia. The phylogeny used in this figure is the molecular tree, and ancestral states are reconstructed with maximum likelihood.

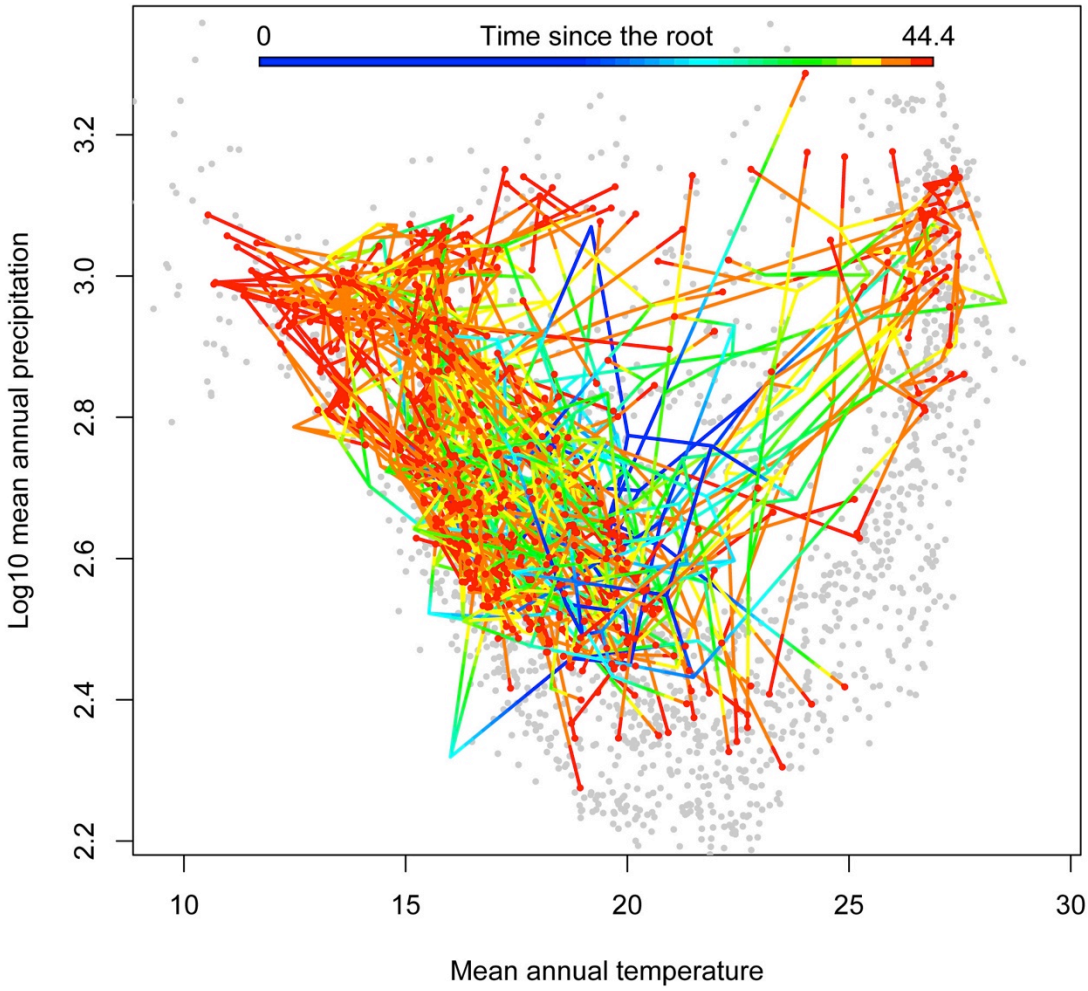

Figure S4.4. Phyloclimatespace figure showing Hakeinae radiation across mean annual temperature and precipitation. Branches are colored from blue to red as a function of distance from the root. Light gray points represent grid-cell averaged climate values, used to show the breadth of climate space available to the Hakeinae in Australia. The phylogeny used in this figure is the randomMCC tree, and ancestral states are reconstructed with the Bayesian method, where a Brownian motion with priors on the root state was the best-supported model.

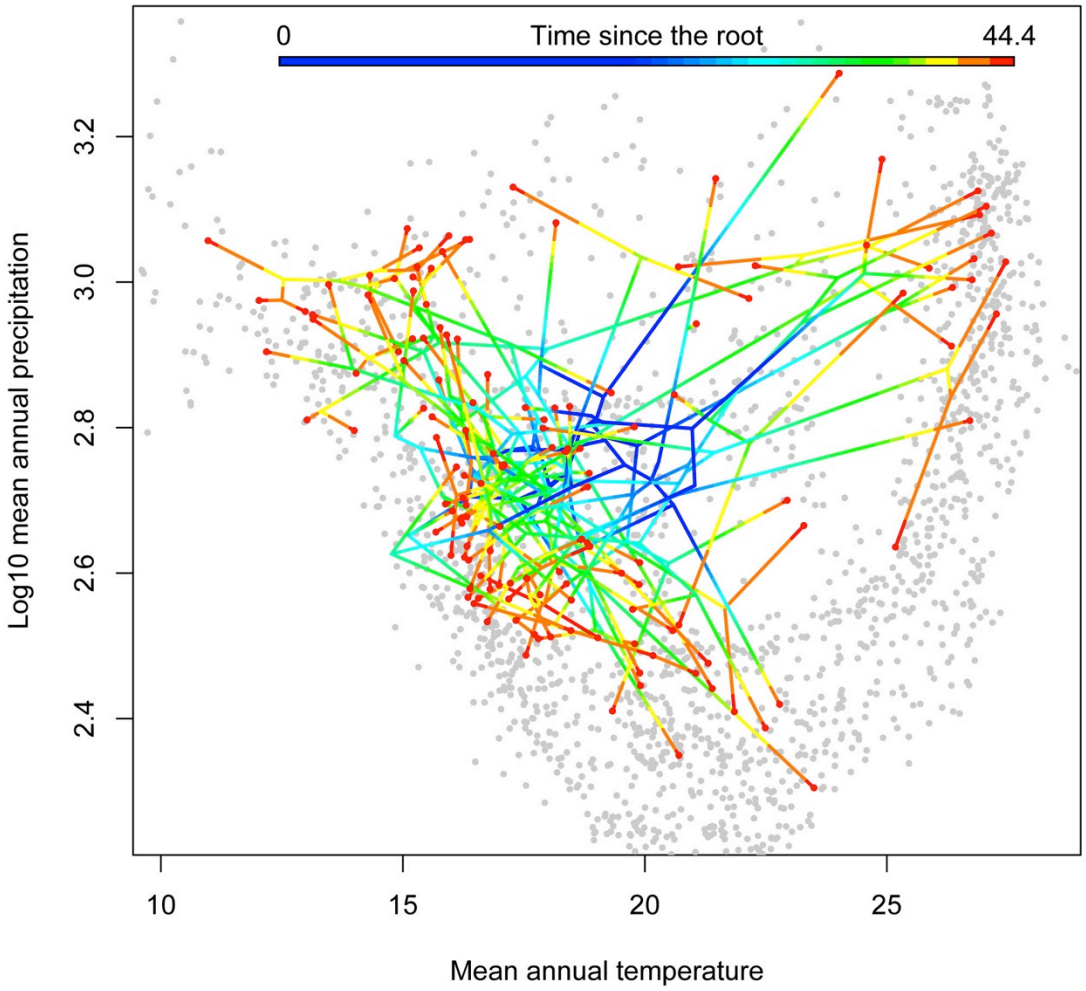

Figure S4.5. Phyloclimatespace figure showing Hakeinae radiation across mean annual temperature and precipitation. Branches are colored from blue to red as a function of distance from the root. Light gray points represent grid-cell averaged climate values, used to show the breadth of climate space available to the Hakeinae in Australia. The phylogeny used in this figure is the molecular tree, and ancestral states are reconstructed with the Bayesian method, where a Brownian motion without priors on the root state was the best-supported model.

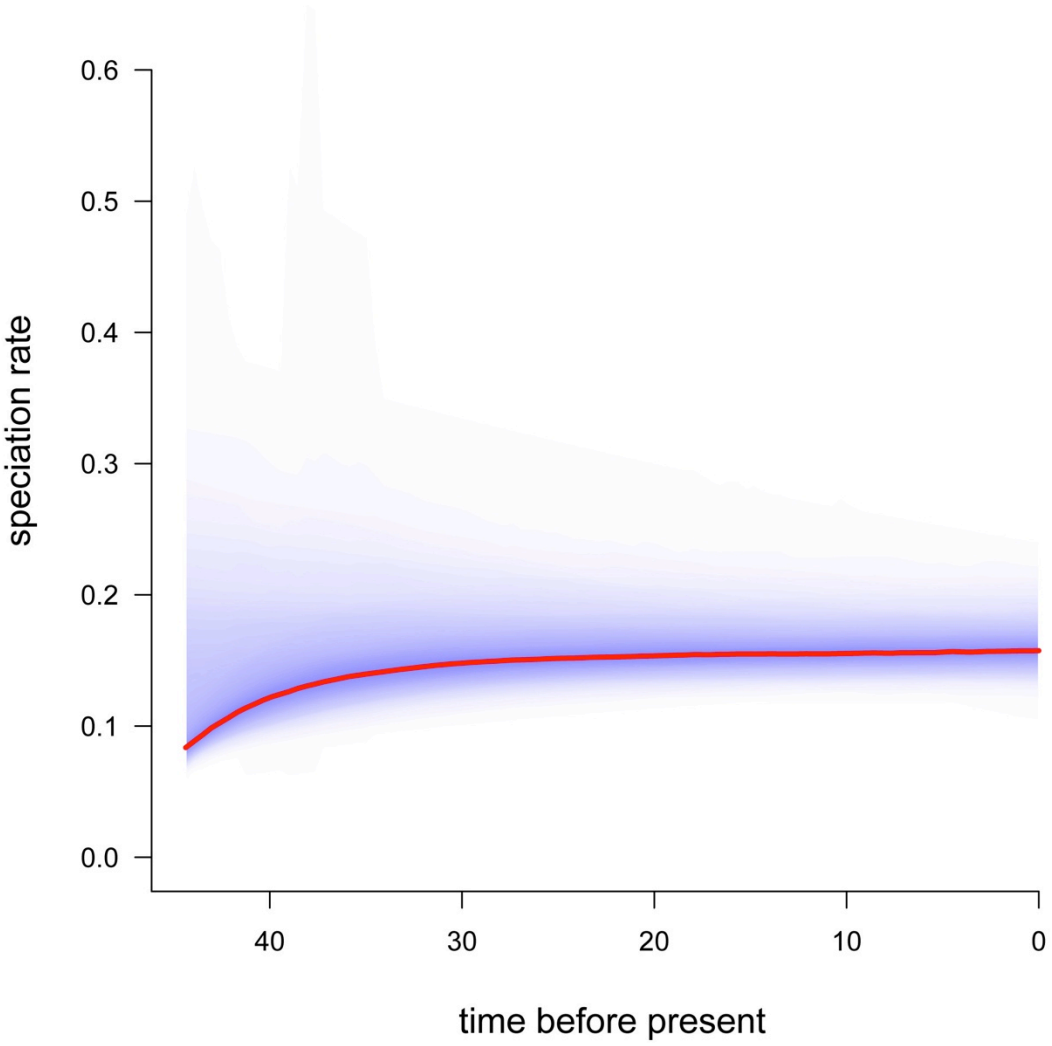

Figure S4.6. Model-averaged speciation rate through time of the molecular tree, as inferred with BAMM.

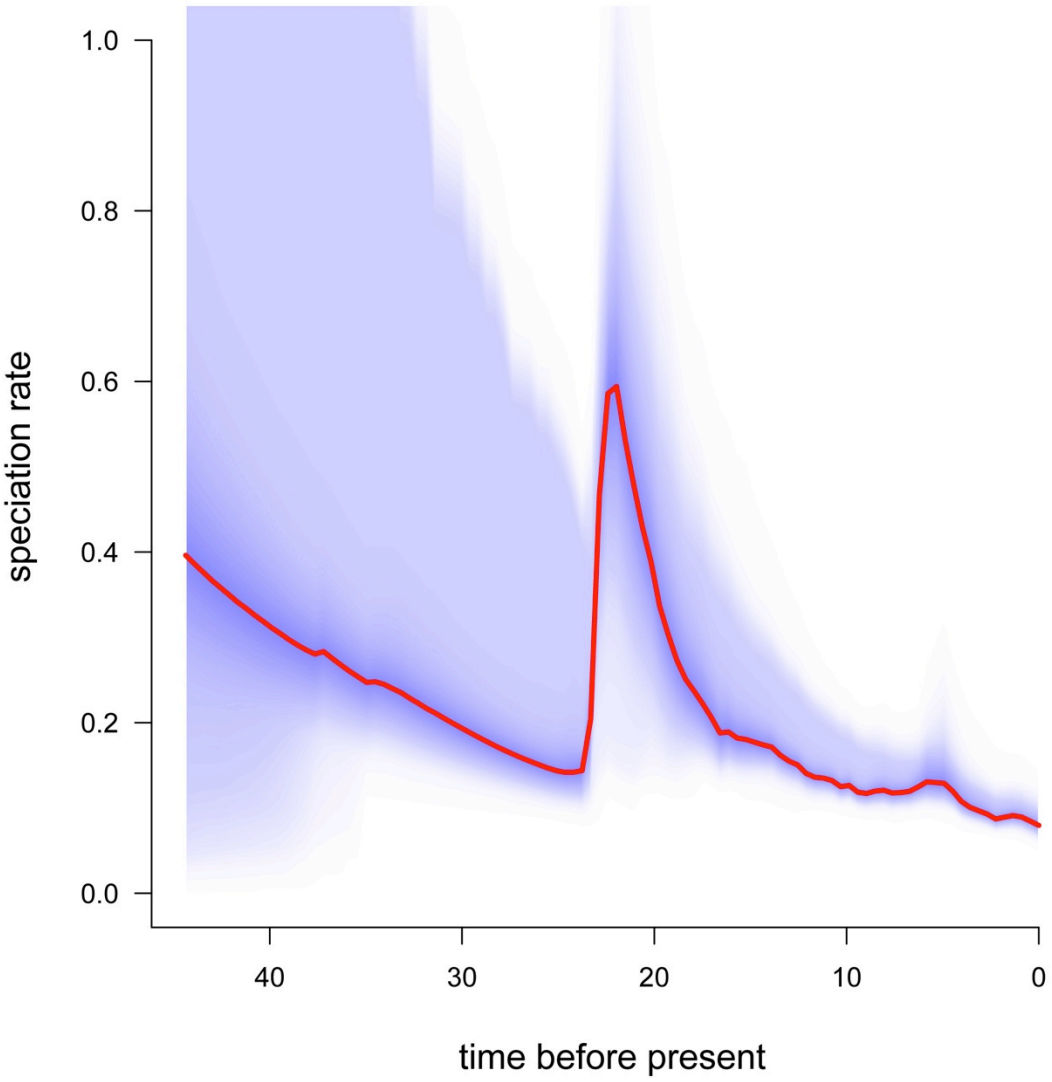

Figure S7. Model-averaged speciation rate through time of the stemMCC tree, as inferred with BAMM.

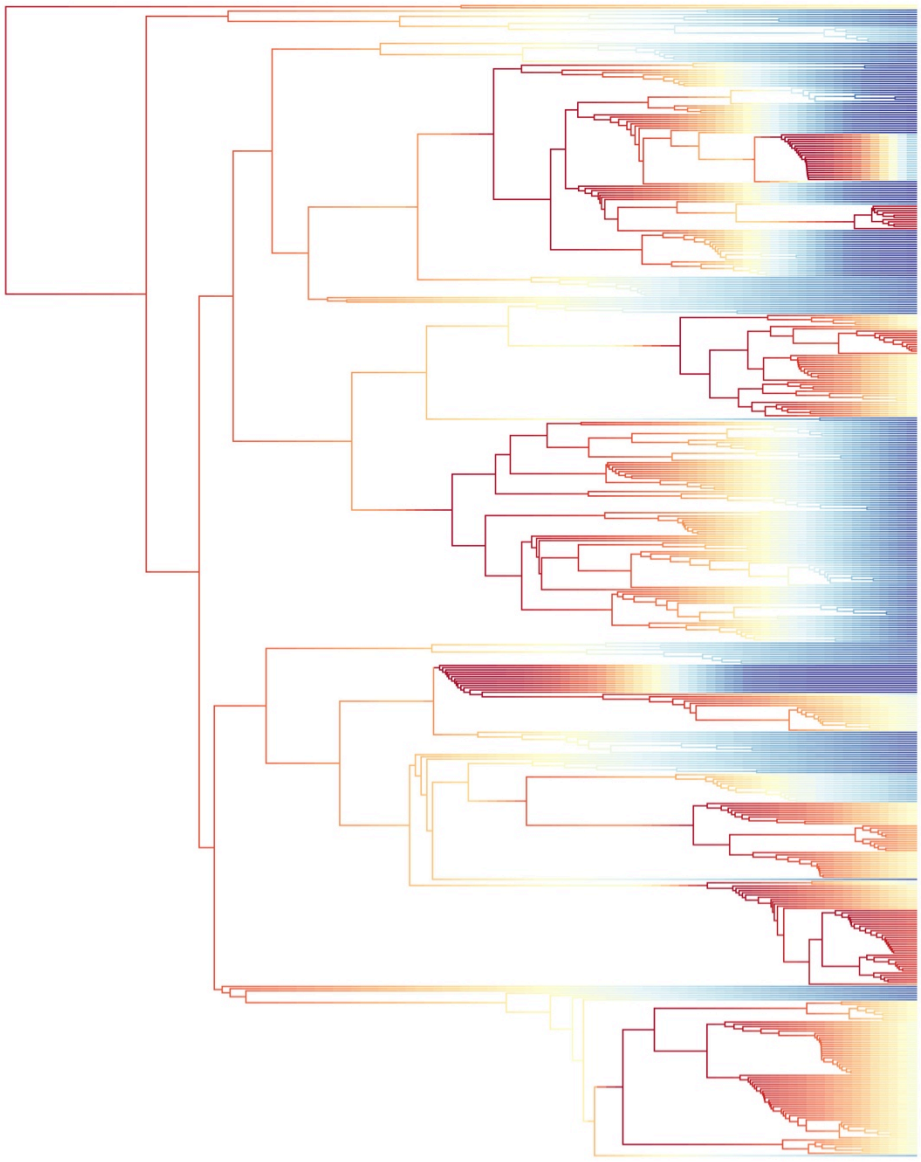

Figure S4.8. Maximum clade-credibility phylogeny of the Australian *Hakea* and *Grevillea* after addition of missing taxa using the stemwards method. Branches are colored from blue to red as a function of the model-averaged lineage-specific speciation rate as calculated in BAMM.

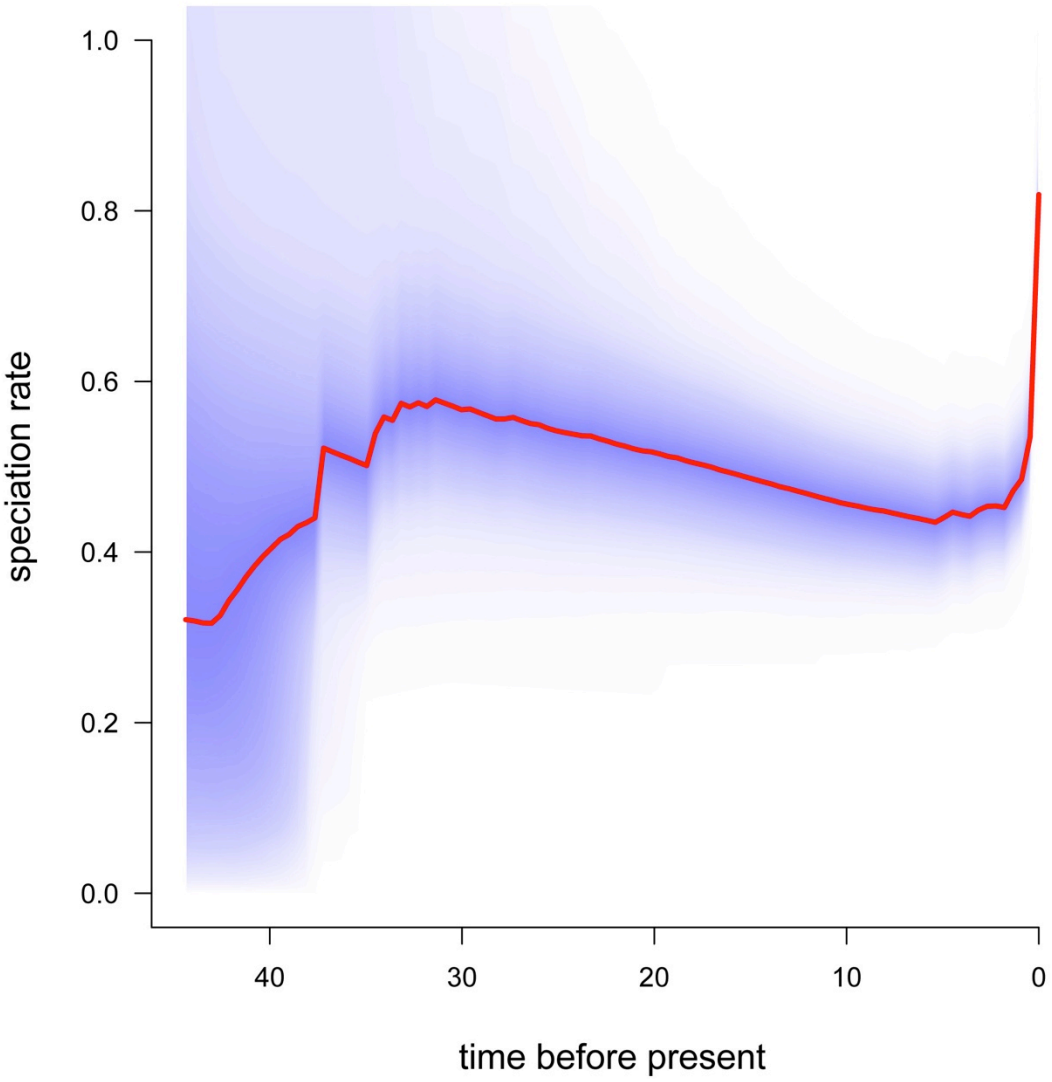

Figure S4.9. Model-averaged speciation rate through time of the crownMCC tree, as inferred with BAMM.

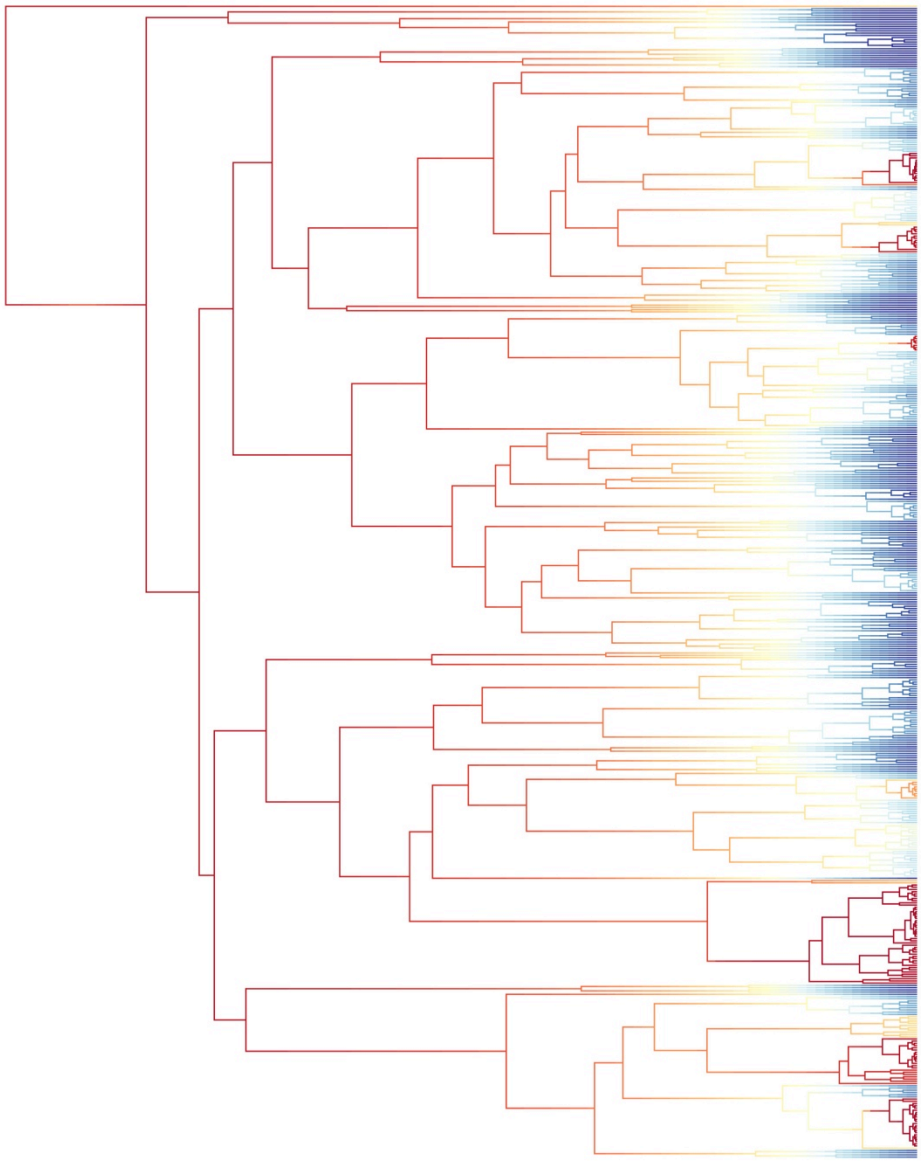

Figure S4.10. Maximum clade-credibility phylogeny of the Australian *Hakea* and *Grevillea* after addition of missing taxa using the crownwards method. Branches are colored from blue to red as a function of the model-averaged lineage-specific speciation rate as calculated in BAMM.

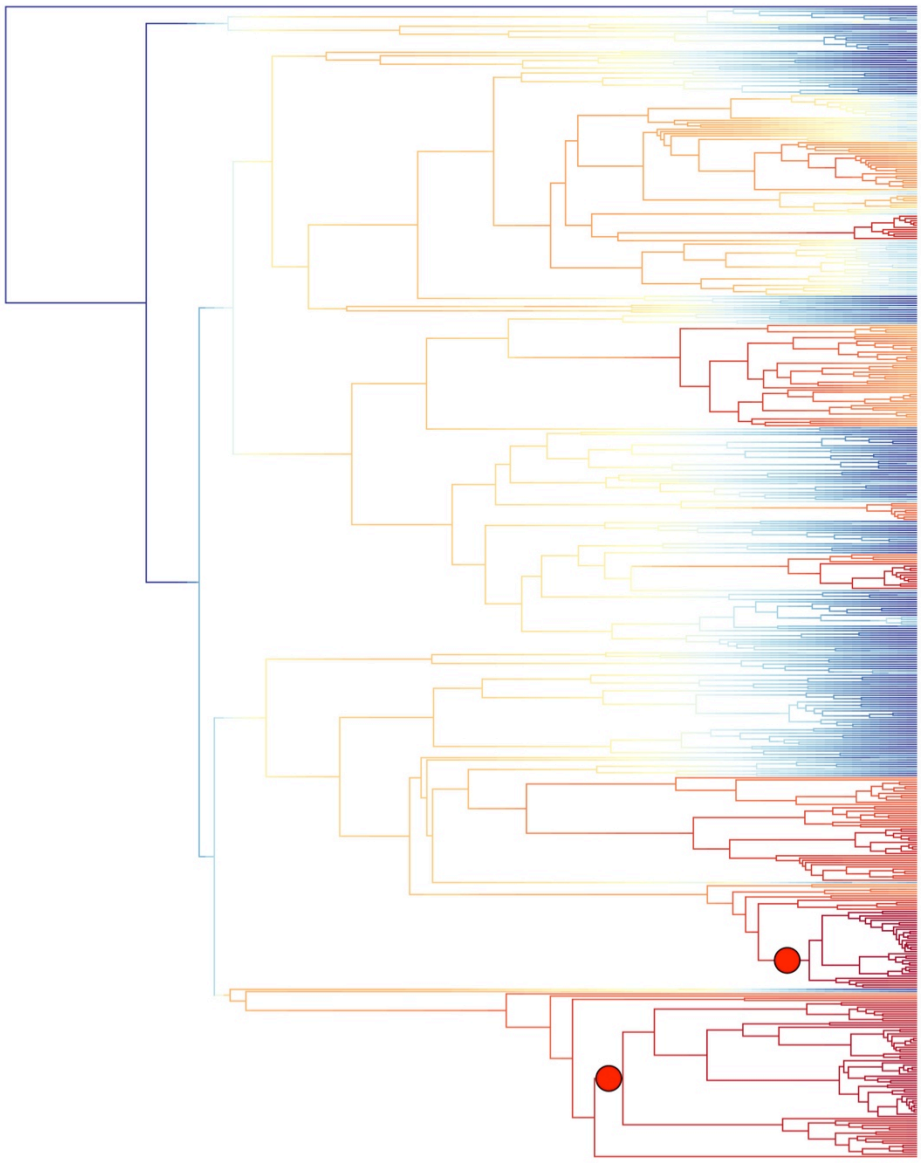

Figure S4.11. Maximum clade-credibility phylogeny of the Australian *Hakea* and *Grevillea* after addition of missing taxa using the stemwards method. The first red dot identifies a clade composed of members of the *Grevillea* Linearifolia group. The second red dot identifies a clade composed of members of the *Grevillea* Pteridifolia group. These two groups were detected as showing an elevated rate of speciation compared to the rest of the Hakeinae.

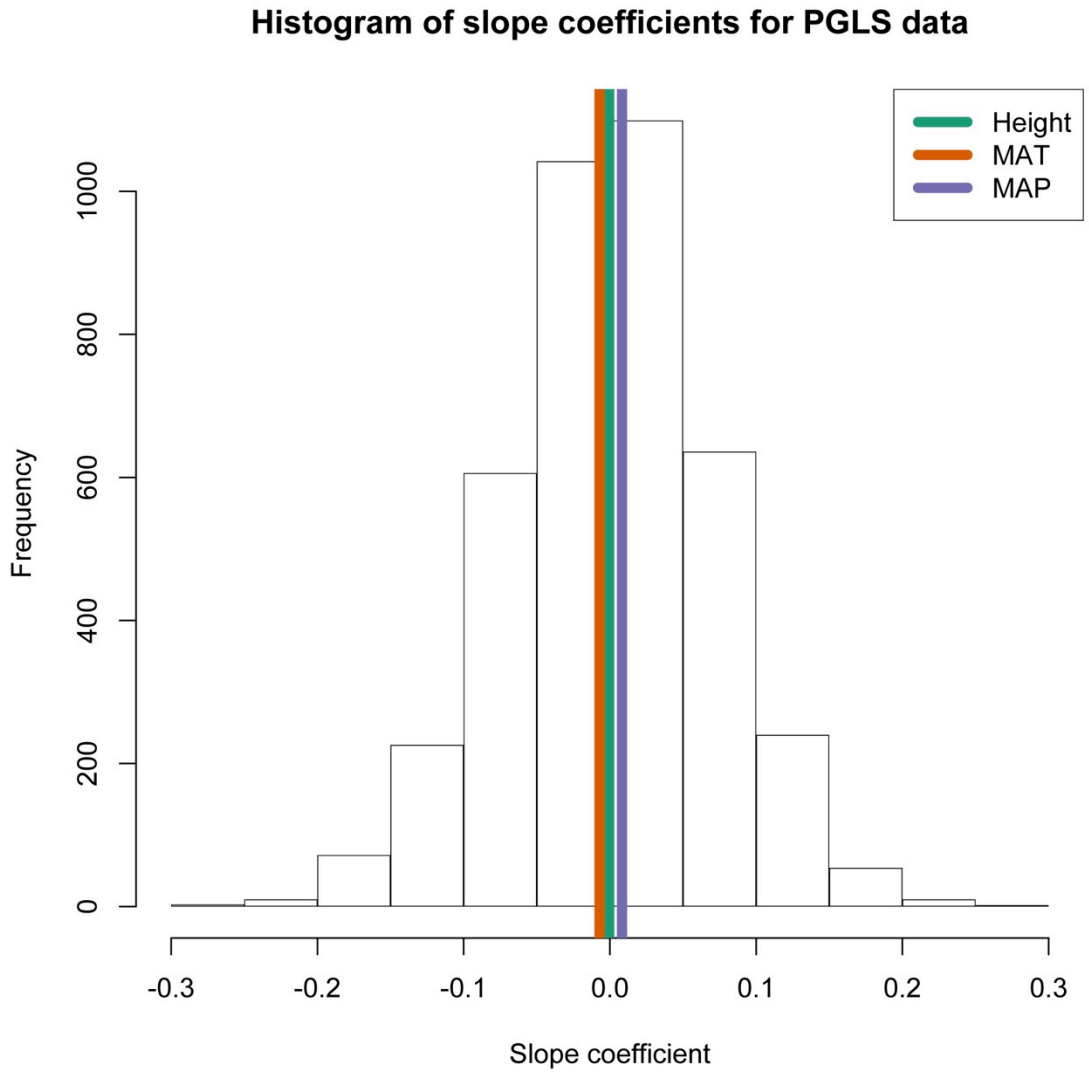

Figure S4.12. Distribution of the phylogenetic generalized least squares (PGLS) correlation coefficients of 1,000 simulated Brownian-motion traits with the lineage-specific speciation rates from the randomMCC tree. The observed PGLS correlation coefficients of height, temperature and precipitation with these speciation rates are shown with vertical colored bars.

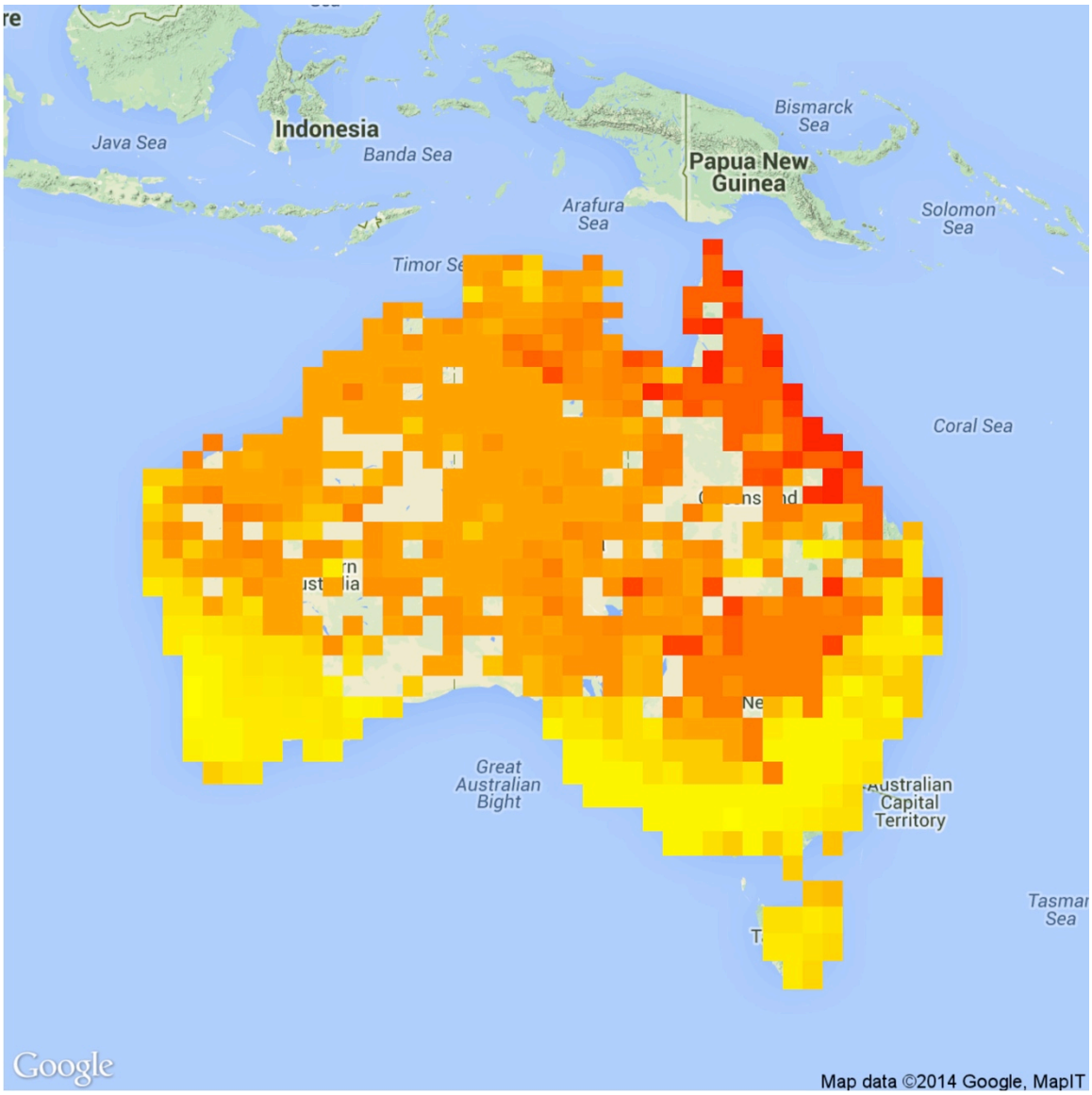

Figure S4.13. Map of grid-cell Hakeinae median heights, where red corresponds to the tallest cells.

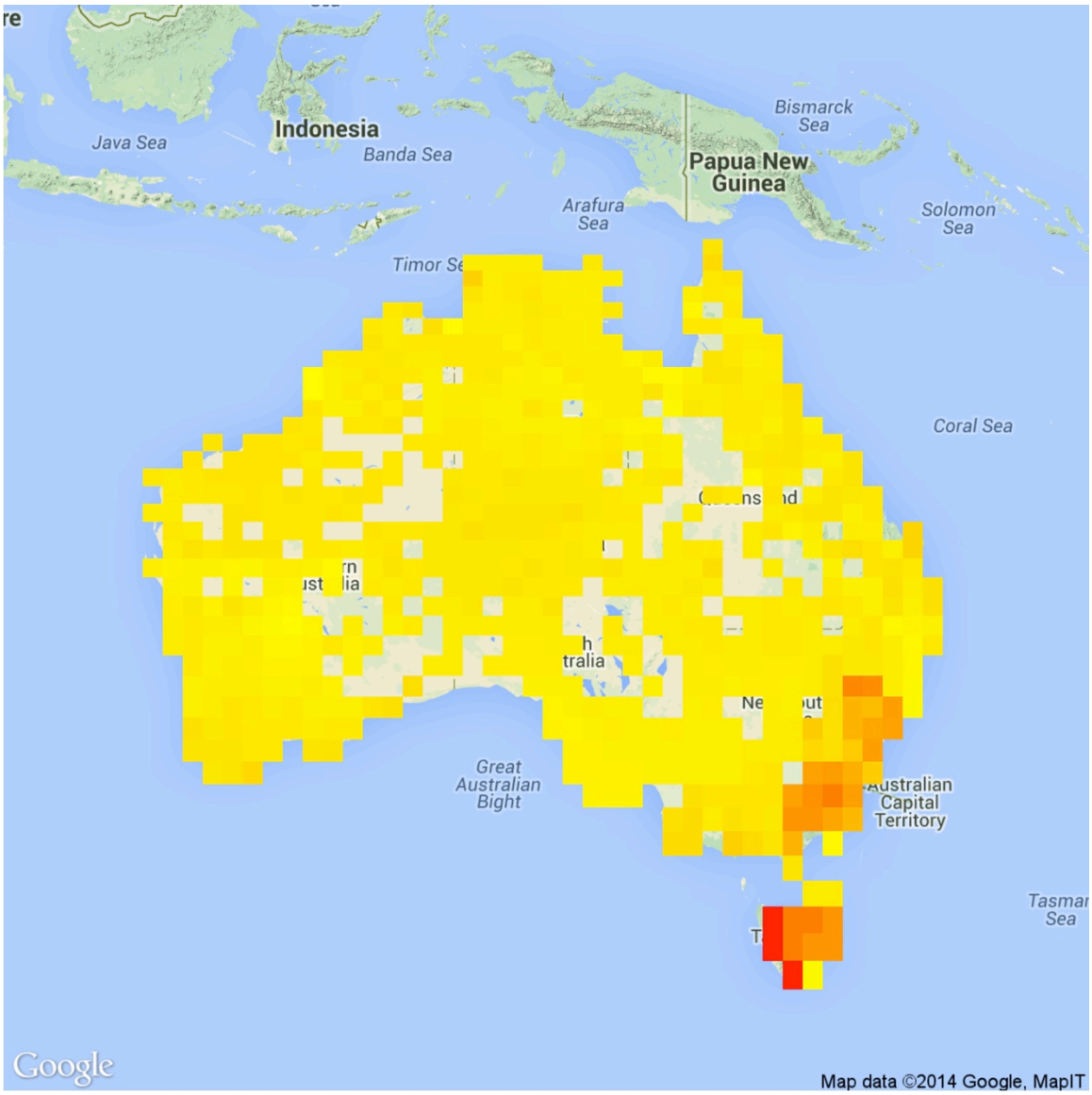

Figure S4.14. Grid-cell averaged diversification rates across Australia, where red represents the fastest rates. The phylogeny used in this figure is the molecular tree.

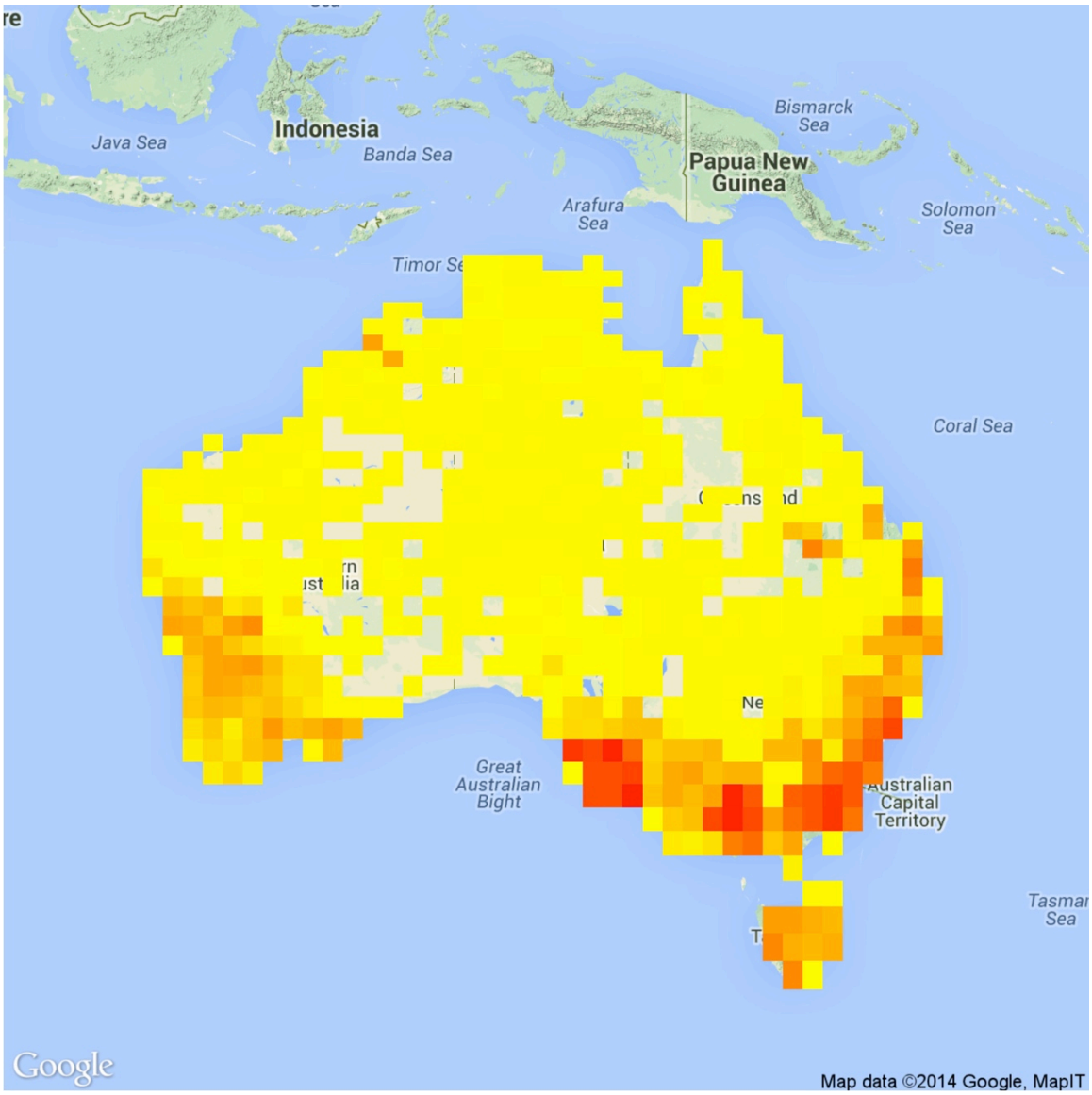

Figure S4.15. Grid-cell averaged diversification rates across Australia, where red represents the fastest rates. The phylogeny used in this figure is the crownMCC tree.

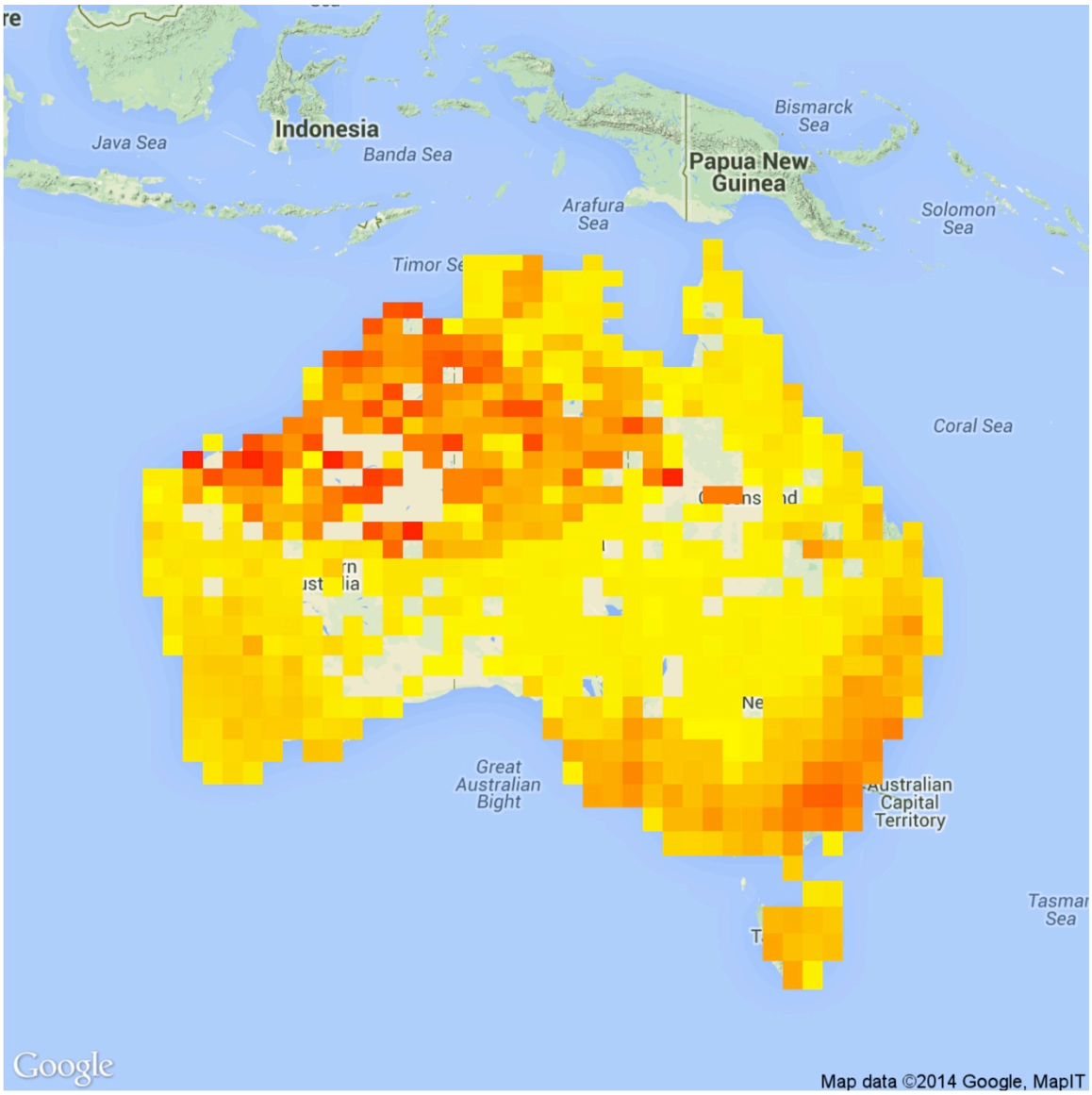

Figure S4.16. Grid-cell averaged diversification rates across Australia, where red represents the fastest rates. The phylogeny used in this figure is the stemMCC tree.

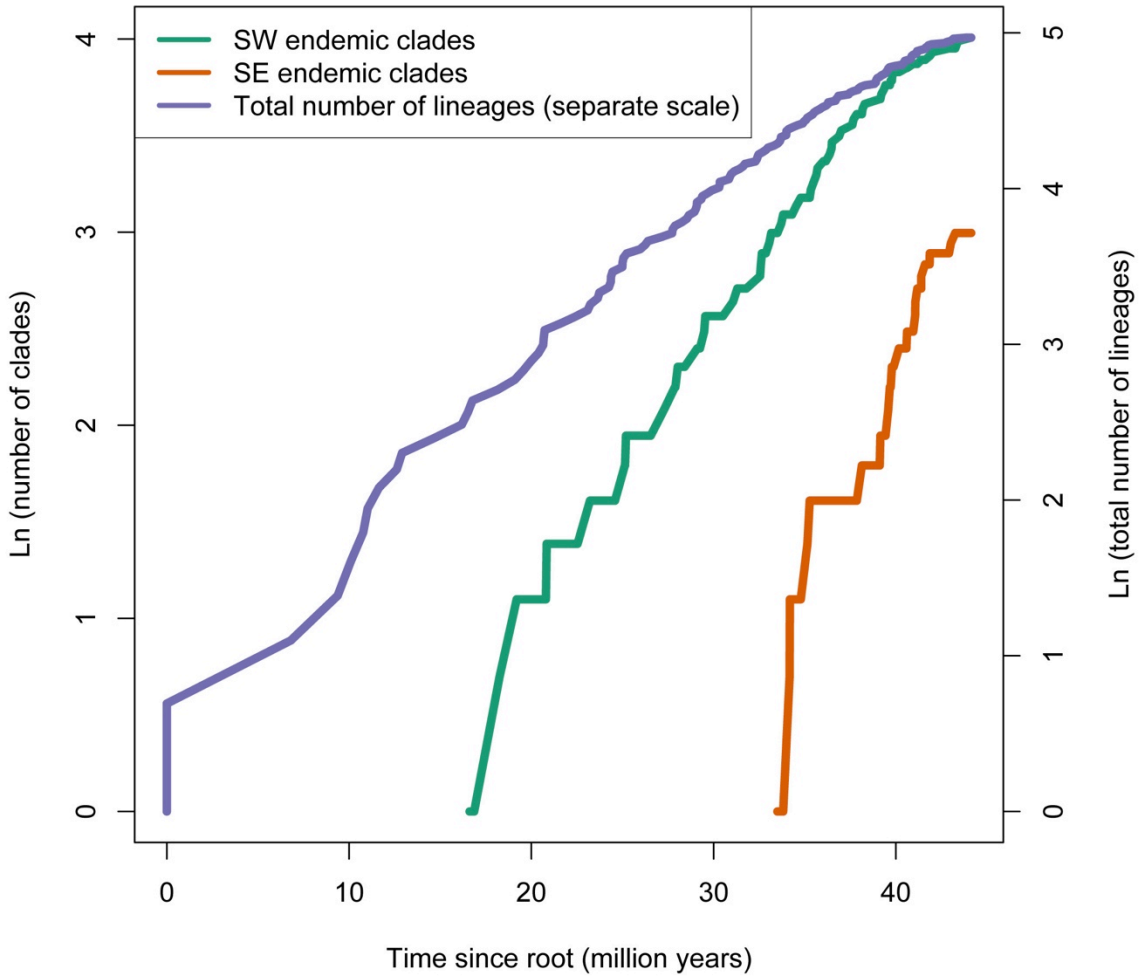

Figure S4.17. A lineage through time plot (right axis) and the accumulation of southwest and southeast endemic clades over time (node through time plot, left axis). This is derived from the molecular phylogeny.

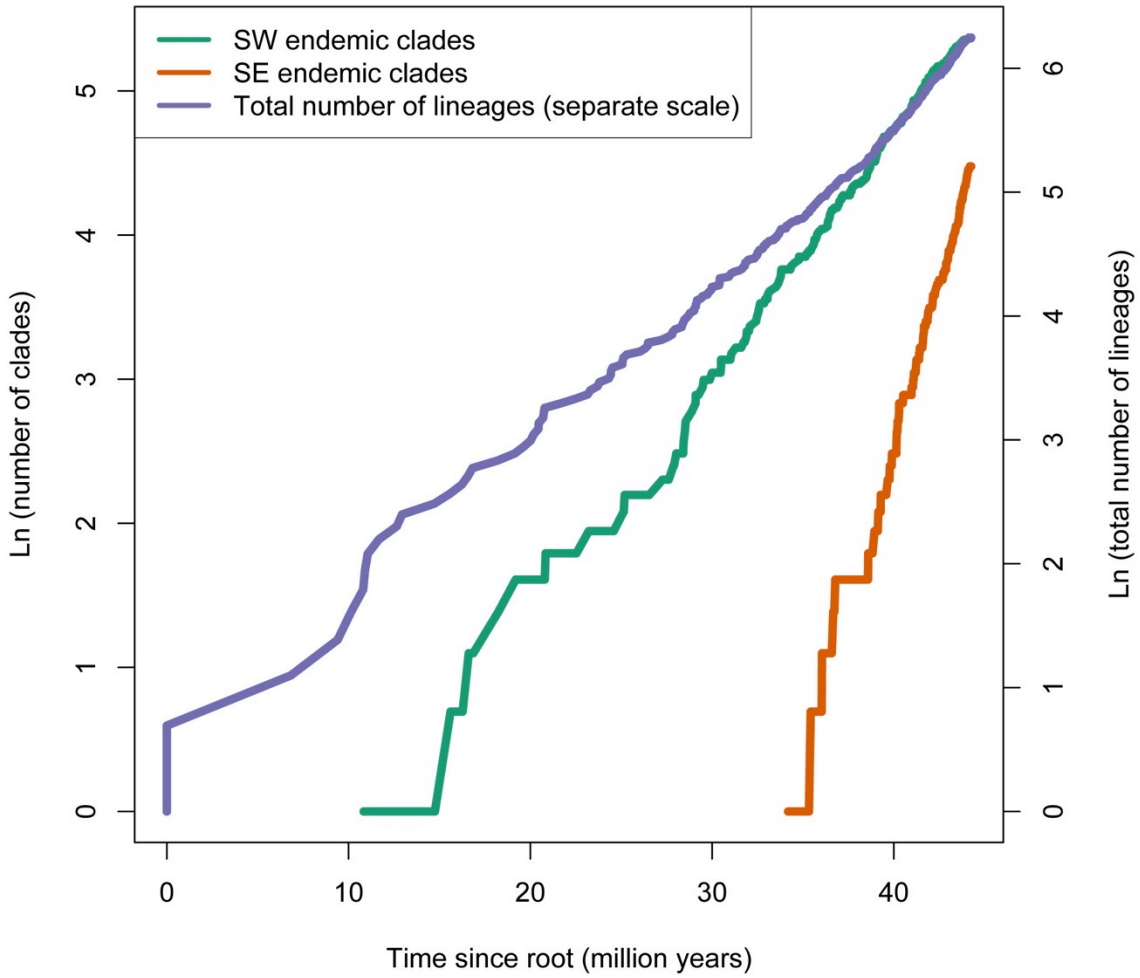

Figure S4.18. A lineage through time plot (right axis) and the accumulation of southwest and southeast endemic clades over time (left axis). This is derived from the randomMCC tree.

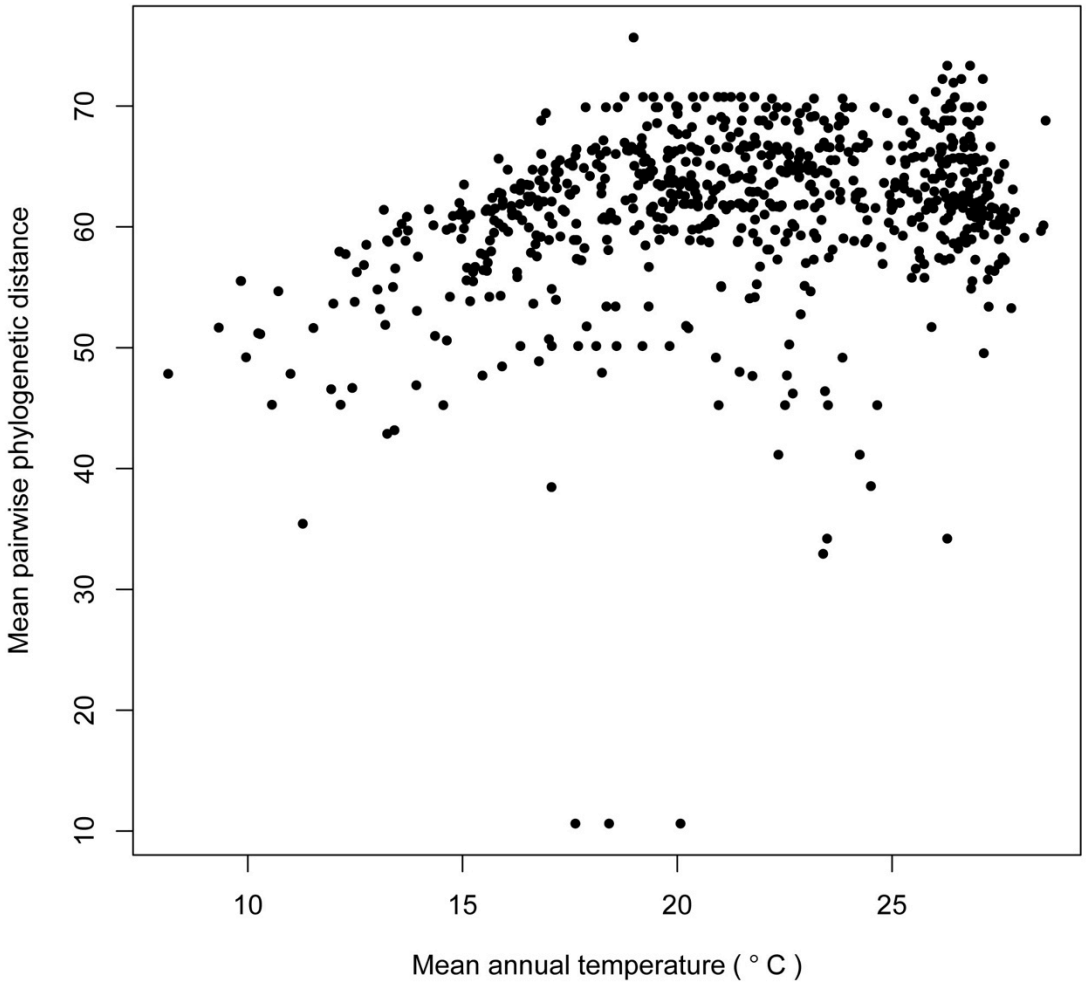

Figure S4.19. Mean pairwise phylogenetic distance (MPD) as a function of mean annual temperature. This was calculated as the average of 1,000 MPD calculations from the same number of complete trees created with the random addition method to the molecular tree. There is a tendency for the most phylogenetically overdispersed sites to occur near the ancestral temperature regime of ~19.9 °C.

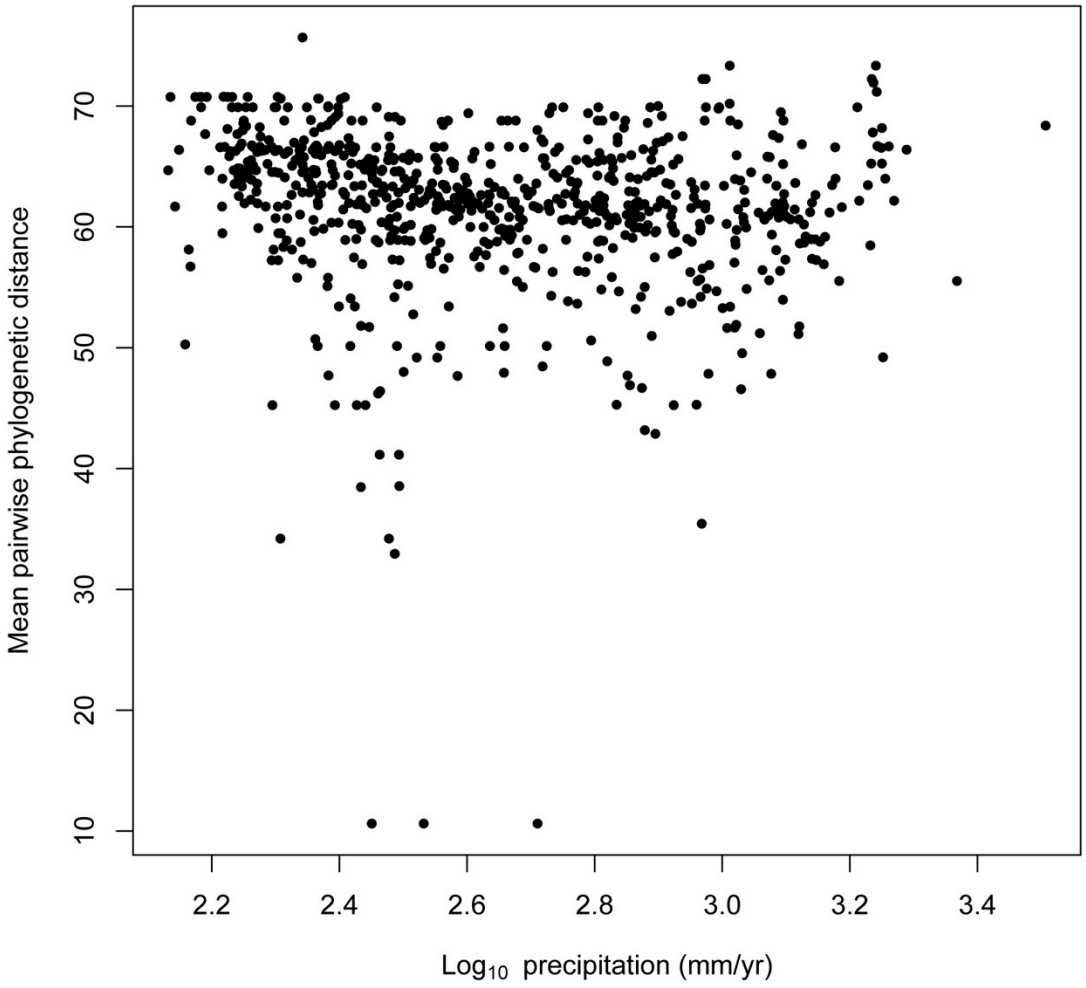

Figure S4.20. Mean pairwise phylogenetic distance (MPD) as a function of the $\log_{10}$ of mean annual precipitation. This was calculated as the average of 1,000 MPD calculations from the same number of complete trees created with the random addition method to the molecular tree. Very little of the variance in MPD can be explained by precipitation.

Figure S4.21. Photographs of members of the *Grevillea* Linearifolia group. Clockwise from top left corner. (1) *Grevillea reptans* in-situ in heath habitat in Great Sandy National Park, pollination syndrome unknown. (2) The bird-pollinated *Grevillea speciosa* from Garigal National Park. (3) *Grevillea sericea* from Muogamarra Nature Reserve. While possibly pollinated by insects—here an invasive *Apis mellifera* visits it—it is also visited by nectarivorous birds like the Meliphagidae *Acanthorhynchus tenuirostris*. (4) *Grevillea speciosa* from Yengo National Park, growing under a *Eucalyptus*-dominated canopy in dry sclerophyll forest on a rocky sandstone slope. All photographs by Eliot Miller.

Figure S4.22. Photographs of members of the *Grevillea* Pteridifolia group. Clockwise from top left corner. (1) An undescribed taxon currently included in *Grevillea hookeriana*, growing in tall heath/stunted forest in Dryanda State Forest. (2) *Grevillea eriostachya* growing on red sand dunes near Uluru National Park. (3) A closer view of the flowers of *G. eriostachya*, illustrating the copious, sticky nectar accumulated on the inflorescence. (4) *Grevillea pteridifolia* growing in vine forest in Iron Range National Park. (5) *Grevillea excelsior* growing in remnant mulga South of Payne's Find, Western Australia. All photographs by Eliot Miller.

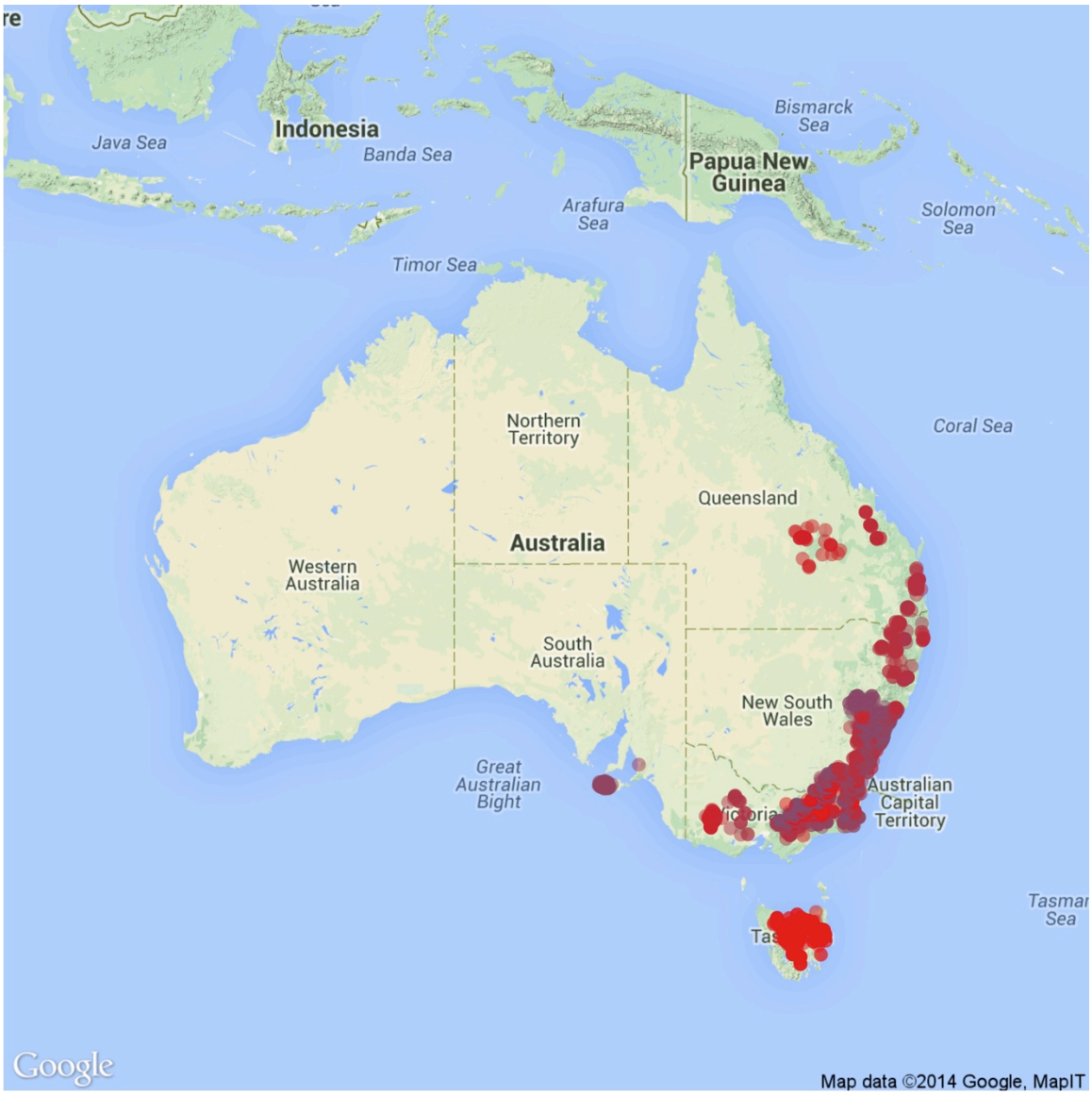

Figure S4.23. Map showing the distribution of the members of the Linearifolia group that showed significantly elevated rates of speciation. Each species is given a unique color.

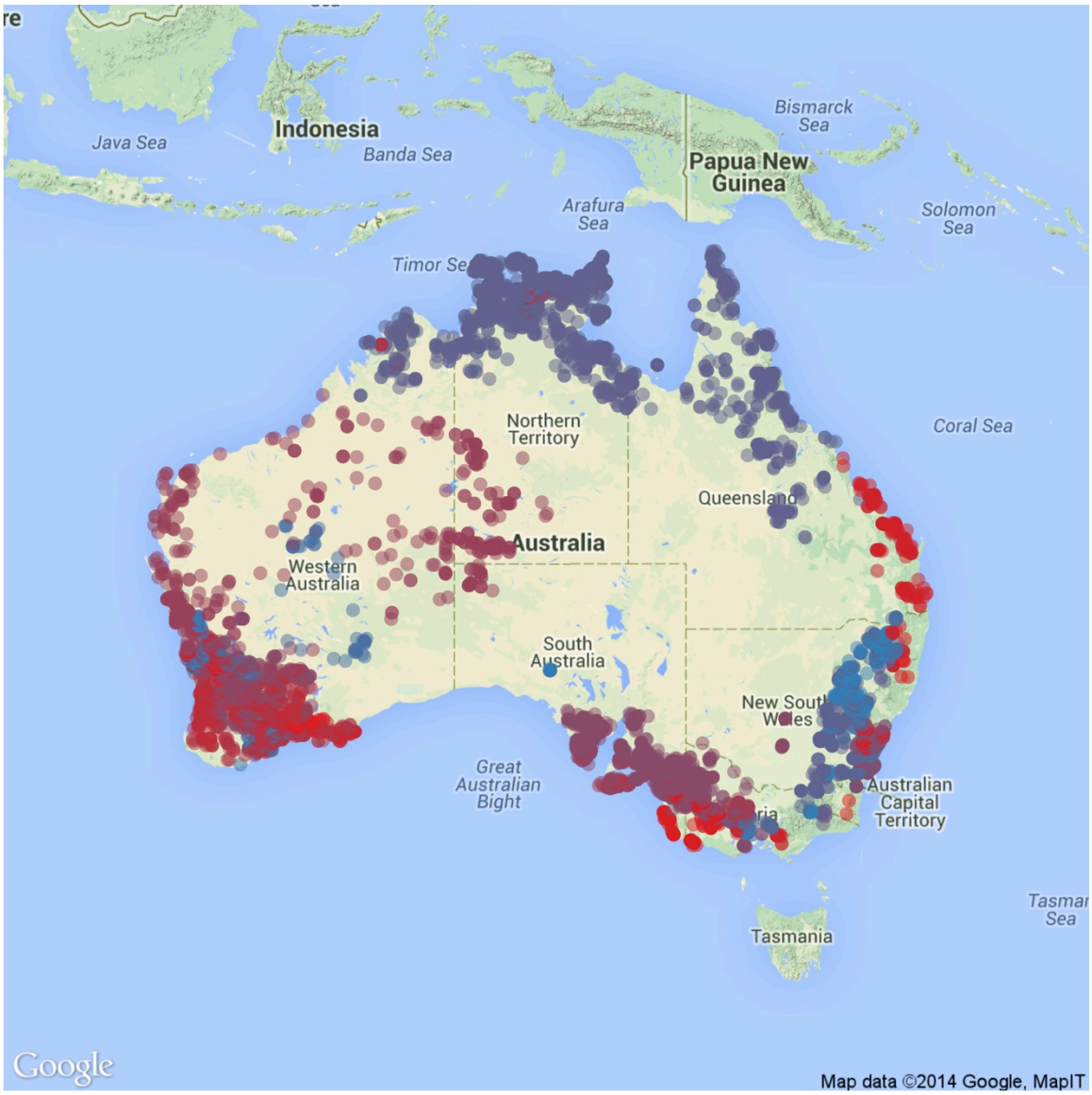

Figure S4.24. Map showing the distribution of the members of the Pteridifolia group that showed significantly elevated rates of speciation. Each species is given a unique color.

Figure S4.25. Photograph of an individual of *Xanthotis macleayanus*, Meliphagidae, feeding on an inflorescence of *Grevillea pteridifolia*, Kingfisher Lodge, Julatten, northeast Queensland. Photograph by Bryan Suson.

Appendix S5. Animated geographic reconstruction of Hakeinae radiation

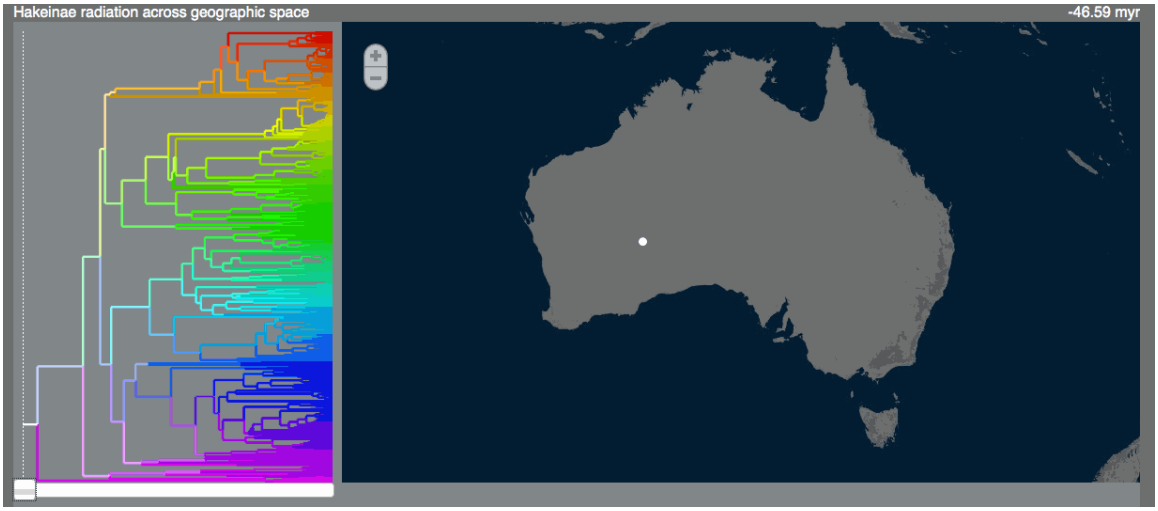

Open with a web browser. Animated reconstruction of Hakeinae radiation across Australian geographic space. Created with *phylowood* and *R2phylowood*.

Does competition matter?

Eliot T. Miller

Sarah K. Wagner

Mark Westoby

Robert E. Ricklefs

ABSTRACT

Resources are finite. Species utilize restricted subsets of the resource pool. A rich history of work examines how species are packed into this available niche space. If competition limits local species richness or the traits of potential immigrants, the signal should manifest itself at any of a few levels. At higher diversity, (1) species may occupy smaller niches, (2) they may be more closely packed in niche space, (3) or total assemblage niche space may simply be larger. With respect to niche overlap, if competition limits similarity, then (4) niche overlap should not increase linearly but, rather, level off with the addition of new species, and (5) observed assemblage niche overlap should be less than expected. To address these possibilities, we used field observations to characterize the niche sizes and positions of a large continental radiation of ecologically diverse birds, the honeyeaters (Meliphagidae). Species occupy characteristic and phylogenetically conserved niches, but many dimensions are needed to accurately describe these. At higher diversity, species occupy larger niches, are more closely packed in niche space, and total assemblage niche space is larger. This provides mixed support for an impact of competition on niche occupancy, and we conclude that niche overlap is the norm. Direct

quantification of overlap, however, suggested that assemblage-level overlap was significantly less than would be expected if constituent species utilized available resources without regards to co-occurring species, and, as compared with a null model, this overlap decreased with increases in diversity. Thus, while species clearly overlap greatly in resource use, we do find some evidence for niche partitioning. Competition appears to influence community assembly in the honeyeaters. We suggest that it is a relatively minor determinant of the process, and operates "after" such things as phylogenetic niche conservatism and stochastic factors have shaped which lineages occur where.

INTRODUCTION

Most researchers probably agree that somewhere between the view that communities are predictably assembled, discrete entities of beautifully co-evolved organisms (MacArthur 1958, 1970), and the view that communities are assembled entirely via dispersal probabilities and stochastic processes (Hubbell 2001), lies reality. Yet, many research questions seem to orbit around one or the other of these worldviews. An issue that has plagued researchers focused on demonstrating predictable community assembly processes like niche filling, competitive exclusion, and habitat filtering is a lack of fine-grained ecological data; when results do not support hypotheses, it can be difficult to determine if this is merely a shortcoming of the data. To what degree might our traditional ecological conceptions be borne out, given ideal ecological data?

The Meliphagidae, or honeyeaters, are a diverse family of passerines distributed predominantly in Australia, New Guinea and the Pacific Islands. They occupy a wide

range of ecological niches, with at least one species occurring almost everywhere in Australia, including Tasmania, where there are four endemic species. Most species take some nectar, but some are also largely frugivores, and others are dedicated insectivores (Higgins *et al.* 2001). Owing both to ease of observation, and a history of interest in Australia, their foraging behavior has been studied in some detail (Recher 1971; Ford & Paton 1976, 1982; Paton 1980; Pyke 1980; Recher *et al.* 1985; Ford 1990). These studies have laid the foundation upon which the current study is based. While these studies have often been descriptive in nature, it is quantitative foraging data like these that are frequently lacking when investigating community assembly patterns.

In this paper we test the hypotheses that limiting similarity structures bird assemblages, and that species partition niche space. In this paper we are concerned with the Eltonian niche (Elton 1927). We adopt the definition that this is, for a species, the position in and breadth of use of a resource pool within a habitat on which that species depends. Support for these hypotheses would provide indirect evidence contradicting the Eltonian Noise Hypothesis (Soberón & Nakamura 2009), which states that the milieu of biotic interactions do not shape species' distributions at the continental scale. Support for our hypotheses might be exhibited at any of a variety of levels. At higher diversity, (1) species may occupy smaller niches, (2) be more closely packed in niche space, (3) or total assemblage niche space may simply be larger. With respect to niche overlap directly, if competition limits similarity, then (4) observed niche overlap should not increase linearly with the addition of new species, i.e. show at most asymptotic growth, and (5) observed assemblage niche overlap should be less than expected; diverse assemblages should show evidence of saturation (Ricklefs 1987). These predictions

follow from a number of cherished ecological ideas: that niche space in any given assemblage is limited (Hutchinson 1957); that in order for a population to persist, individuals must compete more with individuals of their own species than with members of other species (Lotka 1925; Volterra 1926); and that, because of these facts, species from diverse communities are, over an evolutionary time-scale, able/forced to carve out more specialized, smaller portions of available niche space (May & MacArthur 1972).

To address these predictions, we collected foraging data on the Australian Meliphagide. We use these data to quantify species' Eltonian niches (Elton 1927; Soberón & Nakamura 2009; Peterson *et al.* 2011). While we acknowledge spatio-temporal limitations in the dataset, it provides greater detail to address these hypotheses than any other dataset of which we are aware. Rather than species' means, it is composed of species-specific sets of observations, intended to delineate the bounds of species' niches. Rather than proxies of niche space, such as morphology or plant functional traits, it is focused on the actual resources consumed by the Meliphagidae.

METHODS

Our methods of data collection followed Miller & Wagner (2014). These are based on standardized methods of quantifying foraging behavior (Remsen & Robinson 1990). In brief, between July 2009 and May 2014, we spent 295 field days throughout continental Australia, Kangaroo Island, and Tasmania (Fig. 1). When not driving between sites, we spent the daylight hours walking transects, searching for and observing honeyeaters, and recording what they were eating and how they were getting it. We recorded the time, location, substrate the bird foraged on (e.g., flower, branch), the attack maneuver

employed (e.g., sally-strike, glean, probe), whether the bird was hanging while performing it, the height of the foraging bird, the height of the surrounding canopy, the distance of the bird from the trunk, and the density of foliage around the foraging bird. These last two variables were recorded on an ordinal scale. Note then that these data contain continuous, ordinal, and discrete variables.

To minimize biases, we discarded the first foraging maneuver we saw, if that was what drew our attention to the bird. Otherwise, if for instance we located the bird by vocalizations, we recorded the first maneuver we saw. We endeavored to only record one observation per individual per day. To better understand individual variation in foraging behavior, in some cases we did record multiple observations from single birds. However, we considered a series of observations like these to collectively represent a single data point (methods for weighting such series explained below). We had insufficient data to calculate the niche size of one species (see results). Rather than exclude it from analyses, since it is known to forage similarly to its congeners (Higgins *et al.* 2001), we included it as the average of those species.

To provide ease of access to the data, and to facilitate its analysis, we wrote an R package, available from GitHub. The package contains the raw data and functions that: (1) provide detailed metadata on each measure, (2) appropriately convert raw observations to species' averages, and (3) convert raw observations into metrics of species' niche sizes.

We define communities at the 100 x 100 km grid cell level. In many cases in Australia, it is reasonable that all species in a grid cell could interact ecologically. For instance, during a single day's survey, we saw a mean of 40% of the bird species

recorded from a given grid cell (n = 27, SD = 16, max = 100%, min = 21%). We acknowledge that it is not always the case that two species in a given grid cell could reasonably interact, and in the future would like to incorporate finer-scale spatial partitioning. Whenever possible, we weight all our metrics by the grid-cell level relative abundance of each species, which serves to diminish the influence of vagrants. We used the spatial dataset from Miller *et al.* (2013). This taxonomically and spatially cleaned dataset contains 2,273,404 points across all Meliphagidae species. The data were downloaded and concatenated from eBird (Sullivan *et al.* 2009) and the Atlas of Living Australia (http://www.ala.org.au/).

A significant advantage of our foraging dataset is the ability to quantify both the position and size of species' niches. Two difficulties arise, however. First, the dataset includes a combination of variable types. To contend with this, we calculated the Gower distances among all observations (Gower 1971). The Gower method calculates distances among both continuous and discrete variables. We weighted all variables equally, and treated ordinal variables with the method proposed by Podani (1999). We considered whether the foraging substrate was dead (e.g., a dead leaf, Rosenberg 1990) to be a binary asymmetric variable.

We ordinated the distance matrix with non-metric multidimensional scaling (NMDS). We chose the number of dimensions to use in the NMDS by ordinating the same distance matrix across a range of dimensions and examining how stress decreased with the addition of dimensions. Based on an elbow in the plot, we chose a ten-dimensional niche space. Results were qualitatively identical based on either the NMDS or a 792-dimension principal coordinates analysis (PCoA, see below).

The other difficulty with the dataset is the uneven sampling across species (Fig. S1). Volumes such as would be calculated with convex hulls, for instance, are strongly influenced by outliers and the number of points in the hyper-volume. We therefore employed a measure of functional dispersion (FDis) that is robust to variation in sample size (Laliberté & Legendre 2010). FDis was developed to quantify the functional diversity of communities after ordinating, with PCoA, species based on their mean traits (i.e. a single point per species). Thus, we modify the definition slightly here, as the weighted mean absolute deviation of each species' foraging observations from its weighted centroid. FDis has heretofore been calculated with the R package *FD* (Laliberté & Legendre 2010), which requires that data be ordinated by PCoA. We thus generalized FDis to ordination spaces beyond PCoA, including the NMDS used here. These functions are provided in our data package here. The inputs used by our functions are identical to those used in the *FD* package.

We performed two separate FDis calculations on the same ordination space. In the first, we used the R package *FD* (Laliberté & Legendre 2010) to calculate, in multivariate space, the mean absolute deviation of each species' foraging observations from its centroid. Recall that some observations were serial. Thus, we weighted the influence of each observation on FDis by the inverse of the number of observations in the series; a single, non-serial observation had a weight of one. We refer to this species-level measure of niche size as $FDis_{sp}$.

We also calculated a community level measure, $FDis_{comm}$. To do this, we calculated the weighted mean absolute deviation of all foraging observations from all species present in that community from the centroid of the community. The weights in

the $FDis_{comm}$ calculation were proportional to the relative abundance of each species in that grid cell.

To determine whether the ordination space was a reasonable approximation of niche space based on our experiences in the field, and to determine what drove the ordination axes, we used the *vegan* (Oksanen *et al.* 2013) function envfit. This function fits vectors and factors onto the NMDS space, returning both the loadings of the continuous variables and the centroids of the ordinal and discrete variables. Note that NMDS is an unconstrained ordination; envfit fits linear responses. Responses were unsurprisingly non-linear, and so *vegan* methods like ordisurf are in some ways more appropriate. However, ordisurf is not useful for categorical variables, and we therefore used envfit despite this shortcoming. General interpretations of the ordination space were the same irrespective of whether ordisurf or envfit were used.

To address prediction one, that species have smaller niches in higher diversity assemblages, we calculated the weighted-average niche size per grid cell, where weights were relative to species abundances in the cell. We fit a linear model between these average niche sizes and the diversity in the cell.

To address prediction two, that species are more closely packed in niche space at higher diversity, we used Mahalanobis distances (Mahalanobis 1936) to calculate the mean pairwise distance in multivariate space among species' weighted centroids. The weighting of these centroids follows the $FDis_{sp}$ definition above. We calculated mean pairwise distances both without weighting, and by weighting by the relative abundance of each species in the cell, following the "interspecific" method (Miller *et al.* 2013).

To test prediction three we fit linear models to the relationship of $FDis_{comm}$ and the corresponding species richness of that grid cell.

We used the R package *nicheROVER* (Swanson *et al.* 2014) to address predictions four and five. *nicheROVER* calculates species' pairwise probabilities of niche overlap. This returns a probability that a given point of species A falls within species B's niche, and vice versa. We averaged these two probabilities per species. This is the probability that a randomly selected point of either A or B falls within the niche of the other species. Per grid cell, we calculated a mean pairwise overlap among constituent species. We compared observed mean overlaps to those from a null model that randomized the identity of species observations within grid cells. This null model maintained the total size and position of the original assemblage niche space, species richness and number of observations per-species, but not species' niche sizes. We calculated standardized effect sizes (SES) of these observed pairwise overlaps as the difference of the observed overlap and the mean randomized overlaps, divided by the standard deviation of overlaps, and compared these SES to the richness of the corresponding grid cells.

To further test predictions four and five, we calculated the proportion of observations per grid cell that could be correctly classified to species with a linear discriminant analysis (LDA). Independent of any biological phenomena, these proportions decline with increasing richness (and total observations). Thus, we employed the null model described above to calculate a SES, per grid cell, of the proportion of observations correctly assigned to species as compared with the randomizations.

As additional descriptive checks on our data, and confirm that related species forage similarly, we calculated Pagel's lambda (Pagel 1999), a measure of phylogenetic

signal ("conservatism"). We calculated the signal in species' weighted centroids along each of the 10 axes separately, and explored which axes showed reduced phylogenetic signal; it could be supposed that these axes are important for niche partitioning. We also quantified the phylogenetic signal in $FDis_{sp}$. We used the R package *phytools* (Revell 2012) and the most recent, dated Meliphagidae phylogeny for this (Joseph *et al.* 2014), with the few missing species added manually as in Miller *et al*. (2013)

RESULTS

In sum, we collected 9,595 foraging observations across 74 of 75 species of Australian honeyeater. After accounting for serial observations, the dataset contains 7,302 independent observations. The most-observed species was *Lichmera indistincta* (n=459). The least-observed species included in the dataset was *Glycichaera fallax* (n=20). We observed one individual of *Conopophila whitei*. This observation is excluded from the dataset, and we instead ran analyses considering this species to occupy a niche of average size and position between its congeners.

The ordination space corresponded to our conception of available niche space (Fig. S2). Multiple qualitative general areas of niche space can be discerned. Along the first few axes, nectar feeding, aerial attacks, and gleaning from leaves all sit in clearly distinct regions of multivariate space (Table S1); niche space is non-normally distributed, particularly along the first two dimensions.

Measures of $FDis_{sp}$ ranged from 0.14 (*Trichodere cockerelli*, *Ashbyia lovensis*) to 0.34 (*Lichenostomus fuscus*). In general, ground-foraging insectivores and then inveterate nectarivores tended to have the smallest niches, while well-known generalists (Higgins *et*

al. 2001) like species of *Lichenostomus* (*sensu lato*), *Meliphaga* and *Melithreptus* had the largest niches. These niche sizes were phylogenetically conserved across species (Fig. S3, lambda = 0.75, p = 0.007).

Measures of $FDis_{comm}$ showed little variation (range 0.28-0.33). The FDis of the entire ordination space was 0.32, which is less than some individual grid cells and species. What little variation there was did have a clear regional variation in $FDis_{comm}$; grid cells in the southeast of Australia, including Tasmania, were characterized by the largest available niche spaces (Fig. S4).

We found no support for prediction one. Instead, species' average niche sizes were positively correlated with grid cell richness ($R^2 = 0.31$, $p < 0.001$, Fig. 2). The smallest average niches were exhibited by assemblages in the eastern deserts (Fig. S5).

We found no support for prediction two. There was a weak positive correlation between distances among co-occurring species in multivariate space and the species richness of the corresponding grid cell (unweighted $R^2 = 0.11$, $p < 0.001$, weighted $R^2 = 0.02$, $p = 0.0003$, Fig. S6). Assemblages from both Tasmania and the eastern deserts were the most widely separated in niche space (Fig. S7).

We found some support for prediction three. There was a positive correlation between $FDis_{comm}$ and species richness ($R^2 = 0.12$, $p < 0.001$, Fig. 3); more species-rich communities occupy slightly larger total niche space than communities with fewer species.

We also found support for predictions four and five. Mean observed pairwise niche overlap was always less than expected based on the null model. When the values from the null model were used to derive SES, there was a negative correlation with

species richness ($R^2 = 0.64$, $p < 0.001$, Fig. 4); co-occurring species show increasingly smaller pairwise niche overlaps with increasing diversity. All SES were significant, and observed assemblages showed less pairwise niche overlap than if the species were sampling randomly from available niche space. Considered geographically, mean pairwise overlap was highest in the north of the continent, and lowest in the deserts and Tasmania (Fig. S8). SES were lowest (most finely partitioned) in the southeast (Fig. S9).

Across the entire ordination space, including allopatric species from around the continent, 11% of observations could be correctly classified to species. Within grid cells, between 15 and 57% of observations could be correctly classified. As expected, fewer points could be correctly classified at higher species richness. When values from the null model were used to derive SES, there was a positive correlation between these SES and species richness ($R^2 = 0.31$, $p < 0.001$, Fig. 5). Species show increasingly distinct usage of niche space as diversity increases.

Foraging behavior showed a notable degree of phylogenetic signal (Table S2). Species' positions along the 10 NMDS axes tended to be conserved. Only axis 10 did not show significant phylogenetic signal. This axis was driven by unusual foraging maneuvers like pecking, gaping, and hanging, and substrates like spider webs, woody fruits (e.g., *Eucalyptus*), and hanging bark (Table S1).

DISCUSSION

Community assembly rules have intrigued ecologists for well over 250 years. Darwin (1859) famously proposed that, owing to competition, potential invasive species will have more difficulty establishing in novel areas if a congeneric species already exists in

that area than if they do not. Interspecific competition can structure species' territories (Orians & Willson 1964), primary forest tree species ultimately outcompete pioneer species (Buffon 1742), competition has been shown to influence phenotypes (Schluter & Grant 1984), and we see interspecific squabbles at our bird feeders. Yet, at larger scales, the Eltonian Noise Hypothesis (Soberón & Nakamura 2009) reigns (see de Araújo *et al.* 2014 for a specific test of the hypothesis, though researchers have been interested in the idea long before it had a name). Indeed, ideas such as neutral theory likely have been well received in part because of this noise (Hubbell 2001).

In this study, we addressed five, non-mutually exclusive predictions that follow from the hypotheses that limiting similarity structures bird assemblages, and that species partition niche space. As diversity increases, to compensate, (1) species may occupy smaller niches, (2) become more closely packed in niche space, (3) or total assemblage niche space may grow as incoming species occupy peripheral niche positions. Also, if competition limits similarity, then (4) observed niche overlap should not increase linearly with the addition of new species, and (5) observed assemblage niche overlap should be less than expected.

We found mixed support for the predictions. At higher species richness, co-occurring species occupied larger niches (Fig. 2), showed little response in their average position (and distance from co-occurring species) in niche space (Fig. S6), and occupied larger total niche space (Fig. 3). Niche overlap is the norm in Australian honeyeater assemblages, as evidenced by the NMDS plot (Fig. S2) and these and previous results (e.g. Ford & Paton 1976).

At the same time, observed niche overlap was always less than if co-occurring species sampled randomly from available niche space and, as compared with a null model, this niche partitioning increased with species richness (Fig. 4). Species became increasingly more identifiable by their foraging behavior as richness increased (Fig. 5). The most diverse communities showed the best evidence of niche partitioning.

Readers may question to what extent our data and methods are suitable to address these fundamental issues of ecology and evolutionary biology. With regards to the data quality itself, both niche size and position showed pronounced phylogenetic signal (Table S2), implying that the level of signal to noise ratio in the data was low, and that the ordination did indeed provide a reasonable multivariate descriptor niche space. Well-known generalist species (e.g., *Lichenostomus sensu lato*) had large niches, while more specialized, ground-foraging insectivores and highly nectarivorous species had small niches. Within assemblages, 15-57% of observations could be correctly classified to species, and even at the continental-scale, with the entire dataset, 11% of observations could be correctly classified. Our niche space was ten-dimensional. While it may strike some readers as potentially over-fitting, we suggest that more than ten dimensions may best describe true niche space. Future studies should carefully consider potential niche space and its possible dimensions.

With regards to the applicability of these data to the questions, we know of no other dataset providing this level of detail. We acknowledge spatio-temporal biases, but we believe it is unlikely that additional data would change our conclusions. Our analyses account for differences in sample size among species. More data would provide more detail, but it would not dramatically alter the results.

We show here that species exhibit tremendous overlap in niche space. Whether or not this niche overlap is more than predicted by mathematical models remains to be tested (May & MacArthur 1972). Despite this overlap, species occupy characteristic niches, which corroborates our field-based intuition that species utilize subsets of niche space, and obtain these resources in species-specific manners. Evidence of niche partitioning was less obvious, and required the use of null models to demonstrate.

Based on maps of niche sizes and partitioning, it appears that some of the lowest levels of niche overlap occurred in the eastern deserts and Tasmania. The desert species occupied a small total niche space, and co-occurring species had small, widely separated individual niches. Tasmanian assemblages occupied large total niche spaces. Constituent species there exhibited large individual niches and were widely separated in space. It seems possible that populations in both of these regions are unable to grow large enough to buffer species from extinction given strong competition for niche space. In the case of the deserts, this process may lead to local extinction (i.e., an inability of immigrants to settle) of species with large niche overlap with residents, whereas in Tasmania it may have led to a small adaptive radiation into divergent niche spaces (Keast 1970).

The worldview that emerges from these results is one where species show some evidence of niche partitioning, particularly in low resource and insular habitats, but the general community assembly pattern is one of widespread niche overlap. Such a pattern can be explained if "local" communities (on any scale, including the acknowledged artificial scale employed here) are not inviolable evolutionary units, but merely geographically overlapping assemblages of species (Ricklefs 2008), each subject to a unique combination of the effects of competition, habitat filtering, and manifold

additional extrinsic and intrinsic factors. In the title of the paper, we ask, "does competition matter?" Based on our results here, competition appears to influence community assembly in the honeyeaters, but we suggest that it is a relatively minor determinant of the process, and operates "after" such things as phylogenetic niche conservatism and stochastic factors have shaped which lineages occur where.

ACKNOWLEDGEMENTS

ETM is grateful for financial support from the National Science Foundation (GRFP #1051698), the St. Louis Audubon Society, a Trans-World Airlines Scholarship from the University of Missouri, and Macquarie University Higher Degree Research Office. We thank Leo Joseph, Árpád Nyári, Brian Venebles, Stephen Murphy, Hugh Ford, Harry Recher, Phillip Maher, Mick Roderick, Dick Cooper, David Watson, Keith and Lindsay Fisher, Alex Anderson, Bryan Suson, and Amy Zanne for invaluable discussion and advice on study sites, identification tips, and help in the field. Some of our analyses were run on the University of Missouri Lewis Cluster, and the University of Missouri, St. Louis Grethor Cluster.

REFERENCES

1.

De Araújo, C.B., Marcondes-Machado, L.O. & Costa, G.C. (2014). The importance of biotic interactions in species distribution models: a test of the Eltonian noise hypothesis using parrots. *J. Biogeogr.*, 41, 513–523.

2.

Buffon, G.L.L. (1742). *Mémoire sur la culture des forêts.* Mémoires des Académie royale des Sciences.

3.

Darwin, C. (1859). *On the origin of species by means of natural selection, or the preservation of favoured races in the struggle for life*. John Murray, London.

4.

Elton, C.S. (1927). *Animal ecology*. University of Chicago Press, Chicago, IL.

5.

Ford, H.A. (1990). Relationships between distribution, abundance and foraging specialization in Australian landbirds. *Ornis Scand.*, 133–138.

6.

Ford, H.A. & Paton, D.C. (1976). Resource partitioning and competition in honeyeaters of the genus Meliphaga. *Aust. J. Ecol.*, 1, 281–287.

7.

Ford, H.A. & Paton, D.C. (1982). Partitioning of nectar sources in an Australian honeyeater community. *Aust. J. Ecol.*, 7, 149–159.

8.

Gower, J.C. (1971). A general coefficient of similarity and some of its properties. *Biometrics*, 857–871.

9.

Higgins, P.J., Peter, J.M. & Steele, W.K. (2001). *Handbook of Australian, New Zealand and Antarctic Birds. Vol. 5: Tyrant-flycatchers to Chats*. Oxford University Press, Melbourne, Australia.

10.

Hubbell, S.P. (2001). *The unified neutral theory of biodiversity and biogeography*. Princeton University Press, Princeton, NJ.

11.

Hutchinson, G.E. (1957). Concluding remarks. Cold Springs Harbor Symp. Quant. *Biol*, 22, 415–427.

12.

Joseph, L., Toon, A., Nyári, Á.S., Longmore, N.W., Rowe, K., Haryoko, T., *et al.* (2014). A new synthesis of the molecular systematics and biogeography of honeyeaters (Passeriformes: Meliphagidae) highlights biogeographical and ecological complexity of a spectacular avian radiation. *Zool. Scr.*, 43, 235–248.

13.

Keast, A. (1970). Adaptive Evolution and Shifts in Niche Occupation in Island Birds. *Biotropica*, 2, 61–75.

14.

Laliberté, E. & Legendre, P. (2010). A distance-based framework for measuring functional diversity from multiple traits. *Ecology*, 91, 299–305.

15.

Lotka, A.J. (1925). *Elements of physical biology*. Williams & Wilkins company, Baltimore, MD.

16.

MacArthur, R. (1970). Species packing and competitive equilibrium for many species. *Theor. Popul. Biol.*, 1, 1–11.

17.

MacArthur, R.H. (1958). Population ecology of some warblers of northeastern coniferous forests. *Ecology*, 39, 599–619.

18.

Mahalanobis, P.C. (1936). On the generalized distance in statistics. *Proc. Natl. Inst. Sci.*, 2, 49–55.

19.

May, R.M. & MacArthur, R.H. (1972). Niche overlap as a function of environmental variability. *Proc. Natl. Acad. Sci.*, 69, 1109–1113.

20.

Miller, E.T. & Wagner, S.K. (2014). The ecology of the Australian sandstone *Meliphaga* honeyeater species. *Aust. Field Ornithol.*, In press.

21.

Miller, E.T., Zanne, A.E. & Ricklefs, R.E. (2013). Niche conservatism constrains Australian honeyeater assemblages in stressful environments. *Ecol. Lett.*, 16, 1186–1194.

22.

Oksanen, J., Blanchet, F.G., Kindt, R., Legendre, P., Minchin, P.R., O'Hara, R.B., *et al.* (2013). *vegan: Community Ecology Package*.

23.

Orians, G.H. & Willson, M.F. (1964). Interspecific territories of birds. *Ecology*, 45, 736–745.

24.

Pagel, M. (1999). Inferring the historical patterns of biological evolution. *Nature*, 401, 877–884.

25.

Paton, D.C. (1980). The importance of manna, honeydew and lerp in the diets of honeyeaters. *Emu*, 80, 213–226.

26.

Peterson, A.T., Soberón, J., Pearson, R.G., Anderson, R.P., Martínez-Meyer, E., Nakamura, M., *et al.* (2011). *Ecological niches and geographic distributions*. Princeton University Press, Princeton, NJ.

27.

Podani, J. (1999). Extending Gower's general coefficient of similarity to ordinal characters. *Taxon*, 331–340.

28.

Pyke, G.H. (1980). The foraging behaviour of Australian honeyeaters: a review and some comparisons with hummingbirds. *Aust. J. Ecol.*, 5, 343–369.

29.

Recher, H.F. (1971). Sharing of habitat by three congeneric honeyeaters. *Emu*, 71, 147–152.

30.

Recher, H.F., Holmes, R.T., Schulz, M., Shields, J. & Kavanagh, R. (1985). Foraging patterns of breeding birds in eucalypt forest and woodland of southeastern Australia. *Aust. J. Ecol.*, 10, 399–419.

31.

Remsen, J.V. & Robinson, S.K. (1990). A classification scheme for foraging behavior of birds in terrestrial habitats. *Stud. Avian Biol.*, 13, 144–160.

32.

Revell, L.J. (2012). phytools: an R package for phylogenetic comparative biology (and other things). *Methods Ecol. Evol.*, 3, 217–223.

33.

Ricklefs, R.E. (1987). Community diversity: relative roles of local and regional processes. *Science*, New Series, 235, 167–171.

34.

Ricklefs, R.E. (2008). Disintegration of the ecological community. *Am. Nat.*, 172, 741–750.

35.

Rosenberg, K.V. (1990). Dead-leaf foraging specialization in tropical forest birds: measuring resource availability and use. *Stud. Avian Biol.*, 13, 360–368.

36.

Schluter, D. & Grant, P.R. (1984). Determinants of morphological patterns in communities of Darwin's finches. *Am. Nat.*, 123, 175–196.

37.

Soberón, J. & Nakamura, M. (2009). Niches and distributional areas: concepts, methods, and assumptions. *Proc. Natl. Acad. Sci.*, 106, 19644–19650.

38.

Sullivan, B.L., Wood, C.L., Iliff, M.J., Bonney, R.E., Fink, D. & Kelling, S. (2009). eBird: A citizen-based bird observation network in the biological sciences. *Biol. Conserv.*, 142, 2282–2292.

39.

Swanson, H.K., Lysy, M., Power, M., Stasko, A.D., Johnson, J.D. & Reist, J.D. (2014). A new probabilistic method for quantifying n-dimensional ecological niches and niche overlap. *Ecology*, In review.

40.

Volterra, V. (1926). Fluctuations in the abundance of a species considered mathematically. *Nature*, 118, 558–560.

FIGURES

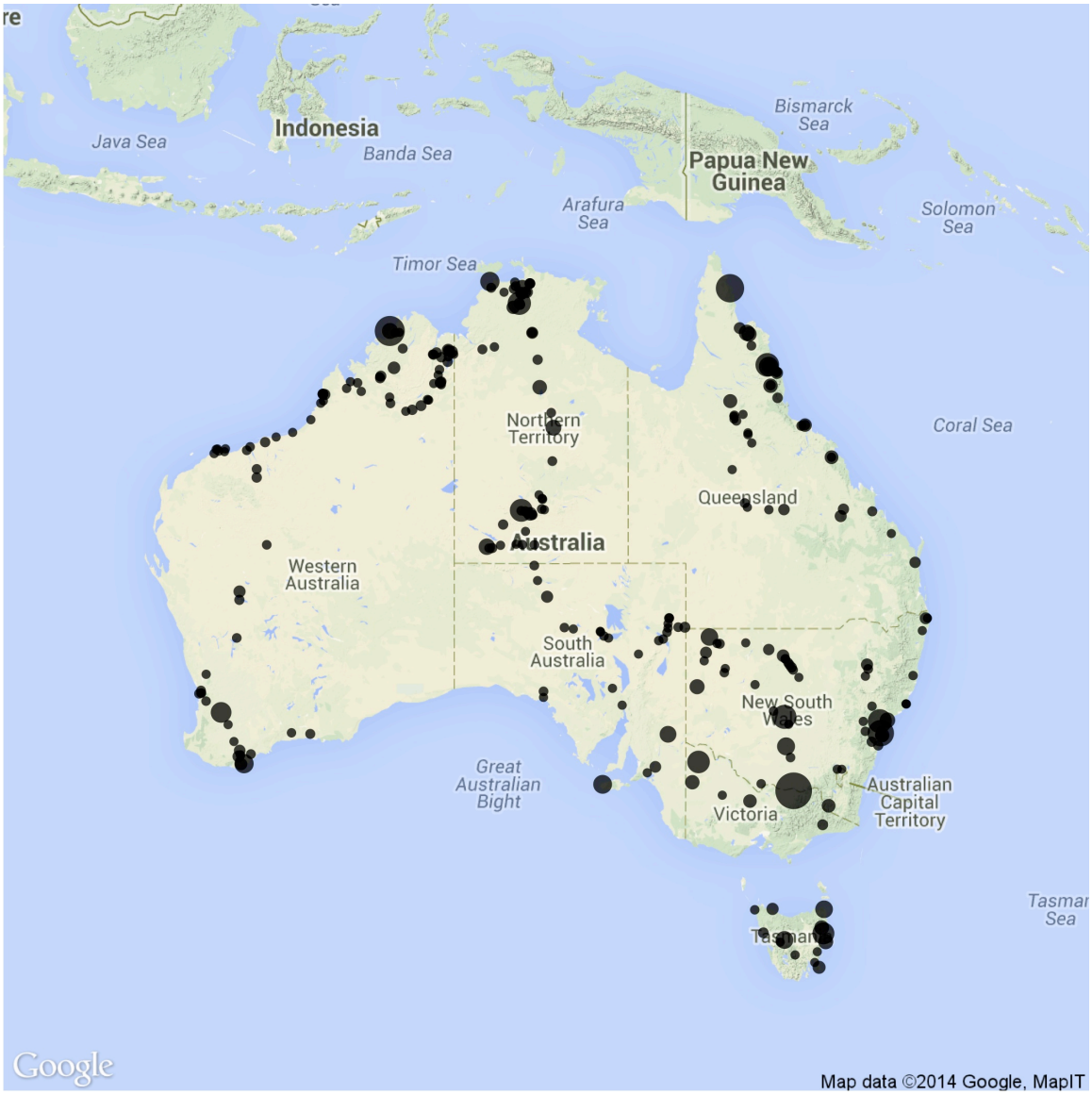

Figure 1. Map of study sites across Australia. The size of the dot corresponds to the number of foraging observations we recorded at that site.

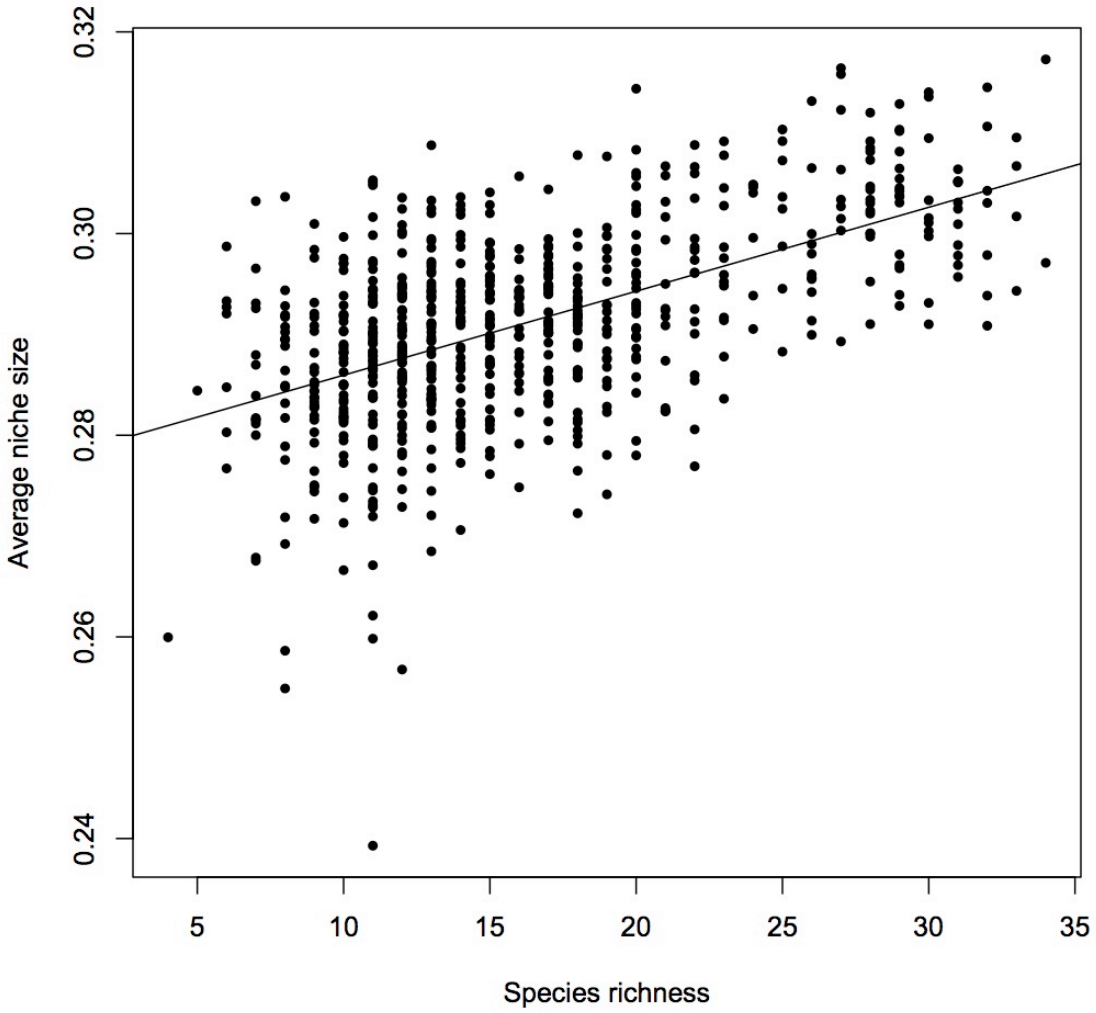

Figure 2. Average species niche size per grid cell as a function of the richness of the grid cell. Species from the most species-rich grid cells occupy larger foraging niches on average ($R^2 = 0.31$, $p < 0.001$).

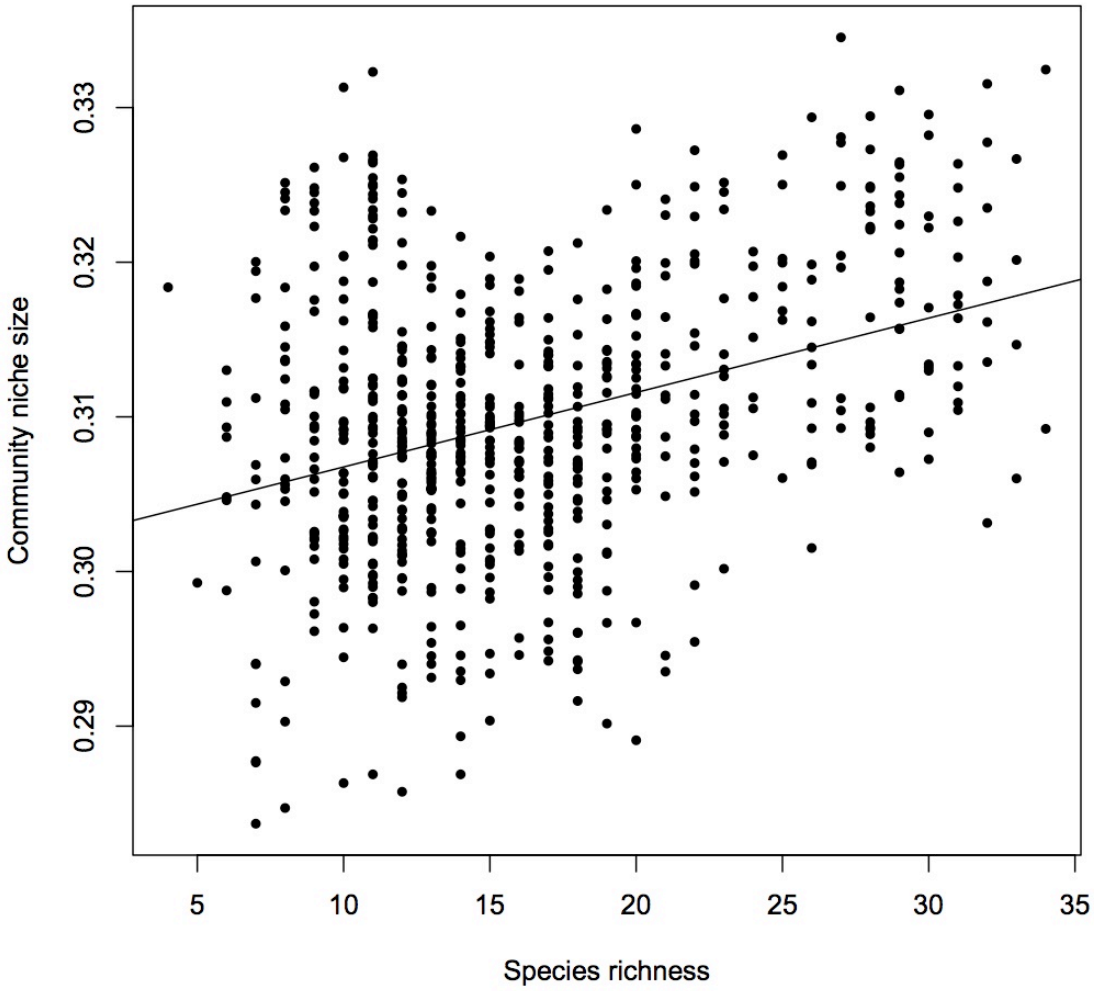

Figure 3. Assemblage-level functional dispersion, i.e. total niche size, as compared with species richness. The most species-rich assemblages occupy the largest total niches, though there is little absolute variation in the measure ($R^2 = 0.12$, $p < 0.001$).

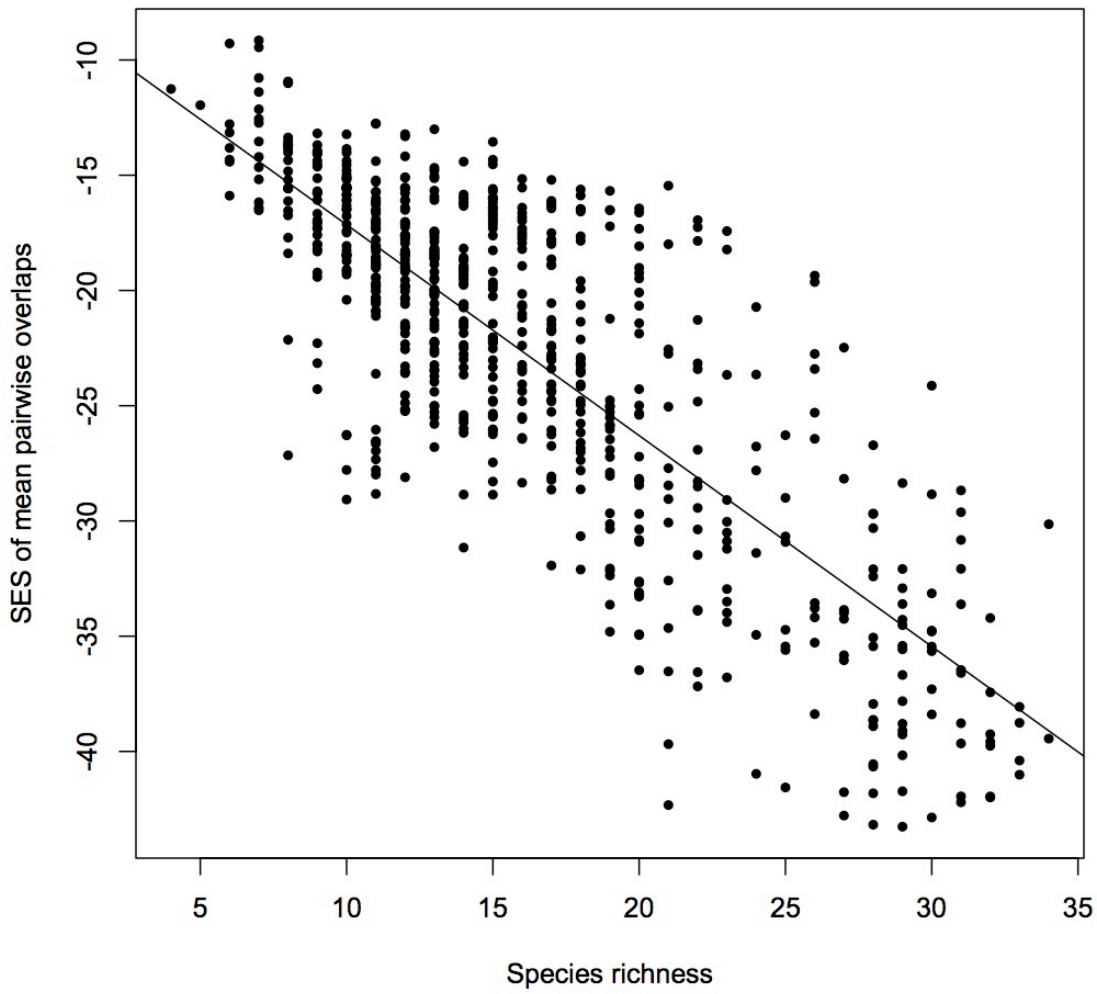

Figure 4. Standardized effect sizes (SES) of mean pairwise niche overlap per grid cell as a function of the species richness of the cell. The SES are based on null model simulations where observations were randomly re-assigned per grid cell ($R^2 = 0.64$, $p < 0.001$).

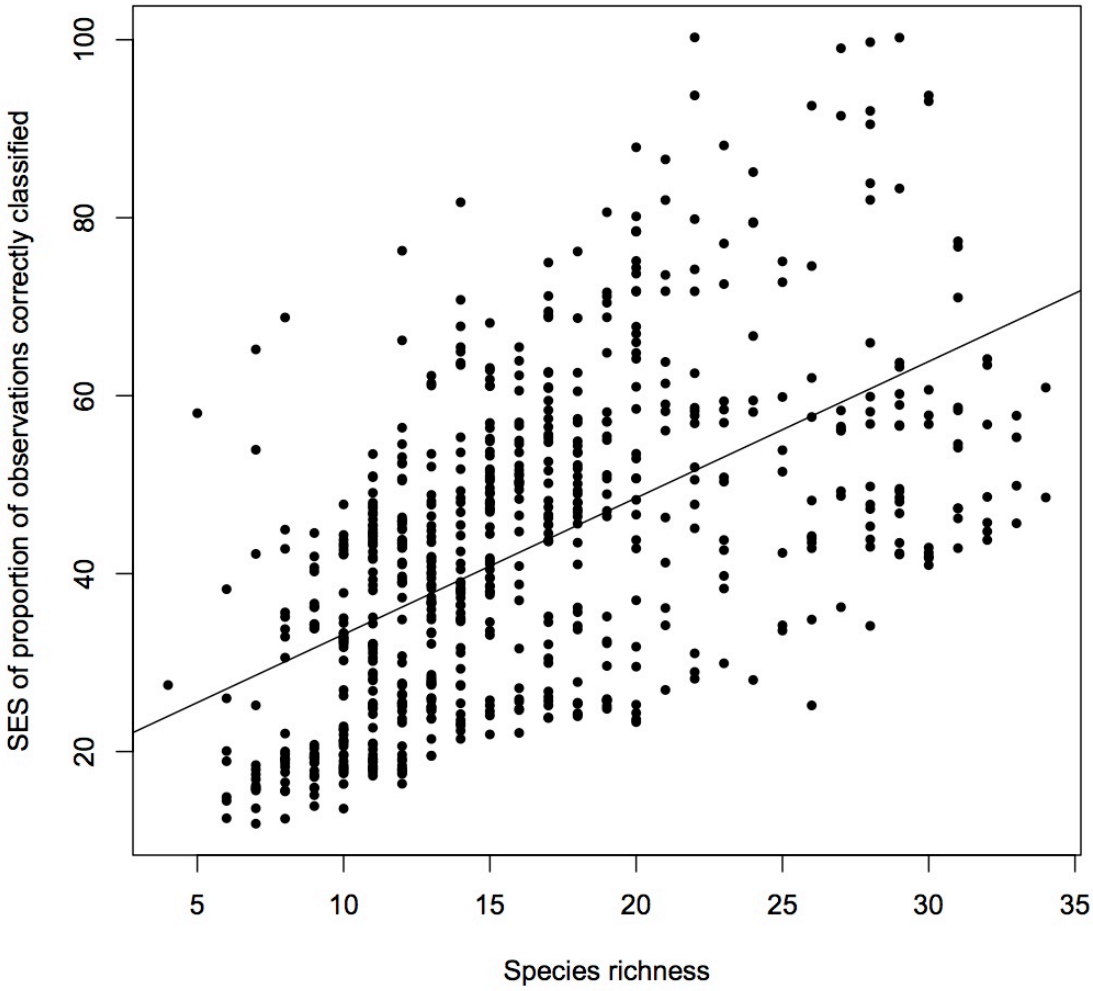

Figure 5. Standardized effect sizes (SES) of proportion of observations correctly classified to species per grid cell as a function of the species richness of the cell. The SES are based on null model simulations where observations were randomly re-assigned per grid cell ($R^2 = 0.31$, $p < 0.001$).

SUPPLEMENTARY FIGURES

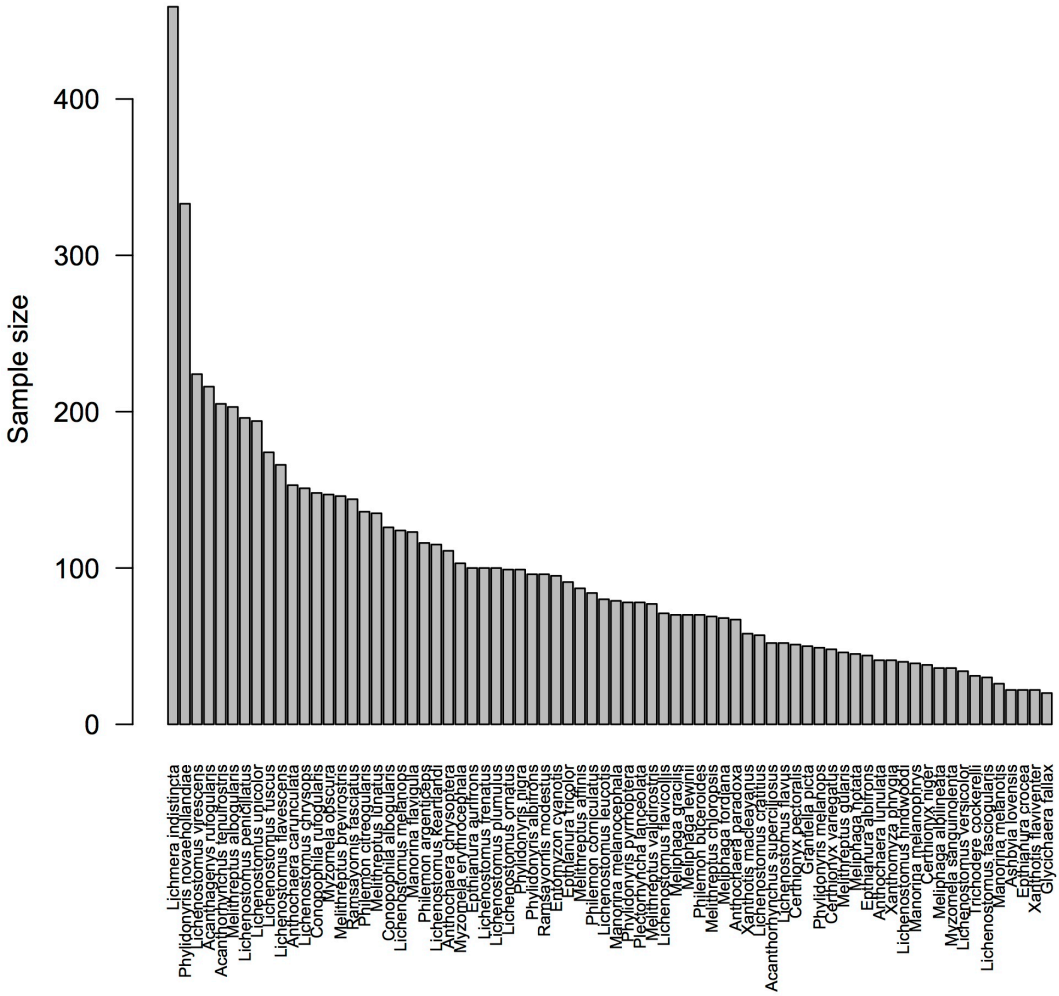

Figure S1. A bar graph showing sample size (number of independent foraging observations) across the 74 species of Meliphagidae included in the dataset.

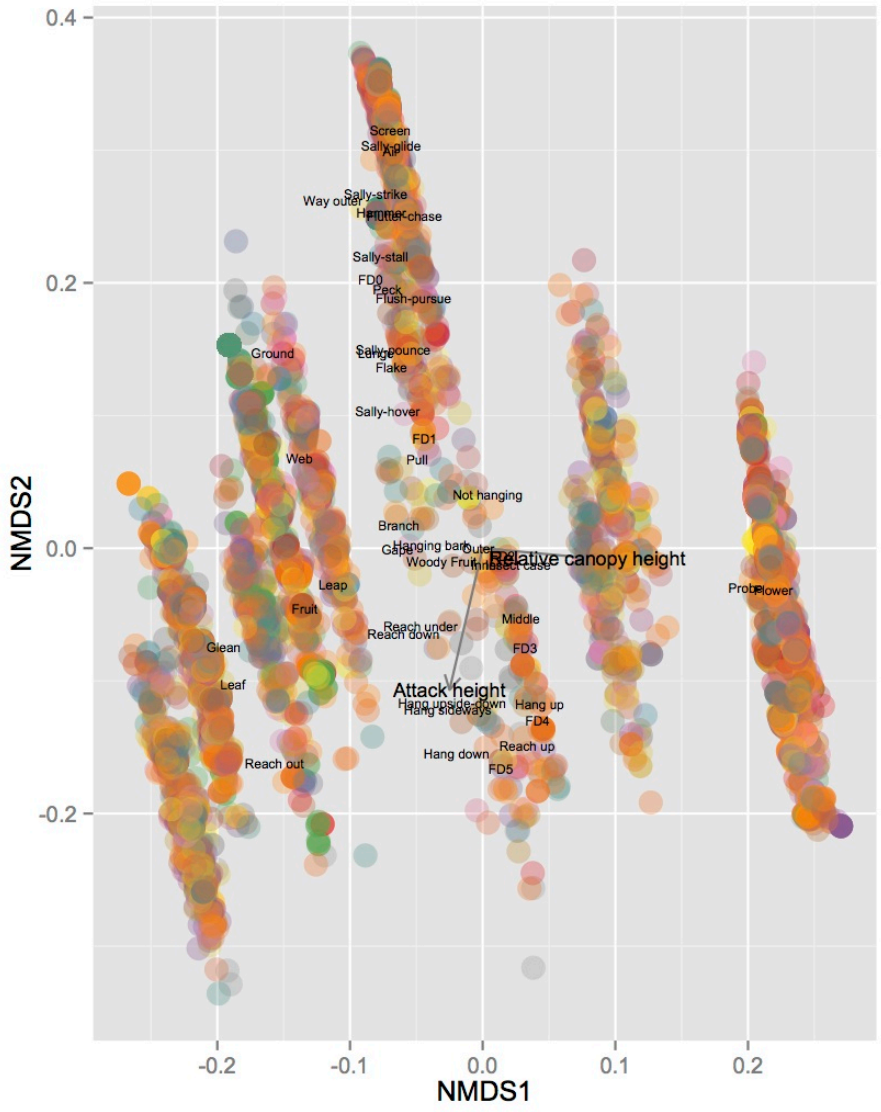

Figure S2. Ordination showing the first two axes from the non-metric multidimensional scaling of all 9,595 foraging observations. Continuous variable loadings are indicated with arrows. Centrodis of categorical variables such as foraging substrates, attack maneuvers, foliage density (FD), and distance from trunk (outer, middle, etc.) are denoted by text at the appropriate position. Each point, color-coded by species, corresponds to a unique foraging observation.

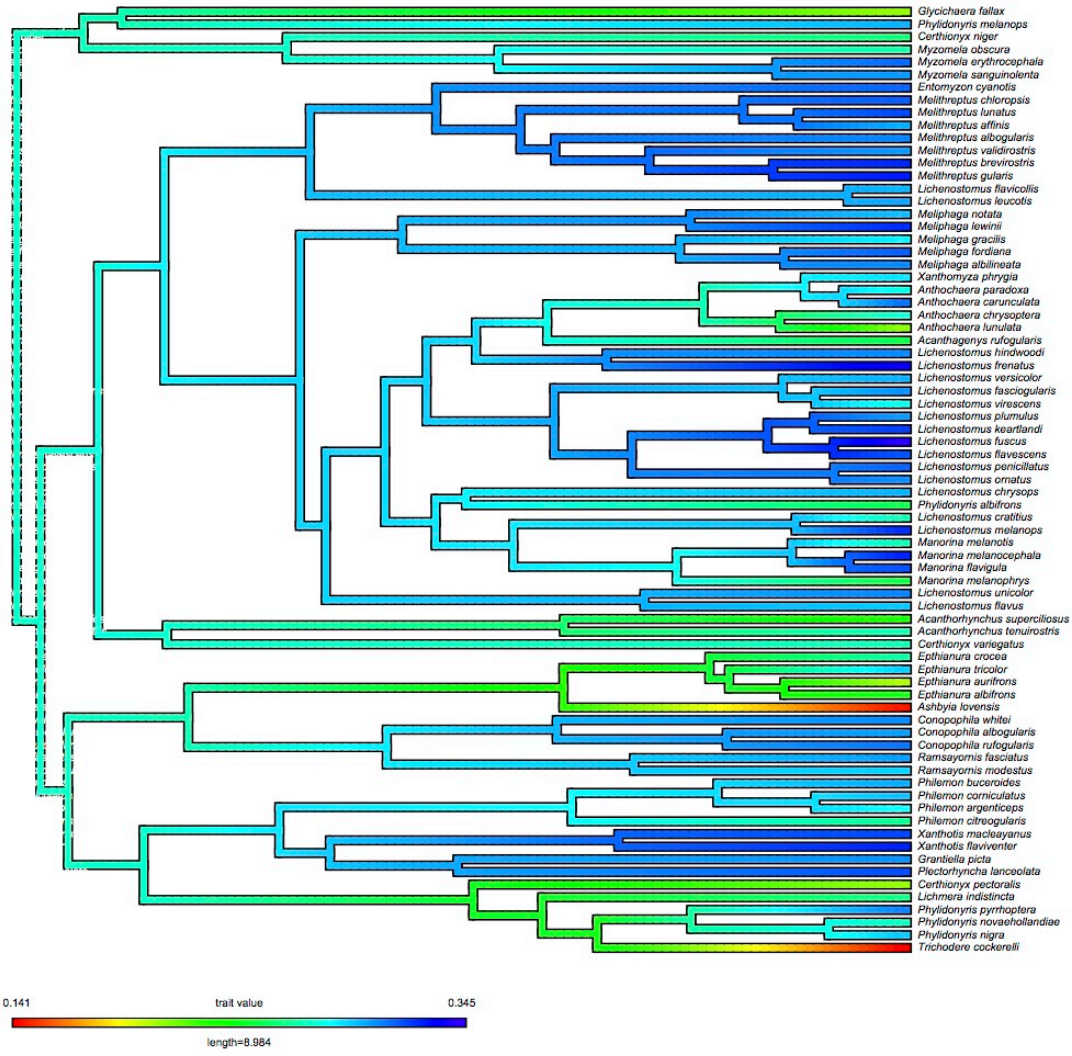

Figure S3. Dated Meliphagidae phylogeny showing the evolution of niche size. Species with small niches are colored red, while species with large niches are colored in dark blue. A significant degree of phylogenetic signal was found in niche size (Pagel's lambda = 0.75, p = 0.007).

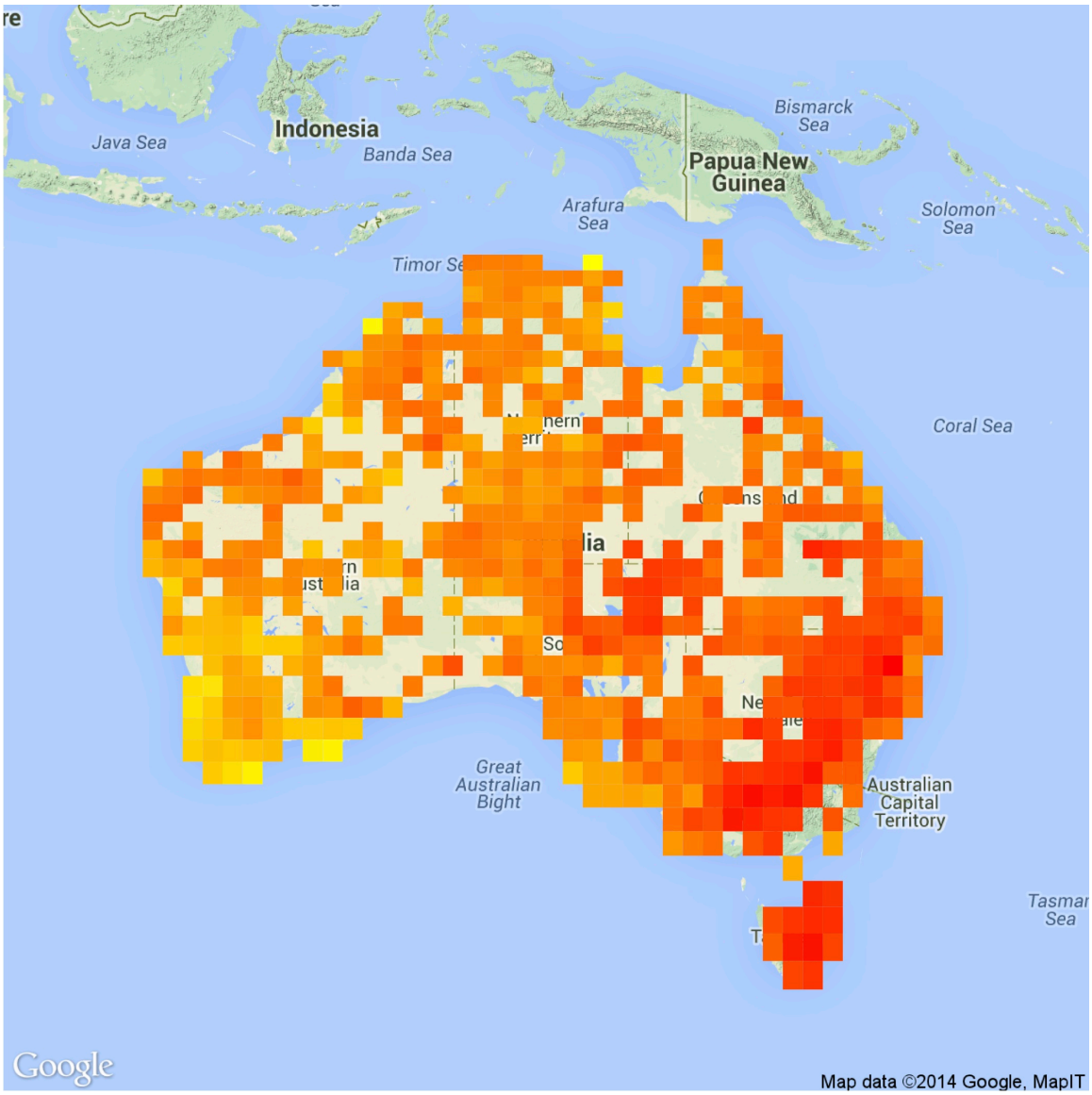

Figure S4. Functional dispersion at the community level, mapped across Australia. Yellow corresponds to small total community niche sizes, red to large. There is little absolute variation in the measure, but southwest Australia does have communities of slightly smaller total niche spaces.

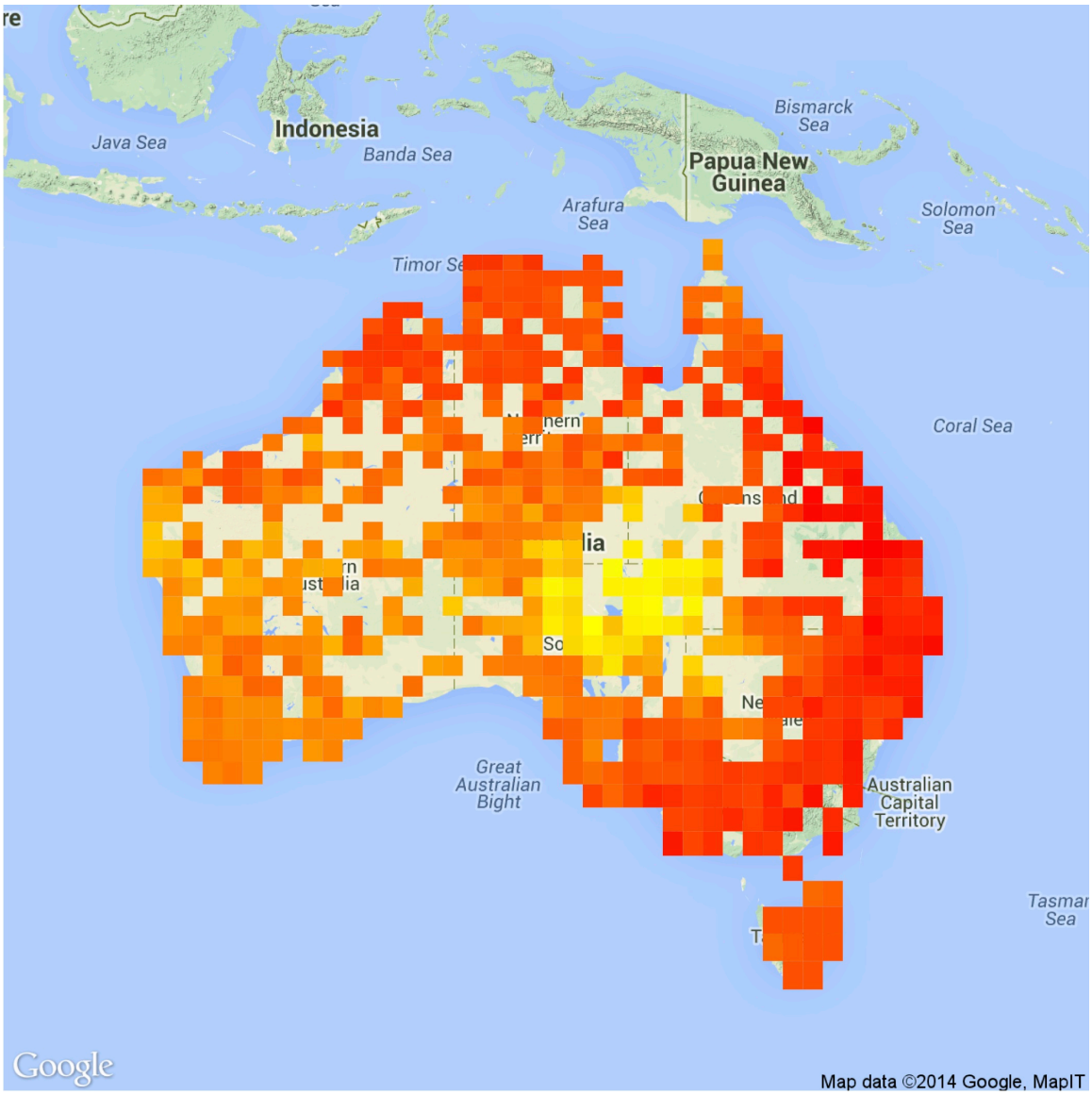

Figure S5. Average species niche size mapped across Australia. Yellow corresponds to small average niches, red to large. Species from the deserts of eastern Australia and, to a lesser degree, southwest Australia, tend to occupy smaller average niches.

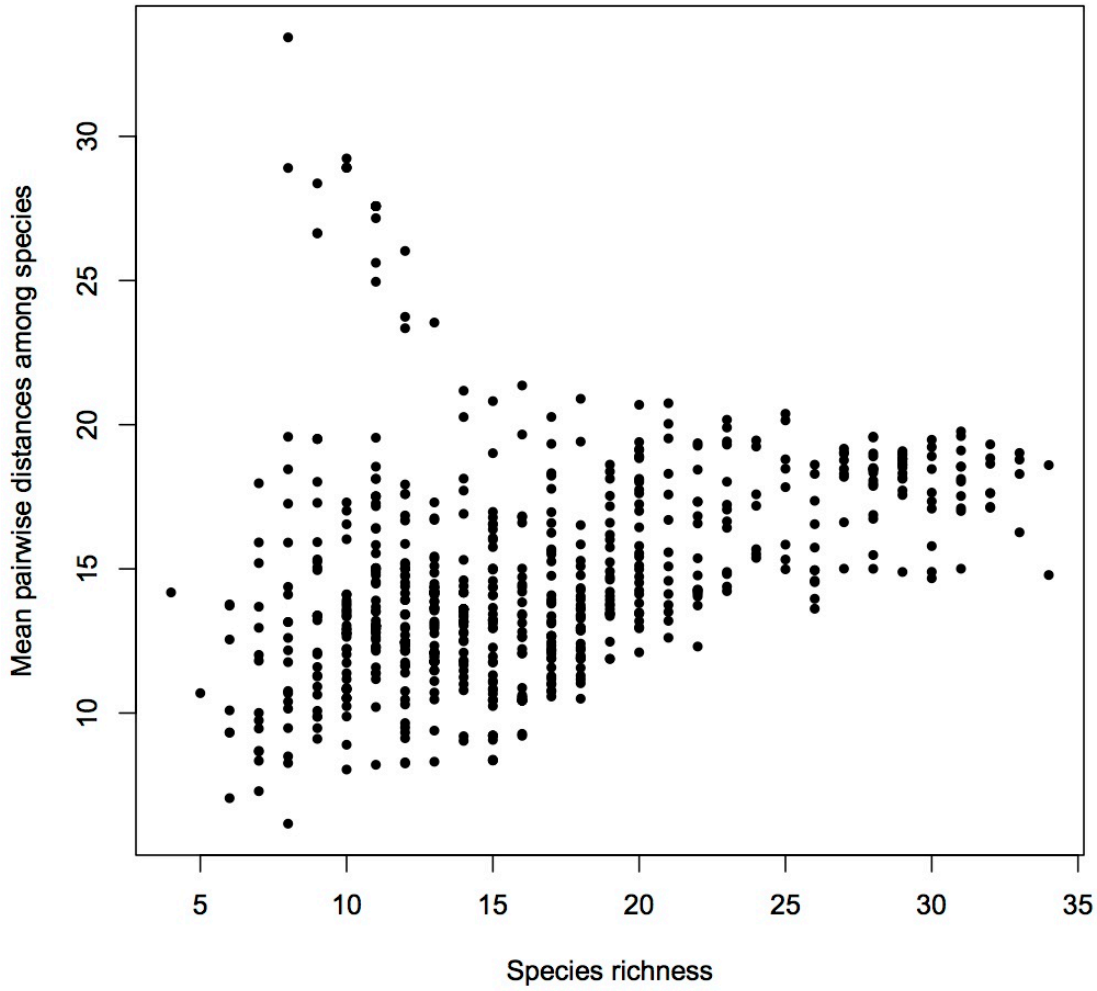

Figure S6. Mean pairwise Mahalanobis' distances among species across the 10 dimensions of the NMDS ordination, plotted against species richness. There is little pattern in the relationship, and more diverse assemblages do not appear more closely packed in niche space ($R^2 = 0.11$, $p < 0.001$).

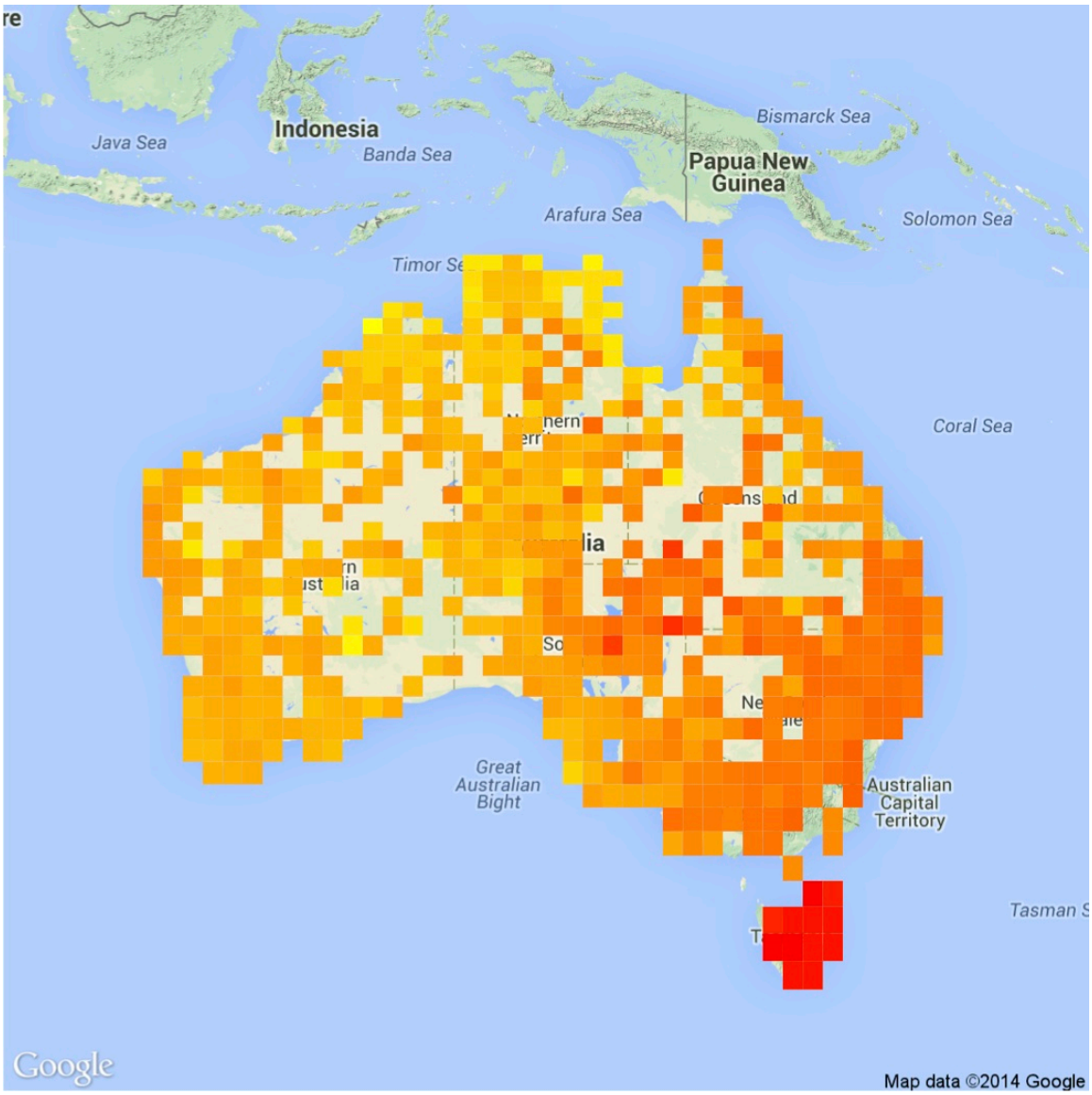

Figure S7. Mean pairwise Mahalanobis' distances among species mapped across Australia. Yellow corresponds to shorter distances, red longer. Species from assemblages in Tasmania and the eastern deserts are more widely separated in available niche space than are species in other regions of the continent.

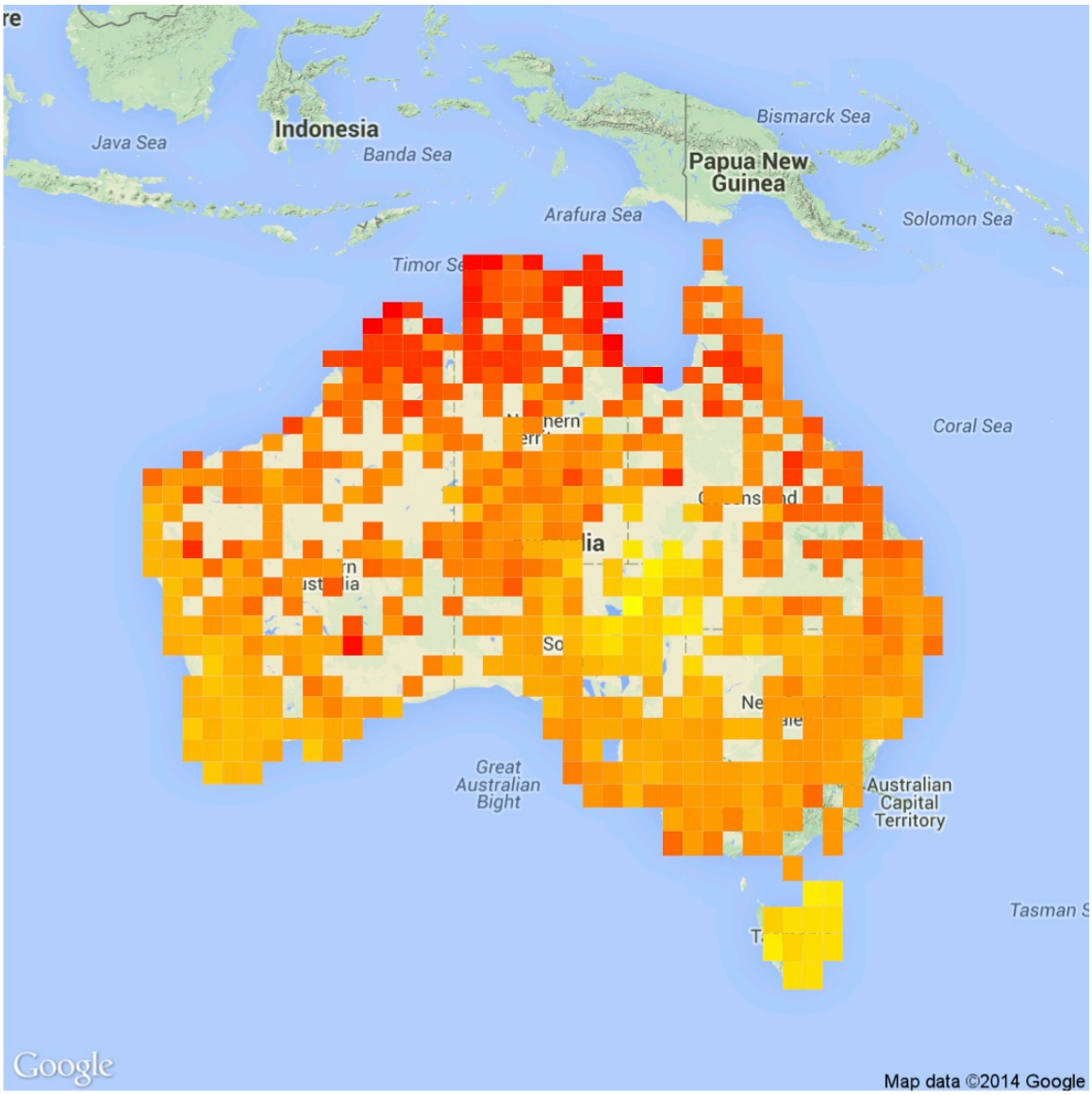

Figure S8. Mean pairwise niche overlap mapped across Australia. Yellow corresponds to lower levels of niche overlap, red to more. Species from Tasmania and the eastern deserts show the least absolute niche overlap.

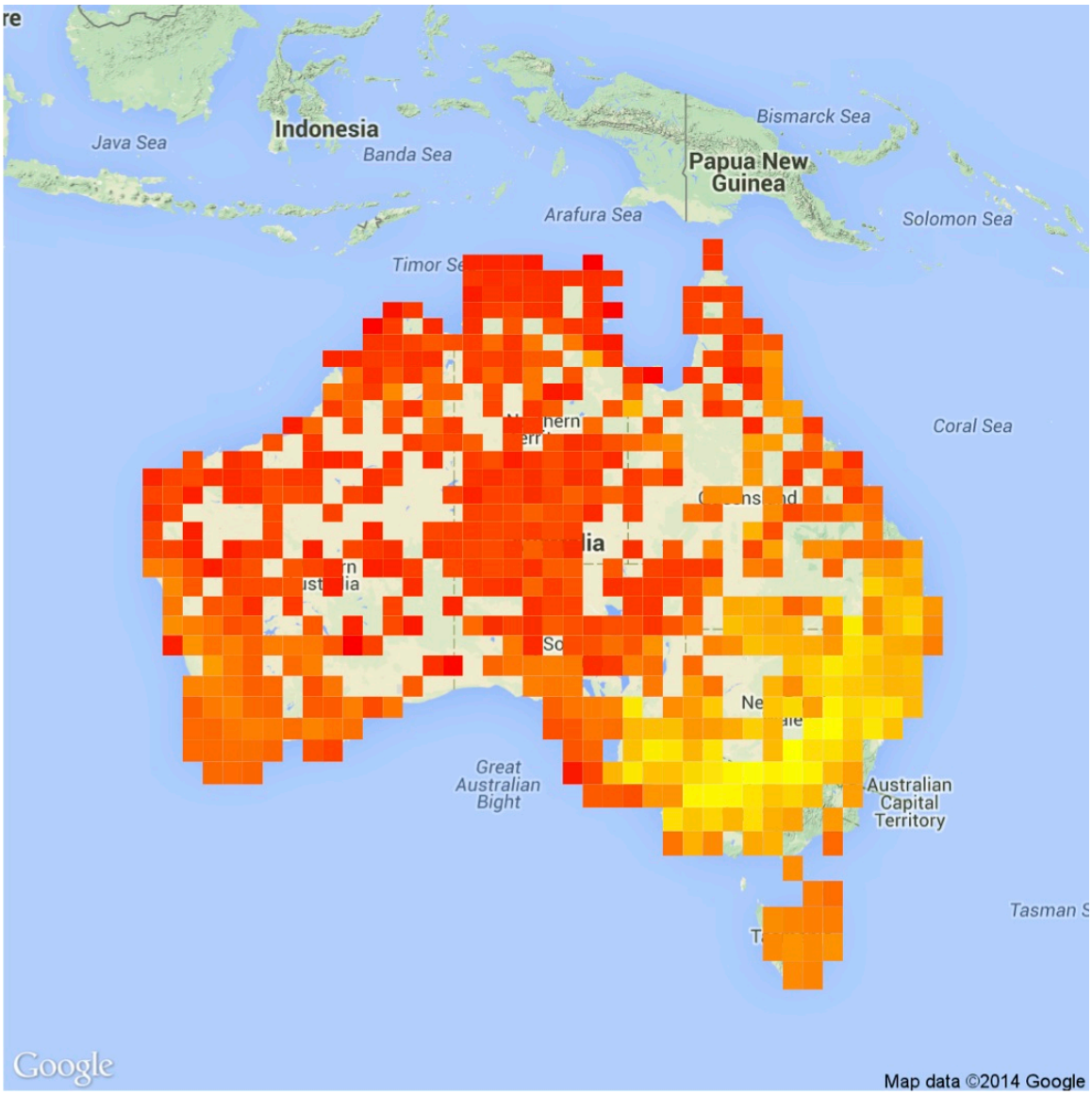

Figure S9. Standardized effect size of mean pairwise niche overlap mapped across Australia. Yellow corresponds to the most negative SES, which are grid cells that show the most significant niche partitioning as compared with the null randomizations.

SUPPLEMENTARY TABLES

Table S1. Table of loadings for continuous vectors and centroids of categorical variables across the ten dimensions of the non-metric multidimensional scaling ordination (NMDS). The continuous (including asymmetric binary) variables are on the first three rows. Foraging maneuvers and factor centroids begin with row "flake". Hang directions begin with row "hang down," and substrates begin with row "air." Foliage density and then distance from trunk are the final rows.

	NMDS1	NMDS2	NMDS3	NMDS4	NMDS5	NMDS6	NMDS7	NMDS8	NMDS9	NMDS10
Dead	-0.10	-0.10	0.03	-0.10	-0.07	0.48	-0.84	0.10	0.04	-0.14
Attack height	-0.03	-0.11	-0.06	0.73	0.39	-0.17	-0.21	-0.18	0.33	0.28
Relative canopy height	0.04	0.00	-0.30	0.81	0.34	-0.35	-0.10	-0.07	-0.07	-0.05
Flake	-0.07	0.14	0.18	-0.03	-0.12	0.00	-0.05	0.00	0.10	0.06
Flush-pursue	-0.05	0.19	-0.02	0.03	0.04	0.09	0.10	-0.11	-0.10	0.01
Flutter-chase	-0.06	0.25	0.01	-0.01	-0.04	0.07	0.11	-0.15	-0.09	0.01
Gape	-0.06	0.00	0.10	0.03	0.04	0.16	0.00	0.02	0.03	0.07
Glean	-0.20	-0.07	0.02	-0.02	0.00	-0.03	0.01	0.00	-0.01	0.00
Hammer	-0.08	0.25	0.05	-0.23	-0.23	-0.12	-0.11	0.09	0.08	-0.02
Leap	-0.11	-0.03	-0.17	-0.10	-0.01	0.15	-0.04	0.14	0.10	-0.01
Lunge	-0.08	0.15	0.00	-0.16	-0.07	0.03	-0.07	0.04	0.05	0.02
Peck	-0.07	0.20	0.08	-0.14	-0.11	-0.05	-0.09	0.09	0.09	0.07
Probe	0.20	-0.03	0.01	0.00	0.00	0.00	-0.01	0.01	0.00	0.00
Pull	-0.05	0.07	0.10	0.06	0.00	0.10	-0.01	-0.03	0.07	-0.04
Sally-glide	-0.07	0.30	-0.05	0.13	-0.08	-0.12	0.00	-0.05	0.05	0.05
Sally-	-0.07	0.10	-0.08	-0.03	0.03	0.08	-0.13	-0.09	0.02	0.06

hover										
Sally-pounce	-0.07	0.15	0.08	-0.17	0.00	0.02	-0.05	0.03	0.10	0.02
Sally-stall	-0.08	0.22	-0.07	0.09	-0.01	-0.07	-0.05	-0.03	0.03	0.01
Sally-strike	-0.08	0.27	-0.07	0.10	-0.02	0.08	0.06	0.04	0.01	-0.01
Screen	-0.07	0.32	-0.08	0.16	-0.09	-0.18	-0.02	0.00	0.01	0.01
Hang down	-0.02	-0.15	0.06	0.09	-0.13	0.02	0.01	-0.10	0.09	-0.03
Hang sideways	-0.03	-0.12	0.12	0.10	-0.05	0.02	0.01	0.04	-0.07	0.17
Hang up	0.04	-0.12	0.10	0.08	-0.06	0.02	0.02	0.10	-0.07	-0.14
Hang upside-down	-0.02	-0.12	0.10	0.11	-0.07	0.01	-0.03	0.10	-0.02	-0.03
Not hanging	0.00	0.04	-0.03	-0.03	0.03	-0.01	0.00	0.00	0.00	0.00
Reach down	-0.06	-0.06	0.20	0.09	-0.01	0.03	-0.02	0.05	0.03	-0.02
Reach out	-0.16	-0.16	0.04	0.07	-0.07	0.00	0.04	0.05	-0.04	-0.01
Reach under	-0.05	-0.06	0.23	0.09	0.00	0.00	0.00	0.00	-0.01	-0.03
Reach up	0.03	-0.15	0.03	0.13	-0.05	0.00	0.00	0.02	-0.06	0.00
Air	-0.07	0.30	-0.05	0.09	-0.04	0.05	0.07	-0.01	-0.01	0.00
Branch	-0.06	0.02	0.20	0.03	0.13	0.00	0.00	0.02	0.05	0.00
Flower	0.22	-0.03	-0.02	-0.01	-0.01	-0.02	0.00	-0.01	-0.01	0.00
Fruit	-0.13	-0.05	0.00	-0.09	0.04	-0.10	0.19	-0.05	-0.01	0.00
Ground	-0.16	0.15	0.08	-0.24	-0.14	-0.13	-0.03	0.04	0.04	0.02
Hanging bark	-0.04	0.00	0.16	0.06	-0.03	0.03	-0.03	-0.01	-0.15	0.10
Insect case	0.03	-0.01	0.05	0.01	-0.02	0.04	0.03	0.04	0.08	0.02

Leaf	-0.19	-0.10	-0.07	0.00	-0.01	0.03	-0.04	0.00	0.00	0.00
Web	-0.14	0.07	0.08	-0.04	0.00	-0.09	-0.01	-0.10	-0.10	-0.01
Woody Fruit	-0.03	-0.01	0.04	0.06	0.02	-0.05	0.03	0.05	-0.02	-0.02
FD0	-0.08	0.20	0.06	0.02	-0.03	-0.01	-0.01	0.00	0.00	0.00
FD1	-0.04	0.08	0.07	0.00	0.01	0.01	-0.04	-0.01	-0.02	-0.01
FD2	0.02	-0.01	0.01	0.00	0.00	0.00	-0.03	-0.01	-0.01	-0.01
FD3	0.03	-0.07	-0.03	0.00	0.00	0.00	0.02	0.00	0.01	0.00
FD4	0.04	-0.13	-0.07	-0.02	0.02	0.01	0.06	0.01	0.02	0.01
FD5	0.01	-0.17	-0.07	-0.07	0.07	0.09	0.07	0.02	0.01	0.00
Inner	0.00	-0.01	0.15	-0.01	0.12	0.08	0.00	-0.02	-0.04	-0.01
Middle	0.03	-0.05	0.02	-0.01	0.04	0.02	0.01	-0.01	-0.01	0.00
Outer	0.00	0.00	-0.02	0.01	-0.03	-0.01	-0.01	0.00	0.00	0.00
Way outer	-0.11	0.26	-0.02	0.00	-0.11	-0.07	-0.01	0.04	0.03	0.01

Table S2. Pagel's lambda (a measure of phylogenetic signal) of species' mean positions along each of the ten NMDS dimensions. Lambda ranges between 0 and 1, where 1 equals Brownian motion evolution. All axes except 10 showed significant phylogenetic signal.

NMDS axis	Lambda	*p*
1	0.715	< 0.001
2	0.907	< 0.001
3	0.565	< 0.001
4	0.813	< 0.001
5	0.545	< 0.001
6	0.960	< 0.001
7	0.980	< 0.001
8	0.789	< 0.001
9	0.390	0.026
10	0.279	0.192